Structured models for dengue epidemiology

Woodall, Hannah

Award date:
2015

Awarding institution:
University of Bath

Structured models for dengue epidemiology

submitted by

Hannah Woodall

for the degree of Doctor of Philosophy

of the

University of Bath

Department of Mathematical Sciences

September 2014

Summary

Dengue is a vector-borne disease. Around 2.5 billion people are thought to be at risk of infection. It is spread primarily through the *Aedes aegypti* mosquito, and is endemic in tropical and subtropical regions. There are four distinct serotypes which co-circulate. Whilst infection from one serotype provides homologous immunity it does not provide heterologous immunity.

In this thesis we use a range of modelling techniques to examine how the epidemiological dynamics of dengue are affected by immunological interaction between serotypes and age–dependent variation in the extent to which people are exposed to the mosquito population. We initially consider transmission dynamics for multi–serotype dengue infections and present a new framework for how secondary infections are modelled. We move on to consider age–structure and introduce a method to quantify differences between seroprevalence profiles when age–independent and age–dependent transmission rates are implemented. We combine these ideas and find that parameters associated with transmission of secondary infections can interact with age–structure and affect how easy it is to detect age–dependence in seroprevalence profiles. Finally we consider how age–dependent variation in the exposure people have to mosquitoes affects the probability of an epidemic and the optimal prevention strategy that should be implemented to ensure that the introduction of isolated infections does not lead to large epidemics.

Our results show it is necessary to understand the underlying dynamics of dengue and implement the correct model, as dynamics can differ substantially. They also show the importance of public health strategies to ensure that all age–groups exposure to mosquitoes is as minimal as possible to decrease the risk of an epidemic. Therefore we have found relevant results that help to further understand the dynamics of dengue.

ACKNOWLEDGEMENTS

I would like to thank my supervisor, Ben Adams, for all his support and guidance throughout my PhD. I would also like to thank the EPSRC for their funding which allowed me to undertake this work.

There have been a lot of people who have helped me over the past three years, keeping me sane, helping me when I have had problems and encouraging me on. Special thanks go to David, Jack, Siân and Tara for this. I would also like to thank everyone who I have shared 4W1.15 with and everyone in 4W1.11.

Finally thanks go to my amazing family who have always believed in me. To Vicky, Dan and Mark for always being there if I need them and for looking after me. To Carl, who has constantly had to listen to me ramble on about my work, and has helped and encouraged me throughout. Lastly to my Mum and Dad who have listened, advised, made me laugh, helped me through the tough times and supported me in the good.

I couldn't have done this without any of you.

CONTENTS

LIST OF FIGURES

LIST OF TABLES

CHAPTER 1

INTRODUCTION

1.1 Dengue

Dengue is a viral mosquito-borne infection which is widespread across Africa, the Americas and Southeast Asia (Gubler and Kuno, 2004; World Health Organisation, 2014a). It is primarily transmitted by the *Aedes aegypti* mosquito, however other mosquitoes can also transmit it (Gubler and Kuno, 2004). There are four antigenetically distinct co-existing serotypes of dengue, DENV-1, DENV-2, DENV-3 and DENV-4. Infection from one serotype results in homologous immunity, however subsequent infection from a second serotype can increase the risk of a more severe infection leading to dengue hemorrhagic fever (DHF, also called severe dengue) (Gubler and Kuno, 2004). DHF can cause complications leading to a patient contracting dengue shock syndrome (DSS). Estimates from the World Health Organisation (2014a) state that over two fifths of the world's population is at risk from dengue, with 50–100 million infections per year. Other estimates range to 390 million dengue infections per year of which 96 million are symptomatic in some way (Bhatt et al., 2013). The World Health Organisation (2014a) estimate that 500,000 people are hospitalized with DHF each year, of which around 2.5% die.

If a susceptible mosquito bites an infectious person, the infection may be passed to that mosquito. Then, after an incubation period of 4–10 days, if the mosquito bites a susceptible person infection can be transmitted to the human host. The mosquito remains infected for the duration of its life. Once a person is infected there is an incubation period which usually lasts 4–5 days, followed by an infectious period where the

person can transmit the infection if bitten by a susceptible mosquito. This usually lasts 4–5 days, with a maximum of 12, after symptoms appear. Once a person has recovered, they have homologous immunity to the serotype for life. However, there is only partial and temporary cross-immunity to the other serotypes (Sabin, 1952; Reich et al., 2013). After this period of temporary cross–immunity it is thought that individuals are more susceptible to a severe secondary infection due to antibody–dependent enhancement (ADE). It is thought that the primary infection leaves cross–reactive, non–neutralizing antibodies which interact with the virus. This leads to increased viral production, increased viraemia and hence a more severe secondary infection (Gubler and Kuno, 2004; Guzman and Vazquez, 2010).

It is interesting to note that in recent years a secondary vector, *Aedes albopictus*, has been more prominent in spreading infection. Increased trade between Asia and North America and Europe of items such as used tyres means that the the mosquito has reached new areas. This, combined with the fact that *Aedes albopictus* is high adaptive and able to survive in these cooler regions, means that dengue has spread further afield (World Health Organisation, 2014a).

Dengue is endemic in more than 100 countries (Gubler, 2002). In countries where dengue is endemic the prevalence of each serotype oscillates with an 8–10 year cycle (Nisalak et al., 2003; Recker et al., 2009). Dengue epidemics can also occur in populations which have not previously seen given serotypes, such as in Cuba in 1997 (Guzmán et al., 2000), on Easter Island, Chile in 2002 (Chowell et al., 2013) and in Madeira in 2012 (Lourenço and Recker, 2014). Dengue is therefore a threat not only in endemic areas, but also those where the disease has not been seen before.

Dengue fever can be symptomatic or asymptomatic; symptoms can include high fever, headaches, rash, loss of appetite, nausea and muscle pain (Guzman and Kouri, 2002; Gubler and Kuno, 2004). Symptoms usually last for 2–7 days (World Health Organisation, 2014a). The symptoms associated with DHF are more severe and can include vomiting, abdominal pain and bleeding alongside the fever (Halstead, 1976). In order for survival it is necessary for early diagnosis so that appropriate treatment can be given.

There is no specific treatment for dengue and there are also no vaccines. At present, the vaccine in the most clinically advanced state is a tetravalent vaccine (World Health Organisation, 2014b). Results of the study showed that the vaccine was effective against only three of the four serotypes (Sabchareon *et al.* (2012), cited in Rodriguez–Barraquer et al. (2014); World Health Organisation (2014b)). While models for expected dynamics should a vaccine become available can be found (WHO–VMI Dengue Vaccine Modelling Group, 2012; Rodriguez–Barraquer et al., 2014), in the interim it is also necessary to

focus on control and prevention strategies. Most control strategies prioritise attempts to decrease the interaction between humans and mosquitoes. This can include the use of insecticides on both adult and larval mosquitoes, and altering human behaviour to reduce the possibility of mosquitoes laying eggs. Examples of this are the emptying and cleaning of water storage containers (World Health Organisation, 2014a).

1.2 Mathematical modelling

Mathematical modelling is used as a way to analyse infectious diseases. The conventional method involves separating the population into different compartments according to their immune–status, such as susceptible to, infected with and recovered from an infectious disease. This modelling approach was initially proposed by Kermack and McKendrick (1927), and forms the base of mathematical modelling of infectious diseases. Use of SIR type models is now frequently seen, with extensions including adding an exposed class to model latency, adding compartments to account for vaccinations, or including multiple strains of a disease, among others (Schenzle, 1984; Anderson and May, 1991; Hethcote, 2000; Keeling and Rohani, 2008; Aparicio and Castillo-Chavez, 2009). The history of mathematical models is discussed further in Anderson and May (1991); Hethcote (2000).

As well as including extensions increasing the number of host compartments, the basic SIR model can be extended to incorporate vectors and the interaction that the host and vector have to model transmission. For dengue this is important as the disease is spread between humans by an intermediary, the mosquito. The framework of including the vector was first established by MacDonald (1957), cited in Keeling and Rohani (2008). This built on work by Ross (1908, 1911), cited in Reiner et al. (2013). Since then host–vector models have been used to study many infectious diseases including dengue, malaria and yellow fever among others (Anderson and May, 1991). Reiner et al. (2013) give a comprehensive review of models for mosquito–borne transmission, comparing and contrasting them with the initial Ross–MacDonald model. We therefore use these ideas when modelling the spread of dengue in a population.

The SIR–type model can be, and has been previously, used in numerous forms to model the spread of infectious diseases. Ordinary differential equations (ODEs), partial differential equations (PDEs), and stochastic models have all been used to model dynamics of different infectious diseases. There are many reviews and books which give examples of these which have been used previously, for example Dietz (1967); Anderson and May (1991); Hethcote (2000); Keeling and Rohani (2008).

Mathematical models can be used for analysis regarding prevalence of disease and

thresholds for epidemic potential (Diekmann and Heesterbeek, 2000; van den Driessche and Watmough, 2008), thresholds for epidemic probability (Allen and Lahodny Jr, 2012; Bacaër and Ait Dads, 2012), and can be adapted to implement controls to decrease the prevalence of a disease (Lenhart and Workman, 2007). The tools needed for analysis depend on the model being implemented.

1.3 Thesis outline

In this thesis we implement and add to existing models for dengue, alongside applying new methodologies to contrast and compare different aspects of the models. The chapters of the thesis are closely connected, but also self–contained. Each chapter has an introduction that provides background and context for the research that is discussed. Models are then built up from this starting point. Chapter 2 introduces ideas relating to partial and temporary immunity which can occur after a primary dengue infection. We implement a new framework for a two–serotype ODE model for dengue and analyse it. In Chapters 3 and 4 we develop an age structured model using PDEs. In Chapter 3 we initially implement a single serotype model and study numerical schemes to solve the system. We then implement a methodology to see if we can quantifiably determine differences in seroprevalence profiles when an age–dependent and age–independent contact rate are implemented. This is developed further in Chapter 4 for a two serotype model where vectors are implicitly included in the model. In Chapter 5 we develop the age structure model into a stochastic model to determine the probability of an epidemic. We assume that age groups have varying exposure to the mosquitoes and determine how this affects the probability of an epidemic. In Chapter 6 we study optimal prevention for the age structured single serotype model to find the most efficient way to ensure that when an infection enters the population it does not lead to an epidemic. Finally, in Chapter 7 we discuss our results and bring the conclusions for each of the chapters together.

CHAPTER 2

PARTIAL CROSS–ENHANCEMENT FOR DENGUE TRANSMISSION

Summary

In this chapter we start by introducing antibody–dependent enhancement (ADE); the idea that due to cross–reactive antibodies secondary dengue infections are more severe than primary infections. We initially analyse an existing, well–known model which includes ADE and extend it, introducing a new framework which incorporates the idea that not all secondary infections are enhanced. Instead, we implement a model where a proportion of secondary infections are enhanced while the rest are subjected to cross–protection, providing research which gives credence to this idea. We then implement temporary cross–immunity in the model; this is the period after a primary infection where it is thought an individual has complete immunity to the serotype previously infected with, but only temporary heterologous immunity to other serotypes. We analyse an existing model which includes both these mechanisms, and extend it to apply our new framework. We analyse both models implementing our new approach, compare them with the conventional framework, and discuss the merits of using this methodology for modelling dengue.[1]

[1]Parts of the work from Chapter 2 have been published (Woodall and Adams, 2014).

2.1 Introduction

As stated in Chapter 1, there are four antigenetically distinct serotypes of dengue virus. Whilst infection from one serotype provides complete homologous immunity, it potentially provides only partial and temporary heterologous immunity against other serotypes (Sabin, 1952; Reich et al., 2013), although this is not fully known. It is thought that as any heterologous immunity wanes there is then a period of time when enhanced secondary infections can occur, caused by antibody-dependent enhancement (ADE). During a primary infection cross–reactive antibodies are produced. Upon secondary infection these bind to the new virus, leading to increased viral production. This then leads to higher viraemia within an individual and consequently a more severe secondary infection (Guzman and Vazquez, 2010).

There are different modelling approaches which have been undertaken, with many studies considering two-serotype models (Ferguson et al., 1999a; Kawaguchi et al., 2003; Adams et al., 2006; Aguiar et al., 2011a), four-serotype models (Wearing and Rohani, 2006; Chikaki and Ishikawa, 2009; Recker et al., 2009) and even n–serotype models (Bianco et al., 2009). Some of these models include both temporary cross–immunity and ADE (for example Wearing and Rohani (2006); Aguiar et al. (2011a)), whilst others only include enhancement (for example Ferguson et al. (1999a); Recker et al. (2009)). The first paper which included ADE for a dengue model was Ferguson et al. (1999a). The results show that including ADE in the model can cause either cyclical behaviour in the seroprevalence of two dengue serotypes or can cause chaotic dynamics. Several papers have implemented this idea and used compartmentalized models to work further on this (for example Schwartz et al. (2005); Bianco et al. (2009)). Wearing and Rohani (2006) include temporary cross–protection as well as ADE in their model. They show that temporary cross–immunity alone is enough to allow for periodic dynamics that can be seen in empirical data for dengue.

The standard framework for incorporating ADE into models assumes that all secondary infections are subject to enhancement. This has been modelled by an increased susceptibility to infection (for example Wearing and Rohani (2006)) or through an increased transmission probability of those with a secondary infection (for example Ferguson et al. (1999a)). It has been shown that the impact on the dynamics is similar whether ADE acts through either mechanism (Ferguson and Andreasen, 2002; Adams and Boots, 2006). ADE has also been modelled through a decreased susceptibility as if enhanced infections result in hospitalization this ultimately decreases infectivity in the general population (Aguiar et al., 2008).

A common feature of all these models is that they assume all secondary infections

are enhanced. However, only 2–4 % of individuals with a secondary infection had DHF in an outbreak in Cuba in 1997 (Guzmán et al., 2000; Guzman and Kouri, 2002). This was only the second serotype to enter the population, after a previous epidemic between 1977–1979. Further to this, a cohort study of children in Thailand from 2006–2009 found that in the majority of cases were secondary secondary infection; 95% of DHF cases and 88.7% of dengue fever cases (Sabchareon et al., 2012). This indicates that many secondary infections were not enhanced. The question then arises as to where the model should be separated into those that suffer an enhanced infection and those that do not. It could be straight after a primary infection or after the second period of susceptibility. The former suggests that there is some form of predisposition (possibly genetic) as to why some people are affected by ADE and have an enhanced secondary infection. The latter assumes that ADE is based on chance, depending on chemical reactions in the body which randomly occur.

Research has shown that it is likely that certain individuals have a predisposition to an enhanced secondary infection via ADE. This could be related to factors such as age, ethnicity, genetic composition including FCγRIIa receptors[2], human leukocyte antigen (HLA) alleles[3] and prior T and B cell immunity, and pre-existing medical conditions (Mathew and Rothman, 2008; Guzman and Vazquez, 2010; Whitehorn and Simmons, 2011).

Guzmán et al. (2002) conducted a study of a population that had been exposed to DENV-1 in an initial epidemic and were then exposed to DENV-2 in a second outbreak in 1981. They calculated the age–specific rates at which people had been hospitalized from DHF/DSS or had died. Their results, considering secondary infections only, show that children are more susceptible to DHF/DSS as secondary infections than adults; the death rate for 3–4 year olds was 25.4 per 10,000 secondary DENV-2 infections which is nearly five–fold more than the rate for 10–14 year olds. It is worth noting that there may also be other factors such as different immune histories which also affect the rate of susceptibility and therefore infection as well as age. Anders et al. (2011) also show that age is an important factor for infection; for their study of three Vietnamese hospitals, children aged 6–10 had the highest percentage of case fatality rate associated with DSS when considering children aged 0–15. They also believe that gender may impact on ADE through a higher mortality due to DSS in girls than in boys. However, the authors note that further investigation may be needed to determine factors influencing behaviours around seeking care for girls and boys and any potential effects this may have on their results. These studies give credence to the idea that some individuals

[2]FCγ receptors contribute to protective functions of the immune system
[3]related to immune system function

have a predisposition to ADE, for example due to their age or gender.

Halstead et al. (2001) use data from Haiti to speculate there is a dengue resistant gene in black populations. This is due to the lack in the number of cases of DHF/DSS in Haitian children compared to the number that would be expected due to the annual infection rate. The arrival of US military who quickly contracted the disease also argues for a dengue resistant gene in black populations. Halstead et al. (2001) also cite examples of the outbreaks in Cuba where blacks were hosptizalised at a lower rates than whites with no preferential hosptitalizaition to argue their case for a dengue resistant gene in black populations. la C. Sierra et al. (2007) produce a review which provides results indicating that ethnicity can be a risk factor for DHF. By comparing the number of white, mixed race and black individuals who contracted DHF for different outbreaks in Cuba, they are able to show that a greater proportion of the population who contracted and died from DHF were white or mixed race. These studies also support the idea that some individuals may have a predisposition to ADE, in this case due to their ethnicity.

There has been much research into dengue outbreaks that have occurred in Cuba. This is because due to its location any epidemics have to be brought in from other places. Therefore it is possible to clearly map infections and use the information for genetic studies regarding dengue. Garciá et al. (2010) discuss the role of the RR variant of the FCγRIIa receptor, showing evidence for the polymorphism to provide an inherited risk factor for DHF/DSS in Cubans. This has also been seen in Vietnamese individuals (Loke et al., 2002). Polymorphisms at some HLA loci may also be important factors with some HLA alleles associated with protection while others are pathogenic genetic variants (Sierra et al., 2007; Mathew and Rothman, 2008).

The above studies indicate some individuals may have a predisposition to an enhanced secondary infection, rather than these being a product of chance. Therefore for our modelling the population will be separated into two groups at the point of susceptibility to secondary infections. The first compartment will be the proportion of the population who are susceptible to an enhanced secondary infection (and therefore have a greater chance of contracting DHF or DSS), whilst the second compartment will have either the same force of infection as a primary infection, or a decreased susceptibility to secondary infection.

To investigate these ideas further we will initially set up the model used in Ferguson et al. (1999a) and simulate the dynamics for this model. We will then extend this model to include our new framework and determine the effect that this has on the system. We will then also do this for the Wearing and Rohani (2006) model and investigate how the different parameters within the model affect the dynamics we see.

2.2 Model I: Two serotype SIR model with ADE

2.2.1 Model Ia: Two serotype SIR overlapping compartmental model with ADE (Ferguson et al., 1999a)

Ferguson et al. (1999a) present a model which includes ADE, exploring the dynamics surrounding when previous exposure to a serotype may increase the probability of transmission of a second serotype. The model is described as a set of seven differential equations, where some compartments overlap. Let the serotype be defined by subscript i, j, where $i, j = 1, 2$, $i \neq j$. Let x_i be the fraction of the population already exposed to serotype i, s be the proportion of the population susceptible to both serotypes, y_i be the proportion of the population with primary infection of serotype i, and y_{ji} be the proportion of the population with a secondary infection of serotype i having previously had primary infection of serotype j. Therefore the system is described by

$$\frac{\mathrm{d}x_i}{\mathrm{d}t} = (1 - x_i)\lambda_i - \mu x_i \tag{2.1a}$$

$$\frac{\mathrm{d}s}{\mathrm{d}t} = \mu - s\sum_k \lambda_k - \mu s \tag{2.1b}$$

$$\frac{\mathrm{d}y_i}{\mathrm{d}t} = s\lambda_i - \sigma y_i \tag{2.1c}$$

$$\frac{\mathrm{d}y_{ji}}{\mathrm{d}t} = (1 - x_i - s)\lambda_i - \sigma y_{ji} \tag{2.1d}$$

where μ is the mortality rate of the host, λ_i is the force of infection of serotype i and σ is the rate of recovery. Table 2.1 gives the parameter definitions and values used in the simulations. It is worth noting that the equation for y_{ji} is slightly different to Ferguson et al. (1999a) where the first term is given as $(1 - x_j - s)$. The term represents the fraction of the population that are not susceptible or have not been previously exposed to serotype j. Two reasons are now given as to why this expression should be given by $(1 - x_i - s)$ instead. Firstly, individuals enter the class x_i by becoming infectious with a primary or secondary infection of serotype i. Using the notation from the paper this is at rate $s\lambda_i$ for a primary infection and at rate $(1 - x_j - s)\lambda_i$ for a secondary infection. Adding these together would give $(1 - x_j)\lambda_i$ which is not the equation given for x_i. Secondly, we are interested in those who have not been exposed to serotype i. We know that $(1 - x_i)$ is the proportion of the population not exposed to serotype i. Therefore $(1 - x_i - s)$ is the proportion of the population not susceptible to both infections and that have not been exposed to serotype i. Therefore this is the expression which we give in the equations above.

Parameter	Definition	Value
μ	Host mortality rate	0.02
σ_i	Host recovery rate	99.98
β	Transmission rate	200
ϕ_i	Enhancement/cross–protection of serotype i (Model 1a)	$\phi_2 = 2$
ρ	Enhancement prevalence (Model 1c)	
χ	Enhancement intensity (Model 1c)	
η	Cross–protection (Model 1c)	

Table 2.1: Parameter definitions and values used where kept constant for Models Ia, Ib and Ic. All rates are given per year.

Ferguson et al. (1999a) assume that ADE acts to increase (or decrease) the transmission probability of an individual with a secondary infection. Therefore the force of infection is given by

$$\lambda_i = \beta_i \left(y_i + \phi_i y_{ji}\right) \tag{2.2}$$

where β_i is the transmission rate of serotype i and ϕ_i is the level of enhancement ($\phi_i > 1$) or cross–protection ($0 < \phi_i < 1$) acting on the model due to antibody interaction in secondary infections. This can be combined with equations (2.1c)–(2.1d) to give

$$\frac{\mathrm{d}\lambda_i}{\mathrm{d}t} = \beta_i \lambda_i (s + \phi_i (1 - x_i - s)) - \sigma \lambda_i. \tag{2.3}$$

We can recreate the bifurcation diagram shown in Figure 1(c) in Ferguson et al. (1999a). Our results show that for x_1 the shape of the figure is similar to that seen in Ferguson et al. (1999a), however translated downwards by around 0.2. Plotting the cross–protection parameter (ϕ_1) against the proportion of the population already exposed to serotype 2 (x_2) yields a graph which, when plotting the local maxima and minima, looks very similar to Figure 1(c) of the paper. The maxima and minima can be seen in Figure 2-2 as the black dots.

As previously stated this model is formed of overlapping compartments. However, to implement our new framework where only a proportion of the population has an enhanced secondary infection, it will be easier to work with non-overlapping compartments. This will also make it easier to interpret results. Therefore we now compartmentalize Model Ia.

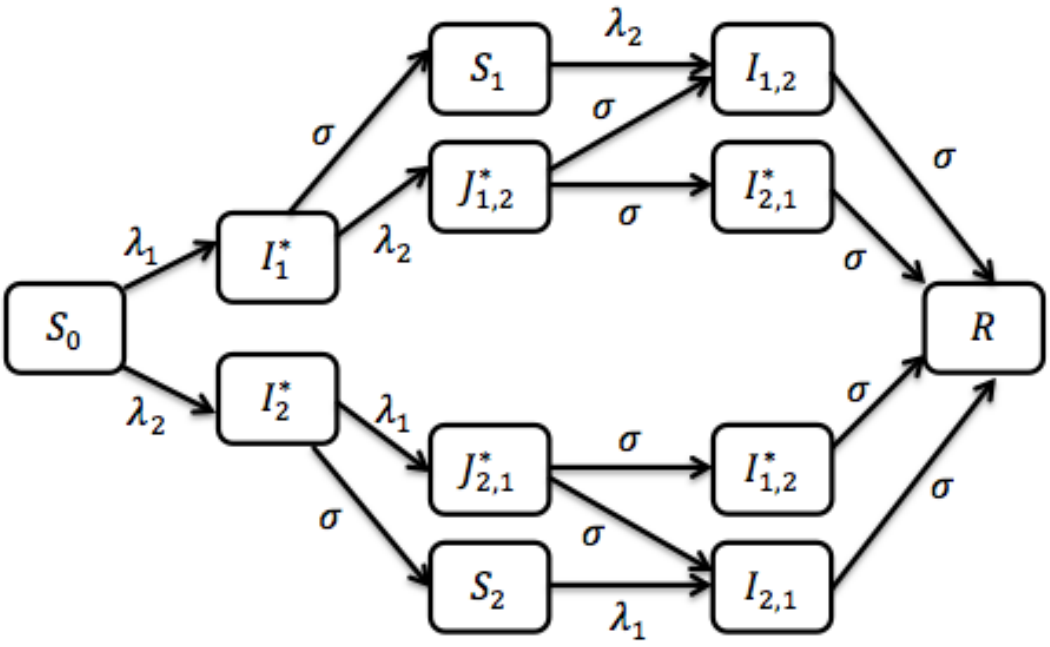

Figure 2-1: Flow diagram showing the compartmentalized Ferguson et al. (1999a) SIR model with enhancement or cross–protection of serotype i (ϕ_i) acting on transmission. For clarity demography has not been included.

2.2.2 Model Ib: Two serotype SIR model with ADE

To compartmentalize the model in Ferguson et al. (1999a) it is necessary to differentiate between primary and secondary infections. This is because of their importance within the force of infection term as enhancement is acting on transmission. Figure 2-1 shows a flowchart of how individuals move between the different compartments. Note that some compartments may initially seem superfluous but after consideration of this model we are able to simplify it. The hosts can be defined by the states susceptible to both serotypes (S_0), actively infected with primary infection serotype i (I_i^*), recovered from infection with serotype i and susceptible to serotype j (S_i), actively infected with secondary infection serotype j having previously been infected with serotype i ($I_{i,j}$), co-infected with serotypes i and j where serotype i was the primary infection ($J_{i,j}^*$), actively infected with primary infection of serotype j and recovered from serotype i ($I_{i,j}^*$) and recovered from both serotypes (R). The asterix (*) keeps track of which have not recovered from their primary infections. The system is then given by

$$\frac{\mathrm{d}S_0}{\mathrm{d}t} = \mu - (\lambda_1 + \lambda_2)S_0 - \mu S_0, \tag{2.4a}$$
$$\frac{\mathrm{d}I_1^*}{\mathrm{d}t} = \lambda_1 S_0 - (\lambda_2 + \sigma + \mu)I_1^*, \tag{2.4b}$$
$$\frac{\mathrm{d}I_2^*}{\mathrm{d}t} = \lambda_2 S_0 - (\lambda_1 + \sigma + \mu)I_2^*, \tag{2.4c}$$
$$\frac{\mathrm{d}J_{1,2}^*}{\mathrm{d}t} = \lambda_2 I_1^* - (2\sigma + \mu)J_{1,2}^*, \tag{2.4d}$$
$$\frac{\mathrm{d}J_{2,1}^*}{\mathrm{d}t} = \lambda_1 I_2^* - (2\sigma + \mu)J_{2,1}^*, \tag{2.4e}$$
$$\frac{\mathrm{d}S_1}{\mathrm{d}t} = \sigma I_1^* - (\lambda_2 + \mu)S_1, \tag{2.4f}$$
$$\frac{\mathrm{d}S_2}{\mathrm{d}t} = \sigma I_2^* - (\lambda_2 + \mu)S_2, \tag{2.4g}$$
$$\frac{\mathrm{d}I_{1,2}}{\mathrm{d}t} = \lambda_2 S_1 + \sigma J_{1,2}^* - (\sigma + \mu)I_{1,2}, \tag{2.4h}$$
$$\frac{\mathrm{d}I_{2,1}^*}{\mathrm{d}t} = \sigma J_{1,2}^* - (\sigma + \mu)I_{2,1}^*, \tag{2.4i}$$
$$\frac{\mathrm{d}I_{1,2}^*}{\mathrm{d}t} = \sigma J_{2,1}^* - (\sigma + \mu)I_{1,2}^*, \tag{2.4j}$$
$$\frac{\mathrm{d}I_{2,1}}{\mathrm{d}t} = \lambda_1 S_2 + \sigma J_{2,1}^* - (\sigma + \mu)I_{2,1}, \tag{2.4k}$$
$$\frac{\mathrm{d}R}{\mathrm{d}t} = \sigma(I_{1,2} + I_{2,1}^* + I_{1,2}^* + I_{1,2}) - \mu R, \tag{2.4l}$$

where μ, σ and λ_i have the same meaning as in Model Ia and are given in Table 2.1. However, we need to adapt the equation for the force of infection. We initially describe the state variables used in the force of infection in Model Ia by the state variables in Model Ib. In Model Ia the force of infection was made by terms describing the primary and secondary infection. Therefore we have

$$y_1 = I_1^* + J_{1,2}^* + I_{2,1}^*, \tag{2.5a}$$
$$y_2 = I_2^* + J_{2,1}^* + I_{1,2}^*, \tag{2.5b}$$
$$y_{21} = J_{2,1}^* + I_{2,1}, \tag{2.5c}$$
$$y_{12} = J_{1,2}^* + I_{1,2}. \tag{2.5d}$$

Hence the forces of infection of serotypes one and two are given by

$$\lambda_1 = \beta_1 \left(I_1^* + J_{1,2}^* + I_{2,1}^* + \phi_1 \left(J_{2,1}^* + I_{2,1} \right) \right), \tag{2.6a}$$

$$\lambda_2 = \beta_2 \left(I_2^* + J_{2,1}^* + I_{1,2}^* + \phi_2 \left(J_{1,2}^* + I_{1,2} \right) \right) \tag{2.6b}$$

respectively, where β_i is the transmission co-efficient of serotype i and ϕ_i is the degree of enhancement ($\phi_i > 1$) or cross–protection ($0 < \phi_i < 1$), $i = 1, 2$.

The state variables not used in the force of infection in Model Ia can also be written in terms of the new variables for Model Ib. For example, x_1 is the fraction of the population exposed to serotype 1, which can be written in terms of all compartments which involve being infected by or recovered from serotype 1. Therefore, in terms of the new state variables x_1 is given by

$$x_1 = I_1^* + J_{1,2}^* + J_{2,1}^* + S_1 + I_{1,2} + I_{2,1}^* + I_{1,2}^* + I_{2,1} + R. \tag{2.7a}$$

Similarly we can define the other state variables from Model Ia as

$$x_2 = I_2^* + J_{1,2}^* + J_{2,1}^* + S_2 + I_{1,2} + I_{2,1}^* + I_{1,2}^* + I_{2,1} + R, \tag{2.7b}$$

$$s = S_0. \tag{2.7c}$$

Using equations (2.4) we plot the maxima and minima of x_2 for various values of cross–protection parameter ϕ_1. These can be seen as the red dots overlaying the original bifurcation diagram for Model Ia (Ferguson et al., 1999a) in figure 2-2(a). For $\phi_1 > 0.5$ there is good agreement, which clearly follows the trend of the bifurcation diagram for the overlapping model. For smaller values of ϕ_1 there is a difference, however in this region there are chaotic dynamics. Therefore, as the overall trend of the graphs are followed we are happy with this model.

Although providing an acceptable fit to the overlapping model (Model Ia, equations (2.1)), the non-overlapping model (equations (2.4)) is quite cumbersome to use. Co-infection alongside keeping track of primary and secondary infections means there are several compartments. Due to the short duration of infection, a good assumption is that an individual cannot be infected with two serotypes at once. This is an assumption which is widely implemented for dengue (Bianco et al., 2009; Recker et al., 2009; Aguiar et al., 2011a). Therefore, a simpler model can be seen in figure 2-3, and described by the system of equations

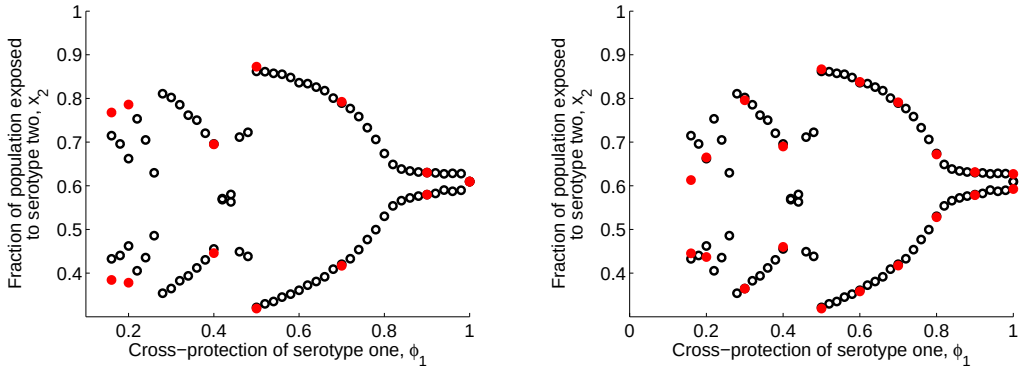

(a) (b)

Figure 2-2: (a) Bifurcation diagram plotting the local maxima and minima of x_2 against ϕ_1 for the full compartmentalized model (equations (2.4)) as red circles overlaying the maxima and minima for Model Ia. (b) Bifurcation diagram plotting the local maxima and minima of x_2 against ϕ_1 for the simpler compartmentalized model (equations (2.8)) as red circles overlaying the maxima and minima for Model Ia. The first 900 years were discarded from the time series to allow convergence to any equilibrium point or limit cycle. All parameters are given in Table 2.1.

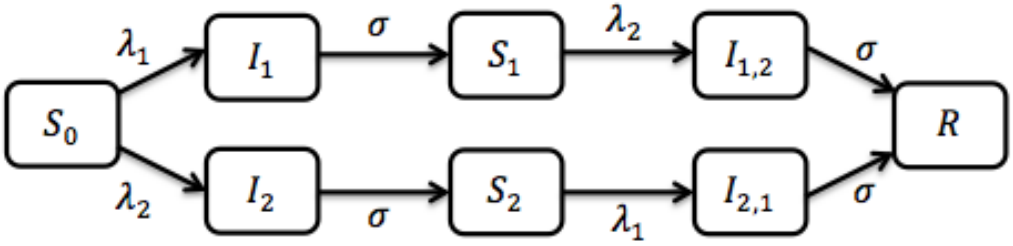

Figure 2-3: Flow diagram showing the simplified compartmentalized Ferguson et al. (1999a) SIR model (no co-infection) with enhancement or cross–protection ϕ_i acting on transmission. For clarity demography has not been included.

$$\frac{\mathrm{d}S_0}{\mathrm{d}t} = \mu - (\lambda_1 + \lambda_2)S_0 - \mu S_0, \tag{2.8a}$$
$$\frac{\mathrm{d}I_1}{\mathrm{d}t} = \lambda_1 S_0 - (\sigma + \mu)I_1, \tag{2.8b}$$
$$\frac{\mathrm{d}I_2}{\mathrm{d}t} = \lambda_2 S_0 - (\sigma + \mu)I_2, \tag{2.8c}$$
$$\frac{\mathrm{d}S_1}{\mathrm{d}t} = \sigma I_1 - (\lambda_2 + \mu)S_1, \tag{2.8d}$$
$$\frac{\mathrm{d}S_2}{\mathrm{d}t} = \sigma I_2 - (\lambda_1 + \mu)S_2, \tag{2.8e}$$
$$\frac{\mathrm{d}I_{1,2}}{\mathrm{d}t} = \lambda_2 S_1 - (\sigma + \mu)I_{1,2}, \tag{2.8f}$$
$$\frac{\mathrm{d}I_{2,1}}{\mathrm{d}t} = \lambda_1 S_2 - (\sigma + \mu)I_{2,1}, \tag{2.8g}$$
$$\frac{\mathrm{d}R}{\mathrm{d}t} = \sigma(I_{1,2} + I_{2,1}) - \mu R, \tag{2.8h}$$

where μ, σ and λ_i have the same meaning as in the previous models. We again have to redefine the forces of infection for each of the serotypes as

$$\lambda_1 = \beta_1 \left(I_1 + \phi_1 I_{2,1}\right), \tag{2.9a}$$
$$\lambda_2 = \beta_2 \left(I_2 + \phi_2 I_{1,2}\right), \tag{2.9b}$$

and in this case the original state variable x_2 can be written as

$$x_2 = I_2 + S_2 + I_{1,2} + I_{2,1} + R. \tag{2.10}$$

All other states from Model Ia can be calculated in a similar manner. Figure 2-2(b) shows the maxima and minima of x_2 for various values of cross–protection parameter ϕ_1 under system (2.8) in red overlaying the initial bifurcation diagram. We can see a good agreement across the different parameter values implemented, meaning that the simpler model is an acceptable approximation to use for Model Ia. Therefore, for further analysis and the extension of the model using our new framework, we are going to implement the simpler compartmentalized version (equations (2.8)) as our base model.

2.2.3 Model Ic: Two serotype SIR model with ADE and partial cross–enhancement

We now implement our new framework into the simplified two serotype SIR compartmentalized model (Model Ib). As stated previously, we separate the population into those who are predisposed to an enhanced secondary infection and those that are not immediately after primary infection, shown in Figure 2-4. As before, an individual can be susceptible to both serotypes (S_0), be actively infected with primary infection of serotype i (I_i) or recovered from both serotypes (R). The state of homologous immunity to serotype i and susceptible to serotype j (S_i) is now composed of those who are susceptible to an enhanced secondary infection and those who are not (S_i^E, S_i^P respectively). This carries on to the active secondary infection with serotype j having previously been infected with serotype i ($I_{i,j}^E$, $I_{i,j}^P$).

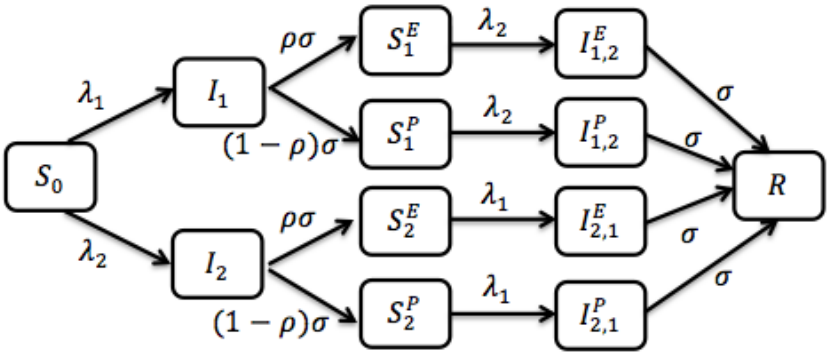

Figure 2-4: Flow diagram showing our new framework acting on the compartmentalized Ferguson et al. (1999a) SIR model. Enhancement intensity χ acts on transmission of the ρ proportion of the population with an enhanced secondary infection and cross–protection η acts on transmission of the other $(1-\rho)$ proportion. For clarity demography has not been included.

The system can be modelled by

$$\frac{\mathrm{d}S_0}{\mathrm{d}t} = \mu - (\lambda_1 + \lambda_2 + \mu)S_0, \tag{2.11a}$$
$$\frac{\mathrm{d}I_1}{\mathrm{d}t} = \lambda_1 S_0 - (\sigma + \mu)I_1, \tag{2.11b}$$
$$\frac{\mathrm{d}I_2}{\mathrm{d}t} = \lambda_2 S_0 - (\sigma + \mu)I_2, \tag{2.11c}$$
$$\frac{\mathrm{d}S_1^E}{\mathrm{d}t} = \rho\sigma I_1 - (\lambda_2 + \mu)S_1^E, \tag{2.11d}$$
$$\frac{\mathrm{d}S_1^P}{\mathrm{d}t} = (1-\rho)\sigma I_1 - (\lambda_2 + \mu)S_1^P, \tag{2.11e}$$
$$\frac{\mathrm{d}S_2^E}{\mathrm{d}t} = \rho\sigma I_2 - (\lambda_1 + \mu)S_2^E, \tag{2.11f}$$
$$\frac{\mathrm{d}S_2^P}{\mathrm{d}t} = (1-\rho)\sigma I_2 - (\lambda_1 + \mu)S_2^P, \tag{2.11g}$$
$$\frac{\mathrm{d}I_{1,2}^E}{\mathrm{d}t} = \lambda_2 S_1^E - (\sigma + \mu)I_{1,2}^E, \tag{2.11h}$$
$$\frac{\mathrm{d}I_{1,2}^P}{\mathrm{d}t} = \lambda_2 S_1^P - (\sigma + \mu)I_{1,2}^P, \tag{2.11i}$$
$$\frac{\mathrm{d}I_{2,1}^E}{\mathrm{d}t} = \lambda_1 S_2^E - (\sigma + \mu)I_{2,1}^E, \tag{2.11j}$$
$$\frac{\mathrm{d}I_{2,1}^P}{\mathrm{d}t} = \lambda_1 S_2^P - (\sigma + \mu)I_{2,1}^P, \tag{2.11k}$$
$$\frac{\mathrm{d}R}{\mathrm{d}t} = \sigma\left(I_{1,2}^E + I_{1,2}^P + I_{2,1}^E + I_{2,1}^P\right) - \mu R, \tag{2.11l}$$

where

$$\lambda_1 = \frac{\beta I_1 + \chi I_{2,1}^E + \eta I_{2,1}^P}{N} \quad \text{and} \quad \lambda_2 = \frac{\beta I_2 + \chi I_{1,2}^E + \eta I_{1,2}^P}{N}. \tag{2.12}$$

For consistency with Ferguson et al. (1999a) ADE is included in the model through increased transmission. Under the new framework a proportion ρ of the population have a predisposition to ADE, and suffer an enhanced infection with enhancement intensity χ. The other $(1-\rho)$ of the population have an infection which exhibits no infectivity ($\eta = 0$), has infectivity with the same intensity as a primary infection ($\eta = 1$) or has a level of cross–protection ($0 < \eta < 1$). Therefore we have $0 \leq \eta \leq 1$. We term ρ the degree of enhancement prevalence and η the level of cross–protection.

This model can be analysed and results compared with Ferguson et al. (1999a). As in Ferguson et al. (1999a) we assume the recovery rates of each serotype are identical. However, we also set the enhancement intensities and cross–protection for each serotype to be identical, as we are not assuming that one serotypes has a greater effect than another.

2.2.4 Results

There are three variables which can be varied in the analysis; the enhancement prevalence (ρ), the enhancement intensity (χ) and the cross–protection (η). It is worth noting that if $\rho = 1$ all individuals suffer an enhanced secondary infection and the model can be reduced to Model Ib with $\chi = \phi_i$ and η being irrelevant. Similarly if $\rho = 0$ no individuals suffer an enhanced secondary infection and the model can be reduced to Model Ib with $\eta = \phi_i$ and χ being irrelevant.

To begin with we vary the enhancement prevalence from 1 (everyone has an enhanced secondary infection) to 0 (no one has an enhanced secondary infection). We initially assume that $\eta = 1$ (all secondary infections which are not enhanced have the same infectivity as a primary infection) and vary the enhancement intensity acting on enhanced secondary infections (figure 2-5(a)). For all of the enhancement intensities as the enhancement prevalence increases so too does the proportion of the population infected with serotype 1 (shown in figure 2-5, consider right to left). This is to be expected as when ρ is increased, the proportion of the population affected by ADE increases. This means there is greater proportion of the population that the higher transmission probability acts on in the force of infection, and therefore more individuals can become infected. As χ increases the proportion of the population infected with serotype 1 also increases. Again this is intuitive; when the enhancement intensity increases the transmission probability also increases within those that ADE affects, and therefore the proportion of the population infected with serotype 1 increases.

As the enhancement intensity χ increases the dynamics of the system change. When $\chi = 2$ (low levels of enhancement) the system is stable for all enhancement prevalences. However, as χ is increased the system becomes unstable and exhibits chaotic dynamics when the enhancement prevalence (ρ) is large. As ρ decreases this is replaced by periodic oscillations which then return to a stable endemic equilibrium. We can see that as χ increases the point of the Hopf bifurcation where the system changes from stable to periodic behaviour decreases. This means that the chaotic behaviour occurs for smaller enhancement prevalences. This behaviour can be seen for both of the different levels of cross–protection in Figure 2-5.

Figure 2-5(b) shows that there is qualitatively similar behaviour as ρ and χ are varied when $\eta = 0$. Note that in this case for the proportion of the population that do not suffer an enhanced secondary infection there is no effect on transmission. Whilst qualitatively the behaviour is the same as in figure 2-5(a), quantitatively there is a difference. As the cross–protection decreases (η increases) for a given enhancement intensity the chaotic behaviour occurs for lower enhancement prevalences. For example when $\eta = 1$ and $\chi = 5$ the Hopf bifurcation occurs when $0.7 < \rho < 0.8$ and when $\eta = 0$

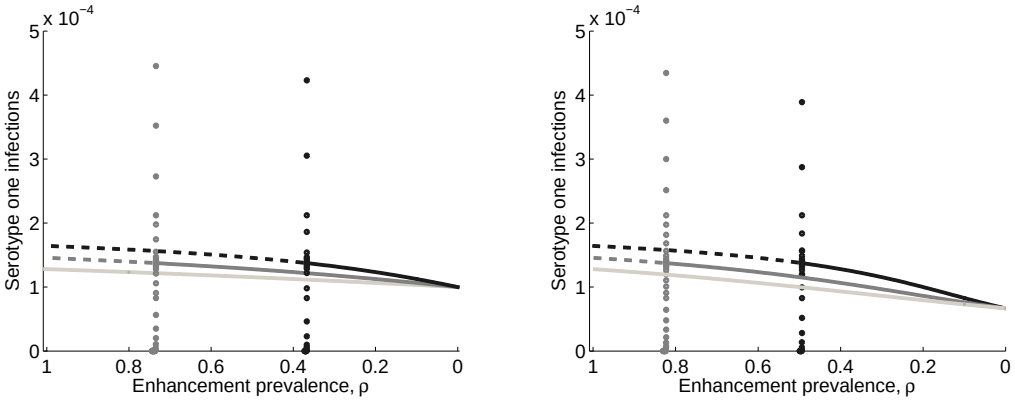

Figure 2-5: Bifurcation diagrams for the two serotype SIR model with enhancement and cross–protection acting on transmission. The graphs show the proportion of individuals infected with serotype 1 ($I_1 + I^E_{2,1} + I^P_{2,1}$) at equilibrium as the enhancement prevalence is varied. In (a) $\eta = 1$; those who do not suffer an enhanced secondary infection have the same transmissibility as those with a primary infection. In (b) $\eta = 0$; those who do not suffer an enhanced secondary infection have complete protection. In both graphs the enhancement intensity is increased, showing $\chi = 2$ (light grey), $\chi = 3$ (dark grey) and $\chi = 5$ (black). All other parameters are given in Table 2.1.

between $0.8 < \eta < 0.9$.

We are also interested in the dynamical changes to the system as the enhancement intensity is varied. Figure 2-5 shows us that for low enhancement prevalences the system remains stable as the enhancement intensity increases. For larger enhancement prevalences, where chaotic behaviour can occur, it is interesting to understand the range of enhancement intensity parameters for which the oscillations start. To do this we consider two-parameter bifurcation diagrams where both the enhancement intensity and the enhancement prevalence are varied.

Figure 2-6(a) shows the two parameter bifurcation diagram as the enhancement prevalence (ρ) and the enhancement intensity (χ) are varied. Therefore it is showing the location of the Hopf bifurcation in the (ρ, χ) parameter space. We can see that as the degree of cross–protection decreases (η increases, line colours become lighter) that the position of the Hopf bifurcation decreases with respect to both enhancement prevalence and enhancement intensity. Above the lines there is unstable behaviour while below the lines the endemic equilibrium is stable. This means that as the cross–protection increases a lower enhancement intensity is required for chaotic dynamics to start. This behaviour occurs because when $\eta = 1$ there is a larger force of infection and this drives the oscillations at lower enhancement prevalences.

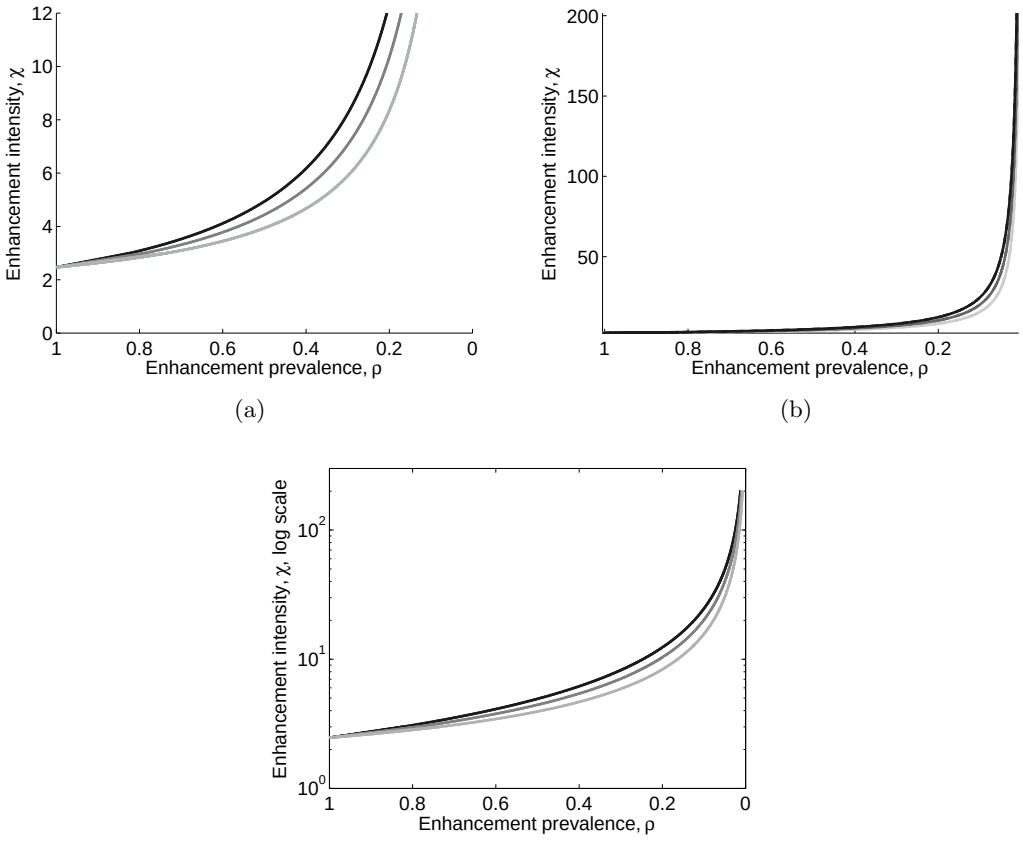

Figure 2-6: Two parameter bifurcation diagrams showing the point of the Hopf bifurcation for the two serotype SIR model with enhancement and cross–protection acting on transmission. In (a) the focus is on smaller enhancement intensities whilst (b) shows the rapid increase in enhancement intensities needed as the enhancement prevalence decreases. (c) Shows the increase on a log scale. In all graphs the cross–protection is varied from $\eta = 0$ (black) to $\eta = 0.5$ (dark grey) to $\eta = 1$ (light grey). All other parameters are given in Table 2.1.

Figure 2-6(b) shows the bifurcation diagram for smaller enhancement prevalences. As the enhancement prevalence decreases, the enhancement intensity needed for oscillations to occur increases rapidly. The rapid increase leads to potentially unrealistic levels of enhancement intensities for small enhancement parameters. This is further exemplified by the log plot (figure 2-6(c)) where there is still not a linear relationship between the enhancement prevalence and the enhancement intensity. We can also see that for small enhancement prevalences, the level of cross–protection acting on the model has little effect on the position of the Hopf bifurcation.

2.2.5 Summary

The results show there are a range of dynamic behaviours that can be seen as the enhancement prevalence, enhancement intensity and cross–protection parameters are varied. Our new framework shows that oscillations will only occur if either the enhancement intensity is very high or if the enhancement prevalence is large. When including ADE in a model, through either increased infectivity or increased susceptibility, there are varied estimates used. However, to obtain oscillatory behaviour in this model the effect of ADE needs to be much higher than those seen in other literature. It is also thought that whilst secondary infections are seen, not all of these cause DHF, and many individuals with secondary infections have the same symptoms as a primary infection. This would also indicate that the value of ρ needed to obtain oscillatory behaviour that can be seen in empirical data is also too high in this model; in these cases an endemic equilibrium is found. Therefore the combination of a low enhancement prevalence and a high enhancement intensity to obtain oscillatory dynamics is unlikely. Overall this indicates that ADE alone is unlikely to drive the oscillations that are seen in data for dengue. What is needed to drive this may be the period of temporary cross–immunity which occurs after a primary infection, which we consider in Section 2.3.

2.3 Model II: Two serotype SIR host–vector model with temporary cross–immunity and ADE

2.3.1 Model IIa: Two serotype SIR host–vector model with temporary cross–immunity and ADE (Wearing and Rohani, 2006)

The model implemented in Wearing and Rohani (2006) includes temporary cross–immunity after a primary infection and ADE acting on secondary infections. The model given in the Supplementary Material is the two serotype host–vector model. For the host and vector dynamics they implement a non-standard method, where the forces of latency and infection are modelled rather than, in the case of the host, all secondary latent and active infections. As in Section 2.2 for the host model we will implement a SIR type set-up. However, we keep their notation for the vector where over-lapping compartments are allowed. Unlike Ferguson et al. (1999a), Wearing and Rohani (2006) include ADE in the model through increased susceptibility to infection. Therefore, we now incorporate ADE in this way (see changes in host equations and the force of infection). We also include a period of latency in the model, to allow the new framework to be directly comparable with that of Wearing and Rohani (2006).

Let the different serotypes be represented by subscripts $i, j = 1, 2$, $i \neq j$. The host

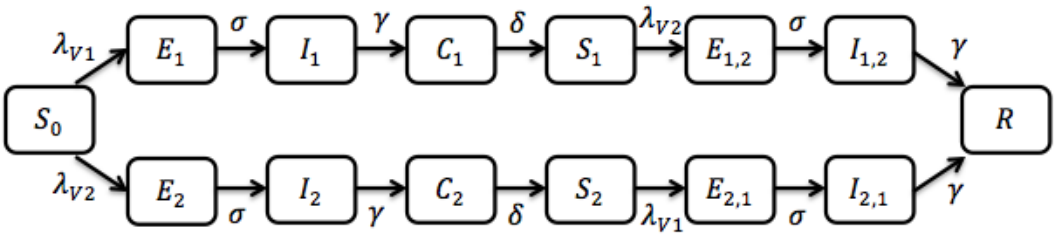

(a)

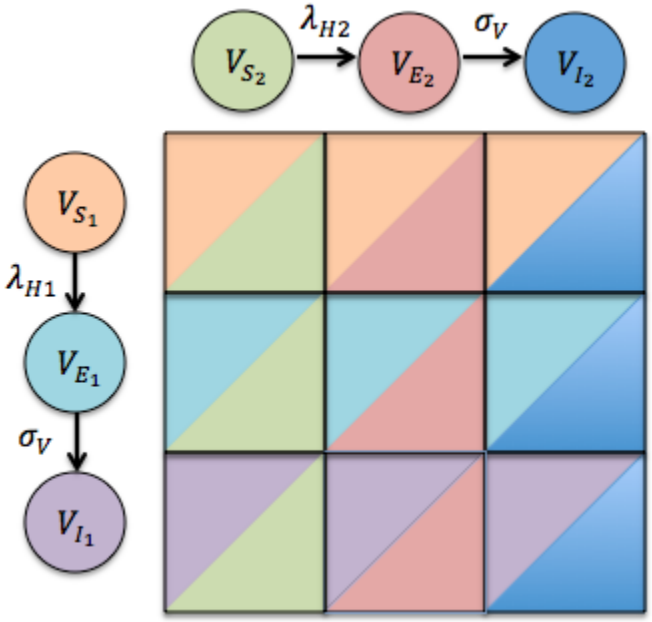

(b)

Figure 2-7: Flow diagram showing the compartmentalized Wearing and Rohani (2006) SIR host–vector model with enhancement χ acting on susceptibility of hosts. (a) The host population. (b) The vector population, formed of overlapping compartments. A vector can be in any one of nine states, where the mosquito is in one immune–status compartment for each serotype. Therefore, for example, a vector susceptible to serotype 1 is also either susceptible to, latently infected with, or actively infected with serotype two. For clarity demography has not been included in either diagram.

model is therefore shown in figure 2-7(a) with compartments representing the states susceptible to both serotypes (S_0), latent primary infection with serotype i (E_i), active primary infection with serotype i (I_i), permanent homologous immunity to serotype i and temporary cross–protection against serotype j (C_i), permanent homologous immunity to serotype i and susceptible to serotype j (S_i), latent secondary infection with serotype j ($E_{i,j}$), active secondary infection with serotype j ($I_{i,j}$) and recovered from

both serotypes (R). The model equations for the host population are therefore

$$\frac{\mathrm{d}S_0}{\mathrm{d}t} = (N_H - S_0)\mu - (\lambda_{V1} + \lambda_{V2})\frac{S_0}{N_H}, \tag{2.13a}$$
$$\frac{\mathrm{d}E_i}{\mathrm{d}t} = \lambda_{Vi}\frac{S_0}{N_H} - (\sigma + \mu)E_i, \tag{2.13b}$$
$$\frac{\mathrm{d}I_i}{\mathrm{d}t} = \sigma E_i - (\gamma + \mu)I_i, \tag{2.13c}$$
$$\frac{\mathrm{d}C_i}{\mathrm{d}t} = \gamma I_i - (\delta + \mu)C_i, \tag{2.13d}$$
$$\frac{\mathrm{d}S_i}{\mathrm{d}t} = \delta C_i - \chi\lambda_{Vj}\frac{S_i}{N_H} - \mu S_H, \tag{2.13e}$$
$$\frac{\mathrm{d}E_{i,j}}{\mathrm{d}t} = \chi\lambda_{Vj}\frac{S_i}{N_H} - (\sigma + \mu)E_{i,j}, \tag{2.13f}$$
$$\frac{\mathrm{d}I_{i,j}}{\mathrm{d}t} = \sigma E_{i,j} - (\gamma + \mu)I_{i,j}, \tag{2.13g}$$
$$\frac{\mathrm{d}R}{\mathrm{d}t} = \gamma \sum_{i,i\neq j} I_{i,j} - \mu R, \tag{2.13h}$$

where the natural mortality rate is μ and individuals who are susceptible to all serotypes are born at rate μN_H meaning a constant population. The force of infection of the vector acting on the host is given by $\lambda_{Vi} = bp_iV_{Ii}$ where b is the biting rate of mosquitoes, p_i is the probability that a bite results in infection, and V_{Ii} is the total number of vectors infected with serotype i. Assuming that $p_i = p \ \forall \ i$ this reduces to $\lambda_{Vi} = \beta V_{Ii}$, where β is the probability of infection given a bite by an infectious mosquito. We assume this to be equal for all serotypes. The average length of the latent period is $1/\sigma$, the average length of the active infectious period is $1/\gamma$ and the average length of time with temporary cross–immunity is $1/\delta$.

In Wearing and Rohani (2006) parameters are included which allow for asymmetry in virulence of the different serotypes, therefore incorporating disease induced mortality. We assume that asymmetry in virulence is the same for both serotypes, and that this is equal to zero; therefore this is not included in the model equations. As stated previously we assume that ADE acts to increase susceptibility to infections, modelled by the parameter χ ($\chi > 1$), and is the same for all serotypes.

Alongside the host dynamics we need the vector dynamics, shown in figure 2-7(b). The model allows for seasonality in the vector population and, unlike the host population, does not allow for recovery after infection. For the vector we implement a system of differential equations which includes susceptible vectors and defines the dynamics of the forces of latency and infection as given in Wearing and Rohani (2006). This is for

two reasons; firstly unlike the host the vector can acquire multiple infections making this model easier to track. In Thailand which is where the data in Wearing and Rohani (2006) is from, it has been shown that mosquitoes can have multipled infections (Thavara et al., 2006). Secondly, the ADE parameters only act on the host population meaning that we are able to easily work with the overlapping model. This means the states the vector population can take are susceptible to serotype i (V_{S_i}), and we also mode the dynamics of the force of latency (ϵ_{Vi}) and the force of infection (λ_{Vi}). Therefore the model equations for the vector population are

$$\frac{\mathrm{d}V_{S_i}}{\mathrm{d}t} = (kN_H(1 - a\cos(2\pi t)) - V_{S_i})\,\mu_V - \lambda_{Hi}\frac{V_{S_i}}{N_H}, \tag{2.14a}$$

$$\frac{\mathrm{d}\epsilon_{Vi}}{\mathrm{d}t} = \lambda_{Hi}\frac{V_{S_i}}{N_H} - (\sigma_V + \mu_V)\epsilon_{Vi}, \tag{2.14b}$$

$$\frac{\mathrm{d}\lambda_{Vi}}{\mathrm{d}t} = \beta_i\sigma_V\epsilon_{Vi} - \mu_V\lambda_{Vi}, \tag{2.14c}$$

where the natural mortality rate of the mosquito is μ_V and k is the average number of female mosquitoes per person. If $a = 0$ there is no seasonality in the model and the vector population is constant over time. The average length of time a vector is latently infected is $1/\sigma_V$. The force of infection exerted by the host on the vector is given by $\lambda_{Hi} = bq_iH_{Ii}$ where b is the biting rate of mosquitoes, q_i is the probability that a bite results in infection, and H_{Ii} is the total number of hosts infected with serotype i. Assuming that $q_i = q\ \forall\ i$ this reduces to $\lambda_{Hi} = \beta H_{Ii}$, where β is the probability of infection given a bite by an infectious mosquito. We assume that the transmission probability is the same for host to vector transmission as vector to host transmission (Wearing and Rohani, 2006; Newton and Reiter, 1992). In equation (2.14) the force of infection is divided by the total host population to give the proportion of bites on infected hosts. In Wearing and Rohani (2006) the force of infection is found explicitly using the host equations. As the model has been written in a different form it is not possible to directly use λ_{Hi} in the same way. We therefore need to define H_{Ii}, which can easily be found from the compartments already introduced. As stated, H_{Ii} is the total number of individuals infected with serotype i. Therefore

$$H_{Ii} = I_i + I_{j,i}, \tag{2.15}$$

which we can use in equations (2.14) for the vector dynamics. All parameter values used in modelling for the host and vector are given in Table 2.2.

Parameter	Definition	Value
Host		
N_H	Host population size	10^6
μ	Host mortality rate	0.02
σ	Latency rate	73
γ	Recovery rate	60.8
β	Transmission rate	70
χ	Enhancement intensity	
η	Cross–protection	
ρ	Enhancement prevalence	
Vector		
k	Average number female vectors per host	2
μ_V	Vector mortality rate	26.1
σ_V	Vector latency rate	36.5
a	Seasonality	0.05

Table 2.2: Parameter definitions and values used where kept constant for Models IIa and IIb. All rates are given per year.

2.3.2 Model IIb: Two serotype SIR host–vector model with ADE, temporary cross–immunity and partial cross–enhancement

We now implement our new framework into the Wearing and Rohani (2006) model, where the host equation framework is shown in figure 2-8. The state variables are similar to in Model Ic, however it is after the period of temporary cross–immunity following a primary infection that individuals enter either the permanent homologous immunity to serotype i and susceptible to serotype j with a predisposition to an enhanced secondary infection (S_i^E) or the permanent homologous immunity to serotype i and susceptible to serotype j without a predisposition to an enhanced secondary infection (S_i^P). These splits carry through to the latent secondary infection with serotype j ($E_{i,j}^E, E_{i,j}^P$) and active secondary infection with serotype j ($I_{i,j}^E, I_{i,j}^P$) compartments. Therefore the model equations for the host population are

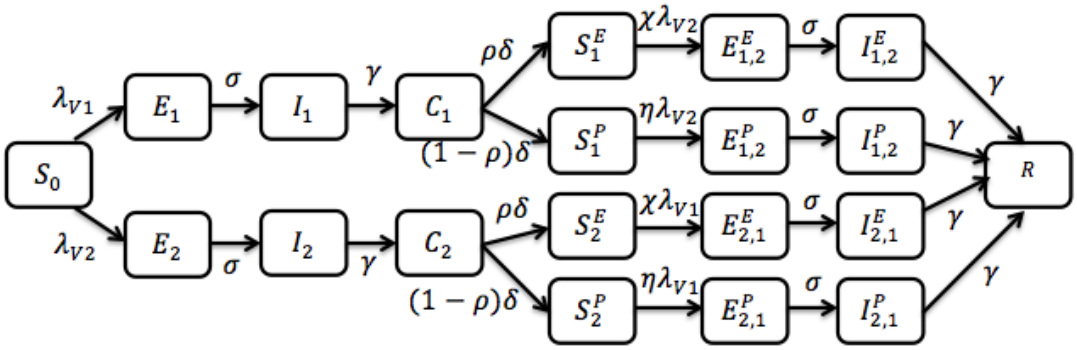

Figure 2-8: Flow diagram showing our new framework in the host population acting on the compartmentalized Wearing and Rohani (2006) SIR host–vector model. Enhancement intensity χ acts on susceptibility of the ρ proportion of the population with an enhanced secondary infection and cross–protection η acts on susceptibility of the other $(1-\rho)$ proportion. For clarity demography has not been included.

$$\frac{\mathrm{d}S_0}{\mathrm{d}t} = (N_H-\mu)S_0 - (\lambda_{V_1}+\lambda_{V_2})\frac{S_0}{N_H}, \tag{2.16a}$$

$$\frac{\mathrm{d}E_i}{\mathrm{d}t} = \lambda_{V_i}\frac{S_0}{N} - (\sigma+\mu)E_i, \tag{2.16b}$$

$$\frac{\mathrm{d}I_i}{\mathrm{d}t} = \sigma E_i - (\gamma+\mu)I_i, \tag{2.16c}$$

$$\frac{\mathrm{d}C_i}{\mathrm{d}t} = \gamma I_i - (\delta+\mu)C_i, \tag{2.16d}$$

$$\frac{\mathrm{d}S_i^E}{\mathrm{d}t} = \rho\delta C_i - \chi\lambda_{V_j}\frac{S_i^E}{N} - \mu S_i^E, \tag{2.16e}$$

$$\frac{\mathrm{d}S_i^P}{\mathrm{d}t} = (1-\rho)\delta C_i - \eta\lambda_{V_j}\frac{S_i^P}{N} - \mu S_i^P, \tag{2.16f}$$

$$\frac{\mathrm{d}E_{i,j}^E}{\mathrm{d}t} = \chi\lambda_{V_i}\frac{S_j^E}{N} - (\sigma+\mu)E_{i,j}^E, \tag{2.16g}$$

$$\frac{\mathrm{d}E_{i,j}^P}{\mathrm{d}t} = \eta\lambda_{V_i}\frac{S_j^P}{N} - (\sigma+\mu)E_{i,j}^P, \tag{2.16h}$$

$$\frac{\mathrm{d}I_{i,j}^E}{\mathrm{d}t} = \sigma E_{i,j}^E - (\gamma+\mu)I_{i,j}^E, \tag{2.16i}$$

$$\frac{\mathrm{d}I_{i,j}^P}{\mathrm{d}t} = \sigma E_{i,j}^P - (\gamma+\mu)I_{i,j}^P, \tag{2.16j}$$

$$\frac{\mathrm{d}R}{\mathrm{d}t} = \sigma(I_{2,1}^E + I_{2,1}^P + I_{1,2}^E + I_{1,2}^P) - \mu R. \tag{2.16k}$$

The two serotype model for the vector population is identical to that of Model IIa (equation (2.14)) with

$$H_{Ii} = I_i + I^E_{j,i} + I^P_{j,i}. \tag{2.17}$$

All parameters in the model have the same meaning as in Wearing and Rohani (2006), given in Table 2.2. As in Section 2.2.3 ρ is the enhancement prevalence, χ is the enhancement intensity (the strength of ADE), and η is the cross–protection for the $(1-\rho)$ proportion of the population that do not suffer an enhanced infection.

The models applying the new framework based on Wearing and Rohani (2006) (Model IIb) and Ferguson et al. (1999a) (Model Ic) are different for a number of reasons. Firstly the base model itself is extended and now includes a period of temporary cross–immunity after a primary infection. Secondly, ADE is included in the model through increased susceptibility to infection rather than through increased transmission. This is due to the differences in the base models which we are comparing the new frameworks to. Finally, due to the model now including temporary cross–immunity, rather than the separation of compartments due to only a proportion of the population suffering an enhanced secondary infection occurring immediately after a primary infection, it occurs after the period of temporary cross–immunity. From the literature previously studied the split in the model comes after the period of temporary cross–immunity, as we believe there to be a predisposition as to whether an individual suffers an enhanced secondary infection. The model has been kept as similar to that of Wearing and Rohani (2006) in all other aspects so that comparisons between the models can be made as accurately as possible.

2.3.3 Results

The results that we wish to compare with Wearing and Rohani (2006) are those where both the length of temporary cross–immunity and the enhancement intensity of secondary infections (the strength of ADE) are varied to determine the effect on the dominant period of any multi–annual oscillations. We also have two new variables which can be changed; the enhancement prevalence (ρ) and the cross–protection (η). We therefore wish to understand how the parameters from our new framework can affect the dynamics of the system.

As in Section 2.2.3 if $\rho = 1$ then all secondary infections are enhanced, η is irrelevant and in this case the model reduces to that of Wearing and Rohani (2006). If $\rho = 0$ then no secondary infections are enhanced, χ is irrelevant and the model

reduces to that of Wearing and Rohani (2006) where η in our model framework (equations (2.16)) equals χ in the original model (equations (2.13)). This can be seen more clearly in figure 2-9 where $\rho = 1$. The whole population suffers an enhanced secondary infection and figures 2-9(b) and (d) resemble those presented in Wearing and Rohani (2006). Figure 2-9(a) shows the time series of the host population of those infected with serotype 1 ($I_1 + I^E_{2,1} + I^P_{2,1}$) under a moderate enhancement intensity ($\chi = 2$). When temporary cross–immunity lasts for a short period of time (5 weeks) there are annual oscillations. However, as the length of temporary cross–immunity increases (15 weeks) so too do the period of the multi–annual oscillations, showing a dominant period of 7.4 years. We see that as the period of temporary cross–immunity increases further to 22 weeks the dynamics can change and there can be multi–annual oscillations which occur more frequently (dominant period 4 years). Figure 2-9(b) shows the generalities of these findings for a single serotype as the duration of temporary cross–immunity and the enhancement intensity are varied. We see that for short periods of temporary cross–immunity there are annual oscillations, however as the enhancement intensity increases there are 'enhancement–induced' oscillations. As the period of temporary cross–immunity increases to between around 8-15 weeks we start to see multi–annual oscillations of around 6–8 years. Increasing the length of cross–immunity further can cause the system to show differences in the dominant period of the oscillations as the enhancement intensity increases, where for a single serotype the multi–annual oscillations range between 4–10 years. For durations of cross–immunity lasting between 6–15 weeks we see, in general, that increasing the enhancement intensity serves to decrease the period of the multi–annual oscillations.

Figures 2-9(c) and (d) show similar results for the aggregate dynamics. Figure 2-9(c) shows the time series for three durations of temporary cross–immunity. Whilst increasing the duration of cross–immunity affects the periodicity, the change in dominant period is not as great as for the single serotype; for 5 weeks there are annual oscillations, for 15 weeks the dominant period is 3.6 years and for 22 weeks the dominant period is 4 years. This is generalized in figure 2-9(d), where there is smoother gradation on the changes in the duration of the dominant period than for the single serotype. As in the case of the single serotype there are annual oscillations when the duration of temporary cross–immunity is short which can give rise to 'enhancement–induced' oscillations as the enhancement intensity increases. As the duration of temporary cross–immunity increases the multi–annual oscillations that occur for the aggregate dynamics are shorter than those of the single serotype, with periods of 2–5 years for a wide range of parameters in the enhancement intensity–duration of cross–immunity parameter space.

Figure 2-10 shows the time series of individuals infected with serotype 1 for given

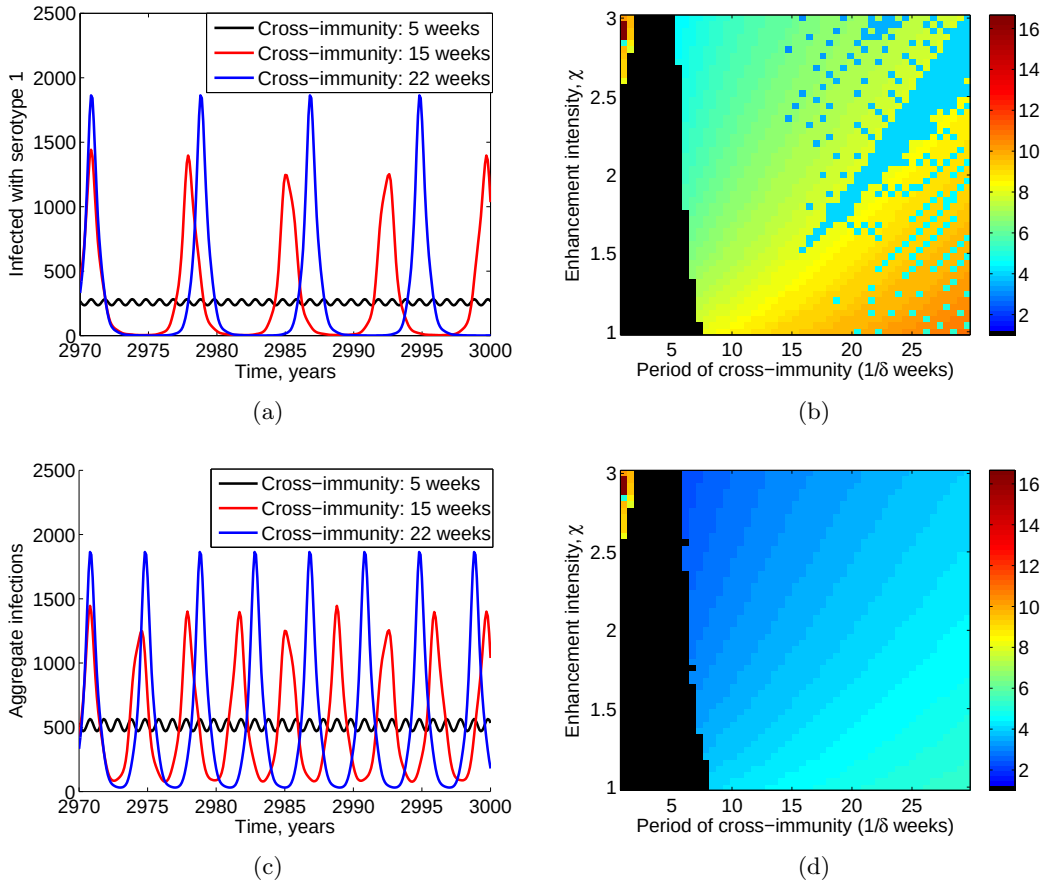

Figure 2-9: (a) Time series showing the total number of hosts infected with serotype 1 when the length of cross–immunity is 5 weeks (black line), 15 weeks (red line) and 22 weeks (blue line) when the enhancement intensity is $\chi = 2$. (b) The dominant period in serotype 1 dynamics for increasing enhancement intensity (χ) and period of temporary cross–immunity (δ). (c) Time series showing the aggregate infections when the length of cross–immunity is 5 weeks (black line), 15 weeks (red line) and 22 weeks (blue line) when the enhancement intensity is $\chi = 2$. (d) The dominant period in the aggregate dynamics for increasing enhancement intensity (χ) and period of temporary cross–immunity (δ). All parameters are given in Table 2.2 with $\rho = 1$. This means the model is the same as Wearing and Rohani (2006) where η can take any value.

enhancement intensity $\chi = 2$ as the level of cross–protection is varied (different colours) and the enhancement prevalence is decreased (different subfigures). If we decrease the enhancement prevalence from $\rho = 1$ (Wearing and Rohani (2006) model) to $\rho = 0.75$ this means that 75% of the population are predisposed to an enhanced secondary infection. Figure 2-10(a) shows the time series after any transient behaviour has settled. We see that as the value of η increases (cross–protection decreases) the number of individu-

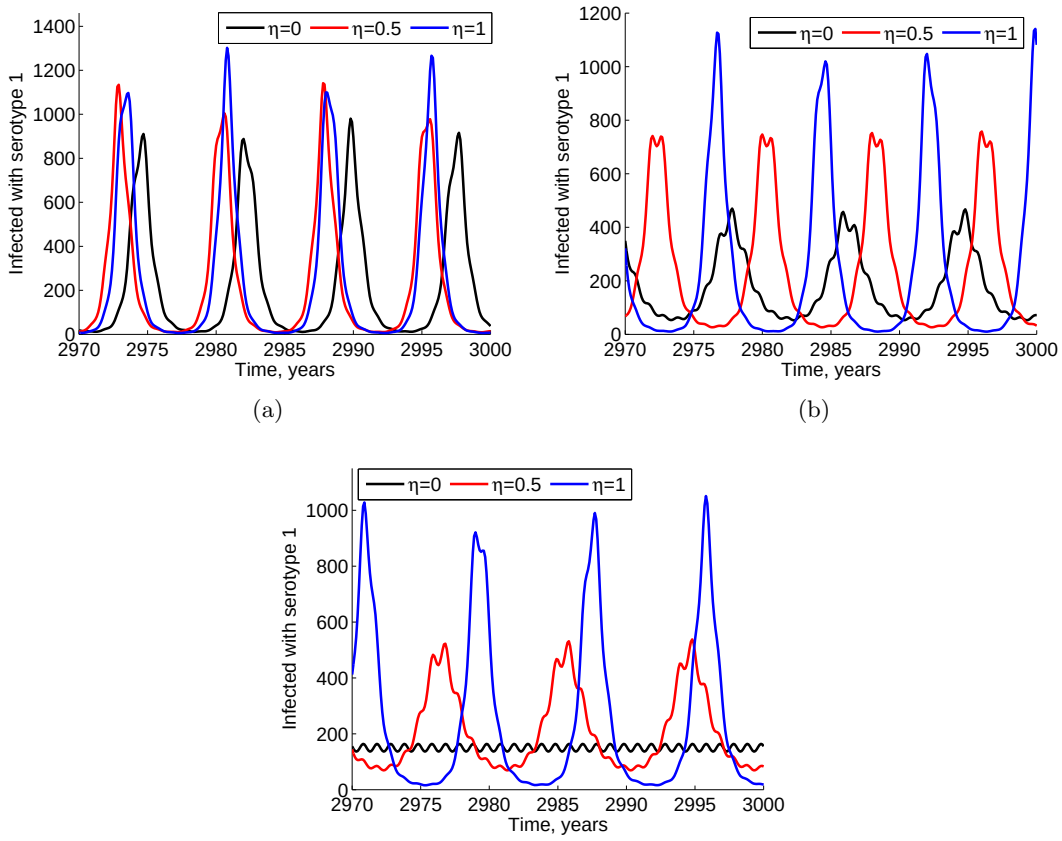

Figure 2-10: Time series showing the total number of hosts infected with serotype 1. In (a) the enhancement prevalence is $\rho = 0.75$, in (b) the enhancement prevalence is $\rho = 0.5$ and in (c) the enhancement prevalence is $\rho = 0.25$. In all graphs the cross–protection levels are $\eta = 0$ (black line), $\eta = 0.5$ (red line) and $\eta = 1$ (blue line), the duration of cross–immunity is 15 weeks and the enhancement intensity is $\chi = 2$. All other parameters are given in Table 2.2.

als infected with serotype 1 increases slightly. This is to be expected; if cross–protection is decreasing then a greater number of individuals can become infected. We also see that the increase in cross–protection has little effect on the period of the oscillations, with all time series showing oscillations of around 7-8 years. Decreasing the enhancement prevalence further ($\rho = 0.5$, figure 2-10(b)) shows a greater change in the number of individuals infected with serotype 1 as the level of cross–protection decreases. This is again to be expected; a lower enhancement prevalence means a greater proportion of the population experience secondary infections which cross–protection acts on. Therefore this parameter becomes more important in the model. Decreasing the cross–protection (increasing η) again has little effect on the period of the multi–annual oscillations, which

is 8–9 years. However, it is worth noting that the period is slightly longer than when the enhancement prevalence was higher. Finally, figure 2-10(c) shows the time series when only 25% of the population suffer an enhanced secondary infection. In this case if an individual with a non-enhanced secondary infection has complete immunity ($\eta = 0$) there are annual dynamics. Decreasing cross–protection then causes an increase in the period, to between 8–10 years.

The time series show that if the enhancement prevalence is large enough, for a given enhancement intensity and duration of cross–protection if the system exhibits multi–annual oscillations then varying the level of cross–protection has little effect on the period of the oscillations (figures 2-10(a) and (b)). However, as the enhancement prevalence decreases the period of the multi–annual oscillations increases as the cross–protection decreases (figure 2-10(c)). We can consider the generalities of these findings by finding the dominant period in oscillation as the enhancement intensity and the duration of cross–immunity are increased, shown in figure 2-11.

Initially 75% of the population suffer an enhanced secondary infection ($\rho = 0.75$, figures 2-11(a), (b) and (c)). The dynamics are similar to when the whole population suffers an enhanced secondary infection, where for short durations of temporary cross–immunity there are annual oscillations. As the duration of temporary cross–immunity increases multi-annual oscillations can then be seen, which in general last between 6–10 years. Further increases can cause more differences in the period as the enhancement intensity increases, with oscillations ranging from 4–10 years. When all secondary infections were subject to enhancement ($\rho = 1$) for short durations of temporary cross–immunity and high enhancement intensities there were 'enhancement–induced' oscillations. However, decreasing the enhancement prevalence causes these to no longer be seen for the parameter range studied here. Decreasing the level of cross–protection (increasing η, moving through figures 2-11(a) to (c)) shows that a lower duration of cross–immunity is needed for mutli-annual oscillations to be seen. The lower level of cross–protection also enables greater variation in the periodicity of the multi–annual oscillations for longer durations of temporary cross–immunity and enhancement intensities. Figures 2-11(d)–(f) and (g)–(i) show similar qualitative behaviours when the enhancement prevalence is set to $\rho = 0.5$ and $\rho = 0.25$ respectively.

It is interesting to note what happens for a given level of cross–protection as the enhancement prevalence is decreased, and less people suffer an enhanced secondary infection. When those who do not suffer an enhanced secondary infection have complete immunity ($\eta = 0$, figures 2-11(a), (d) and (g)) as the enhancement prevalence is decreased the system exhibits annual oscillations for a greater range of durations of cross–immunity and enhancement intensities. When only 25% of the population suffer

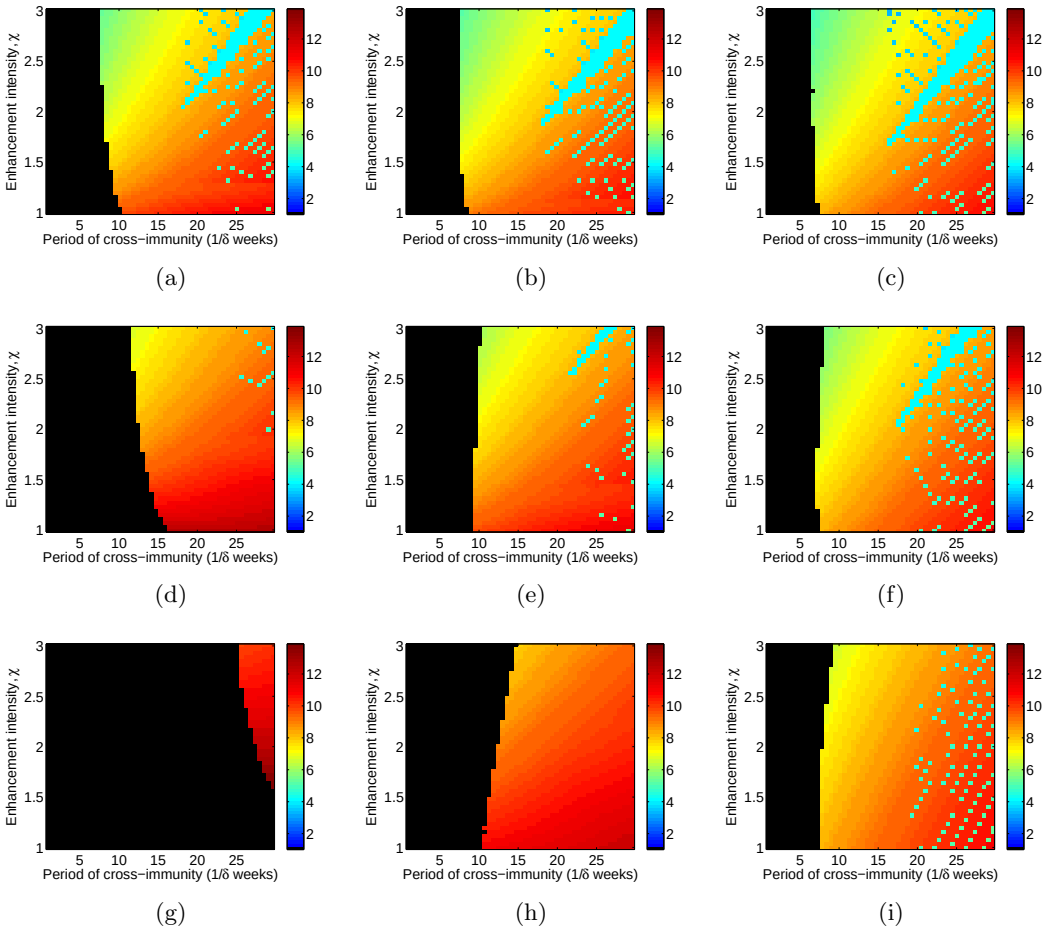

Figure 2-11: The dominant period of a single serotype for the two serotype SIR type model for increasing enhancement intensity and duration of temporary cross-immunity. In (a), (b) and (c) $\rho = 0.75$, in (d), (e) and (f) $\rho = 0.5$, in (g), (h) and (i) $\rho = 0.25$. In (a), (d) and (g) $\eta = 0$, in (b), (c) and (h) $\eta = 0.5$ and in (c), (f) and (i) $\eta = 1$. All other parameters are given in Table 2.2.

an enhanced secondary infection (figure 2-11(g)) multi-annual oscillations can only be seen for long durations of cross–immunity and high enhancement intensities. We see that as the cross–protection decreases (figure 2-11(h)) this behaviour is not seen to the same extent, and multi–annual oscillations are seen for a much greater range of durations of temporary cross–protection. It is also interesting to note that under the new model framework there are longer mutli-annual oscillations, up to 12 years, than for the initial model implemented (compare figure 2-9 with figure 2-11).

In figure 2-11(g) where there is a low enhancement prevalence and high cross–protection there are different dynamics to the rest of the parameter combinations that we have shown. The annual oscillations occur for a far greater range of parameters

in the enhancement prevalence–enhancement intensity parameter space. Figure 2-12 looks at this in more detail, showing the transitionary period between this behaviour and the more 'standard' behaviour by considering cross–protection of between $\eta = 0.1$ and $\eta = 0.2$.

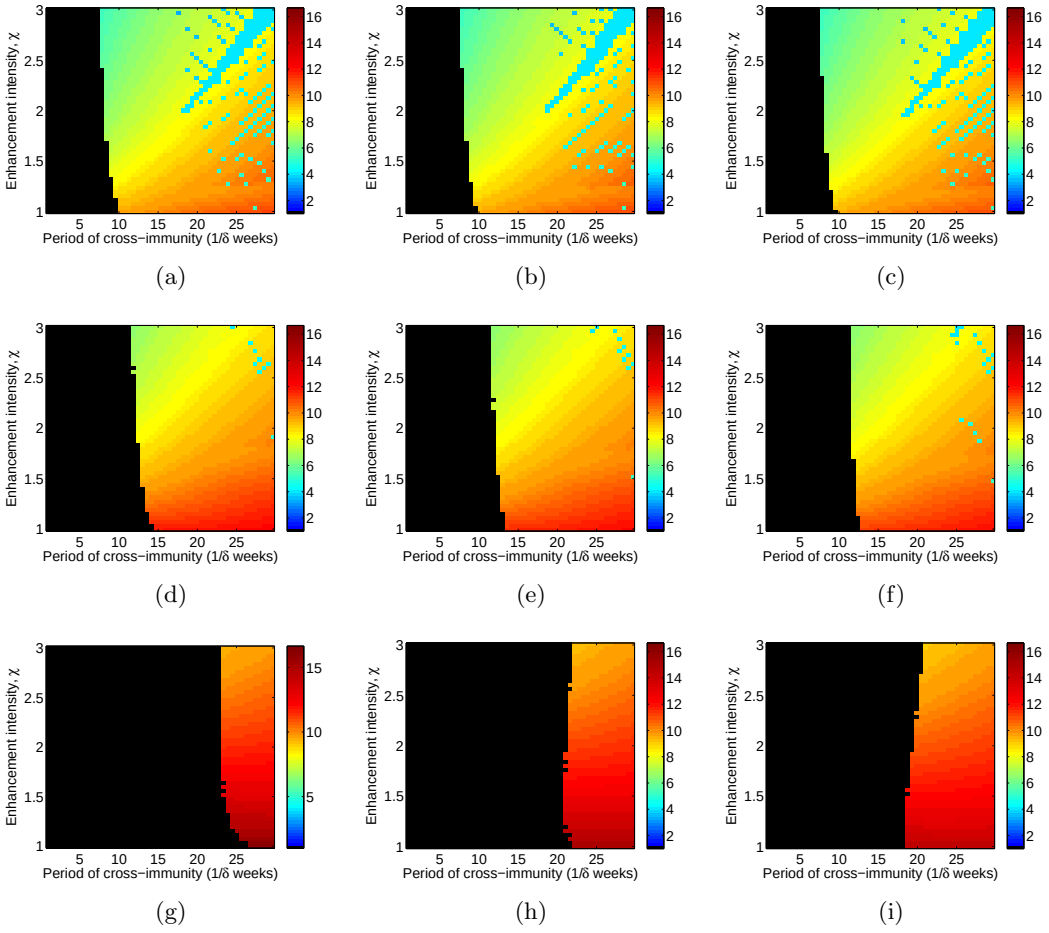

Figure 2-12: The dominant period of a single serotype for the two serotype SIR type model for increasing enhancement intensity and duration of temporary cross-immunity. In (a), (b) and (c) $\rho = 0.75$, in (d), (e) and (f) $\rho = 0.5$, in (g), (h) and (i) $\rho = 0.25$. In (a), (d) and (g) $\eta = 0.1$, in (b), (c) and (h) $\eta = 0.15$ and in (c), (f) and (i) $\eta = 0.2$. All other parameters are given in Table 2.2.

When $\rho = 0.75$ (figures 2-12 (a)–(c)) the behaviour for all cross–protection parameters is similar to that seen for the larger cross–protection values. Small durations of partial immunity lead to annual oscillations, which give rise to multi–annual oscillations as the duration of partial immunity increases. However, as the enhancement prevalence decreases the dynamics of the system changes for small values of η (high cross–protection). When $\rho = 0.5$ for low enhancement intensities there is a greater area

where annual oscillations can be seen (figure 2-12 (d)) and the changes in period of multi–annual oscillations for longer durations of partial immunity are rarely seen. This is again true for all the cross–protection values (figures 2-12 (d)–(f)). Decreasing the enhancement prevalence further to $\rho = 0.25$ shows the change in dynamics (figures 2-12 (g)–(l)). Only a very small subset of parameter combinations produce multi–annual oscillations, needing both a long duration of cross–immunity and high enhancement intensity for them to be produced. Decreasing cross–protection (increasing η) increases the parameter range where multi–annual oscillations occur.

We also consider the aggregate dynamics. We would expect the results to be similar to those seen for the single serotype, but with a different periodicity. Figure 2-13 shows this to be the case; in general multi-annual oscillations last between 4–6 years if there are not annual dynamics. It is interesting to note that the differences in period of multi–annual oscillations that can be seen in the single serotype dynamics for large durations of cross–immunity are not seen as readily in the aggregate dynamics. This is due to the interaction of the two serotypes.

It is noteworthy that for both the single serotype and aggregate dynamics for some combinations of enhancement prevalence and duration of cross–immunity the direction of slope where the annual dynamics change to multi–annual oscillations changes (e.g. figures 2-13(g)–(i)). We have found no immediate cause for this, however a high cross–protection (low η) appears to facilitate this change. As this was not the focus of this research and the number of interactions in the model is great, we have not focussed on this. However, if looking in more detail at the interactions within the model, this is an area which would be interesting to consider.

2.3.4 Summary

The results show that for some parameter combinations the multi–annual cycles that can be seen are similar to those found under the more traditional framework. However, the inclusion of the enhancement prevalence and cross–protection parameters do interact with the enhancement intensity and duration of cross–immunity. This shows that the new framework provides an alternative approach to modelling dengue which shows a greater range of dynamics than previous models. Data show that only a small proportion of the population have an enhanced secondary infection. For the single serotype dynamics using a lower value of ρ sees less jumps in the lengths of period in the simulations. However, for some values of ρ there needs to be low cross–protection (high η) to ensure multi–annual oscillations for a range of enhancement intensities and durations of cross–immunity. A low cross–protection value is likely; serological testing regularly shows secondary infections, many of which are not not enhanced (Sabchareon

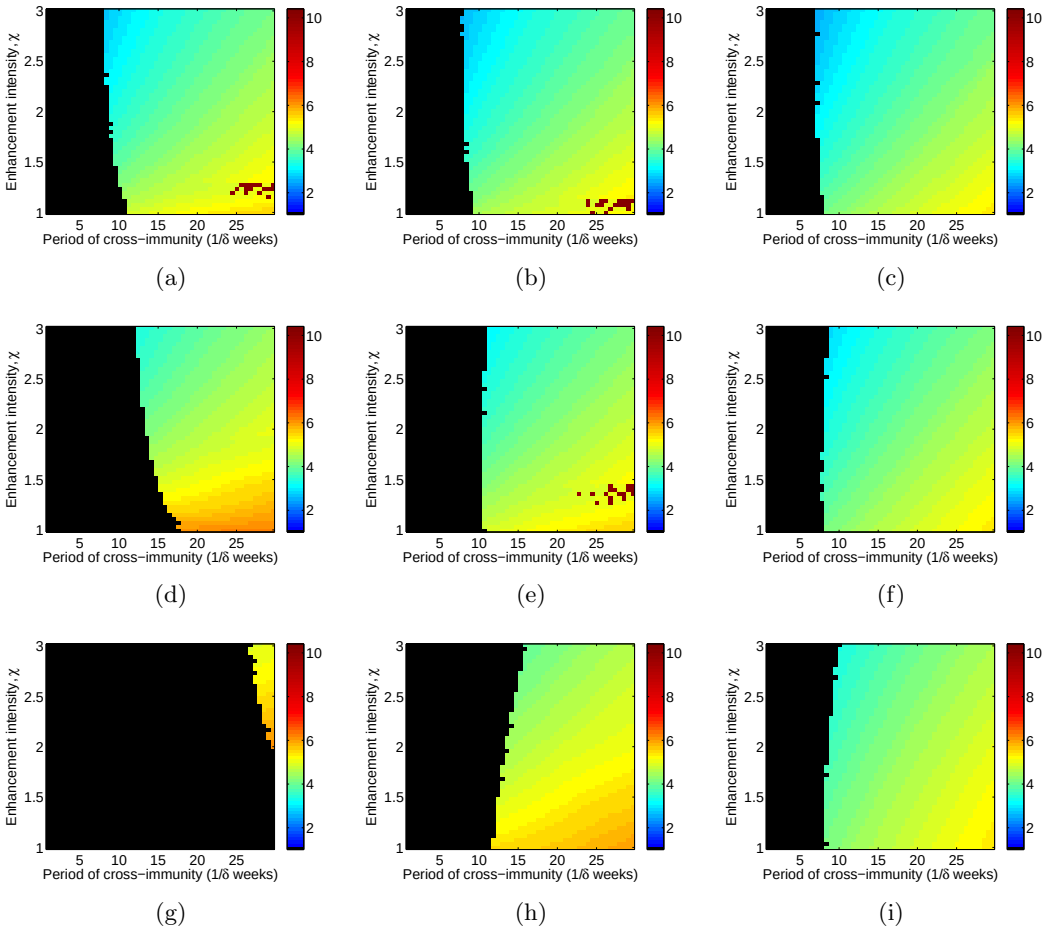

Figure 2-13: The dominant period of the aggregate dynamics for the two serotype SIR type model for increasing enhancement intensity and duration of temporary cross-immunity. In (a), (b) and (c) $\rho = 0.75$, in (d), (e) and (f) $\rho = 0.5$, in (g), (h) and (i) $\rho = 0.25$. In (a), (d) and (g) $\eta = 0$, in (b), (c) and (h) $\eta = 0.5$ and in (c), (f) and (i) $\eta = 1$. All other parameters are given in Table 2.2.

et al., 2012). This means it is likely that the cross–protection is not complete.

2.4 Discussion

Conventional two–serotype SIR type models for dengue may include periods of temporary cross–immunity (Wearing and Rohani, 2006; Aguiar et al., 2011b) and/or mechanisms such as antibody–dependent enhancement (ADE) (Ferguson et al., 1999a; Recker et al., 2009). After recovery from a primary infection these models assume that the whole population is subject to an enhanced secondary infection. However, we have reviewed literature which suggests that not all secondary infections are enhanced. We

have therefore presented a new framework which accounts for this, and compared the results of existing models to our new framework.

Standard two–serotype SIR models which implement enhancement on secondary infections (e.g. Ferguson et al. (1999a)) show that a small amount of enhancement acting on the transmission term can cause oscillatory dynamics. Our new framework has shown that splitting the population into those who suffer an enhanced secondary infection and those that do not affects the point at which the multi-annual oscillations start. For multi–annual oscillations to occur there needs to be either a high proportion of the population that suffer an enhanced secondary infection, or a high enhancement intensity. This is true no matter what the level of cross–protection in the model.

The original model and new framework imply that ADE alone is not the sole driver of multi–annual oscillations that can be seen in empirical data for dengue. We therefore then examined the new framework in a model that incorporated both ADE and temporary cross–immunity. At this point, to maintain consistency with the model being tested against we changed enhancement to act on susceptibility rather than transmission. Previous work analysing enhancement of transmission and susceptibility has shown the impact on the dynamics to be similar (Ferguson and Andreasen, 2002; Adams and Boots, 2006).

In a standard two serotype SIR model which implements temporary cross–protection and ADE (e.g. Wearing and Rohani (2006)) it has been shown that a period of temporary cross–immunity to all serotypes after a primary infection can allow for multi–annual oscillations which coincide with empirical data. However, the duration of the epidemic cycle is influenced by the level of enhancement (Wearing and Rohani, 2006) or cross–protection (Aguiar et al., 2011b) that subsequently act on susceptibility to or transmission of secondary infections. By implementing our new framework and separating the population into those who suffer an enhanced secondary infection and those who do not we can see multi–annual oscillations that are driven by temporary cross–immunity. However, the strength of enhancement intensity and, perhaps more importantly, the level of cross–protection on infections that are not enhanced, can have a large impact on what enhancement prevalence the multi–annual oscillations can start. Our results help to compound the findings that temporary cross–immunity is likely to have a large influence on the period of oscillations in models. However, we also indicate there is a complex interaction between the different mechanisms which occur during the course of primary and secondary dengue infections.

This work therefore points to the fact that separating the population into those that suffer an enhanced secondary infection and those that do not affects the dynamics that can be seen. Changes to the dynamics are especially apparent if the level of

enhancement prevalence is low, which studies indicate that it may be. Therefore the implementation of this framework may prove beneficial in future modelling approaches, where the level of enhancement intensity and cross–protection are being studied.

CHAPTER 3

AGE STRUCTURED EPIDEMIOLOGICAL MODELS

Summary

In this chapter we will examine an age structured SIR partial differential equation (PDE) model which includes different functional forms of the contact rate. We wish to study the seroprevalence profiles produced by different contact rates, and determine a way to quantify the difference between them. Therefore, we initially examine different numerical schemes that can be used to solve non–linear PDEs. We then use existing literature to determine the basic reproductive number for a PDE model. We implement age–independent and age–dependent contact rates and use these to determine the probability an individual in a given age group is seroprevalent. We then use likelihood ratios to determine which of the contact rates a seroprevalence profile sampled from an age–independent contact rate is likely to have come from. We also consider which age groups are the main source and recipients of infection under the age–dependent contact rates implemented. Finally, we discuss the advantages of modelling using an age structured model and how changes in the contact rate affect the seroprevalence of infection in a population.

3.1 Introduction

In many epidemiological models age structure is not explicitly included. Contacts are assumed to be homogeneous across the population, with the law of mass action being used to model contacts between hosts. However, contacts are rarely identical between all age groups. Theory tells us that age–dependent variation in the contact rate affects the dynamics of infectious disease, whether this is the epidemic trajectory, equilibria or stability properties (Schenzle, 1984; Greenhalgh, 1987; Inaba, 1990; Anderson and May, 1991). Simulations have shown that some of these changes, for example to the epidemic trajectory, can be used to better explain the dynamics of certain childhood illnesses such as measles (Schenzle, 1984). Inclusion of age structure can also be beneficial when it is known that different ages play an important role in the dynamics of the disease, such as tuberculosis (Aparicio and Castillo-Chavez, 2009). Therefore understanding how different aged individuals affect transmission dynamics is vital.

Understanding that different age groups have varied interactions is important to be able to implement age–dependent transmission in an epidemiological model. Edmunds et al. (1997) undertook one of the first studies attempting to quantify contacts between human hosts. They sampled 92 individuals and found that the degree of mixing depended not only on age but on the number of contacts made. Since then other studies have been performed, including Mossong et al. (2008), who studied 7290 individuals over 8 countries. Their results, similar for each country, showed that contact rates are assortative with age, and that those aged between 5–19 years old are expected to suffer highest incidence at the start of an epidemic. Del Valle et al. (2007) find that children interact mostly with other children, whilst adults interact with individuals over a greater age–range. Therefore mixing patterns and the number of contacts individuals have are relevant to consider when modelling transmission of infectious diseases. The effective reproduction number, R, can also give an indication of transmission in different age groups. Glass et al. (2012) study the 2009 influenza A pandemic (H1N1) and determine that the effective reproduction numbers are different for adults and children. This indicates a difference in contact patterns for the ages. Variable mixing patterns therefore provide credibility for the use of age–dependent contact rates in epidemiological models.

Several methods for including age structure in a model have been explored. The population can be split into discrete age groups and modelled by a series of ODEs (Mello and Castilho, 2014). Individuals move through distinct age groups, as well as different immune status compartments. Examples of where this is appropriate can include grouping children by school years as individuals are generally of a similar age,

or considering high risk and low risk groups when studying transmission of sexually transmitted diseases (Keeling and Rohani, 2008). An alternative approach is to use a continuous age–time PDE model (Anderson and May, 1991; Hethcote, 2000; Thieme, 2001). The system is usually formed of hyperbolic PDEs, however these are more complex to solve than a corresponding system of ODEs with distinct age classes. PDEs have been used to study epidemics of measles (Schenzle, 1984), cholera (Alexanderian et al., 2011) and tuberculosis (Aparicio and Castillo-Chavez, 2009) among others.

Serological studies from around the world for dengue indicate the possibility of age–dependent transmission. In a cohort of schoolchildren in Nicaragua Balmaseda et al. (2006) found that the seroprevalence for DENV antibodies increased from 75% to 100% from children aged 4–16 over a two year period, indicating that children have been highly exposed to dengue. Thai et al. (2011) used age–specific seroprevalence data and a community longitudinal study and found the median age of dengue fever patients changed between primary (12 years) and secondary (20 years) infections. Braga et al. (2010) performed a population based household survey in Brazil. Whilst primarily considering different socio–economic groups for control, they found that in deprived areas the force of infection increased with age. These results suggest that inclusion of age structure in an epidemiological model for dengue may help to understand how dengue affects different age groups and the resulting seroprevalence.

Previous models involving age structure in populations for dengue have included ODE modelling. This has included structured two age–class modelling considering stability analysis (Pongsumpun and Tang, 2003) and the inclusion of vaccination (Supriatna et al., 2008). Time discrete age structure models have also been implemented (Mello and Castilho, 2014) and their analytical properties studied. This model was also used to analyse age structured data and provide an estimate for the basic reproductive number. Statistical models to fit simulations to age profiles have also been implemented for dengue (Cummings et al., 2009). Statistical analysis has also been used on PDE models (Ferguson et al., 1999b), however in the analysis of the serotype specific force of infection age structure was ignored. Cochran and Xu (2014) implement an age structured PDE model in both the host and vector population and simulate different scenarios, yielding a range of different behaviours depending on parameter choice.

Although there is analysis on models with age structure (both for dengue and other diseases), there is little comparing models that do and do not implement age structure in the contact rate. Laverty and Adler (2010) examine how age–dependence affects the survivorship function in a model of Sin Nombre virus in deer mice, showing a change in the baseline model without age–dependence. However, they do not quantify the difference that they see. In this chapter we aim to address this quantification for a

single serotype age structure model for dengue, and determine how strong the imprint of age–dependence is likely to be in seroprevalence data.

To this end we initially examine a simple PDE model and numerical schemes which can be used to solve it. We then consider the basic reproductive number for a PDE model. Using these structures we implement a PDE model including an age–independent and two age–dependent contact rates. After finding seroprevalence profiles under these contact rates, we implement likelihood analysis to determine whether a sampled seroprevalence profile is likely to have come from an age–independent or age–dependent contact rate as a way to quantify the difference between them. We implement this analysis at the endemic equilibrium and the peak of the initial epidemic. Finally, we consider the main sources and recipients of infection over the initial epidemic to determine which age groups are more important over the course of infection.

3.2 Numerical schemes

3.2.1 A simple SIR PDE model

Initially we study a simple compartmentalized SIR system composed of PDEs. An individual aged a at time t can be susceptible ($S(a,t)$), infected ($I(a,t)$) or recovered ($R(a,t)$). Therefore the model equations are given by

$$\frac{\partial S}{\partial t} + \frac{\partial S}{\partial a} = -\lambda(a,t)S - \delta(a)S, \tag{3.1a}$$

$$\frac{\partial I}{\partial t} + \frac{\partial I}{\partial a} = \lambda(a,t)S - (\gamma + \delta(a))I, \tag{3.1b}$$

$$\frac{\partial R}{\partial t} + \frac{\partial R}{\partial a} = \gamma I - \delta(a)R, \tag{3.1c}$$

with initial conditions

$$S(a,0) = S_0(a), \qquad I(a,0) = I_0(a), \qquad R(a,0) = R_0(a), \tag{3.2}$$

and boundary conditions

$$S(0,t) = \int_0^\infty b(a)N(a,t)\mathrm{d}a, \qquad I(0,t) = 0, \qquad R(0,t) = 0, \tag{3.3}$$

where $\delta(a)$ is the natural morality rate of an individual aged a, γ is the recovery rate (which is independent of age) and $\lambda(a,t)$ is the force of infection of an individual aged a at time t. The boundary conditions assume that all individuals are born susceptible, where $b(a)$ is the reproductive rate of an individual aged a. The total population aged

a at time t is $N(a,t) = S(a,t) + I(a,t) + R(a,t)$. The force of infection is given by

$$\lambda(a,t) = \int_0^\infty c(a,\alpha)I(\alpha,t)d\alpha \tag{3.4}$$

where $c(a,\alpha)$ is the contact rate of an individual aged a with individuals aged α per unit time. We assume random and proportionate mixing, meaning the contact rate can be written in the separable form $c(a,\alpha) = f(a)f(\alpha)$ (Hethcote, 1996). Let $\beta(a)$ be the average number of people contacted per unit time by an individual aged a and $N(a)$ be the steady age distribution of the population. Therefore the total number of contacts per unit time is

$$D = \int_0^\infty \beta(\alpha)N(\alpha)\mathrm{d}\alpha, \tag{3.5}$$

and under random and proportionate mixing

$$c(a,\alpha) = \frac{\beta(a)\beta(\alpha)}{D}. \tag{3.6}$$

Therefore the force of infection can be written as

$$\begin{aligned}
\lambda(a,t) &= \int_0^\infty c(a,\alpha)I(\alpha,t)d\alpha && \text{(3.7a)}\\
&= \int_0^\infty \frac{\beta(a)\beta(\alpha)}{D}I(\alpha,t)d\alpha && \text{(3.7b)}\\
&= \beta(a)\frac{\int_0^\infty \beta(\alpha)I(\alpha,t)\mathrm{d}\alpha}{\int_0^\infty \beta(\alpha)N(\alpha)\mathrm{d}\alpha} && \text{(3.7c)}
\end{aligned}$$

Hethcote (1996, 2000). In this case the spread of infection is solely dependent on the number of contacts that individuals have.

3.2.2 Methods of solving PDEs

There is a lot of literature surrounding age structured PDE systems. Greenhalgh (1987) examined the equilibrium and stability properties of an SIR model under different transmission functions and death rates, while Iannelli (1995) finds the endemic steady state and determines its asymptotic behaviour for a generalized SIS model. There are different methods for solving age structured PDE systems, however these often depend on the complexity of the system such as the number of differential equations being solved. For example, an age structured model of the whole population (defined by one PDE with corresponding initial and boundary conditions) can be analysed using the method of characteristics (Li and Brauer, 2008). However, this can only be used in specific cases, and with the non–linear terms in equation (3.1) this is not feasible.

Therefore, we need a numerical scheme to solve the system of PDEs.

There are different numerical schemes which can be used to solve the hyperbolic system of PDEs given in equation (3.1). For single populations the Lax–Wendroff Scheme has been implemented (Sulsky, 1993), whilst Abia et al. (2005) provide a review of characteristic curves and numerical solutions for solving age structured models for a single population. Numerical schemes can also be implemented to solve models with more than one compartment. Alexanderian et al. (2011) use a forward-time backward-space finite difference scheme to solve an age structured hyperbolic system of PDEs and ODEs for the spread of cholera, whilst Iannelli et al. (1997) discuss convergence, stability and non-negativity of a splitting scheme for an SI model.

As the forward–time backward-space method and the splitting scheme have both previously been implemented for systems of hyperbolic differential equations, we focus on these two methods. We introduce the two different finite difference schemes and then test them using error analysis to determine which of the schemes we should implement for our analysis.

Forward-time backward-space (upwind) scheme

The upwind scheme uses a forward difference approximation for the time derivative and a backward difference approximation for the age derivative. It is fully explained in Strikwerda (1989), while as previously stated Alexanderian et al. (2011) successfully implement the scheme in an age structured model for cholera.

Let us define a grid of points in the age–time (a, t) plane. Let $h, k > 0$, meaning a point in the grid $(a_m, t_n) = (mh, nk)$ for arbitrary $m, n \in \mathbb{Z}$. The approximation to $S(a_m, t_n)$ will be given using the numerical scheme as $\bar{S}^n_m$, and similarly for $I(a_m, t_n)$, $R(a_m, t_n)$ and $N(a_m, t_n)$. We assume that age and time are both progressing at the same rate and therefore $h = k$, which allows for a vast simplification of the upwind scheme. Hence, the scheme to solve system (3.1) is given by

$$\bar{S}^{n+1}_m = \bar{S}^n_{m-1} - k(\Lambda^n_{m-1} + \Delta_{m-1})\bar{S}^n_{m-1}, \tag{3.8a}$$

$$\bar{I}^{n+1}_m = \bar{I}^n_{m-1} + k\Lambda^n_{m-1}\bar{S}^n_{m-1} - k(\gamma + \Delta_{m-1})\bar{I}^n_{m-1}, \tag{3.8b}$$

$$\bar{R}^{n+1}_m = \bar{R}^n_{m-1} + k\gamma\bar{I}^n_{m-1} - \Delta_{m-1}\bar{R}^n_{m-1}, \tag{3.8c}$$

with initial conditions

$$\bar{S}^0_m = \bar{S}_0(a_m), \qquad \bar{I}^0_m = \bar{I}_0(a_m), \qquad \bar{R}^0_m = \bar{R}_0(a_m), \tag{3.9}$$

and boundary conditions

$$\bar{S}_0^n = \sum_{j=0}^{J} h\omega_j b_j(\bar{S}_j^n + \bar{I}_j^n + \bar{R}_j^n), \qquad \bar{I}_0^n = 0, \qquad \bar{R}_0^n = 0, \tag{3.10}$$

where Δ_j are the discretized mortality rates of age group j, b_j are the discretized birth rates of age group j and ω_j are the weights associated with the composite trapezoidal rule ($\omega_0 = \omega_J = 1/2$ and $\omega_j = 1$ for $1 \leq j \leq J-1$). We assume that the recovery rate γ is identical for all age groups and therefore no discretization is needed. In contrast to this the force of infection depends on both age and time. As for the boundary condition on the susceptible population, we implement the composite trapezoidal rule. Therefore, discretizing equation (3.7) the force of infection is given by

$$\Lambda_m^n = \hat{\beta}_m \frac{\sum_{j=0}^{J} \omega_j \hat{\beta}_j \bar{I}_j^n}{\sum_{j=0}^{J} \omega_j \hat{\beta}_j \bar{N}_j^n} \tag{3.11}$$

where $\hat{\beta}_j$ is the discretized contact rate and ω_j are as given in equation (3.10)

Splitting scheme

The splitting scheme has been successfully implemented and analysed by Iannelli et al. (1997). Their scheme, adapted for our parameters and $n \geq 1$, is given for the susceptible class by

$$\frac{\bar{S}_m^{n-1/2} - \bar{S}_{m-1}^{n-1}}{k} + \Delta_m \bar{S}_m^{n-1/2} = 0 \tag{3.12a}$$

$$\frac{\bar{S}_m^n - \bar{S}_m^{n-1/2}}{k} = -\Lambda_{m-1}^{n-1} s_m^n, \tag{3.12b}$$

the infected class by

$$\frac{\bar{I}_m^{n-1/2} - \bar{I}_{m-1}^{n-1}}{k} + \Delta_m \bar{I}_m^{n-1/2} = 0 \tag{3.12c}$$

$$\frac{\bar{I}_m^n - \bar{I}_m^{n-1/2}}{k} + \gamma \bar{I}_m^n = \Lambda_{m-1}^{n-1} \bar{S}_m^n, \tag{3.12d}$$

and the recovered class by

$$\frac{\bar{R}_m^{n-1/2} - \bar{R}_{m-1}^{n-1}}{k} + \Delta_m \bar{R}_m^{n-1/2} = 0 \tag{3.12e}$$

$$\frac{\bar{R}_m^{n} - \bar{R}_m^{n-1/2}}{k} = \gamma \bar{I}_m^{n}. \tag{3.12f}$$

The initial and boundary conditions are as for the upwind scheme (equations (3.9)–(3.10)), the force of infection is given in equation (3.11) and the weights in the boundary condition and the force of infection are the same as those previously given for the composite trapezoidal rule. Taking the susceptible compartment equations as an example, we can eliminate the $\bar{S}_m^{n-1}$ term. Rearranging equation (3.12a) we get

$$\bar{S}_m^{n-1/2} - \bar{S}_{m-1}^{n-1} + k\Delta_m \bar{S}_m^{n-1/2} = 0 \tag{3.13a}$$

$$(1 + k\Delta_m)\, \bar{S}_m^{n-1/2} = \bar{S}_{m-1}^{n-1} \tag{3.13b}$$

$$\bar{S}_m^{n-1/2} = \frac{\bar{S}_{m-1}^{n-1}}{(1 + k\Delta_m)}. \tag{3.13c}$$

This can then be substituted into equation (3.12b). Repeating this for the infected and recovered compartments then yields one equation for each compartment, given by

$$\bar{S}_m^{n} = \frac{1}{(1 + k\Lambda_{m-1}^{n-1})(1 + k\Delta_m)} \bar{S}_{m-1}^{n-1}, \tag{3.14a}$$

$$\bar{I}_m^{n} = \frac{1}{(1 + k\gamma)(1 + k\Delta_m)} \left[\bar{I}_{m-1}^{n-1} + k(1 + k\Delta_m)\Lambda_{m-1}^{n-1} \bar{S}_m^{n} \right], \tag{3.14b}$$

$$\bar{R}_m^{n} = \frac{1}{(1 + k\Delta_m)} \left[\bar{R}_{m-1}^{n-1} + k\gamma(1 + k\Delta_m) \bar{I}_m^{n} \right], \tag{3.14c}$$

which can be combined with the initial and boundary conditions and force of infection previously given to solve the system of equations (3.1).

3.2.3 Analytic results for testing numerical schemes

We next analyse both the upwind and splitting schemes to determine which is the most efficient and gives the most accurate results when being used to find an approximation to the system of equations (3.1). To achieve this we need an empirical value to test the schemes against. Following the work of Greenhalgh (1987) we calculate the age–profiles at the equilibrium by initially factoring out the death rate in equations (3.1). We will then be able to run the numerical scheme to equilibrium and test for errors between the analytic solution and the schemes.

Starting with equations (3.1) we initially divide each of the population densities by

the density of the total population, giving

$$x(a,t) = \frac{S(a,t)}{N(a,t)}, \quad y(a,t) = \frac{I(a,t)}{N(a,t)}, \quad z(a,t) = \frac{R(a,t)}{N(a,t)}. \tag{3.15}$$

Taking the partial derivatives of $S(a,t)$ with respect to age and time we get

$$\frac{\partial S}{\partial t} + \frac{\partial S}{\partial a} = x\frac{\partial N}{\partial t} + N\frac{\partial x}{\partial t} + x\frac{\partial N}{\partial a} + N\frac{\partial x}{\partial a}, \tag{3.16}$$

which we can substitute into equation (3.1a). This yields

$$N\frac{\partial x}{\partial t} + N\frac{\partial x}{\partial a} = -(\lambda+\delta)xN - x\left(\frac{\partial N}{\partial t} + \frac{\partial N}{\partial a}\right). \tag{3.17}$$

We know that $N_t + N_a = -\delta N$. Using this fact, dividing by N and rearranging we find that

$$\frac{\partial x}{\partial t} + \frac{\partial x}{\partial a} = -\lambda x. \tag{3.18}$$

We can follow the same process for the infected and recovered compartments, giving a new system of equations

$$\begin{aligned}
\frac{\partial x}{\partial t} + \frac{\partial x}{\partial a} &= -\lambda x, && \text{(3.19a)}\\
\frac{\partial y}{\partial t} + \frac{\partial y}{\partial a} &= \lambda x - \gamma y, && \text{(3.19b)}\\
\frac{\partial z}{\partial t} + \frac{\partial z}{\partial a} &= \gamma y. && \text{(3.19c)}
\end{aligned}$$

As the death rate has been factored out we need an upper bound on the age of the population as individuals do not live forever. Therefore equation (3.19) is valid for ages $0 \leq a \leq L$, where L is the maximum age of an individual in the population.

To test the numerical schemes we assume a constant transmission rate ($\beta(a) = \beta \ \forall \ a$). This allows for easier manipulation of the force of infection term, which is given by

$$\lambda(t) = \beta\frac{\int_0^L y(a,t)N(a,t)\mathrm{d}a}{\int_0^L N(a,t)\mathrm{d}a}. \tag{3.20}$$

The associated boundary conditions for the system are are

$$x(0,t) = 1, \quad y(0,t) = 0, \quad z(0,t) = 0. \tag{3.21}$$

The age–equilibrium solutions can then be calculated by setting the time derivatives

to zero in equations (3.19) and solving them simultaneously, yielding

$$\bar{x}(a) = e^{-\lambda a}, \tag{3.22a}$$

$$\bar{y}(a) = \frac{\lambda}{\gamma - \lambda}\left(e^{-\lambda a} - e^{-\gamma a}\right), \tag{3.22b}$$

$$\bar{z}(a) = \frac{\gamma}{\gamma - \lambda}\left(1 - e^{-\lambda a}\right) - \frac{\lambda}{\gamma - \lambda}\left(1 - e^{-\gamma a}\right). \tag{3.22c}$$

This can be done because β is constant and hence λ is no longer dependent on age. We then substitute the expression for $\bar{y}$ into equation (3.20), giving the force of infection as

$$\begin{aligned}\lambda &= \beta \int_0^L \bar{y}(a)\bar{N}(a)\mathrm{d}a \Big/ \int_0^L \bar{N}(a)\mathrm{d}a \\ &= \beta \int_0^\infty \frac{\lambda}{\gamma - \lambda}\left(e^{-\lambda a} - e^{-\gamma a}\right)\bar{N}(a)\mathrm{d}a \Big/ \int_0^L \bar{N}(a)\mathrm{d}a. \end{aligned} \tag{3.23}$$

We use this result to determine the equilibria for the system of equations (3.1).

To do this in our model system, equation (3.1), we assume a type I mortality rate (Anderson and May, 1991). This assumes everyone survives until age L and then dies, and is given by the function

$$\delta(a) = \begin{cases} 0 & \text{if } 0 \le a \le L, \\ \infty & \text{if } a \ge L. \end{cases} \tag{3.24}$$

We assume that the population is at equilibrium and that the birth rate ($b(a)$) is constant for all ages. Then the per capita birth rate is given by L^{-1}, where L is the average lifespan of an individual. Assuming

$$P(t) = \int_0^L S(a,t)\mathrm{d}a + \int_0^L I(a,t)\mathrm{d}a + \int_0^L R(a,t)\mathrm{d}a = \bar{P}, \tag{3.25a}$$

the boundary condition for the susceptible population is $S(0,t) = \bar{P}/L$. In order to determine the population densities at equilibrium we need to know $N(a)$. This is easily calculated, giving

$$N(a) = \frac{\bar{P}}{L}\exp\left[-\int_0^a \delta(\xi)\mathrm{d}\xi\right] = \frac{\bar{P}}{L}, \qquad 0 \le a \le L. \tag{3.26}$$

This is because if $a < L$ then $\delta = 0$ meaning the exponential equals 1. If $a > L$ then $\delta = \infty$ and the exponential tends to zero. We know $S(a) = x(a)N(a)$, and similarly for the infected and recovered classes, meaning for type I mortality (equation (3.24))

the equilibrium densities are given by

$$S(a) = \frac{\bar{P}}{L} e^{-\lambda a}, \qquad 0 \leq a \leq L \tag{3.27a}$$

$$I(a) = \frac{\lambda}{\gamma - \lambda} \frac{\bar{P}}{L} (e^{-\lambda a} - e^{-\gamma a}), \qquad 0 \leq a \leq L \tag{3.27b}$$

$$R(a) = \frac{\gamma}{\gamma - \lambda} \frac{\bar{P}}{L} (1 - e^{-\lambda a}) - \frac{\lambda}{\gamma - \lambda} \frac{\bar{P}}{L} (1 - e^{-\gamma a}) \qquad 0 \leq a \leq L. \tag{3.27c}$$

The last element to calculate is the force of infection. Substituting $N(a)$ into equation (3.23) we see the solutions are $\lambda = 0$ or the solutions of the equation

$$1 = \frac{\beta}{\gamma - \lambda} \frac{\bar{P}}{L} \int_0^L \left(e^{-\lambda a} - e^{-\gamma a} \right) \mathrm{d}a \Big/ \frac{\bar{P}}{L} \int_0^L \mathrm{d}a \tag{3.28a}$$

$$= \frac{\beta}{\gamma - \lambda} \frac{1}{L} \left[\frac{e^{-\lambda a}}{-\lambda} - \frac{e^{-\gamma a}}{-\gamma} \right]_0^L \tag{3.28b}$$

$$= \frac{\beta}{\gamma - \lambda} \frac{1}{L} \left(\frac{1 - e^{-\lambda L}}{\lambda} - \frac{1 - e^{-\gamma L}}{\gamma} \right). \tag{3.28c}$$

We are then able to use a MATLAB function, such as `fzero`, to solve equation (3.28). We therefore establish the age–profiles for each of the immune status compartments when the system is at the endemic equilibrium, as well as the total number of individuals in each compartment at this time. We can use this to determine which of the numerical schemes produce a better approximation at the endemic equilibrium to the system of PDEs (3.1).

3.2.4 Error analysis: L_2 norm

One method to estimate the error of numerical schemes is the L_2 norm (Strikwerda, 1989). Let u_m^n be the solution at the endemic equilibrium using the numerical scheme and $U(a_m, t^n)$ be the accurate solution at the endemic equilibrium found using equations (3.27)–(3.28). The L_2 norm is then defined by

$$E(t) = ||U(\cdot, t) - u^n||_2,$$

$$= \left(h \sum_m \frac{|U(a_m, t^n) - u_m^n|^2}{|U(a_m, t^n)|^2} \right)^{\frac{1}{2}}. \tag{3.29}$$

Using this definition we determine the relative error across the age–profile for the susceptible, infected and recovered compartments. For this analysis we will use $t = 1000$ years in the numerical schemes.

We can determine the L_2 norm in different ways for the compartments in the system. For each step size k we can either sum the error at each age interval to find the overall error or use the trapezoidal rule to determine the total number of individuals in each compartment and calculate the error based on this. Figure 3-1 shows the error for the former of these. Results for the latter were very similar and are shown in Appendix A. The error is calculated separately for each of the compartments as they all have their own endemic equilibrium age–profiles. For all compartments (figures 3-1(a)–(c)) we can see that for larger step sizes the error is smaller for the splitting scheme than the upwind scheme. As the step size is reduced to less than $k = 0.004$ the error is either very similar for both schemes or slightly smaller using the splitting scheme. It is worth noting that the error for both schemes is much larger for the infected compartment than the susceptible or recovered compartments.

Figure 3-1 shows that the decrease in error as the step size decreases is approximately linear for the splitting method and exponentially decreasing for the upwind scheme. This means that increasing the step size initially has less of an effect on the accuracy of the splitting method than it does on the upwind scheme.

It is also important to consider how long each of the schemes takes to approximate the system at the endemic equilibrium. We calculate this using the `tic` function in MATLAB. Figure 3-2(a) shows that the upwind scheme takes longer to solve to equilibrium for all step sizes. As the times for both schemes follow a negative exponential curve this means that as the step size decreases the difference in time taken to solve to equilibrium under the two schemes will increase. This can be seen further in the log log plot, figure 3-2(b), where there is a linear relationship between the terms. This indicates that the time taken to solve the system as the step size is reduced increases according to power laws under both schemes.

From this we conclude that it is better to use the splitting scheme than the upwind scheme. The former reaches equilibrium quicker than the latter and for small step sizes has a similar (and in many cases better) error approximation to the analytic solution. We will choose a step size of $k = 0.005$; the splitting scheme has good accuracy whilst only taking around four minutes to solve to equilibrium.

3.3 Basic reproductive number for PDE models

The basic reproductive number is the number of secondary infections in a population when one infected individual is placed in a naïve population (Diekmann and Heesterbeek, 2000; Keeling and Rohani, 2008). For an age structured PDE model it is given by the expected number of new infections produced by a typical individual in a naïve

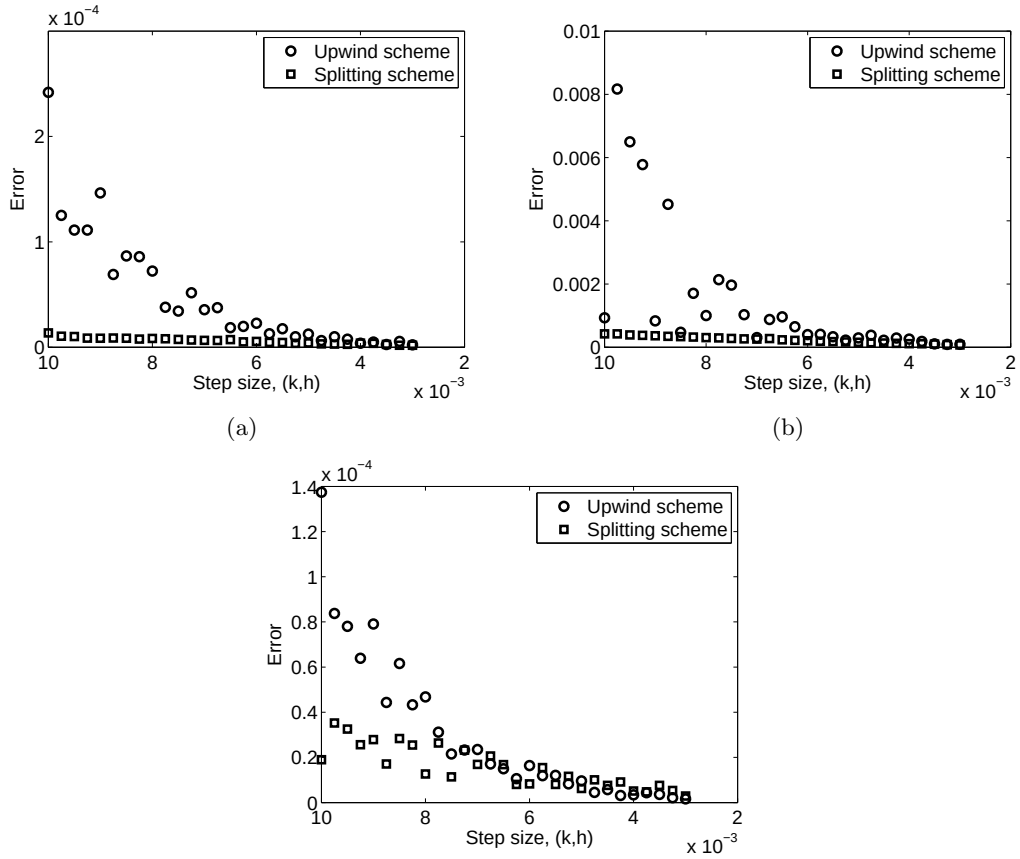

Figure 3-1: The relative error (equation (3.29)) for the upwind scheme (circles) and the splitting scheme (squares) when $t = 1000$ years as the step size is reduced. The error is calculated at each of the points on the age profile. (a) Shows the error in the schemes for the susceptible compartment, (b) shows the error in the schemes for the infected compartment and (c) shows the error in the schemes for the recovered compartment. The parameters are given by $N = 10000$, $\gamma = 60$, $\beta = 2\gamma$ and $b = 1/60$.

population. The infected individual is distributed across all infection types in a given way, according to the eigenvector which corresponds to the basic reproductive number R_0 (Diekmann and Heesterbeek, 2000). When studying different contact rates it is important that the basic reproductive number is kept constant to ensure homogeneity when performing later analysis. For a system of PDEs finding R_0 is substantially different than for a system of ODEs, as it is dependent on the age structure of the infected population. We therefore follow the work of Diekmann and Heesterbeek (2000) in finding R_0 for a PDE system.

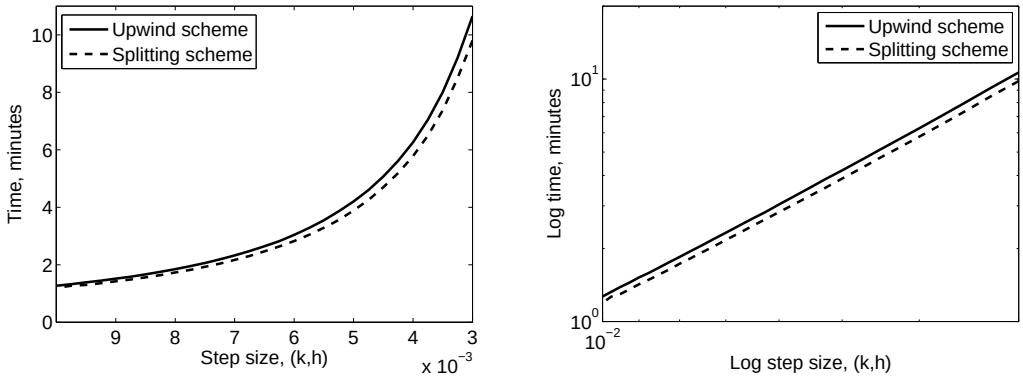

(a) (b)

Figure 3-2: Time taken to reach the endemic equilibrium under the upwind scheme (solid line) and splitting scheme (dashed line) when $\bar{T} = 1000$ years. The parameters are given by $N = 10000$, $\gamma = 60$, $\beta = 2\gamma$ and $b = 1/60$.

To find R_0 we need to find the spectral radius of the next–generation operator

$$(K\phi)(a) = \int_0^\infty k(a,\alpha)\phi(\alpha)\mathrm{d}\alpha, \tag{3.30}$$

where $k(a,\alpha)$ is the kernel of the next–generation operator. The kernel is given by

$$k(a,\alpha) = \int_0^\infty h(\tau,\alpha)c(a,\alpha+\tau)\frac{F_d(\alpha+\tau)}{F_d(\alpha)}\mathrm{d}\tau, \tag{3.31}$$

where $h(\tau,\alpha)$ is the probability of transmission time τ after infection, $c(a,\alpha+\tau)$ is the rate of contact per unit time an individual aged $(\alpha+\tau)$ has with individuals aged a and $\frac{F_d(\alpha+\tau)}{F_d(\alpha)}$ is the probability an individual survives to age $(\alpha+\tau)$ given they have survived until age α. By integrating over time τ, the kernel gives the expected number of infections from one individual infected at age α.

We assume a short–disease approximation, which allows for simplifications to the kernel and subsequently the next–generation operator. The short–disease approximation means the disease has an infectious period which is much shorter than the average human lifespan. Therefore we assume that due to the short infectious period the probability of individuals dying whilst infected is very small, hence

$$\frac{F_d(\alpha+\tau)}{F_d(\alpha)} \approx 1. \tag{3.32}$$

Secondly, we assume that the contact rate does not change over the course of infection,

meaning

$$c(a, \alpha + \tau) = c(a, \alpha). \tag{3.33}$$

To construct R_0 we discretize the system and allow for age intervals to be able to calculate the contact rate. Let us introduce age–intervals i, $i = 1, 2, \ldots, n$. Then the contact rate can be defined as

$$c(a, \alpha) = c_{ij} \text{ for } a \in i \text{ and } \alpha \in j. \tag{3.34}$$

For this to be used in our kernel function we introduce the characteristic function χ_i, defined as

$$\chi_i(a) = \begin{cases} 1 & \text{if } a \in i, \\ 0 & \text{otherwise.} \end{cases}$$

We can therefore write the contact rate using this function as

$$\begin{aligned} c(a, \alpha) &= \sum_{k,l=1}^{n} c_{kl} \chi_k(a) \chi_l(\alpha) && (3.35) \\ &= \sum_{k=1}^{n} \chi_k(a) \sum_{l=1}^{n} c_{kl} \chi_l(\alpha). && (3.36) \end{aligned}$$

We know that the rate of recovery is γ. Therefore the probability of transmission time τ after infection is given by $\exp(-\gamma\tau)$. Substituting this into the kernel gives

$$\begin{aligned} k(a, \alpha) &= \int_0^\infty h(\tau, \alpha) c(a, \alpha) \mathrm{d}\tau && (3.37) \\ &= \int_0^\infty \exp(-\gamma\tau) \sum_{k=1}^{n} \chi_k(a) \sum_{l=1}^{n} c_{kl} \chi_l(\alpha) \mathrm{d}\tau \\ &= \sum_{k=1}^{n} \chi_k(a) \psi_k(\alpha), && (3.38) \end{aligned}$$

where

$$\psi_k(\alpha) = \int_0^\infty \exp(-\gamma\tau) \sum_{l=1}^{n} c_{kl} \chi_l(\alpha) \mathrm{d}\tau. \tag{3.39}$$

Finally, the kernel can be substituted into the next-generation operator, yielding

$$(K\phi)(a) = \sum_{k=1}^{n} \chi_k(a) \int_0^L \psi_k(\alpha) \phi(\alpha) \mathrm{d}\alpha. \tag{3.40}$$

Note the change in the integral bounds in the next–generation operator due to the

assumption of type I mortality. Therefore the range of K is spanned by $\{\chi_k\}_{k=1}^n$. Let

$$\phi(a) = \sum_{j=1}^{n} q_j \chi_j(a), \tag{3.41}$$

where $\mathbf{q}$ is a vector of constants. This means the next–generation matrix becomes

$$\begin{aligned}(K\phi)(a) &= \sum_{k=1}^{n} \chi_k(a) \int_0^L \psi_k(\alpha) \sum_{j=1}^{n} q_j \chi_j(\alpha) \mathrm{d}\alpha \\ &= \sum_{k=1}^{n} d_k \chi_k(a), \end{aligned} \tag{3.42}$$

where

$$d_k = \sum_{j=1}^{n} q_j \int_0^L \psi_k(\alpha)\chi_j(\alpha)\mathrm{d}\alpha. \tag{3.43}$$

Hence the vector $\mathbf{q}$ is transformed into $\mathbf{d} = M\mathbf{q}$ where M is the matrix with elements

$$m_{ij} = \int_0^L \psi_i(\alpha)\chi_j(\alpha)\mathrm{d}\alpha. \tag{3.44}$$

R_0 is the dominant eigenvalue of the matrix M with elements m_{ij}. We can explicitly calculate $\psi_k(\alpha)$ as

$$\begin{aligned}\psi_k(\alpha) &= \int_0^\infty \exp(-\gamma\tau) \sum_{l=1}^{n} c_{kl}\chi_l(\alpha)\mathrm{d}\tau \\ &= \frac{1}{\gamma}\left[\sum_{l=1}^{n} c_{kl}\chi_l(\alpha)\right]. \end{aligned} \tag{3.45}$$

Hence the elements of the matrix M are

$$m_{ij} = \frac{1}{\gamma}\int_0^L \sum_{l=1}^{n} c_{il}\chi_l(\alpha)\chi_j(\alpha)\mathrm{d}\alpha \tag{3.46a}$$

$$= \frac{1}{\gamma}\int_0^L c_{i1}\chi_1(\alpha)\chi_j(\alpha) + c_{i2}\chi_2(\alpha)\chi_j(\alpha) + ... + c_{ij}\chi_j(\alpha)\chi_j(\alpha) + ... + c_{in}\chi_n(\alpha)\chi_j(\alpha)\mathrm{d}\alpha \tag{3.46b}$$

$$= \frac{1}{\gamma}\int_0^L c_{ij}\chi_j(\alpha)\chi_j(\alpha)\mathrm{d}\alpha, \tag{3.46c}$$

$$\approx \frac{1}{\gamma}c_{ij}. \tag{3.46d}$$

Having found an expression to calculate the basic reproductive number, we now need to determine the elements in the contact rate. An individual aged α makes $\beta(\alpha)$ contacts per unit time. Again, we discretize the populations into different age groups, $(a, a+\delta a)$. The total number of contacts made by individuals of all ages per unit time is

$$\int_0^L \beta(\nu)N(\nu,t)\mathrm{d}\nu, \tag{3.47}$$

and the total contacts made by individuals of age $(a, a+\delta a)$ per unit time is

$$\int_a^{a+\delta a} \beta(\nu)N(\nu,t)\mathrm{d}\nu. \tag{3.48}$$

Therefore the rate of contact an individual aged α has with individuals in the interval $(a+\delta a)$ is given by

$$\beta(\alpha)\frac{\int_a^{a+\delta a}\beta(\nu)N(\nu,t)\mathrm{d}\nu}{\int_0^L \beta(\nu)N(\nu,t)\mathrm{d}\nu}. \tag{3.49}$$

Therefore we find that the discretized contact rate of an individual aged α with individuals aged a, c_{ij}, is given by

$$c_{ij} = \hat{\beta}_i \frac{\hat{\beta}_j N_j}{\sum_k \hat{\beta}_k N_k} \text{ for } \alpha \in i \text{ and } a \in j, \tag{3.50}$$

where $\hat{\beta}_i$ is the average number of contacts made by individuals in the age class i,

$$\hat{\beta}_i = \frac{1}{\delta a}\int_a^{a+\delta a} \beta(\alpha)\mathrm{d}\alpha. \tag{3.51}$$

We need to compare the PDE model above with the corresponding ODE model with discrete age classes. This allows us to relate the contact rate found in equation (3.50) to the force of infection in the PDE model (equation 3.7) to ensure consistency. To do this we implement an ODE system with distinct age classes at the start of an epidemic and find the contact rate. Letting $\delta a \to 0$ we can then obtain a continuous expression for the force of infection in the PDE model. We assume individuals are separated into age groups i, $i = 1, \ldots, n$. When infection is introduced into a naïve population we can describe the dynamics by the system of ODEs

$$\frac{\mathrm{d}S_i}{\mathrm{d}t} = N_i, \tag{3.52a}$$

$$\frac{\mathrm{d}I_i}{\mathrm{d}t} = \lambda_i S_i - \gamma I_i, \tag{3.52b}$$

where

$$\lambda_i = \beta_i \frac{\beta_1 I_1 + \beta_2 I_2 + ... + \beta_n I_n}{\beta_1 N_1 + \beta_2 N_2 + ... + \beta_n N_n}. \tag{3.53}$$

The force of infection term has the denominator weighted by the contacts of each age group due to the assumption of frequency dependence in the transmission term. We can approximate the susceptible population by the total population and therefore

$$\frac{\mathrm{d}I_i}{\mathrm{d}t} = \lambda_i N_i - \gamma I_i, \tag{3.54}$$

which means we have

$$\begin{aligned}
\begin{pmatrix} \dot{I}_1 \\ \dot{I}_2 \\ \vdots \\ \dot{I}_n \end{pmatrix} &= \begin{pmatrix} \frac{\beta_1 N_1 \beta_1}{\sum_k \beta_k N_k} & \frac{\beta_1 N_1 \beta_2}{\sum_k \beta_k N_k} & \cdots & \frac{\beta_1 N_1 \beta_n}{\sum_k \beta_k N_k} \\ \frac{\beta_2 N_2 \beta_1}{\sum_k \beta_k N_k} & \frac{\beta_2 N_2 \beta_2}{\sum_k \beta_k N_k} & \cdots & \frac{\beta_2 N_2 \beta_n}{\sum_k \beta_k N_k} \\ \vdots & \vdots & \ddots & \vdots \\ \frac{\beta_n N_n \beta_1}{\sum_k \beta_k N_k} & \frac{\beta_n N_n \beta_2}{\sum_k \beta_k N_k} & \cdots & \frac{\beta_n N_n \beta_n}{\sum_k \beta_k N_k} \end{pmatrix} \begin{pmatrix} I_1 \\ I_2 \\ \vdots \\ I_n \end{pmatrix} + \\
&\qquad \begin{pmatrix} -\gamma & 0 & \cdots & 0 \\ 0 & -\gamma & \cdots & 0 \\ \vdots & \vdots & \ddots & \vdots \\ 0 & 0 & \cdots & -\gamma \end{pmatrix} \begin{pmatrix} I_1 \\ I_2 \\ \vdots \\ I_n \end{pmatrix} \qquad (3.55) \\
&= (T + \Sigma) \begin{pmatrix} I_1 \\ I_2 \\ \vdots \\ I_n \end{pmatrix}, \qquad (3.56)
\end{aligned}$$

where T is the transmission matrix and Σ is the transition matrix. The next–generation matrix, given by $-T\Sigma^{-1}$, yields

$$G = \frac{1}{\gamma} \begin{pmatrix} \frac{\beta_1 N_1 \beta_1}{\sum_k \beta_k N_k} & \frac{\beta_1 N_1 \beta_2}{\sum_k \beta_k N_k} & \cdots & \frac{\beta_1 N_1 \beta_n}{\sum_k \beta_k N_k} \\ \frac{\beta_2 N_2 \beta_1}{\sum_k \beta_k N_k} & \frac{\beta_2 N_2 \beta_2}{\sum_k \beta_k N_k} & \cdots & \frac{\beta_2 N_2 \beta_n}{\sum_k \beta_k N_k} \\ \vdots & \vdots & \ddots & \vdots \\ \frac{\beta_n N_n \beta_1}{\sum_k \beta_k N_k} & \frac{\beta_n N_n \beta_2}{\sum_k \beta_k N_k} & \cdots & \frac{\beta_n N_n \beta_n}{\sum_k \beta_k N_k} \end{pmatrix}. \tag{3.57}$$

Therefore

$$\begin{aligned} g_{ij} &= \frac{1}{\gamma} c_{ij} \\ &= m_{ij}, \end{aligned}$$

and R_0 is the dominant eigenvalue of this matrix, corresponding to the PDE model.

This confirms that the force of infection we used in the PDE model is correct. In the discrete model this was given by equation (3.53) where an individual is in age group i if in the age–interval $(a + \delta a)$. Letting $\delta a \to 0$ we find the continuous form as

$$\lambda(a,t) = \beta(a)\frac{\int_0^L \beta(\alpha)I(\alpha,t)\mathrm{d}\alpha}{\int_0^L \beta(\alpha)N(\alpha,t)\mathrm{d}\alpha}. \tag{3.58}$$

Therefore we have shown that for the PDE model with a force of infection given by equation (3.7) we can use the discretized contact rate $c(a,\alpha)$ (equation (3.50)) to find the basic reproductive number.

3.4 The model and methodologies

3.4.1 The model

Recapping the model from Section 3.2, we have a compartmentalized SIR system composed of PDEs. An individual aged a at time t can be susceptible ($S(a,t)$), infected ($I(a,t)$) or recovered ($R(a,t)$). Therefore the model equations are given by

$$\frac{\partial S}{\partial t} + \frac{\partial S}{\partial a} = -\lambda(a,t)S - \delta(a)S, \tag{3.59a}$$

$$\frac{\partial I}{\partial t} + \frac{\partial I}{\partial a} = \lambda(a,t)S - (\gamma + \delta(a))I, \tag{3.59b}$$

$$\frac{\partial R}{\partial t} + \frac{\partial R}{\partial a} = \gamma I - \delta(a)R, \tag{3.59c}$$

with initial conditions

$$S(a,0) = S_0(a), \qquad I(a,0) = I_0(a), \qquad R(a,0) = R_0(a), \tag{3.60}$$

and boundary conditions

$$S(0,t) = \int_0^\infty bN(a,t)\mathrm{d}a, \qquad I(0,t) = 0, \qquad R(0,t) = 0, \tag{3.61}$$

where $\delta(a)$ is the natural morality rate of an individual aged a, γ is the recovery rate, $\lambda(a,t)$ is the force of infection of an individual age a at time t and b is the reproductive rate. The force of an infection, in its simple form, is given by

$$\lambda(a,t) = \beta(a)\frac{\int_0^\alpha \beta(\alpha)I(\alpha,t)\mathrm{d}\alpha}{\int_0^\infty \beta(\alpha)N(\alpha)\mathrm{d}\alpha} \tag{3.62}$$

where $\beta(a)$ is the average number of people contacted per unit time by an individual aged a. We assume type I mortality, given in equation (3.24). All parameters are given in Table 3.1.

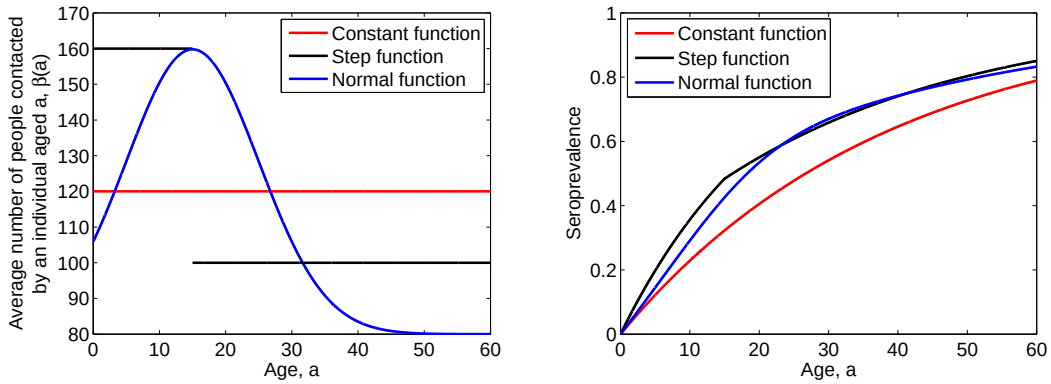

(a) (b)

Figure 3-3: (a) Examples of different functions which can be used to model the average number of people contacted by an individual aged a ($\beta(a)$). The functions are an age–independent function (red line), a step function (black line) and a transposed normal function (blue line). (b) The corresponding seroprevalence profiles at the endemic equilibrium under the different contact rate functions. In both figures $\mu = 15$, $\sigma = 10$, $c_5 = 2000$ and $a^* = 0$. All parameters are given in Table 3.1.

If we set $\beta(a)$ to be different functions this will affect the way that the disease progresses in the population, both in time and across the different age groups. Figure 3-3(a) gives examples of an age–independent and two age–dependent contact rates. Implementing these in model (3.59)–(3.62) yields different age profiles at the endemic equilibrium when considering seroprevalence in the population, shown in figure 3-3(b). Although seroprevalence increases with age under each of the different contact rates, the profiles are different. When the age–independent contact rate is implemented there is a smooth increase in seroprevalence which has a decreasing gradient as age increases. In contrast to this, under the step function there is a smooth increase until age 15, at which point the gradient of the curve substantially changes and there is again a smooth increase at a different rate. It is ages 0–15 which have a higher contact rate and this is why the change in gradient occurs at this point. Under the normal function there is again a smooth increase in seroprevalence with age, however seroprevalence is higher in the population under this contact rate than under the age–independent contact rate. In all cases we have found the basic reproductive ratio using Section 3.3 and set $R_0 \approx 2$.

3.4.2 Quantification

We can qualitatively see differences in the seroprevalence profiles in figure 3-3(b). However, we wish to quantify these differences. To do this we implement likelihood analysis. At the endemic equilibrium and peak of the initial epidemic we will test the null hypothesis

$$H_0\text{: the host population has an age–independent contact rate}$$

against the alternative hypothesis

$$H_1\text{: the host population has an age–dependent contact rate.}$$

To do this we sample a population from the age–independent seroprevalence profile and calculate the likelihood that this sample came from a model simulated using an age–independent or an age–dependent contact rate. Repeating this process several thousand times we can find the type I error - the probability of rejecting the null when it is true. A high type I error indicates similarities between the seroprevalence profiles while a low type I error indicates that the seroprevalence profiles are different. To do this we implement the following algorithm:

1. Using seroprevalence profiles generated at the time point being investigated calculate the seroprevalence density under the null (p_N) and alternative (p_A) hypotheses, i.e. $0 < p_N < 1$ and $0 < p_A < 1$.

2. Choose the number of individuals P in each age group. This is the same for all age groups.

3. For each age group generate P random numbers (r_i, $i = 1, \dots P$) between 0 and 1. If $r_i < p_N$ an individual is seropositive. If $r_i > p_N$ an individual is susceptible. Store the number of seroprevalent individuals in each age group, x.

4. Calculate the likelihood there are $0, 1, \dots, P$ individuals seroprevalent (either infected or recovered) in each age group using the probabilities found in 1.

   (a) We are finding the likelihood there are x seroprevalent individuals of age a out of a possible P in each age group. Therefore, for each age group the likelihood is given by

   $$p(x|\text{model}) = \binom{P}{x} p^x (1-p)^{N-x}. \tag{3.63}$$

5. Using 4 find the likelihood of there being x individuals in each age group under the null and alternative hypothesis.

6. Calculate the likelihood ratio for each age group, given by

$$\frac{p(x|\text{Age–independent model})}{p(x|\text{Age–dependent model})} = \left(\frac{p_N}{p_A}\right)^x \left(\frac{(1-p_N)}{(1-p_A)}\right)^{P-x}. \tag{3.64}$$

7. We define age groups i, $i = 1, \ldots m$. Multiply the likelihood ratios for each age group i together to find the likelihood ratio l for the whole seroprevalence profile. Therefore

$$l = \prod_{i=1}^{m} \frac{p_{N_i}^{x_i}(1-p_{N_i})^{P-x_i}}{p_{A_i}^{x_i}(1-p_{A_i})^{P-x_i}}, \tag{3.65}$$

   where x_i is the number of seroprevalent individuals generated in age group i in 3.

   (a) If $l > 1$ the null hypothesis is accepted and if $l < 1$ the alternative hypothesis is accepted.

8. Repeat steps 3–7 50,000 times. Keep track of the number of times the alternative hypothesis is accepted.

9. Calculate the proportion of times the alternative is chosen - this is the type I error.

It is also possible to calculate type II errors in a similar way. However, the results are qualitatively and quantitatively similar to those for type I error and therefore we concentrate on these results.

3.4.3 Source and recipients of infection

As well as quantifying the difference in the seroprevalence profiles, we are also interested in which age groups are the main source and recipients of infection over the course of the initial epidemic. The source of infection are those age groups which are causing the most infections, while the recipients are those that are getting the most infections.

If we consider the discretized system, the total infections caused by age group j at time t in discretized form is given by

$$\sum_i \hat{\beta}_i \bar{S}_i^n \frac{\hat{\beta}_j \bar{I}_j^n}{\sum_k \hat{\beta}_k \bar{N}_k^n}, \tag{3.66}$$

where $\hat{\beta}_j$ is the average number of contacts made by individuals in age group j, $j = 1, 2, \ldots, n$. The assumption of random and proportionate mixing means we sum over

the contacts with all susceptible individuals. This is then divided by the total number of contacts, leaving the total infections which are caused by age group j. The recipients of infection in age group j at time t are given by the discretized force of infection experienced by age group j, given by

$$\Lambda_j^n \bar{S}_j^n, \tag{3.67}$$

where Λ_j^n is the discretized force of infection, given in equation (3.11).

After calculating the source and the recipients of infection, we rank the different age groups in ascending order from least important to most important. We can then plot these ranks to determine which aged individuals are the most and the least important when considering the source and recipients of infection.

3.4.4 Contact rates

We now formally introduce the different contact rates which we implement. In all cases the contact rates are implemented to ensure that $R_0 \approx 2$, maintaining heterogeneity within the model. As we have numerical approximations we allow for a 2.5% error, meaning $1.95 < R_0 < 2.05$. The basic reproductive number for each contact rate is found using the methodology in Section 3.3. All parameters are given in Table 3.1.

Parameter	**Definition**	**Value**
N	Total population	10^4
L	Maximum age of host	60
γ	Recovery rate	60
h, k	Step size	0.005
c_1	Constant (age–independent function)	120
c_2	Constant (age–dependent step function)	100
c_3	Constant (age–dependent step function)	160
a^*	Age higher contact rate starts	
ν	Number of age groups with higher contact rate	15
c_4	Constant (age–dependent normal function)	80
c_5	Constant (age–dependent normal function)	
μ	Age–group with maximum contact rate (age–dependent normal function)	
σ	Intensity of contacts around μ (age–dependent normal function)	

Table 3.1: Parameter definitions and values used where kept constant. All rates are given per year.

Age–independent contact rate

The first function we implement is an age–independent contact rate, given by

$$\beta(a) = c_1 \ \ \forall a. \tag{3.68}$$

Therefore, no matter the age of an individual the average number of contacts they have is identical. The constant c_1 can be altered accordingly to ensure that $R_0 \approx 2$.

Age–dependent contact rate: Step function

For our first age–dependent contact rate we implement a step function. This allows for two contact rates in the population; a higher one for a certain range of ages and a lower contact rate for the rest of the population. We assume that the higher contact rate starts for individuals aged a^* $(0 \leq a^* \leq L-1)$, and continues for ν age groups following this, where $a^* + \nu \leq L$. Therefore the step contact rate is given by

$$\beta(a) = \begin{cases} c_2 & \text{if } 0 \leq a < a^*, \\ c_3 & \text{if } a^* \leq a < a^* + \nu, \\ c_2 & \text{if } a^* + \nu \leq a, \end{cases} \tag{3.69}$$

where the constants c_2 and c_3 are altered such that $R_0 \approx 2$. It is worth noting that there are different combinations of (c_2, c_3) that can be implemented for a given ν.

Age–dependent contact rate: Normal function

The second age–dependent contact rate we implement is based on a normal function. This allows for a greater range of contacts between different age groups. We assume that the contacts are centered around an age group, μ, and are distributed with a given intensity σ, which are both known. Therefore the normal contact rate is given by

$$\beta(a) = c_4 + c_5 f(a; \mu, \sigma), \tag{3.70}$$

where

$$f(a; \mu, \sigma) = \frac{1}{\sigma\sqrt{2\pi}} \exp\left(\frac{-(a-\mu)}{2\sigma^2}\right), \tag{3.71}$$

and the constants c_4 and c_5 are chosen such that $R_0 \approx 2$. A multiple c_5 of the normal function is added to a constant rate c_4. This allows for a base level in the contact rate, meaning no age group is exempt from transmitting infection. Again, it is worth noting that there are different combinations of (c_4, c_5) which can be implemented to ensure

$R_0 \approx 2$.

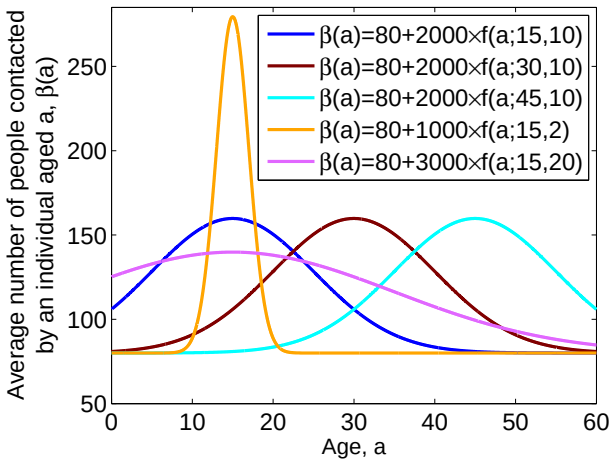

Figure 3-4: Example of how varying the parameters in the age–dependent normal function (equation (3.70)) affects the average number of contacts of an individual aged a ($\beta(a)$). Increasing μ translates the curve to the right. Increasing σ makes the curve less focussed around a given age group.

Figure 3-4 shows examples of how the average number of contacts changes as the age group which makes most contacts (μ) and the intensity of contacts around μ (σ) change. As the age group with the maximum contact rate increases the peak of the average number of contacts made by an individual aged a moves to the right. Changes to the intensity of contacts alter the concentration of contacts at the peak and how the contacts are distributed amongst the different age groups.

3.5 Results I: Step function

3.5.1 At the endemic equilibrium

We initially consider the differences in dynamics at the endemic equilibrium when the constant contact rate (equation (3.68)) and the step function contact rate (equation (3.69)) are implemented. Figure 3-5(a) shows the seroprevalence profiles at the endemic equilibrium for the constant function (equation (3.68)) and several examples of step function (equation (3.69)) where the initial age group which has the highest contact rate (a^*) is changed. The seroprevalence profiles are a similar shape, however for the step function we see a change in gradient for those ages which have a higher contact rate. This is due to the higher transmission among these individuals, which results in fewer susceptible individuals in these age groups, and hence a higher seroprevalence. At

the outset increasing the age group which initially has the highest contact rate pushes the seroprevalence profile towards that of the constant, age–independent function. Increasing further causes seroprevalence for the majority of age groups to be less than when the constant, age–independent function is implemented.

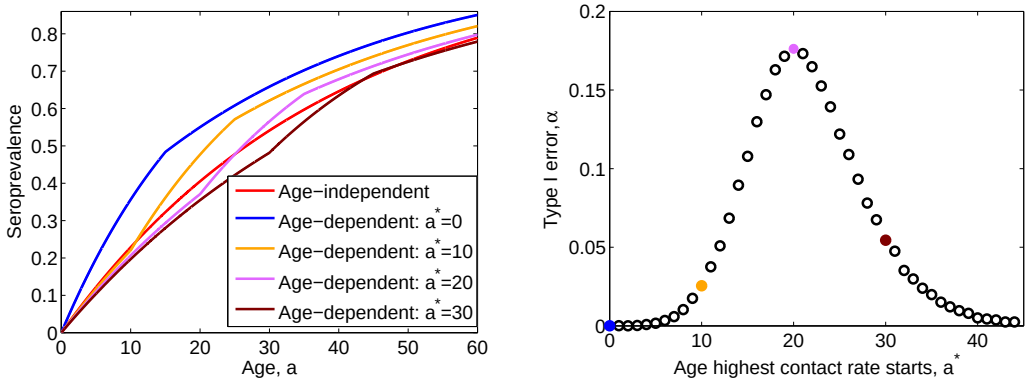

(a) (b)

Figure 3-5: (a) Seroprevalence profiles at the endemic equilibrium for the age–independent contact rate (red line, equation (3.68)) and the age–dependent contact rate (equation (3.69)) where $a^* = 0$ (blue line), $a^* = 10$ (yellow line), $a^* = 20$ (purple line) and $a^* = 30$ (brown line). (b) The probability of type I error at the endemic equilibrium across the seroprevalence profile as the initial age group which has the highest contact rate (a^*) is increased. The colours represent the probability of type I error for the seroprevalence profiles given in figure 3-5 (a). All parameters are given in Table 3.1.

Figure 3-5(b) shows the probability of type I error across the seroprevalence profiles as a^* is increased in the step function (equation (3.69)). If the higher contact rate is among the young or old then the error is small, however if $11 < a^* < 34$ the probability of type I error is above 0.02. This means that it is harder to differentiate between the age–independent and age–dependent seroprevalence profiles than when the higher contact rates were in the younger or older age groups. If the highest contact rate starts at age $a^* = 15$ then over 10% of the time the seroprevalence profiles sampled by the constant contact rate can be better explained by the age–dependent step function. This increases to nearly 18% of the time if the maximum contact rate is among the middle ages. Therefore in these cases the seroprevalence profiles are more similar, and it is harder to determine the impact of the age–dependent contact in the model. However, if the maximum contact rate is among the younger or older age groups then the probability of a type I error is less than 2 in 100. This means that the seroprevalence profiles are sufficiently different to notice the impact that the age–dependent contact

is having in the model.

3.5.2 At the initial epidemic peak

When an age–dependent contact rate is introduced, the dynamics over the initial epidemic also change. Figure 3-6(a) shows the seroprevalence profiles at the peak of the initial epidemic for the constant function (equation (3.68)) and several examples of step function (equation (3.69)) where the initial age group which has the highest contact rate (a^*) is changed. For the constant contact rate the peak of the initial epidemic is at $t = 0.21$ years (approximately 77 days), while for all the step contact rates in figure 3-6(a) the peak of the epidemic is at $t = 0.205$ years (approximately 75 days). Under the age–independent contact rate seroprevalence is identical across all age groups. This is because the initial condition assumes one infected individual spread equally across all age groups. Therefore all the age groups are progressing in the same way and demography has not yet had a chance to make a large impact on the system dynamics. The figure shows that when the age–dependent function is implemented the age range with the higher contact rate $(a^*, a^* + \nu)$ have one seroprevalence level and the other age groups have a second seroprevalence level. However, as in the constant case, there is no variability in these.

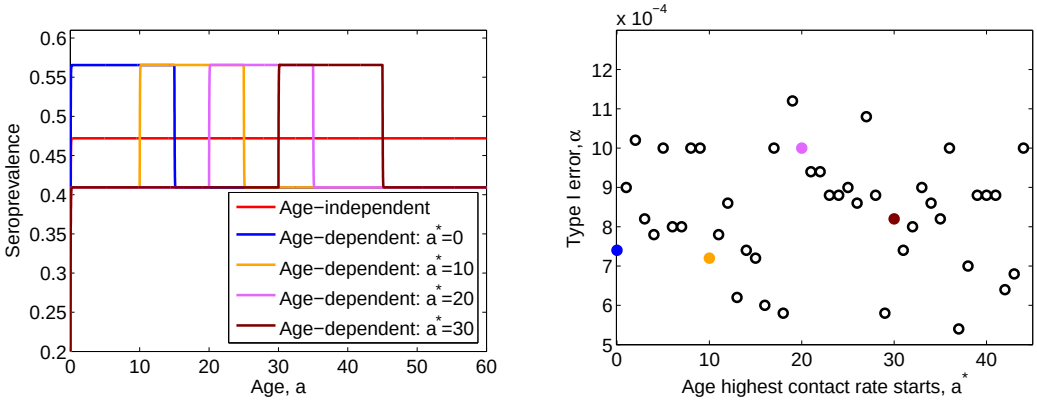

(a) (b)

Figure 3-6: (a) Seroprevalence profiles at the peak of the initial epidemic for the age–independent contact rate (red line, equation (3.68)) and the age–dependent contact rate (equation (3.69)) where $a^* = 0$ (blue line), $a^* = 10$ (yellow line), $a^* = 20$ (purple line) and $a^* = 30$ (brown line). (b) The probability of type I error at the peak of the initial epidemic across the seroprevalence profile as the initial age group which has the highest contact rate (a^*) is increased. The colours represent the probability of type I error for the seroprevalence profiles given in figure 3-6(a). All parameters are given in Table 3.1.

Figure 3-6(b) shows the type I error across the seroprevalence profiles as a^* is increased in the step function (equation (3.69)). We see that the probability of type I error is relatively uniform across all ages. Therefore the probability of rejecting the null when it is true does not overly change when different age groups have a higher contact rate. This is because the step function causes there to be a large jump in the seroprevalence for certain age groups. Considering the seroprevalence profiles themselves, the lack of variability in the probability of type I error is to be expected; the same trends are seen in each of the seroprevalence profiles, just transposed to the right. Therefore, as the age–independent contact rate produces constant seroprevalence across all age groups it is intuitive that the probability of a type I error is similar as a^* is increased. As well as being similar across all ages the probability of type I error is very small (less than 12×10^{-4}). This indicates that the seroprevalence profiles at the peak of the initial epidemic are quite different for the age–independent and age–dependent contact rates. Therefore the age–dependent contact rate is having an effect on the system dynamics.

3.5.3 Source and sink of infection

Figure 3-7(a) shows the source of infection (defined by equation (3.66)) when the step function (equation (3.69)) is implemented with $a^* = 0$. As groups of individuals have the same contact rate, we have groups of individuals who have the same weighting as the source of infection. The boundary at age 0 and then between the two contact rates causes differences in the rankings at these ages. We can see that when $1 < a < 15$ the rank of the source of infection is always higher than $15 < a < 60$. Therefore those with the highest contact rate are the main source of infection. The boundaries cause some variability, however, looking at the two main groups these trends hold.

Figure 3-7(b) shows the recipients of infection (defined by equation (3.67)) when the step function (equation (3.69)) is implemented with $a^* = 0$. We see that at the start of the epidemic the force of infection experienced is greatest amongst those that have a higher contact rate. However, after the initial peak of the epidemic, the force of infection experienced is greater amongst those who have the lower contact rate. This is because those with a higher contact rate have had the infection and recovered. As the epidemic progresses the pool of individuals recovered is mainly those who are younger, and therefore it is those who are older becoming infected. It is important to note that after the initial epidemic it is not that the same number of individuals become infected as before. Instead, those with lower contact rates are becoming more prominent in the population, and thus are receiving more infections than those who have the higher contact rate.

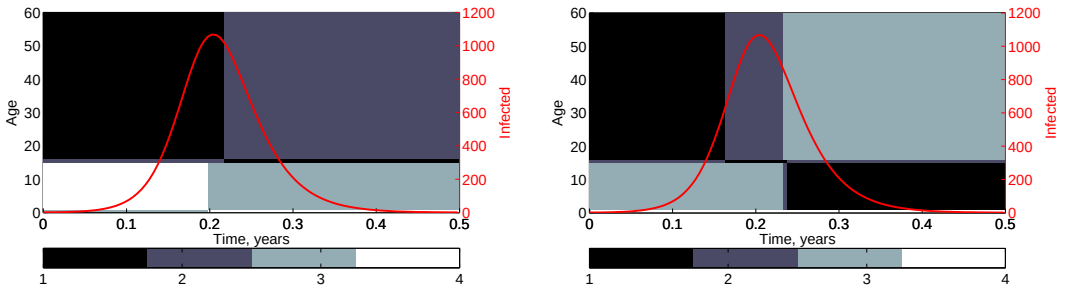

(a) (b)

Figure 3-7: (a) Ranking of those that provide the greatest source of infection over the initial epidemic (equation (3.66)), where one is the least important and four is the most important. (b) Ranking of those that receive the greatest amount of infection over the initial epidemic (equation (3.67)), where one is the least important and four is the most important. The initial age group of highest contact is $a^* = 0$. All other parameters are given in Table 3.1.

3.5.4 Summary

Implementing a step function as the contact rate has provided some interesting results. We have seen that at the endemic equilibrium there are potentially some age–dependent contact rates which produce similar seroprevalence profiles to the age–independent contact rate. However, if contacts are greatest amongst children or the older population then the seroprevalence profiles are different, with the wrong profile being chosen less than 2% of the time. At the peak of the initial epidemic we have seen that the probability of type I error is very small, indicating the seroprevalence profiles are quantifiably different under the age–dependent contact rate.

3.6 Results II: Normal function

3.6.1 At the endemic equilibrium

We again look at the probability of the type I error at the endemic equilibrium, this time with the contact rate modelled using the normal function (equation (3.70)). Figure 3-8(a) shows the seroprevalence profiles of the constant contact rate and three different age–dependent contact rates where the intensity of contacts (σ) is kept the same, but the age group with the maximum number of contacts is changed. All of the seroprevalence profiles increase with age, however the gradient of the curve is dependent on the varied parameter μ. For example, when $\mu = 15$ there is initially a steep increase in the seroprevalence which becomes shallower with age. In contrast to this, when

$\mu = 45$ the gradient of the curve appears to be fairly constant until it tails off for older age groups. The proportion of the population seroprevalent also varies, with a greater proportion of the population seroprevalent when the the highest contact rate is amongst the younger population. As before, we have ensured $R_0 \approx 2$ in each case.

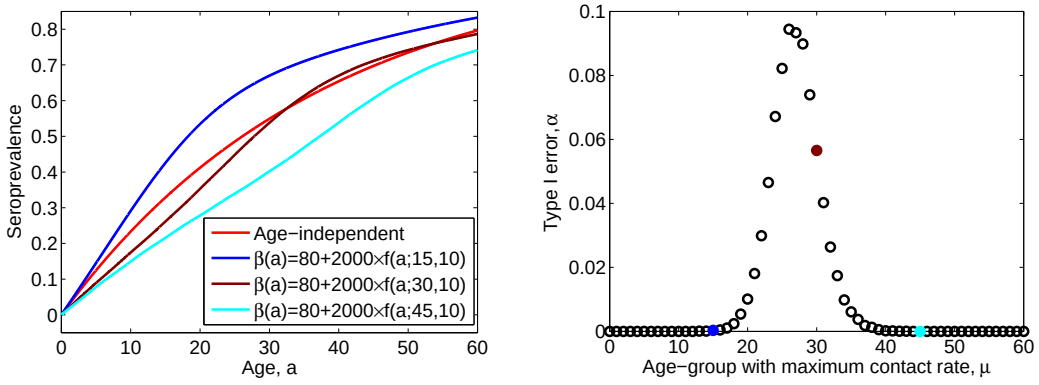

(a) (b)

Figure 3-8: (a) Seroprevalence profiles at the endemic equilibrium for the age–independent contact rate (red line, equation (3.68)) and the age–dependent normal function contact rate (equation (3.70)) where $\mu = 15$ (blue line), $\mu = 30$ (brown line) and $\mu = 45$ (light blue line). The intensity of contacts around μ is $\sigma = 10$ and $c_5 = 2000$. (b) The probability of type I error at the endemic equilibrium across the seroprevalence profiles as the age group which has the highest contact rate is increased. The colours represent the probability of type I error for the seroprevalence profiles given in figure 3-8(a). The intensity of contacts around μ is $\sigma = 10$, and c_5 is varied such that $R_0 \approx 2$. All other parameters are given in Table 3.1.

Figure 3-8(b) shows the probability of type I error as the age group who have the most contacts (μ) is increased. The intensity of contacts around μ is kept constant throughout, however c_5 is varied to ensure the basic reproductive number is 2. We see that when the maximum contact rate is highest amongst the younger or older population there is a very low chance of type I error. This means that the seroprevalence profiles at the endemic equilibrium are sufficiently different and hence it is easy to distinguish between them. The figure shows that the probability of type I error greatly increases when the maximum contact rate is between those aged 20–35, rising to nearly 10%. When considering the seroprevalence profiles it is unsurprising that it is for these ages that the probability of type I error increases, as the profiles look more similar (see $\mu = 30$ in figure 3-8(a)). However, looking at the contact rates themselves (see figure 3-4) we see it is for these age groups that the age–independent and age–dependent contact rates are more similar; the distribution of contacts in the age–dependent case

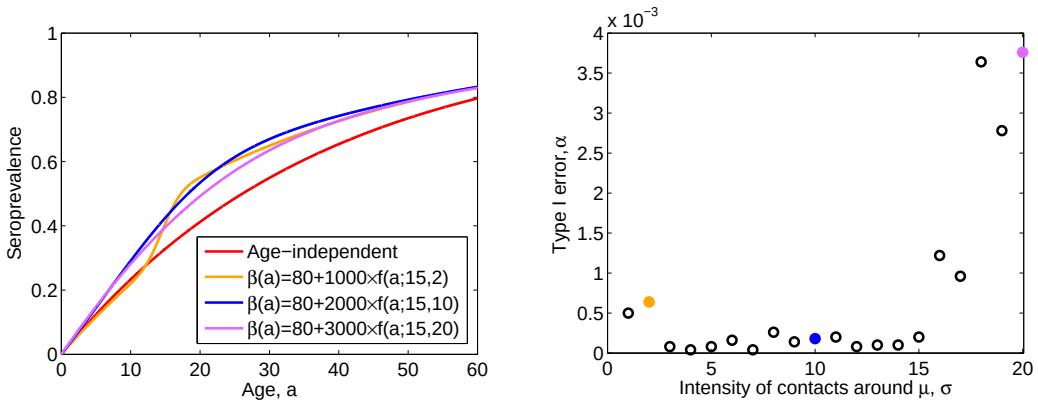

(a) (b)

Figure 3-9: (a) Seroprevalence profiles at the endemic equilibrium for the age–independent contact rate (red line, equation (3.68)) and the age–dependent normal function contact rate (equation (3.70)) where $\sigma = 2$ (yellow line), $\sigma = 10$ (blue line) and $\sigma = 20$ (purple line). The age group with the most contacts is $\mu = 15$. When $\sigma = 2$ $c_5 = 1000$, $\sigma = 10$ $c_5 = 2000$ and when $\sigma = 20$ $c_5 = 3000$. (b) The probability of type I error at the endemic equilibrium across the seroprevalence profiles as the intensity of contacts around μ is decreased (σ is increased). The colours represent the probability of type I error for the seroprevalence profiles given in figure 3-9(a). The age group with the most contacts is $\mu = 15$ and c_5 is varied such that $R_0 \approx 2$. All other parameters are given in Table 3.1.

above and below the constant contact rate is more even. It is interesting to note that the greatest α value is when $\mu = 26$. Due to the symmetry in the normal function and the maximum age being 60 we may expect to see the greatest type I error around 30, however this is not the case. The figure shows that when the age group with the highest contacts is between 20–40 it is harder to distinguish between the constant and age–dependent normal function seroprevalence profiles than for the other ages.

When considering the normal function there are two variables which we can change, and therefore we also examine the probability of type I error when the intensity of contacts around μ is varied. Figure 3-9(a) shows the seroprevalence profiles for the constant contact rate and three examples where the intensity of contacts around μ in the age–dependent contact rate changes. When the intensity of contacts is high (σ low) this produces many contacts around a given age group, and we can see that this causes a change to the seroprevalence profile. The seroprevalence profile resembles those for the step function (compare with figure 3-5); between the ages of 10 and 20 there is a greater increase in seroprevalence than for other age groups. This is because it is for these age groups where contacts are intensified, and for the other age groups the contact rate

is quite similar. The intense contacts mean seroprevalence is greater than otherwise would be seen. However, as the intensity of contacts decreases (σ increases), the normal function becomes flatter. Therefore contacts become more evenly distributed and hence the shape of the seroprevalence profiles tends to that of the constant function.

Figure 3-9(b) shows the probability of type I error at the endemic equilibrium as the intensity of contacts around μ is decreased (σ is increased). As the intensity of contacts is decreased there is initially a small decrease in the probability of type I error. As σ increases from 3 to 15 the probability of type I error stays relatively constant, after which time it increases more dramatically. Considering the scale, we can see that frequently the correct seroprevalence profile is chosen, and hence including age structure in the population affects the seroprevalence profiles. However, overall, as the intensity of contacts around μ decreases the distribution of the number of contacts of individuals increases, and hence the function flattens and starts to tend towards the constant, age–independent contact rate. Therefore the age–independent and age–dependent seroprevalence profiles become slightly harder to differentiate between. Decreasing the intensity of contacts further continues to increase the probability of type I error.

3.6.2 At the initial epidemic peak

Again it is possible to perform a similar analysis at the initial epidemic peak. Figure 3-10(a) shows the seroprevalence for different values of μ at the peak of the initial epidemic. As for the step function, the seroprevalence profiles are highly governed by the contact rate at the peak of the epidemic, as the time period to the peak is much shorter than the demographic dynamics.

Figure 3-10(b) shows the probability of type I error at the peak of the initial epidemic as the age group with the greatest average number of contacts (μ) is increased. We see that there is a similar shape to at the endemic equilibrium (compare with figure 3-8(b)), however there is more variability in the type I error. Whilst there is an increase and then decrease as μ increases, it is not as ordered as at the endemic equilibrium. The probability of type I error at the peak of the initial epidemic is also much smaller than at the endemic equilibrium. This indicates that it is easier to distinguish between the seroprevalence profiles at the peak of the initial epidemic than it is at the endemic equilibrium.

Again we also consider how the intensity of contacts around a given age affects seroprevalence at the peak of the initial epidemic (figure 3-11(a)) and the corresponding type I error (figure 3-11(b)). As in the previous case the seroprevalence curves at the initial epidemic peak are highly influenced by the contact rate. We immediately see

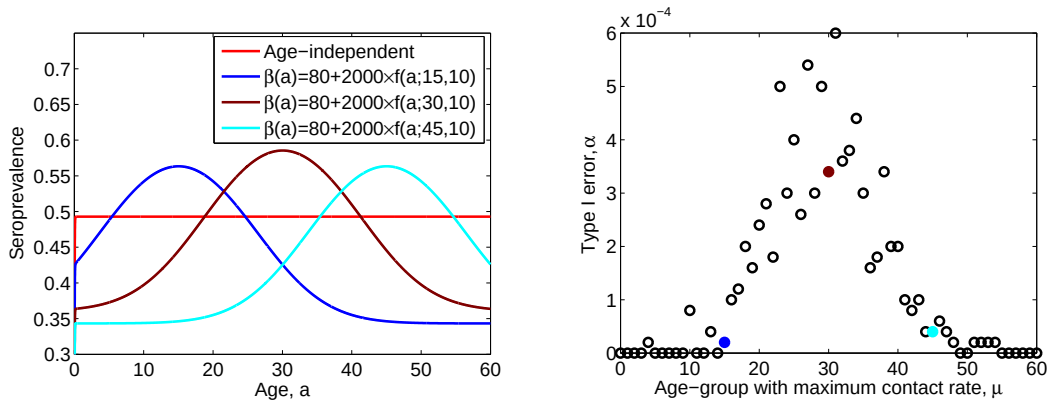

(a) (b)

Figure 3-10: (a) Seroprevalence profiles at the peak of the initial epidemic for the age–independent contact rate (red line, equation (3.68)) and the age–dependent normal function contact rate (equation (3.70)) where $\mu = 15$ (blue line), $\mu = 30$ (brown line) and $\mu = 45$ (light blue line). The intensity of contacts around μ is $\sigma = 10$ and $c_5 = 2000$. (b) The probability of type I error at the peak of the initial epidemic across the seroprevalence profiles as the age group which has the highest contact rate is increased. The colours represent the probability of type I error for the seroprevalence profiles given in figure 3-8(a). The intensity of contacts around μ is $\sigma = 10$ and c_5 is varied such that $R_0 \approx 2$. All other parameters are given in Table 3.1.

the effect this has on seroprevalence; when the intensity of contacts is high (σ low), seroprevalence is highly concentrated amongst certain ages. Decreasing the intensity of contacts causes the seroprevalence to become more uniform across the population. When examining the probability of type I error we see similar qualitative behaviour to at the endemic equilibrium (compare figure 3-11(b) with figure 3-9(b)). However, this time we only see an increase in the probability of type I error as the intensity of contacts around μ decreases. This is because as σ increases the shape of the seroprevalence profile becomes more similar to when the constant contact rate is implemented, making the profiles harder to differentiate between.

3.6.3 Source and recipients of infection

As when studying the step function, we are able to examine the source and recipients of infection over the course of the initial epidemic. For this we consider the age–dependent normal contact rate (equation (3.70)) with $\mu = 15$ and $\sigma = 10$. Figure 3-12(a) shows the rankings of the source of infection (calculated using equation (3.66)). We see that throughout the epidemic it is those with the higher contact rate who are the greatest source of infection. After the peak of the epidemic there is a minimal change and those

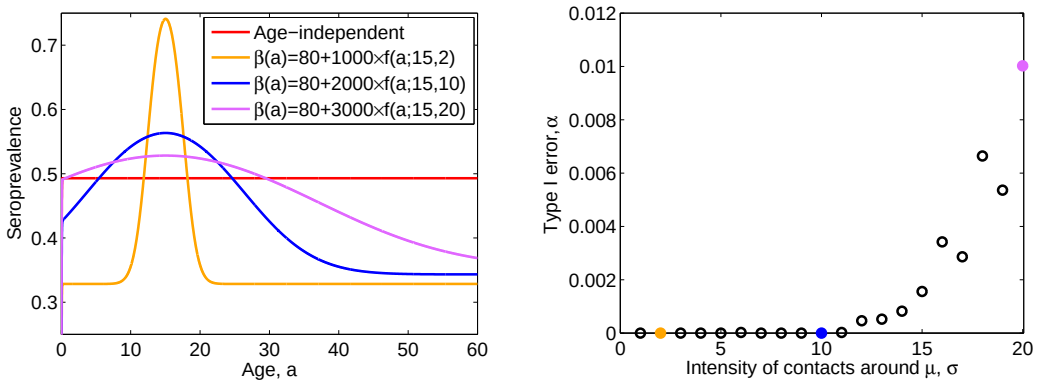

(a) (b)

Figure 3-11: (a) Seroprevalence profiles at the peak of the initial epidemic for the age–independent contact rate (red line, equation (3.68)) and the age–dependent normal function contact rate (equation (3.70)) where $\sigma = 2$ (yellow line), $\sigma = 10$ (blue line) and $\sigma = 20$ (purple line). The age group with the most contacts is $\mu = 15$. When $\sigma = 2$ $c_5 = 1000$, $\sigma = 10$ $c_5 = 2000$ and when $\sigma = 20$ $c_5 = 3000$. (b) The probability of type I error at the peak of the initial epidemic across the seroprevalence profiles as the intensity of contacts around μ is decreased (σ is increased). The colours represent the probability of type I error for the seroprevalence profiles given in figure 3-9(a). The age group with the most contacts is $\mu = 15$ and c_5 is varied such that $R_0 \approx 2$. All other parameters are given in Table 3.1.

aged around ten become the main source of infection. However, the main and least sources of infection do not change significantly over the course of the epidemic.

In contrast to this, the main recipients of infection (calculated using equation (3.67), figure 3-12(b)) do change over the course of the epidemic. Initially it is those with the highest contact rate who are the main recipients of infection. After the epidemic peak there is a wave and the main recipients of infection change. As time continues those with slightly lower contact rates become the main recipients of infection, as those with the highest contact rates are now immune. This is because the duration of infection is small in comparison to life expectancy. Therefore, shortly after the peak of the epidemic those aged 15 become the individuals who are experiencing the least infection. As the epidemic draws to a close those aged 59–60 are receiving the most infections; importance decreases with age until 15–16, and then begins to increase again. It is important to remember in figures 3-12(a) and (b) that it is the rank we are considering. Therefore although at the end of the epidemic it is those aged 59–60 who are receiving the most infection, there are not as many infected individuals as at the start of the epidemic when those aged 15–16 are the most important.

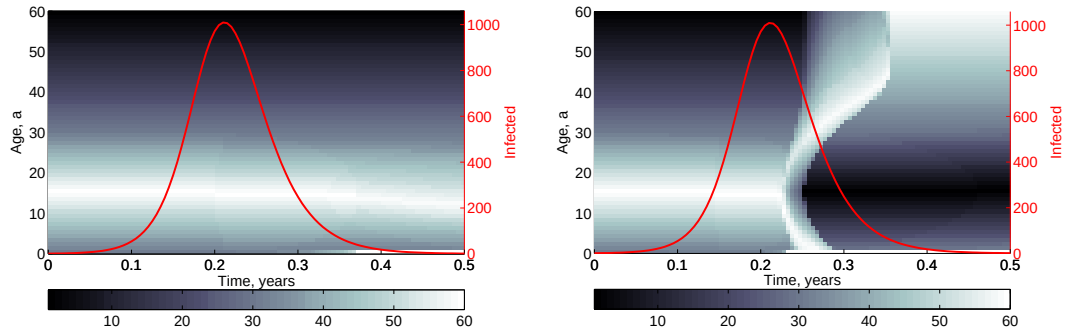

(a) (b)

Figure 3-12: (a) Ranking of those that provide the greatest source of infection over the initial epidemic (equation (3.66)), where one is the least important and 60 is the most important. (b) Ranking of those that receive the greatest amount of infection over the initial epidemic (equation (3.67)), where one is the least important and 60 is the most important. The age group with the maximum contacts is $\mu = 15$ and the intensity of contacts around μ is $\sigma = 10$ with $c_5 = 2000$. All other parameters are given in Table 3.1.

3.6.4 Summary

Implementing the normal function as the age–dependent contact rate has provided different results depending on which parameter in the contact rate we have changed. Increasing the average age of the individuals with most contacts has the same effect at both the endemic equilibrium and the peak of the initial epidemic. There is initially an increase in the probability of type I error, followed by a decrease. However, we find that the probability is much smaller at the peak of the initial epidemic than at the endemic equilibrium. This means that the seroprevalence profiles are easier to differentiate between at the peak of the initial epidemic than the endemic equilibrium, indicating that it is initially important to know whether there is age–dependent contact in the population.

Decreasing the intensity of contacts around a given age group also produced similar results at the endemic equilibrium and at the peak of the initial epidemic, with the probability of type I error increasing as the intensity of contacts around μ decreases. However, in contrast to the previous case, the probability of type I error is higher at the peak of the initial epidemic than at the endemic equilibrium. This indicates that it is easier to differentiate between the seroprevalence profiles at the endemic equilibrium as the intensity of contacts decreases. These results together indicate that the distribution of contacts is highly relevant in determining any differences in seroprevalence profiles

if implementing an age–dependent contact rate.

Throughout the epidemic it is those that have the majority of contacts who are the main source of infection. What is interesting to note is that this is the case even when, after the initial epidemic peak, they are no longer the main recipients of infection. After the peak of the initial epidemic, those who have less contacts become more important, becoming the main recipients of infection.

3.7 Discussion

Age structure has been included in the transmission term when modelling infectious diseases such as cholera (Alexanderian et al., 2011), tuberculosis (Aparicio and Castillo-Chavez, 2009), measles (Schenzle, 1984) and dengue (Cochran and Xu, 2014; Mello and Castilho, 2014). There is much theory on how age structure can be included in models (Anderson and May, 1991; Hethcote, 2000; Thieme, 2001). However, there is little, if any, literature on quantifying the differences that we can see in dynamics when age–independent and age–dependent contact rates are included in models. Therefore we have focussed on implementing methods to quantify the differences in age structured models with age–independent and age–dependent contact rates. We have considered the endemic equilibrium and the peak of the initial epidemic, however the methods could be implemented at any reasonable time point.

When a step contact rate is implemented we see qualitatively and quantitatively different results at the peak of the initial epidemic and at the endemic equilibrium. At the peak of the initial epidemic there is a relatively constant probability of type I error for all ages, which is very low. This means that the seroprevalence profiles are easier to differentiate between and therefore more different from each other. In contrast, at the endemic equilibrium as the age group which initially has the highest contact rate is increased the probability of type I error increases and then decreases. Although at the tails the probability of type I error is low, for medium ages the type I error can reach nearly 18%. This means that it is easier to distinguish between the seroprevalence profiles at the initial epidemic than at the endemic equilibrium.

We see different results when implementing the normal contact rate, particularly at the peak of the initial epidemic where we no longer see linearity in the probability of type I error. Instead, the qualitative behaviour of the type I error is more similar to at the endemic equilibrium where there is an increase and then decrease in the probability of type I error as the age group with the maximum number of contacts varies. However, quantitatively the results differ, showing that where in the course of infection we are interested in affects how readily we can differentiate between age–

independent and age–dependent contact rates. A small type I error indicates that the seroprevalence profiles are dissimilar and therefore easier to differentiate between. At both the endemic equilibrium and the peak of the initial epidemic it is easier to differentiate the seroprevalence profiles if younger or older individuals have the most contacts. At the endemic equilibrium the probability of type I error is much higher than at the peak of the initial epidemic meaning the seroprevalence profiles are more similar. Therefore inclusion of an age–dependent contact rate in a model may be influenced by whether we are interested in short– or long–term dynamics.

We also see qualitatively similar behaviour at the endemic equilibrium and peak of the initial epidemic when the intensity of contacts around a given age group is changed. In contrast to varying the age group with the most contacts, the seroprevalence profiles are more similar at the initial epidemic peak than at the endemic equilibrium. In this case it is therefore not only the short–term dynamics that are affected by an age–dependent contact rate, but the long–term dynamics too.

The results for both age–dependent contact rates indicate the importance of which age groups have the highest contact rate. When the intensity of contacts around a given age group is kept constant, we see that at the endemic equilibrium the type I error is correlated with the age group(s) with the most contacts. This is also true at the peak of the initial epidemic where type I error is very low and hence seroprevalence has been highly affected by the contact rates.

When considering the main sources and recipients of infections we see similar results for both the step and normal functions. The trends can be seen more readily in the normal function results as the discrete step function creates boundaries which have slightly different conditions. The main source of infection is the age group with the highest number of contacts. This helps to explain why measures such as closing schools can be effective (Hens et al., 2009) for certain infectious diseases. The main recipients of infection change throughout the epidemic. Initially the age group with the highest number of contacts are the main recipients. However, as individuals start to recover from infection other age groups become more dominant in receiving infection. Therefore the main recipients of infection become those who have less contacts as the epidemic progresses. This means that any control programmes may need to take this into account as the optimal age group to target over time may vary.

For a simple SIR PDE model we have shown that it is possible to differentiate between given seroprevalence profiles at the peak of the initial epidemic and at the endemic equilibrium. The same analysis could also be used at other times during the course of infection. The results show that we can see a difference in the seroprevalence profiles when age–independent and age–dependent contact rates are implemented. The

amount of difference we can see can change in the short– and long–term, potentially impacting on any control strategies.

We have reviewed literature showing indicators of age structure in the contact rate for dengue. In this chapter we have implemented a single serotype model to investigate the methodology we wish to use to determine differences in seroprevalence profiles. In Chapter 4 we will extend the model for dengue by implementing two serotypes. We quantify the differences in the seroprevalence profiles for one serotype and total seroprevalence as not only the contact rate is changed, but also other prominent parameters in the model.

CHAPTER 4

AGE STRUCTURE IN THE TWO–SEROTYPE DENGUE MODEL

Summary

In this chapter we extend and combine ideas from Chapters 2 and 3. We implement our new framework for the two–serotype model for dengue where certain individuals are predisposed to an enhanced secondary infection while others are not (see Chapter 2) in a partial differential equation setting for age. We then use the preliminary work in Chapter 3 to study age structure in this two–serotype model for dengue. To do this we initially consider how best to include vectors in our age structured model. We then implement likelihood analysis at the endemic equilibrium and under two sets of initial conditions at the peak of the initial epidemic. We conclude that age–dependent transmission can have a significant impact on seroprevalence profiles seen and can interact with the enhancement parameters associated with secondary infections. The initial composition of the population also affects the probability of type I error. Therefore age–dependence is important to include in a model if we wish to understand the impact of age structure on transmission and subsequent seroprevalence in the population.

4.1 Introduction

We now extend the likelihood work introduced in Chapter 3 by incorporating two serotypes of dengue in the model. As stated in Chapter 2, secondary dengue infections

can give rise to antibody–dependent enhancement (ADE) (Sabin, 1952; Wearing and Rohani, 2006; Guzman and Vazquez, 2010), where secondary infections can be more severe. Therefore by modelling two serotypes we can include mechanisms such as this which are applicable to dengue. We use the model framework described in Chapter 2 to separate the population into those that have a predisposition to an enhanced secondary infection and those that do not.

There is growing evidence to suggest that incorporating age structure into models for dengue is applicable. Pongsumpun and Tang (2001) show incidence reports for different age–groups during the 1998 DHF epidemic for three different provinces in Thailand. These all indicate the need for age structure as incidence increases and then decreases as age increases. Kongsomboon et al. (2004) studied age, time and birth cohorts and determined that the age–group at greatest risk in Bangkok, Thailand was 5–9 year olds. In contrast to this in other areas of Thailand, Thai et al. (2011) found that the median age of dengue fever patients in primary infection was 12 years and secondary infections was 20 years. This was using age–specific seroprevalence data and a community longitudinal study. This is complemented by epidemiological data for Thailand which shows that the mean age of DHF patients has steadily risen between 1980 and 2004 (Nagao and Koelle, 2008). Balmaseda et al. (2006) found that in a cohort of schoolchildren from Nicaragua, over two years seroprevalence for DENV antibodies increased from 75% to 100% in children aged from 4 to 16. Dengue can also affect infants; a study in Thailand considering data from 1988–1995 showed that out of 995 0–15 year olds diagnosed with dengue, 7.7% were aged 0–2 (Pancharoen and Thisyakorn, 2001). Halstead et al. (2002) found infant DHF/DSS accounted for 4.6–5% of infants and children hospitalized in Thai, Vietnamese, Myanmar and Indonesian children and infants. They also found differences in observed age–distribution curves for hospitalization of DHF/DSS cases in children; in Yangon the modal age was 4 whilst in Bangkok this was 8.

The above indicates that a model which includes age structure will allow us to incorporate observed epidemiological patterns. This can then help to indicate differences that may occur in the epidemic trajectory and at the equilibrium due to the age–dependence in the model, helping to further understand the disease dynamics for dengue. Although there are many different models for dengue which include attributes associated with the virus, there is less modelling which includes age structure. Pongsumpun and Tang (2001) separate the population into different age–groups and use N ODEs for each immune status compartment to model age structure. They determine that age–dependence should be implemented for predicted incidence rates to be similar to DHF incidence seen in empirical data during the epidemic in Thailand in 1998.

Following on from this, Pongsumpun and Tang (2003) use only two ODEs for each immune status compartment, separating the population into juveniles and adults, and perform stability analysis of the model. Using numerical simulations they show that age structure can affect the underlying dynamics of the model including periodicity and stability analysis. Supriatna et al. (2008) also use a two age–class model and examine the effect of vaccination. By including different effects of the vaccine depending on whether an individual is healthy or is asymptomatic they find that including age structure affects standard results regarding how vaccination should be implemented. A further approach, used by Ferguson et al. (1999b), is implementing PDEs to model age structure. They use parameter estimation to evaluate their model, using age as an indicator of serological patterns. More recently Mello and Castilho (2014) used a time discrete age structured model to show how an estimate for the basic reproductive number (R_0) can be found using age–distributions for the different immune status compartments. They implement the model to find R_0 for an area in Brazil where they had access to dengue serological data. Similarly, work on age structure PDE models has recently been implemented for dengue. Cochran and Xu (2014) include age structure in both the host and vector populations, and find four scenarios which they analyse; the vector dies out, the vector population flourishes and disease is rife, both host and vector survive but disease dies out, and an equilibrium solution where disease is present. Their work shows how changes to parameters can affect the dynamics of the model. Therefore knowledge of age structure and the disease dynamics are vital to understanding and correctly interpreting results. These show some of the ways that age structure has been included in models for dengue already, and the subsequent impact it can have.

As in Chapter 3 whilst we can find examples of age structure for dengue, there is little research examining the differences in models which include age–independent and age–dependent contact rates. Whilst in the previous chapter a host–only model was implemented and therefore contacts themselves can be measured, in this case the mosquito becomes more important as the transmitter of infection. There are, however, areas where vectors are more likely to flourish such as by stagnant water (World Health Organisation, 2014a). If these are, for example, near schools or offices then certain age–groups may be more likely to be bitten by a mosquito, and hence there is greater chance of infection. Therefore understanding age structure in vector borne diseases is also important. We therefore implement a continuous time–age partial differential equation (PDE) system to model the dynamics of a two–serotype model for dengue. We perform a similar analysis to that of Chapter 3 on the model to attempt to determine if we can easily differentiate between age–independent and age–dependent transmission.

This will allow us to understand its importance in affecting seroprevalence and hence its effect on the model. We will also consider how the age–dependence interacts with other parameters in the model which are vital to modelling the attributes associated with dengue, such as ADE. This will allow us to understand not only the importance of age–dependence, but also of the mechanisms of dengue and their interactions.

4.2 Preliminary work I: Single serotype host–vector model

4.2.1 The model

In the previous chapter we implemented ideas to differentiate between age–independent and age–dependent contact rates in seroprevalence profiles. However dengue is not spread via person to person contact. Therefore, we initially extend the model to include the vector population and determine any differences this may make. The host and vector populations can be defined by the states susceptible hosts (S), actively infected hosts (I), recovered hosts (R), susceptible vectors (S_V) and actively infected vectors (I_V). We include age structure in the host population only. Therefore the model equations for the host are given by

$$\begin{aligned}
\frac{\partial S}{\partial a} + \frac{\partial S}{\partial t} &= -\left(\lambda_V(a,t) + \delta(a)\right) S(a,t), && \text{(4.1a)}\\
\frac{\partial I}{\partial a} + \frac{\partial I}{\partial t} &= \lambda_V(a,t)S(a,t) - (\gamma + \delta(a))I(a,t), && \text{(4.1b)}\\
\frac{\partial R}{\partial a} + \frac{\partial R}{\partial t} &= \gamma I(a,t) - \delta(a)R(a,t) && \text{(4.1c)}
\end{aligned}$$

with initial conditions

$$S(a,0) = S_0(a), \qquad I(a,0) = I_0(a), \qquad R(a,0) = R_0(a), \tag{4.2}$$

and boundary conditions

$$S(0,t) = \int_0^\infty \psi(a)N(a,t), \qquad I(0,t) = 0, \qquad R(0,t) = 0, \tag{4.3}$$

where $\delta(a)$ is the natural mortality rate of a host aged a, γ is the recovery rate of the hosts and $\lambda_V(a,t)$ is the force of infection exerted by the vector on a host aged a at time t. As in the previous chapter we assume the total population aged a at time t is $N(a,t)$ and we assume type I mortality (equation (3.24)). The model for the vector

population is given by

$$\frac{\mathrm{d}S_V}{\mathrm{d}t} = (\kappa P(t) - S_V(t))\delta_V - \lambda_H(t)S_V(t), \tag{4.4a}$$

$$\frac{\mathrm{d}I_V}{\mathrm{d}t} = \lambda_H(t)S_V(t) - \delta_V I_V(t), \tag{4.4b}$$

with initial conditions

$$S_V(0) = S_{V_0}, \qquad I_V(0) = I_{V_0}, \tag{4.5}$$

where δ_V is the mortality rate of the vector, $P(t) = \int_a N(\alpha, t)\mathrm{d}\alpha = \bar{P}$ is the total number of hosts at time t, κ is the average number of mosquitoes per person and $\lambda_H(t)$ is the force of infection exerted by the hosts on the vector at time t.

We note that the main difference in contact structure between the host–only model and host–vector model is down to the way that transmission occurs. In the host–only model transmission occurs through person to person contacts, and the number of contacts that different age groups have. In the host–vector model there is a transmission probability which depends on the bite rate of the mosquito and the probability of transmission given a bite between a host of a given age and the vector. Therefore, the force of infection exerted by the host population on the vectors ($\lambda_H(t)$) is given by

$$\lambda_H(t) = qb\frac{\int_0^L p(a)I(a,t)\mathrm{d}a}{\int_0^L p(a)N(a,t)\mathrm{d}a}, \tag{4.6}$$

where b is the biting rate of mosquitoes, q is the transmission probability given a bite, and the fraction term represents the probability a vector bites an infected host. This term is weighted by $p(a)$ which accounts for the fact that some age–groups are more attractive or exposed to mosquitoes than others. We call this the exposure weighting. The force of infection exerted by the vectors on hosts aged a ($\lambda_V(a,t)$) is the total number of infectious bites per unit time multiplied by the probability of being bitten at age a. We assume that the biting rate of susceptible mosquitoes is the same as those that are infected (Wearing and Rohani, 2006), and that the transmission probability from vector to host is the same as from host to vector (Newton and Reiter, 1992). Therefore if an individual is in age–group $(a + \delta a)$ we have

$$\lambda_V(a,t) = qbI_V(t)\frac{\int_a^{a+\delta a} p(\alpha)S(\alpha,t)\mathrm{d}\alpha}{\int_0^L p(\alpha)N(\alpha,t)\mathrm{d}\alpha}. \tag{4.7}$$

As $\delta a \to 0$ the integral in the numerator tends to zero, and hence to solve the system numerically we cannot use the continuous form. However, we can discretize the system as in the previous chapter, and let an individual be in age–group i, $i = 1, 2, \ldots, n$.

Then the force of infection for age–group i is

$$(\lambda_V(t))_i = qbI_V(t)\frac{\bar{p}_i\bar{S}_i(t)}{\sum_k \bar{p}_k\bar{N}_i(t)}, \tag{4.8}$$

where q and b are as in equation (4.6), and $\bar{p}_i$ is the exposure weighting of individuals in age–group i.

We use a splitting method to solve the PDE system for the host (see Chapter 3, Section 3.2.2), combined with a simple Euler scheme to solve the ODE system for the vector. As in Chapter 3 it is possible to solve the system at equilibrium. We use the next generation matrix and the dynamics close to the disease free equilibrium to find R_0 (see Appendix B.1). We ensure that R_0 is consistent when implementing the different forces of infection in the model to ensure the results are comparable.

For our tests we implement an age–independent and age–dependent exposure weighting. The age–independent exposure weighting is given by

$$p(a) = c_1 \ \forall a, \tag{4.9}$$

and the age–dependent exposure weighting is given by

$$p(a) = c_2 + c_3 f(a;\mu,\sigma), \tag{4.10}$$

where

$$f(a;\mu,\sigma) = \frac{1}{\sigma\sqrt{2\pi}}\exp\left(\frac{-(a-\mu)}{2\sigma^2}\right), \tag{4.11}$$

where c_1, c_2 and c_3 are varied to ensure that $R_0 \approx 2$. We set $c_2 = 0.67$ to allow a base level of transmission for all age–groups in the age–dependent case. We can then calculate the probability of type I error at the endemic equilibrium and peak of the initial epidemic. For the host model parameters are given in Table 3.1 in Chapter 3 and for the host–vector model the parameters are the same as those used later in the Chapter, given in Table 4.1.

4.2.2 Results

We compare the probability of type I error at the endemic equilibrium and peak of the initial epidemic under the host model with the normal function contact rate introduced in Chapter 3 and the host–vector model (equations (4.1)–(4.4)) above. It is important to note that although $R_0 \approx 2$ for both models, there is no attempt at this point to link the contact rate in the host model and the exposure weighting in the host–vector model. Rather, we are interested to see if the qualitative behaviour in the probability

of type I error is the same under both models.

Figure 4-1(a) shows the the probability of type I error at the endemic equilibrium as the age–group with the maximum contact/exposure rate is increased. We see that the qualitative behaviour in the probability of type I error is different; in the host model there is an increase and decrease in the type I error as the age–group with the maximum contact rate is increased. In contrast to this under the host–vector model the probability of type I error decreases, then increases to a peak before decreasing and then finally increasing again. At the peak of the initial epidemic (figure 4-1(b)) we again see different behaviour under the two models. When the host–vector model is implemented we see the inverse results to the host model; as the age–group which the maximum exposure rate is increased the type I error initially decreases and then increases for older ages.

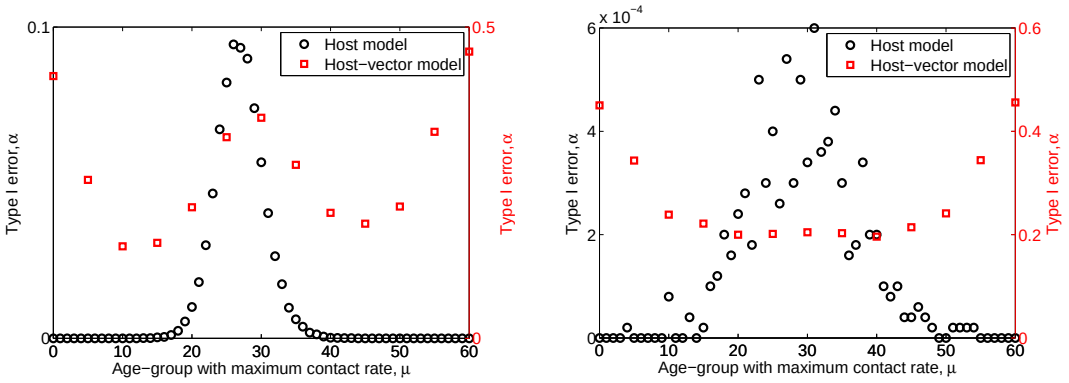

(a) (b)

Figure 4-1: Comparison of type I error under the host model (black circles) and host-vector model (red squares) when the age–group with the maximum contact rate is varied in the age–dependent model. In (a) we consider the endemic equilibrium and (b) the peak of the initial epidemic. For the host model parameters are given in Table 3.1 and for the host–vector model parameters are given in Table 4.1.

As when implementing the host model in Chapter 3 there are two variables which we can change. Figure 4-2(a) therefore shows the type I error at the endemic equilibrium as the intensity of contacts/exposure around μ is increased. Again, we see qualitatively different results at the endemic equilibrium under the two models. Whilst in the host–model as the intensity decreases (σ increases) the probability of type I error increases, under the host–vector model as the intensity decreases so too does the probability of type I error. At the peak of the initial epidemic the host–vector model shows a decrease in the probability of type I error followed by an increase. In contrast the host model simply shows an increase in the probability of type I error as intensity decreases.

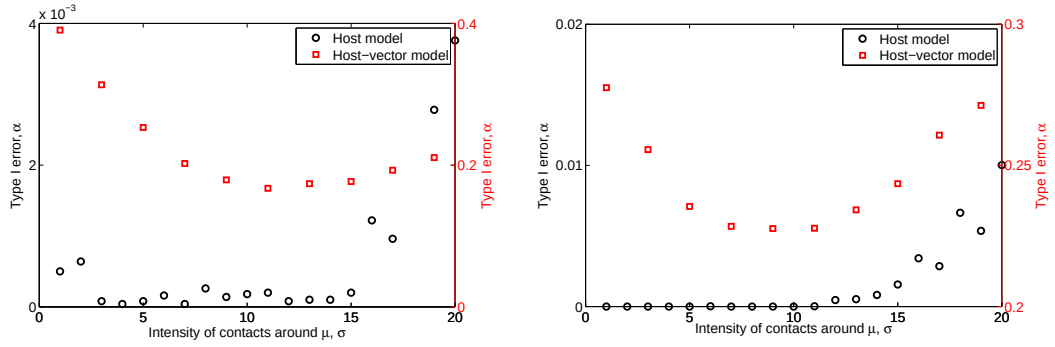

Figure 4-2: Comparison of type I error under the host model (black circles) and host-vector model (red squares) when the age–group with the maximum contact rate is varied in the age–dependent model. In (a) we consider the endemic equilibrium and (b) the peak of the initial epidemic. For the host model parameters are given in Table 3.1 and for the host–vector model parameters are given in Table 4.1.

4.2.3 Summary

The results show that there is a qualitative difference in the probability of type I error brought about by the inclusion of vectors in the model. Therefore, the vector plays an important role in the transmission of dengue. Although there are quantitative differences in the type I error, these have not been adjusted for in this Section. It is the qualitative differences which are important, and which indicate that vectors should be included in the analysis.

4.3 Preliminary work II: Comparison of R_0 in the host and host–vector model

As inclusion of the vector produced different probabilities of type I error at both the endemic equilibrium and the peak of the initial epidemic we need to include them in the model. However, the combined ODE–PDE host–vector model is more complex to implement than its PDE counterpart. In Section 4.2 we ensure $R_0 \approx 2$ in each model and considered the qualitative results. We now try to establish a relationship between the contact rate in the host model and the exposure weighting in the host–vector model so that vectors can implicitly be included in the model. As we have previously introduced both the host and host–vector models we will not do so again here. For reference see equations (3.59) in Section 3.4.1 of Chapter 3 for the host model and equations (4.1) and (4.4) in Section 4.2 for the host–vector model.

4.3.1 Next–generation matrix

Host model

In the age structured host model the force of infection is given by

$$\lambda(a,t) = \beta(a)\frac{\int_0^L \beta(\alpha)I(\alpha,t)\mathrm{d}\alpha}{\int_0^L \beta(\alpha)N(\alpha,t)\mathrm{d}\alpha}, \tag{4.12}$$

where $\beta(a)$ is the average number of people contacted per unit time by an individual aged a. We can discretize the PDE system to calculate the next–generation matrix close to the disease free equilibrium (see Section 3.3 in Chapter 3) to obtain

$$G_{\text{host}} = \frac{1}{\gamma}\begin{pmatrix} \frac{\beta_1 N_1 \beta_1}{\sum_k \beta_k N_k} & \frac{\beta_1 N_1 \beta_2}{\sum_k \beta_k N_k} & \cdots & \frac{\beta_1 N_1 \beta_n}{\sum_k \beta_k N_k} \\ \frac{\beta_2 N_2 \beta_1}{\sum_k \beta_k N_k} & \frac{\beta_2 N_2 \beta_2}{\sum_k \beta_k N_k} & \cdots & \frac{\beta_2 N_2 \beta_n}{\sum_k \beta_k N_k} \\ \vdots & \vdots & \ddots & \vdots \\ \frac{\beta_n N_n \beta_1}{\sum_k \beta_k N_k} & \frac{\beta_n N_n \beta_2}{\sum_k \beta_k N_k} & \cdots & \frac{\beta_n N_n \beta_n}{\sum_k \beta_k N_k} \end{pmatrix}, \tag{4.13}$$

where β_i is the discretized contact rate of age–group i. To find the basic reproductive number we then find the spectral radius of G_{host}.

Host–vector model

In the age structured host–vector model there are two force of infection terms; the force of infection exerted by the host on the vector ($\lambda_H(t)$) and the force of infection exerted by the vector on a host aged a ($\lambda_V(a,t)$). These are given by

$$\lambda_H(t) = b\frac{\int_0^L p(\alpha)I(\alpha,t)\mathrm{d}\alpha}{\int_0^L p(\alpha)N(\alpha,t)\mathrm{d}\alpha}, \tag{4.14a}$$

$$\lambda_V(a,t) = bI_V(t)\frac{\int_a^{a+\delta a} p(\alpha)S(\alpha,t)\mathrm{d}\alpha}{\int_0^L p(\alpha)N(\alpha,t)\mathrm{d}\alpha}, \tag{4.14b}$$

where b is the transmission probability given an infected bite (we have combined terms q and b from equation (4.8) for ease) and $p(a)$ is the exposure weighting of an individual aged a. Using the discretization discussed in Section 4.2 and Appendix B.1 the next–

generation matrix for the associated discrete model is given by

$$G_{\text{host-vector}} = \begin{pmatrix} 0 & 0 & \cdots & 0 & \frac{bp_1N_1}{\delta_V\sum_k p_kN_k} \\ 0 & 0 & \cdots & 0 & \frac{bp_2N_2}{\delta_V\sum_k p_kN_k} \\ \vdots & \vdots & \ddots & \vdots & \vdots \\ 0 & 0 & \cdots & 0 & \frac{bp_nN_n}{\delta_V\sum_k p_kN_k} \\ \frac{bp_1N_V}{\gamma\sum_k p_kN_k} & \frac{bp_2N_V}{\gamma\sum_k p_kN_k} & \cdots & \frac{bp_nN_V}{\gamma\sum_k p_kN_k} & 0 \end{pmatrix}, \tag{4.15}$$

where p_i is the discretized exposure weighting of age–group i. In this case we implement spectral analysis and R_0^2 is the dominant eigenvalue of the next–generation matrix.

4.3.2 The 2×2 case

We are trying to find a link between the basic reproductive number of the host and host–vector models so that the vector population can be included in the model implicitly. Therefore we need to find the dominant eigenvalue of each of the next generation matrices, and equate these to determine $\beta(a)$ in terms of $p(a)$. We will then test the models to ensure the results of the host and host–vector models are similar. We will start by assuming that the population is split into two age–groups ($k = 1, 2$).

Host model

Let ν_1, ν_2 be eigenvalues of G_{host} with $\nu_1 > |\nu_2|$, $\nu_1 > 0$ with associated eigenvectors $\mathbf{v}_1$, $\mathbf{v}_2$. We consider $\det(G_{\text{host}} - \lambda I)$ which is given by

$$\begin{aligned} \det(G_{\text{host}} - \nu I) &= \begin{vmatrix} \frac{\beta_1^2N_1}{\gamma\sum_k \beta_kN_K} - \nu & \frac{\beta_1\beta_2N_1}{\gamma\sum_k \beta_kN_k} \\ \frac{\beta_2\beta_1N_2}{\gamma\sum_k \beta_kN_K} & \frac{\beta_2^2N_2}{\gamma\sum_k \beta_kN_k} - \nu \end{vmatrix} && \text{(4.16a)} \\ &= \left\{ \left(\frac{\beta_1^2N_1}{\gamma\sum_k \beta_kN_k} - \nu \right) \left(\frac{\beta_2^2N_2}{\gamma\sum_k \beta_kN_k} - \nu \right) - \right. \\ &\qquad \left. \left(\frac{\beta_1^2\beta_2^2N_1N_2}{(\gamma\sum_k \beta_kN_k)^2} \right) \right\} && \text{(4.16b)} \\ &= \nu \left(\nu - \frac{\sum_k \beta_k^2N_k}{\gamma\sum_k \beta_kN_k} \right). && \text{(4.16c)} \end{aligned}$$

The eigenvalues are therefore $\nu_2 = 0$ or $\nu_1 = \frac{\sum_k \beta_k^2N_k}{\gamma\sum_k \beta_kN_k} = \text{tr}(G_{\text{host}})$. Therefore R_0 is given by

$$R_0 = \frac{\beta_1^2N_1 + \beta_2^2N_2}{\gamma(\beta_1N_1 + \beta_2N_2)}. \tag{4.17}$$

Host–vector model

We perform similar analysis on the host–vector model. In this case we have

$$\det(G_{\text{host–vector}} - \nu I) = \begin{vmatrix} -\nu & 0 & \frac{bp_1N_1}{\delta_V \sum_k p_k N_k} \\ 0 & -\nu & \frac{bp_2N_2}{\delta_V \sum_k p_k N_k} \\ \frac{\kappa bp_1 \sum_k N_k}{\gamma \sum_k p_k N_k} & \frac{\kappa bp_2 \sum_k N_k}{\gamma \sum_k p_k N_k} & -\nu \end{vmatrix}. \tag{4.18}$$

The elements in the numerators in the third row are found using the fact that $N_V(t) = \kappa P(t) = \kappa \sum_{k=1}^{2} N_k$ where $P(t)$ is the total host population size as previously defined. We perform elementary row and column operations on matrix (4.18) to move the bottom row to the top and the right most column to the left meaning

$$\begin{aligned}
\det(G_{\text{host–vector}} - \nu I) &= \begin{vmatrix} -\nu & \frac{\kappa bp_1 \sum_k N_k}{\gamma \sum_k p_k N_k} & \frac{\kappa bp_2 \sum_k N_k}{\gamma \sum_k p_k N_k} \\ \frac{bp_1N_1}{\delta_V \sum_k p_k N_k} & -\nu & 0 \\ \frac{bp_2N_2}{\delta_V \sum_k p_k N_k} & 0 & -\nu \end{vmatrix} && \text{(4.19a)} \\
&= (-\nu)\begin{vmatrix} -\nu & 0 \\ 0 & -\nu \end{vmatrix} - \frac{\kappa bp_1 \sum_k N_k}{\gamma \sum_k p_k N_k}\begin{vmatrix} \frac{bp_1N_1}{\delta_V \sum_k p_k N_k} & 0 \\ \frac{bp_2N_2}{\delta_V \sum_k p_k N_k} & -\nu \end{vmatrix} + \\
&\qquad \frac{\kappa bp_2 \sum_k N_k}{\gamma \sum_k p_k N_k}\begin{vmatrix} \frac{bp_1N_1}{\delta_V \sum_k p_k N_k} & -\nu \\ \frac{bp_2N_2}{\delta_V \sum_k p_k N_k} & 0 \end{vmatrix} && \text{(4.19b)} \\
&= (-\nu)^3 - \frac{\kappa b \sum_k N_k}{\gamma \sum_k p_k N_k}\left(p_1\left(\frac{bp_1N_1}{\delta_V \sum_k p_k N_k}\right)(-\nu) - \right. \\
&\qquad \left. p_2\left(-\frac{bp_2N_2}{\delta_V \sum_k p_k N_k}\right)(-\nu)\right) && \text{(4.19c)} \\
&= (-\nu)^3 - \frac{\kappa b^2 \sum_k N_k \sum_k p_k^2 N_k}{\gamma \delta_V (\sum_k p_k N_k)^2}(-\nu). && \text{(4.19d)}
\end{aligned}$$

The eigenvalues are therefore $\nu = 0$ or

$$(-\nu)^2 = \frac{\kappa b^2 \sum_k N_k \sum_k p_k^2 N_k}{\gamma \delta_V (\sum_k p_k N_k)^2}. \tag{4.20}$$

As the dominant eigenvalue is $\sqrt{R_0}$ we therefore have that

$$R_0 = \frac{\kappa b^2 \sum_k N_k (p_1^2 N_1 + p_2^2 N_2)}{\gamma \delta_V (p_1 N_1 + p_2 N_2)^2}. \tag{4.21}$$

Equating R_0

In both the host and host–vector models we want R_0 to be equal. By finding a constant c which links the basic reproductive number for the host–only and host–vector model, then we can potentially include vectors implicitly in the host–only model. This will make the model simpler and therefore easier to work with in the following analysis. However, the vector dynamics will still be included in the model which we have shown to be important in Section 4.2. Therefore we let $\beta_1 = cbp_1$ and $\beta_2 = cbp_2$ where $c \in \mathbb{R}^+$. We substitute these into equation (4.17) and equate this to equation (4.21) to find

$$\frac{(cbp_1)^2 N_1 + (cbp_2)^2 N_2}{\gamma((cbp_1)N_1 + (cbp_2)N_2)} = \frac{\kappa b^2 \sum_k N_k (p_1^2 N_1 + p_2^2 N_2)}{\gamma \delta_V (p_1 N_1 + p_2 N_2)^2} \tag{4.22a}$$

$$c\left(\frac{b(p_1^2 N_1 + p_2^2 N_2)}{\gamma(p_1 N_1 + p_2 N_2)}\right) = \frac{\kappa b \sum_k N_k}{\delta_V (p_1 N_1 + p_2 N_2)} \frac{b(p_1^2 N_1 + p_2^2 N_2)}{\gamma(p_1 N_1 + p_2 N_2)}. \tag{4.22b}$$

Hence

$$c = \frac{\kappa b \sum_k N_k}{\delta_V (p_1 N_1 + p_2 N_2)}. \tag{4.23}$$

Therefore if the population is split into two age–groups we have found a constant c needed to equate the host and host–vector models in terms of their R_0 values. We now extend this to when the population is separated into n age–groups.

4.3.3 The $n \times n$ case

Host model

For the $n \times n$ case we have

$$\begin{aligned} G_{\text{host}} &= \frac{1}{\gamma} \begin{pmatrix} \frac{\beta_1 N_1 \beta_1}{\sum_k \beta_k N_k} & \frac{\beta_1 N_1 \beta_2}{\sum_k \beta_k N_k} & \cdots & \frac{\beta_1 N_1 \beta_n}{\sum_k \beta_k N_k} \\ \frac{\beta_2 N_2 \beta_1}{\sum_k \beta_k N_k} & \frac{\beta_2 N_2 \beta_2}{\sum_k \beta_k N_k} & \cdots & \frac{\beta_2 N_2 \beta_n}{\sum_k \beta_k N_k} \\ \vdots & \vdots & \ddots & \vdots \\ \frac{\beta_n N_n \beta_1}{\sum_k \beta_k N_k} & \frac{\beta_n N_n \beta_2}{\sum_k \beta_k N_k} & \cdots & \frac{\beta_n N_n \beta_n}{\sum_k \beta_k N_k} \end{pmatrix} \\ &= \frac{1}{\gamma \sum_k \beta_k N_k} \begin{pmatrix} \beta_1 N_1 \\ \beta_2 N_2 \\ \vdots \beta_n N_n \end{pmatrix} \begin{pmatrix} \beta_1 & \beta_2 & \cdots & \beta_n \end{pmatrix} = \mathbf{c}\mathbf{b}^\intercal. \end{aligned} \tag{4.24}$$

To find the basic reproductive number we again need to find the dominant eigenvalue. When finding the eigenvalues we know that

$$\mathbf{c}\mathbf{b}^\intercal \mathbf{v} = \lambda \mathbf{v} \tag{4.25}$$

Therefore we have

$$\mathbf{c}\mathbf{b}^{\mathsf{T}}\mathbf{v} = \sum_i \beta_i v_i \mathbf{c} = \lambda \mathbf{v} \tag{4.26}$$

Therefore $\mathbf{v} = \alpha\mathbf{c}$. Without loss of generality $\mathbf{v} = \mathbf{c}$ and

$$\lambda = \sum_i \beta_i c_i = \frac{\sum_i \beta_i^2 N_i}{\gamma \sum_k \beta_k N_k} (= R_0) \tag{4.27}$$

Therefore the basic reproductive number is given by $R_0 = \lambda$.

Host–vector model

For the host–vector model the first n rows of the next generation matrix have one element in each which we will call $r_1, r_2, \ldots, r_n$ and the columns $s_1, s_2, \ldots s_n$ where

$$r_i = \frac{bp_i N_i}{\delta_V \sum_k p_k N_k}, \qquad s_i = \frac{\kappa b p_i \sum_k N_k}{\gamma \sum_k p_k N_k}. \tag{4.28}$$

Therefore we have

$$\det(G_{\text{host–vector}} - \nu I) = \begin{vmatrix} -\nu & 0 & \cdots & 0 & r_1 \\ 0 & -\nu & \cdots & 0 & r_2 \\ \vdots & \vdots & \ddots & \vdots & \vdots \\ 0 & 0 & \cdots & -\nu & r_n \\ s_1 & s_2 & \cdots & s_n & -\nu \end{vmatrix}. \tag{4.29}$$

We initially make two row/column operations meaning that the determinants of the matrices are still identical; we move the bottom row of the matrix to the top and the right most column of the matrix to the left. Therefore the determinant is equivalent

to

$$\begin{aligned}
\begin{vmatrix} -\nu & s_1 & s_2 & \cdots & s_n \\ r_1 & -\nu & 0 & \cdots & 0 \\ r_2 & 0 & -\nu & \cdots & 0 \\ \vdots & \vdots & \vdots & \ddots & \vdots \\ r_n & 0 & 0 & \cdots & -\nu \end{vmatrix} &= (-1)^2(-\nu)\begin{vmatrix} -\nu & 0 & \cdots & 0 \\ 0 & -\nu & \cdots & 0 \\ \vdots & \vdots & \ddots & \vdots \\ 0 & 0 & \cdots & -\nu \end{vmatrix} + (-1)^3 s_1 \begin{vmatrix} r_1 & 0 & \cdots & 0 \\ r_2 & -\nu & \cdots & 0 \\ \vdots & \vdots & \ddots & \vdots \\ r_n & 0 & \cdots & -\nu \end{vmatrix} + \\
&\quad (-1)^4 s_2 \begin{vmatrix} r_1 & -\lambda & \cdots & 0 \\ r_2 & 0 & \cdots & 0 \\ \vdots & \vdots & \ddots & \vdots \\ r_n & 0 & \cdots & -\nu \end{vmatrix} + \cdots + (-1)^{n+2} s_n \begin{vmatrix} r_1 & -\nu & \cdots & 0 \\ r_2 & 0 & \cdots & 0 \\ \vdots & \vdots & \ddots & \vdots \\ r_n & 0 & \cdots & 0 \end{vmatrix} \\
&= (-1)^2(-\nu)(\nu)^n + (-1)^3 s_1 (-1)^2 r_1 (-\nu)^{n-1} + (-1)^3 s_2 (-1)^2 r_2 (-\nu)^{n-1} \\
&\quad + \cdots + (-1)^{n+2} s_n (-1)^{n+1} r_n (-\nu)^{n-1} \\
&= (-\nu)^{n-1}\left((-\nu)^2 - \sum_k s_k r_k\right).
\end{aligned}$$

This means that R_0 is given by

$$R_0 = \sum_k s_k r_k = \frac{\kappa b^2 \sum_k N_k \sum_k p_k^2 N_k}{\gamma \delta_V (\sum_k p_k N_k)^2}. \tag{4.31}$$

Equating R_0

Following the same procedure as for the 2×2 example, we let $\beta_i = cbp_i$ ($i = 1, 2, \ldots, n$, $c \in \mathbb{R}^+$). Equating equations (4.27) and (4.31) we find that the constant is formed of the same elements as in the case where $n = 2$, namely

$$c = \frac{\kappa b \sum_k N_k}{\delta_V \sum_k p_k N_k}. \tag{4.32}$$

We now test this result to ensure that we get similar results when implementing $p(a)$ into the host–vector model and $\beta(a) = cbp(a)$ in the host model.

4.3.4 Results

Figure 4-3 shows the probability of type I error at the endemic equilibrium (figures 4-3(a) and (b)) and at the peak of the initial epidemic (figures 4-3(c) and (d)) when varying parameters within the exposure weighting term $p(a)$ (equation (4.10)). At the endemic equilibrium the two models provide results which are both qualitatively and quantitatively similar. As the age–group which has the maximum exposure to mosquitoes is increased (figure 4-3(a)) the maximum absolute value between any two corresponding points is 0.0207. However, for some ages the difference is much smaller.

When decreasing the intensity of contacts around $\mu = 15$ (increasing σ, figure 4-3(b)) we find that the maximum absolute value between any two corresponding points is 0.0069. Therefore at the endemic equilibrium the host model with the adjusted contact rate is a good approximation to the host–vector model.

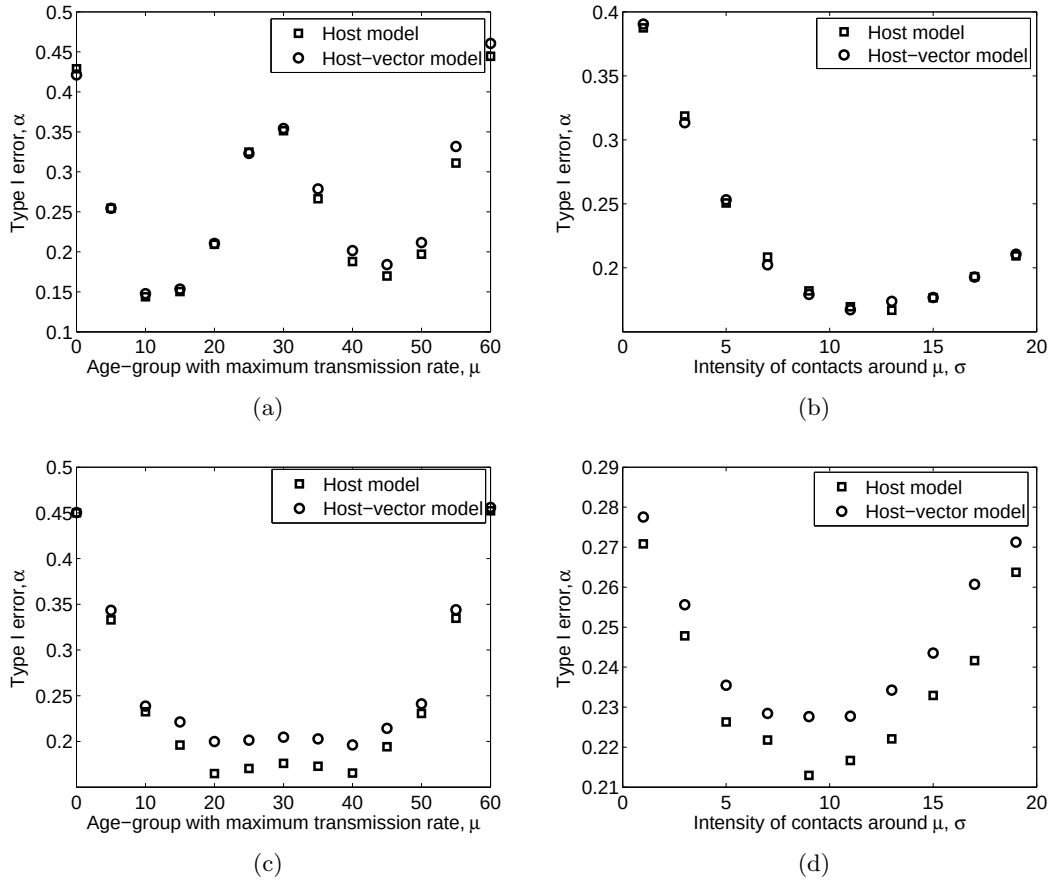

Figure 4-3: (a) Type I error at the endemic equilibrium as the age–group with the maximum contact/exposure rate is increased. (b) Type I error at the endemic equilibrium as the intensity of contacts/exposure around $\mu = 15$ is decreased (σ increased). (c) Type I error at the peak of the initial epidemic as the age–groups with the maximum contact/exposure rate is increased. (d) Type I error at the peak of the epidemic as the intensity of contacts/exposure around $\mu = 15$ is decreased (σ increased). In all figures the type I error for the host model is shown by squares and for the host–vector model by circles. For the host model parameters are given in Table 3.1 with $\beta(a)$ given in equation 3.70 in Chapter 3. For the host–vector model parameters are given in Table 4.1 with $p(a)$ given in equation (4.10).

At the peak of the initial epidemic the probability of type I error for the host–model is slightly less than it is for the host–vector model. This is true both as the age–group

with the maximum exposure weighting is increased (figure 4-3(c)) and the intensity of contacts around $\mu = 15$ is decreased (σ increased, figure 4-3(d)). In the former the maximum absolute value between any two corresponding points is 0.0350, and in the latter the maximum absolute value between any two corresponding points is 0.0191.

4.3.5 Summary

Overall, the difference between the host and host–vector models is greater at the initial epidemic peak than at the endemic equilibrium. This is likely to be because although the force of infections are now equal, the inclusion of vectors in the model will mean that the composition of the population is slightly different. This will have more of an effect at the peak of the initial epidemic than at the endemic equilibrium. However, these results indicate that by adjusting the contact rate in the host–only model to implicitly include the vector population we can obtain similar results to when the vector is modelled explicitly. This helps to simplify the model we are dealing with and our subsequent analysis.

4.4 The model and methodologies

4.4.1 Two serotype host–vector model

We now consider the two–serotype host–vector model, shown in figure 4-4. An individual can be susceptible to both serotypes (S_0), actively infected with primary infection of serotype i (I_i), have homologous immunity to serotype i and susceptible to serotype j with an enhanced or protected secondary infection (S_i^E, S_i^P), be actively infected with serotype j having previously been infected with serotype i with an enhanced or protected secondary infection ($I_{i,j}^E, I_{i,j}^P$) or recovered from both serotypes (R). A vector can be susceptible to both serotypes (S_V) or actively infected with serotype i (I_{Vi}). We assume no co-infection in either the host or vector populations.

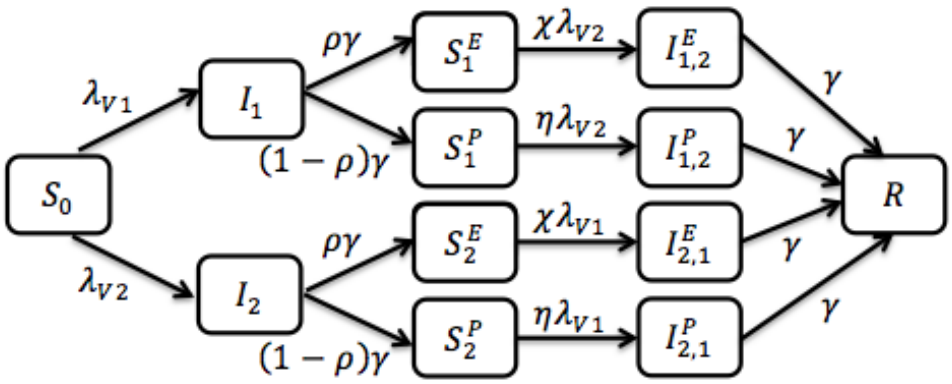

(a)

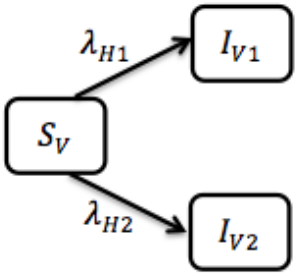

(b)

Figure 4-4: (a) Flow diagram showing the new framework (presented in Chapter 2) acting on a compartmentalized SIR model for the host population for dengue. Enhancement intensity χ acts on susceptibility of ρ proportion of the population with an enhanced secondary infection and cross–protection η acts on susceptibility of the other $(1-\rho)$ proportion. (b) Flow diagram showing the vector dynamics. In both graphs for clarity demography has not been included.

Therefore the model can be described by the following set of differential equations

$$\frac{\partial S_0}{\partial t} + \frac{\partial S_0}{\partial a} = -(\lambda_{V1}(a,t) + \lambda_{V2}(a,t) + \delta(a))S_0(a,t), \tag{4.33a}$$

$$\frac{\partial I_i}{\partial t} + \frac{\partial I_i}{\partial a} = \lambda_{Vi}(a,t)S_0(a,t) - (\gamma + \delta(a))I_i(a,t), \tag{4.33b}$$

$$\frac{\partial S_i^E}{\partial t} + \frac{\partial S_i^E}{\partial a} = \rho\gamma I_i(a,t) - (\chi\lambda_{Vj}(a,t) + \delta(a))S_i^E(a,t), \tag{4.33c}$$

$$\frac{\partial S_i^P}{\partial t} + \frac{\partial S_i^P}{\partial a} = (1-\rho)\gamma I_i(a,t) - (\eta\lambda_{Vj}(a,t) + \delta(a))S_i^P(a,t), \tag{4.33d}$$

$$\frac{\partial I_{i,j}^E}{\partial t} + \frac{\partial I_{i,j}^E}{\partial a} = \chi\lambda_{Vj}(a,t)S_i^E(a,t) - (\gamma + \delta(a))I_{i,j}^E(a,t), \tag{4.33e}$$

$$\frac{\partial I_{i,j}^P}{\partial t} + \frac{\partial I_{i,j}^P}{\partial a} = \eta\lambda_{Vj}(a,t)S_i^P(a,t) - (\gamma + \delta(a))I_{i,j}^P(a,t), \tag{4.33f}$$

$$\frac{\partial R}{\partial t} + \frac{\partial R}{\partial a} = \gamma\sum_{j=1}^{2}\left(I_{i,j}^E(a,t) + I_{i,j}^P(a,t)\right) - \delta(a)R, \tag{4.33g}$$

$$\frac{\mathrm{d}S_V}{\mathrm{d}t} = \delta_V N_V - (\lambda_{H1}(t) + \lambda_{H2}(t) + \delta_V)S_V(t), \tag{4.33h}$$

$$\frac{\mathrm{d}I_{Vi}}{\mathrm{d}t} = \lambda_{Hi}(t)S_V(t) - \delta_V I_i(t), \tag{4.33i}$$

with given initial conditions and the boundary condition on the susceptible population given as

$$S_0(t,0) = \int_0^L \psi(\alpha)N(\alpha)\mathrm{d}\alpha, \tag{4.34}$$

where $\delta(a)$ is the natural mortality rate of the host, $\lambda_{Vi}(a,t)$ is the force of infection of serotype i exerted by the vector on the host aged a at time t, γ is the recovery rate of the host, ρ is the enhancement prevalence, χ is the enhancement intensity, η is the level of cross–protection, $\psi(a)$ is the birth rate of an individual aged a, δ_V is the natural mortality rate of the vector and $\lambda_{Hi}(t)$ is the force of infection of serotype i exerted by the host on the vector.

The force of infection of serotype i exerted by the host on the vector is given by

$$\lambda_{Hi}(t) = b\frac{\int_0^L p(\alpha)\left(I_i(\alpha,t) + I_{j,i}^E(\alpha,t) + I_{j,i}^P(\alpha,t)\right)\mathrm{d}\alpha}{\int_0^L p(\alpha)N(\alpha,t)\mathrm{d}\alpha}, \tag{4.35}$$

and the force of infection of serotype i exerted by the vector on a host aged a is given by

$$\lambda_{Vi}(a,t) = bI_{Vi}(t)\frac{\int_a^{a+\delta a} p(\alpha)S(\alpha,t)\mathrm{d}\alpha}{\int_0^L p(\alpha)N(\alpha,t)\mathrm{d}\alpha}, \tag{4.36}$$

where as in the single serotype model b is the probability of becoming infected given an infected bite and $p(a)$ is the exposure weighting of a host aged a to the vectors.

4.4.2 Host–only model

The host–only model is a simplified version of the host–vector model, where transmission from host to vector to host is approximated by direct transmission between hosts. It can be seen in figure 4-4(a). It is formed of equations (4.33a)–(4.33g) where transmission via the vector is replaced by direct transmission. So, the force of infection $\lambda_{Vi}(a,t)$ is replaced by

$$\lambda_{Vi}(a,t) = \lambda_i(a,t) = \beta(a)\frac{\int_0^L \beta(\alpha)\left(I_i(\alpha,t) + I^E_{j,i}(\alpha,t) + I^P_{j,i}(\alpha,t)\right)\mathrm{d}\alpha}{\int_0^L \beta(\alpha)N(\alpha,t)\mathrm{d}\alpha} \tag{4.37}$$

where $\beta(a)$ is the "effective contact" (implicitly mediated by the vector) per unit time of an individual aged a.

As for the single serotype model we wish to link the effective contact mediated by the vector ($\beta(a)$) in the host–only model and the exposure weighting ($p(a)$) in the host–vector model. The basic reproductive number for multiple serotypes is the same as for single serotypes (van den Driessche and Watmough, 2008). Therefore the constant c implemented for the single serotype model (equation 4.32) can be implemented and we find that in discretized form

$$\beta_k = cbp_k, \tag{4.38}$$

where we have k age–groups, $k = 1, \ldots, n$. We therefore implement the host–only model which implicitly includes vectors in the model via the constant c. When implementing the PDE model we will need this in the continuous form, given by

$$\begin{aligned} \beta(a) &= cbp(a) && \text{(4.39a)} \\ &= \frac{\kappa bP(t)}{\delta_V \int_a p(\alpha)N(\alpha,t)\mathrm{d}\alpha}bp(a), && \text{(4.39b)} \end{aligned}$$

where $P(t)$ is the total population size at time t and $p(a)$ is the exposure weighting of hosts to vectors. It is worth noting that the constant c relates the vector population size, the biting rate and the death rate of the vector to the force of infection i.e. the elements we would usually expect to the associated with the basic reproductive number for a host–vector model. It is also necessary to note that c itself depends on $p(a)$.

As in Chapter 3 we implement an age–independent and an age–dependent trans-

Parameter	Definition	Value
N	Total population	10^4
$b(a)$	Birth rate	$\frac{1}{60}$
L	Maximum age of host	60
γ	Recovery rate	60.8
δ_V	Mortality rate of vector	26.1
b	Transmission rate	40
χ	Enhancement intensity	
η	Cross–protection	
ρ	Enhancement prevalence	
κ	Average number females vectors per host	2
h, k	Step size	0.005
c_2	Constant (age–dependent model)	0.67
c_3	Constant (age–dependent model)	
μ	Age–group with maximum transmission rate	
σ	Intensity of contacts around μ	10

Table 4.1: Parameter definitions and values used where kept constant. All rates given per year.

mission rate. The age–independent exposure rate is given by

$$p(a) = c_1 \ \forall a. \tag{4.40}$$

Due to the formation of the model when the constant exposure rate is implemented we have

$$\beta(a) = \frac{\kappa b P(t)}{\delta_V c_1 \int_a N(\alpha, t) \mathrm{d}\alpha} b c_1 = \frac{\kappa b^2}{\delta_V}. \tag{4.41}$$

The age–dependent exposure rate is given by

$$p(a) = c_2 + c_3 f(a; \mu, \sigma), \tag{4.42}$$

where

$$f(a; \mu, \sigma) = \frac{1}{\sigma\sqrt{2\pi}} \exp\left(\frac{-(a-\mu)}{2\sigma^2}\right). \tag{4.43}$$

Therefore we have

$$\beta(a) = c(\mu, \sigma)\left(c_2 + c_3 f(a; \mu, \sigma)\right). \tag{4.44}$$

Parameters are given in Table 4.1.

To solve the PDE system we implement a splitting scheme in the same way as in Chapter 3.

4.4.3 Quantification

As in Chapter 3 we use the likelihood method to determine how easy it is to differentiate between seroprevalence profiles with an age–independent and an age–dependent force of infection. We will consider this both at the peak of the initial epidemic and at the endemic equilibrium. The method is given in full in Chapter 3, Section 3.4.2, but we will briefly recap the main points.

1. Determine the seroprevalence profile under the age–independent and age–dependent force of infection.

2. Sample the population according to the seroprevalence profile under the age–independent force of infection.

3. Using likelihood methods determine whether the sample is more likely to have come from the age–independent or age–dependent seroprevalence profile.

4. Repeat steps (1)–(3) and count the number of times the sample is more likely to have come from the age–dependent seroprevalence profile. Use this to determine the probability of type I error.

In this chapter the model has become more complex than in Chapter 3. Therefore, at the peak of the initial epidemic we have to implement interpolation to determine more accurately the time of the peak of the epidemic. In doing so we gain greater precision regarding the time of the peak of the epidemic, improving the accuracy of our results.

4.4.4 Initial conditions

We wish to determine how the type I error changes as we vary different parameters within the model. However, the results at the initial epidemic peak may differ depending on the initial conditions that we use, as these affect the subsequent dynamics. Therefore we will consider the type I error under two sets of initial conditions. Under the first set of initial conditions we introduce one individual infected with serotype 1 and two individuals infected with serotype 2 into an otherwise susceptible population. The difference in the initial number infected means that the serotypes do not behave in an identical way. Under the second set of initial conditions we assume serotype 1 is endemic in the population and introduce one individual infected with the second serotype.

For the different initial conditions we determine the type I error at the peak of the initial epidemic for different cases. We need to know seroprevalence of serotype 1,

seroprevalence of serotype 2 and total seroprevalence, given by

$$\begin{aligned}
\text{Serotype 1:} \quad & N(a,t) - S_0(a,t) - I_2(a,t) - S_2^E(a,t) - S_2^P(a,t), \\
\text{Serotype 2:} \quad & N(a,t) - S_0(a,t) - I_1(a,t) - S_1^E(a,t) - S_1^P(a,t), \\
\text{Serotypes 1 \& 2:} \quad & N(a,t) - S_0(a,t).
\end{aligned}$$

4.5 Results I: At the peak of the initial epidemic IC1: $S_0(0) = 9997$, $I_1(0) = 1, I_2(0) = 2$

4.5.1 Varying the enhancement intensity χ

We are now interested in whether we can differentiate between the age–independent and age–dependent seroprevalence profiles and how the parameters in the two–serotype model affect the results that we see. Figure 4-5(a) shows the seroprevalence of serotype 1 at the peak of the initial epidemic under the age–independent and age–dependent transmission rates (equations (4.41) and (4.44) respectively) as the enhancement intensity is varied. We set $\rho = 0.5$ meaning 50% of infections are enhanced. Susceptibility on infections that are not enhanced is the same as for primary infections ($\eta = 1$). As the enhancement intensity increases the seroprevalence of serotype 1 increases, as susceptibility to infection has increased. Although quantitatively having an effect on the seroprevalence, increasing the enhancement intensity does not qualitatively have a great effect on the seroprevalence profiles under either transmission rate. This is exemplified in figure 4-5(b) where the probability of type I error is given as the age–group which has the maximum transmission is increased. For each of the enhancement intensities the qualitative shape is similar and varying the enhancement intensity has little quantitative effect on the probability of type I error.

We also consider how varying the enhancement prevalence affects the seroprevalence profiles and the probability of type I error (figures 4-5(c) and (d)). As the enhancement prevalence decreases seroprevalence decreases, as less individuals suffer an enhanced secondary infection meaning there is less infection in the population as a whole. This is true under both transmission rates. Although minimal, there is a change in the area between the two curves as the enhancement prevalence decreases. This then has an effect on the probability of type I error for each age–group with the highest transmission rate, shown in figure 4-5(d). The higher the enhancement prevalence, the smaller the type I error and therefore the easier it is to differentiate between the seroprevalence profiles. We see qualitatively that for each enhancement prevalence as the age–group with the maximum transmission rate increases the probability of type I error initially

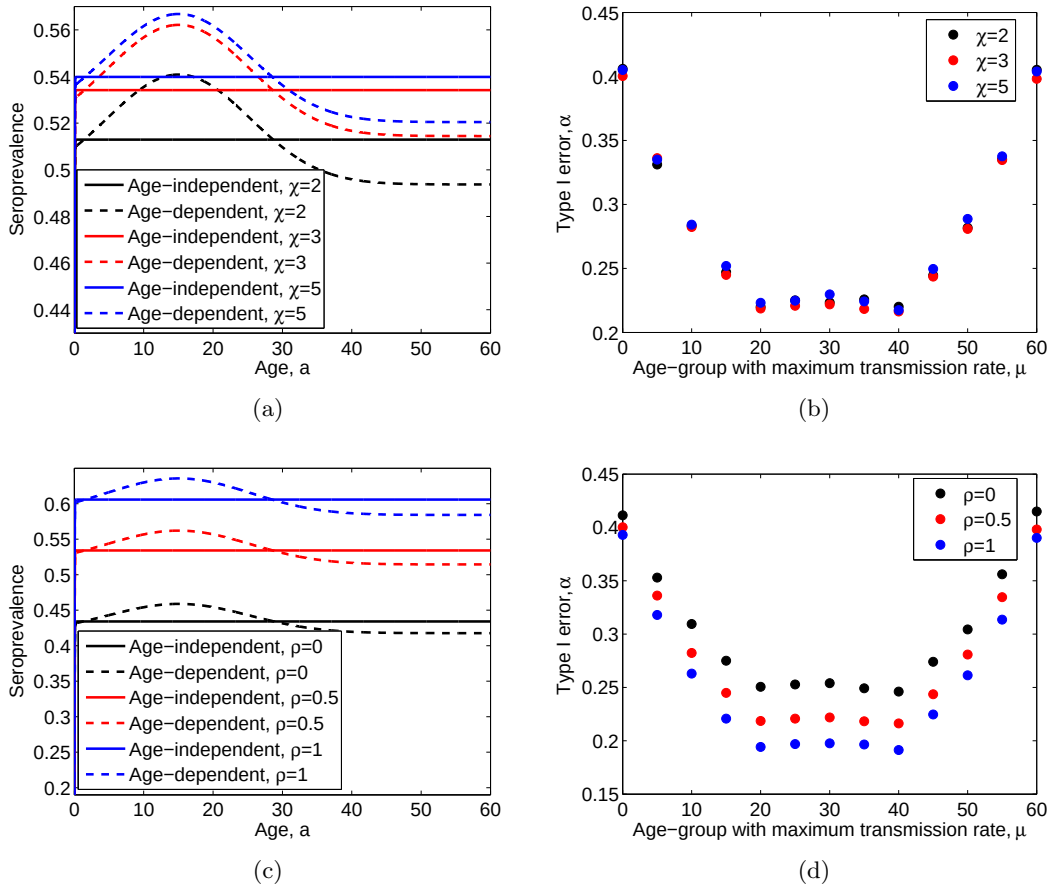

Figure 4-5: (a) Seroprevalence profiles at the peak of the initial epidemic under the age–independent transmission rate (solid lines) and age–dependent transmission rate (dashed lines) when the enhancement intensity is $\chi = 2$ (black lines), $\chi = 3$ (red lines) and $\chi = 5$ (blue lines). (b) The probability of type I error at the peak of the initial epidemic as the age–group with the greatest transmission rate is increased for different enhancement intensities. (c) Seroprevalence profiles at the peak of the initial epidemic under the age–independent transmission rate (solid lines) and age–dependent transmission rate (dashed lines) when the enhancement prevalence is $\rho = 0$ (black lines), $\rho = 0.5$ (red lines) and $\rho = 1$ (blue lines). (d) The probability of type I error at the peak of the initial epidemic as the age–group with the greatest transmission rate is increased for different enhancement prevalences. In (a) $\mu = 15$, $\rho = 0.5$ and $\eta = 1$, in (b) $\rho = 0.5$ and $\eta = 1$, in (d) $\mu = 15$, $\chi = 3$ and $\eta = 1$, in (d) $\chi = 3$ and $\eta = 1$. All other parameters are given in Table 4.1.

decreases. For several age–groups which have the greatest transmission there is then a similar probability of type I error, after which the probability of type I error increases again. This means that when the highest transmission rate is among the middle ages it

is easiest to differentiate between seroprevalence profiles, indicating that they are more different from each other under the age–independent and age–dependent transmission rates.

These findings hold true as we increase the enhancement intensity and vary both the enhancement prevalence and the age–group with the maximum transmission rate. For both the single serotypes and total seroprevalence there is little difference in the probability of type I error as the enhancement intensity is increased. Overall, we find that it is harder to differentiate between seroprevalence profiles for individual serotypes than for total seroprevalence (see Appendix B.2.1).

4.5.2 Varying the cross–protection η

Figure 4-6(a) shows the seroprevalence of serotype 1 at the peak of the initial epidemic under the age–independent and age–dependent transmission rates (equations (4.41) and (4.44) respectively) as the level of cross–protection is varied. As the level of cross–protection decreases (η increases) seroprevalence increases. This is to be expected, as a greater proportion of individuals can be infected with secondary infections which are not enhanced. Although increasing the cross–protection causes a quantitative change in the seroprevalence profile, there is only a small qualitative difference in the age–independent and age–dependent seroprevalence profiles. However, the small difference affects the probability of type I error (and hence how readily we can differentiate between the transmission rates) as the age–group with the greatest transmission rate is increased (figure 4-6(b)). If all secondary infections which are not enhanced have complete protection ($\eta = 0$) then the probability of type I error is higher than when they do not. This indicates that the seroprevalence profiles are more similar when there is total protection and thus harder to differentiate between. Although this may seem surprising considering the profiles themselves, we can calculate the area of difference between the age–independent and age–dependent seroprevalence profiles. We find that this area is increasing as cross–protection decreases, thus the profiles are becoming more different and causing the decrease in the probability of type I error. The figure also shows that when the greatest transmission rate is among the middle ages, the difference in the probability of type I error as the level of cross–protection is varied is greater than when the greatest transmission rate is among the young or the older population.

We show the generalities of these findings in figure 4-6, where we decrease the level of cross–protection (increase η) as both the enhancement prevalence and the age–group with the greatest transmission rate are varied. Figures 4-6(a), (b) and (c) show the type I error for serotype 1 as the level of cross–protection is decreased from everyone

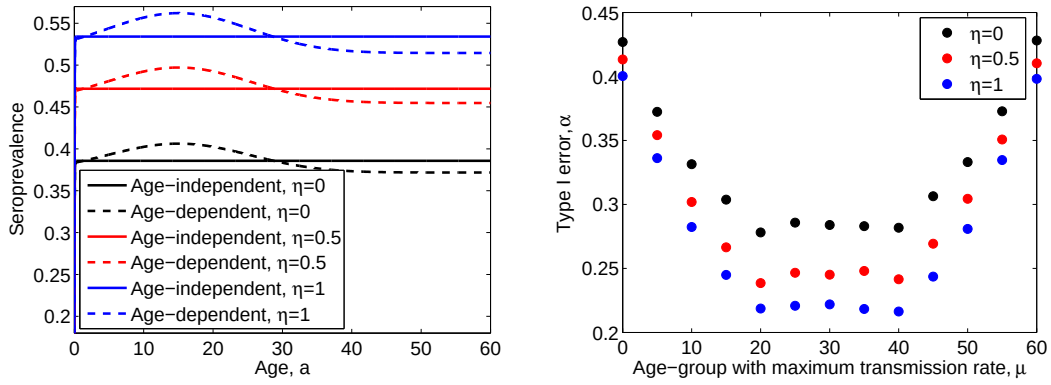

Figure 4-6: (a) Seroprevalence profiles at the peak of the initial epidemic under the age–independent transmission rate (solid lines) and age–dependent transmission rate (dashed lines) when the level of cross–protection is $\eta = 0$ (black lines), $\eta = 0.5$ (red lines) and $\eta = 1$ (blue lines). (b) The probability of type I error at the peak of the initial epidemic as the age–group with the greatest transmission rate is increased for different levels of cross–protection. In (a) $\mu = 15$, $\rho = 0.5$ and $\chi = 3$ and in (b) $\rho = 0.5$ and $\chi = 3$. All other parameters are given in Table 4.1.

is protected if they do not have an enhanced secondary infection ($\eta = 0$) to no one is protected ($\eta = 1$). If the greatest transmission rate is in younger or older age–groups the difference in seroprevalence profiles is relatively uniform across all enhancement prevalences. However, for the ages in between as the enhancement prevalence decreases the probability of type I error increases. This happens at a quicker rate as the age–group with the greatest transmission increases, and then slows again after $\mu = 30$. This means that it is easier to differentiate between the seroprevalence profiles when a greater proportion of the population suffer an enhanced secondary infection. As the level of cross–protection decreases (η increases) we see that the differences in the probability of type I error across the enhancement prevalences decrease. This means that as a greater proportion of the population suffer infections it becomes comparatively easier to differentiate between the age–independent and age–dependent seroprevalence profiles. We see similar behaviour for the serotype 2 dynamics (see Appendix B.2.2).

Unlike the single serotype, there is far more uniformity in the differences in the seroprevalence profiles across the enhancement prevalences for all cross–protection values for total seroprevalence (figures 4-7(d), (e) and (f)). This indicates that the enhancement prevalence is not a large factor in determining differences in the seroprevalence profiles. As when increasing the enhancement intensity, it is easier to differentiate the

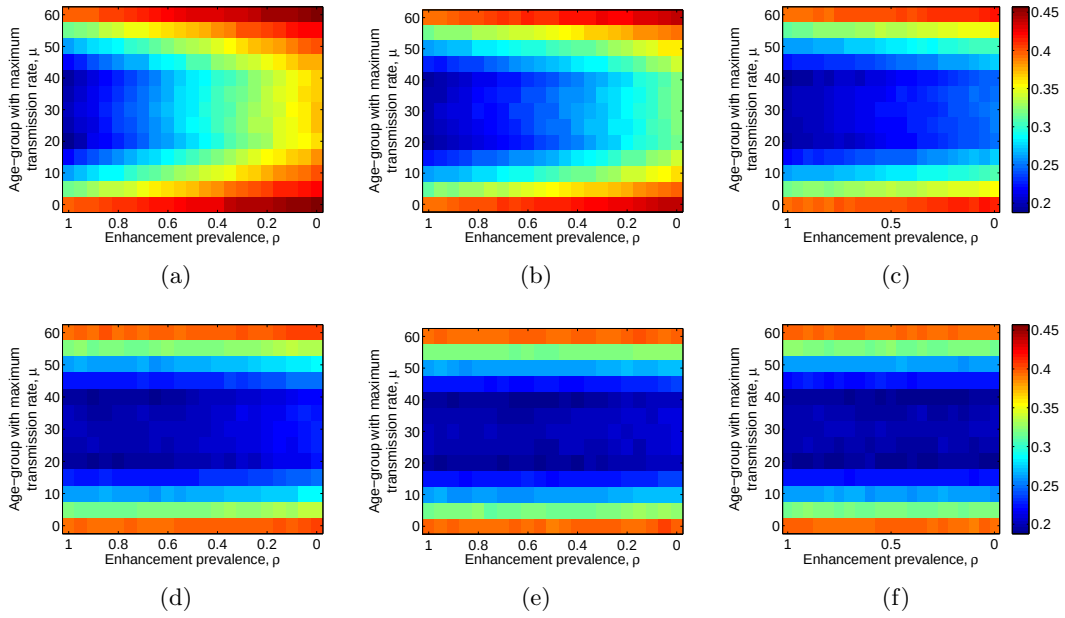

Figure 4-7: Probability of type I error at the peak of the initial epidemic as the enhancement prevalence and the age–group with the greatest transmission rate are varied. (a) (b) and (c) shows the probability of type I error for serotype 1. In (a) $\eta = 0$, in (b) $\eta = 0.5$ and in (c) $\eta = 1$. (d) (e) and (f) shows the probability of type I error for both serotypes. In (d) $\eta = 0$, in (e) $\eta = 0.5$ and in (f) $\eta = 1$. In all figures $\chi = 3$ and all other parameters are given in Table 4.1.

seroprevalence profiles when taking account of all infection in the population than for an individual serotype.

4.5.3 Summary

We have examined the probability of type I error at the peak of the initial epidemic when one individual infected with serotype 1 and two individuals infected with serotype 2 are introduced into a susceptible population. The results show that increasing the enhancement intensity acting on the serotypes has little effect on how easy it is to differentiate between seroprevalence profiles, both of a single serotype and total seroprevalence. For the individual serotypes decreasing the level of cross–protection has a larger effect on the probability of type I error than for total seroprevalence, particularly if the greatest transmission rate is among the middle ages. In both cases we find that decreasing the enhancement prevalence causes an increase in the probability of type I error, making it harder to differentiate between the seroprevalence profiles. In contrast to this, for total seroprevalence the ease of differentiating seroprevalence profiles

does not change with enhancement prevalence. When varying both the enhancement intensity and the level of cross–protection we find that it is easier to differentiate between age–independent and age–dependent transmission in the total seroprevalence age–profiles than in age–profiles for the individual serotypes.

4.6 Results II: At the peak of the initial epidemic IC2: Serotype 1 at endemic equilibrium, $I_2(0) = 1$

4.6.1 Preliminaries

We now start with the population at the endemic equilibrium for serotype 1, meaning there are individuals in the S_0, I_1, S_1^E and S_1^P compartments. Although we can calculate the endemic equilibrium analytically for the age–independent case we cannot for the age–dependent case. Therefore we numerically find the endemic equilibrium age–profiles for these compartments to use as the initial condition, at which point one individual infected with serotype 2 is introduced into the population.

When serotype 1 is at the endemic equilibrium and an individual with serotype 2 is introduced into the population the ensuing dynamics vary according to the parameters. Over the initial period the dynamics of those infected with the endemic serotype range from there being a small initial decrease, followed by an increase (figure 4-8(a)), to there being an increase in the number infected, but at a slower rate to the increase seen in serotype 2 (figure 4-8(b)). In both of these cases the initial epidemic peaks for the two serotypes are not at a similar time. We are interested in the initial epidemic peak, and therefore we restrict our analysis to the serotype which is introduced into the population and the total seroprevalence. We study the total seroprevalence as although it is dominated by the serotype introduced into the population (and so analysis can be done at the initial epidemic peak), it allows us to gain an insight of how the endemic serotype affects the probability of type I error.

4.6.2 Varying the enhancement intensity, χ

Figure 4-9(a) shows the seroprevalence of serotype 2 at the peak of the initial epidemic under the age–independent and age–dependent transmission rates (equations (4.41) and (4.44) respectively) as the enhancement intensity is varied. As in the previous case when varying the enhancement intensity, we assume no cross–protection acting on all other secondary infections ($\eta = 1$). It is immediately clear that the initial conditions have drastically changed the seroprevalence profiles. Rather than constant seroprevalence across all age–groups under the age–independent contact rate, seroprevalence

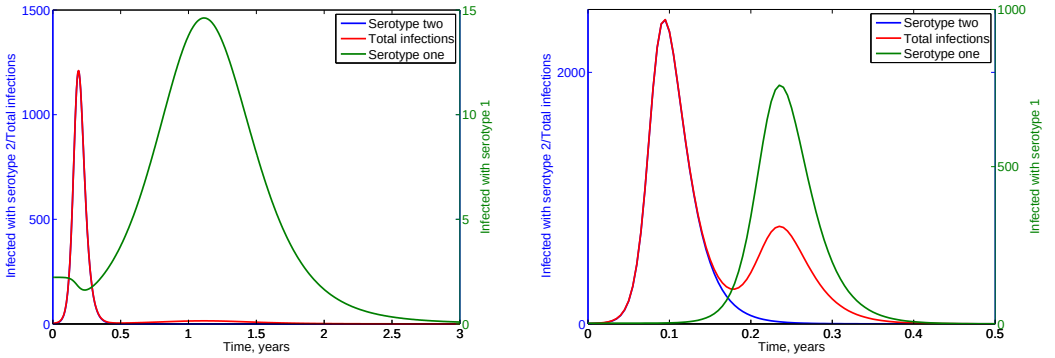

Figure 4-8: The number of individuals infected with serotype 1 which was initially endemic in the population (green line), the newly introduced serotype 2 (blue line) and total infections (red line). In (a) the enhancement prevalence is $\rho = 0.05$ and in (b) the enhancement prevalence is $\rho = 0.95$. The enhancement intensity is $\chi = 3$ and the level of cross–protection is $\eta = 1$. All other parameters are given in Table 4.1.

increases with age (compare with figure 4-5(a)). In Section 4.5 the quantitative behaviour of the seroprevalence changed under different enhancement intensities but the qualitative behaviour did not. Under the new initial conditions the qualitative behaviour also changes under both the age–independent and age–dependent transmission rates; for each enhancement intensity the seroprevalence increases with age, however the gradient of the increase depends on the enhancement intensity. Comparing the age–independent and age–dependent seroprevalence profiles themselves, we see that seroprevalence starts at approximately the same level. Under the age–dependent contact rate the seroprevalence then substantially increases; this is because in this example the age–group with the greatest transmission rate is $\mu = 15$. However, the gradient of the profiles then reduces and hence at age 60 the seroprevalence under the age–independent and age–dependent transmission rates is again very similar.

Figure 4-9(b) shows the probability of type I error as the age–group with the greatest transmission rate is increased for different enhancement intensities. Unlike under the previous initial condition, varying the enhancement intensity has an effect on the probability of type I error; the greater the enhancement intensity the larger the probability of type I error. This means that the seroprevalence profiles under the age–independent and age–dependent transmission rates are more similar than for lower enhancement intensities, and thus more difficult to differentiate between. Although quantitatively different, varying the enhancement intensity has little qualitative effect on the type I error, which is the same behaviour seen at the peak of the initial epidemic under the

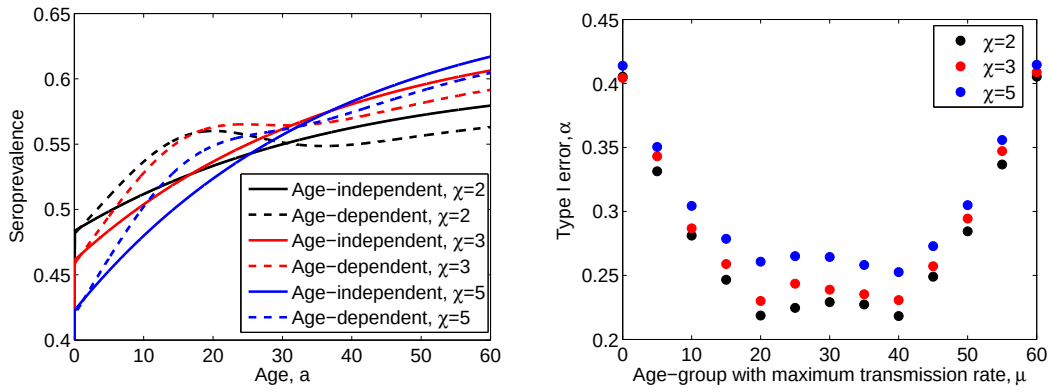

(a) (b)

Figure 4-9: (a) Seroprevalence profiles at the peak of the initial epidemic under the age–independent transmission rate (solid lines) and age–dependent transmission rate (dashed lines) when the enhancement intensity is $\chi = 2$ (black lines), $\chi = 3$ (red lines) and $\chi = 5$ (blue lines). (b) The probability of type I error at the peak of the initial epidemic as the age–group with the greatest transmission rate is increased for different enhancement intensities. In (a) $\mu = 15$, $\rho = 0.5$ and $\eta = 1$, in (b) $\rho = 0.5$ and $\eta = 1$. All other parameters are given in Table 4.1.

first initial conditions (compare with figure 4-5(b)).

Figure 4-10(a) shows the total seroprevalence at the peak of the initial epidemic under the age–independent and age–dependent transmission rates (equations (4.41) and (4.44) respectively). The seroprevalence profiles are much smoother than for the single serotype (compare with figure 4-9(a)). For younger ages the seroprevalence profile is dominated by the serotype 2 dynamics, however for the older age–groups seroprevalence is much higher; this is dominated by the serotype which was initially endemic in the population.

The probability of type I error as the enhancement intensity is increased is shown in figure 4-10(b). The qualitative behaviour in the type I error is different to that for the single serotype, and therefore the endemic serotype is playing a role in how easy it is to differentiate between the age–independent and age–dependent seroprevalence profiles. The qualitative behaviour as the enhancement intensity increases is similar in each graph, however the error does increase minimally as enhancement increases. For the enhancement prevalence, as the age–group with the maximum transmission rates increases there is an initial decrease in the probability of type I error until a minimum is reached. Unlike for the single serotype, this then increases for middle ages, before decreasing again and finally increasing as the older age–groups have the maximum

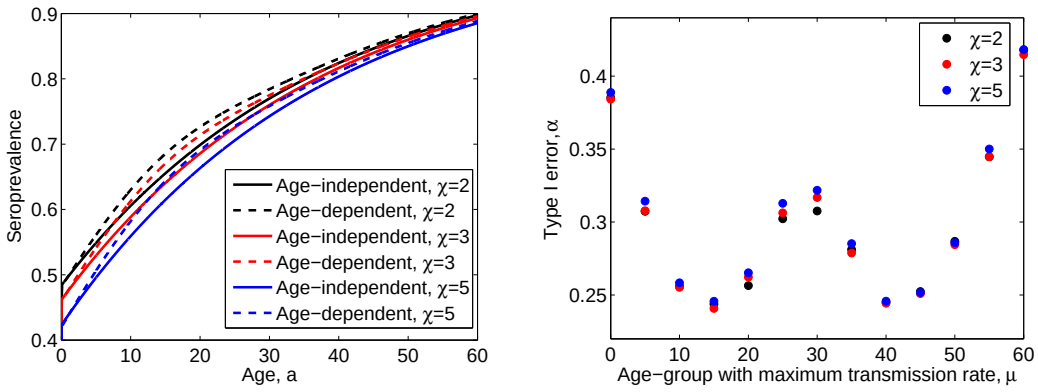

(a) (b)

Figure 4-10: (a) Seroprevalence profiles for total seroprevalence at the peak of the initial epidemic under the age–independent transmission rate (solid lines) and age–dependent transmission rate (dashed lines) when the enhancement intensity is $\chi = 2$ (black lines), $\chi = 3$ (red lines) and $\chi = 5$ (blue lines). (b) The probability of type I error at the peak of the initial epidemic as the age–group with the greatest transmission rate is increased for different enhancement intensities. In (a) $\mu = 15$, $\rho = 0.5$ and $\eta = 1$, in (b) $\rho = 0.5$ and $\eta = 1$. All other parameters are given in Table 4.1.

transmission rate.

The generalities of these findings for both the single serotype and total seroprevalence are the same as the enhancement prevalence and age–group with maximum transmission rate are varied. It is, however, interesting to note that for nearly all parameter combinations the probability of type I error is greater for the total seroprevalence than for the individual serotype. This is in contrast to when the previous set of initial conditions was implemented (see Appendix B.3.1).

4.6.3 Varying the cross–protection, η

Figure 4-11(a) shows the seroprevalence of serotype 2 at the peak of the initial epidemic under the age–independent and age–dependent transmission rates (equations (4.41) and (4.44) respectively) as the level of cross protection is varied. As the level of cross–protection decreases (η increases) the seroprevalence increases, which we also saw under the first set of initial conditions. However, unlike under the first set of initial conditions, the seroprevalence profiles qualitatively change as the level of cross–protection decreases. Under the age–independent transmission rate the gradient of the profile increases with age and gets steeper as cross–protection decreases. The same is true under the age–dependent transmission rate, however there is also an increase in gradient

around the age–groups which have the greatest transmission rate. Figure 4-11(b) shows the probability of type I error of the seroprevalence profiles as the age–group with the highest transmission rate is varied. We see very similar qualitative and quantitative behaviour as to under the first set of initial conditions (compare with figure 4-6(b)). As the cross–protection decreases (η increases) it becomes easier to differentiate the seroprevalence profiles at the peak of the initial epidemic.

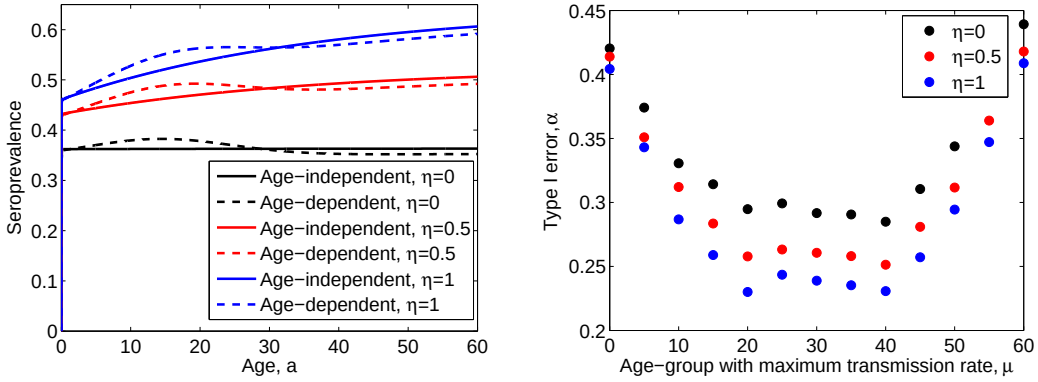

(a) (b)

Figure 4-11: (a) Seroprevalence profiles at the peak of the initial epidemic under the age–independent transmission rate (solid lines) and age–dependent transmission rate (dashed lines) when the level of cross–protection is $\eta = 0$ (black lines), $\eta = 0.5$ (red lines) and $\eta = 1$ (blue lines). (b) The probability of type I error at the peak of the initial epidemic as the age–group with the greatest transmission rate is increased for different levels of cross–protection. In (a) $\mu = 15$, $\rho = 0.5$ and $\chi = 3$ and in (b) $\rho = 0.5$ and $\chi = 3$. All other parameters are given in Table 4.1.

We show the generalities of these findings in figure 4-12, where we decrease the level of cross–protection (increase η) as both the enhancement prevalence and the age–group with the greatest transmission rate are varied. For the case where $\chi = 3$, $\eta = 0$, $\rho = 0$ the dynamics do not lend themselves to an initial epidemic peak, and therefore in this case we have started the analysis at $\rho = 0.05$. This is because the initial conditions mean there is a decrease in the number of infected individuals before damped oscillations occur.

Figures 4-12(a), (b) and (c) show the probability of type I error for the serotype introduced into the population. As the level of cross–protection decreases the type I error decreases across all parameter combinations in the $(\rho - \mu)$ parameter space. This means that as cross–protection decreases it becomes easier to differentiate between the seroprevalence profiles. This is especially true when the greatest transmission rate is

among the middle ages. The graphs also change qualitatively as the level of cross–protection decreases. When cross–protection acts on secondary infections that are not enhanced (figures 4-12(a) and (b)), as the enhancement prevalence decreases the type I error increases. This means that the greater the proportion of the population with enhanced secondary infections, the harder it is to differentiate between age–independent and age–dependent seroprevalence profiles. However, as the level of cross–protection decreases (η increases, figure 4-12(c)), the probability of type I error becomes more uniform across the enhancement prevalences.

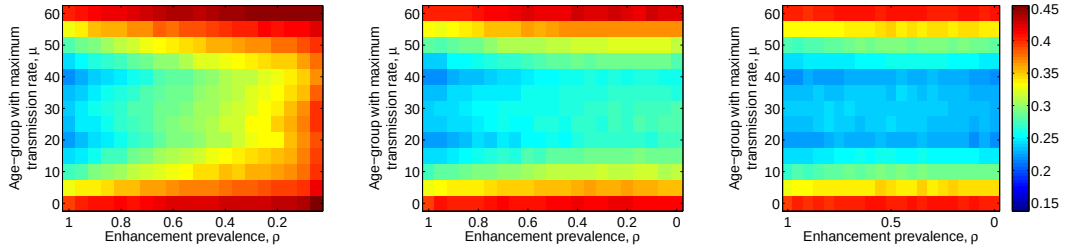

(a) (b) (c)

Figure 4-12: Probability of type I error at the peak of the initial epidemic as the enhancement prevalence and the age–group with the greatest transmission rate are varied for serotype 1. In (a) $\eta = 0$, in (b) $\eta = 0.5$ and in (c) $\eta = 1$. In all figures $\chi = 3$ and all other parameters are given in Table 4.1.

For total seroprevalence we see the same qualitative behaviour as when varying the enhancement intensity. Therefore we again have a different qualitative behaviour between the single serotype and the total seroprevalence. This indicates that although serotype 1 does not peak at the same time as the introduced serotype, the dynamics still influence total seroprevalence.

4.6.4 Summary

We have considered the probability of type I error at the peak of the initial epidemic when serotype 1 is at equilibrium and one individual infected with serotype 2 is introduced into the population. The results show that increasing the level of enhancement has a small effect on how easy it is to differentiate seroprevalence profiles at the peak of the initial epidemic. As the enhancement intensity increases there is less uniformity in the probability of type I error across enhancement prevalences. We find that decreasing the level of cross–protection makes it easier to differentiate between age–independent and age–dependent seroprevalence profiles at the peak of the initial epidemic for the serotype which is introduced into the population. This is also true for total seropreva-

lence. We also see that there is different qualitative behaviour in how easy it is to differentiate seroprevalence profiles when examining the single serotype and total seroprevalence. This is due to one serotype being at the endemic equilibrium when infection with the other serotype is introduced into the population.

4.7 Results III: At the endemic equilibrium

Running the system to the endemic equilibrium means that the initial conditions are unimportant as we are no longer interested in the initial transient behaviour. We therefore proceed using the first set of initial conditions. We also increase the step size in the numerical scheme to $k, h = 0.01$ so that the system is able to reach equilibrium faster. As before, we want to determine how the probability of type I error changes as we vary the enhancement prevalence and the age–group which has the maximum transmission rate. We follow the same algorithmic steps as for finding the probability of type I error at the peak of the initial epidemic. However, in some cases a stable endemic equilibrium is not reached and there are periodic dynamics. In these cases we are unable to perform the likelihood analysis and hence find the probability of type I error. This is because we need a specific point where the time profiles are comparable which we will not be able to find if the system is unstable.

4.7.1 Varying the enhancement intensity, χ

Figure 4-13(a) shows the seroprevalence of serotype 1 at the endemic equilibrium under the age–independent and age–dependent transmission rates (equations (4.41) and (4.44) respectively) as the enhancement intensity is varied. As the enhancement intensity increases so too does seroprevalence under both transmission rates. We can see that the profiles themselves follow a similar trajectory under both the age–independent and age–dependent transmission rates. Figure 4-13(b) shows the probability of type I error as the age–group with the greatest transmission is increased. The differences in seroprevalence profiles are fairly similar for each of the enhancement intensities. As the age–group with the greatest transmission rate increases there is initially a decrease in the probability of type I error, followed by an increase for the middle ages, followed by a second decrease before finally increasing as the age–group with the maximum transmission is in the older ages. These results indicate that the age–group with the maximum transmission rate is highly important in determining how similar the seroprevalence profiles are at the endemic equilibrium, and thus how easy it is to determine the importance of age–dependence in the model.

The generalities of these findings are the same as the enhancement prevalence and

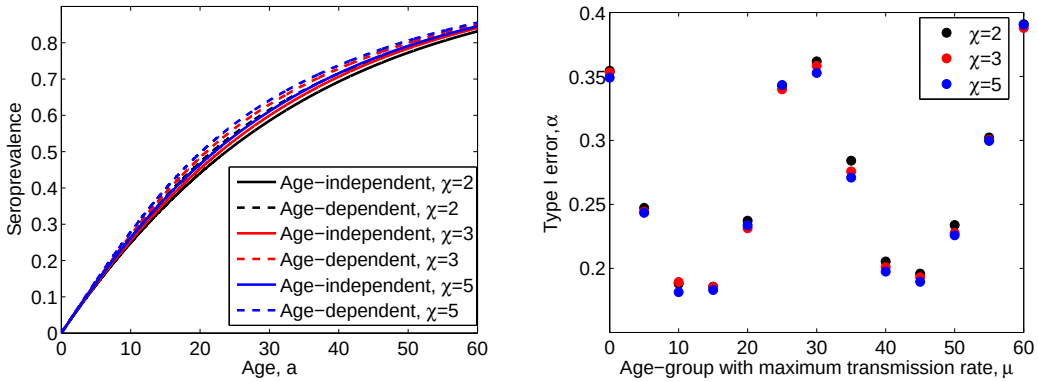

(a) (b)

Figure 4-13: (a) Seroprevalence profiles at the endemic equilibrium under the age–independent transmission rate (solid lines) and age–dependent transmission rate (dashed lines) when the enhancement intensity is $\chi = 2$ (black lines), $\chi = 3$ (red lines) and $\chi = 5$ (blue lines). (b) The probability of type I error at the endemic equilibrium as the age–group with the greatest transmission rate is increased for different enhancement intensities. In (a) $\mu = 15$, $\rho = 0.2$ and $\eta = 1$, in (b) $\rho = 0.2$ and $\eta = 1$. All other parameters are given in Table 4.1.

age–group with the maximum transmission rate are varied. This is true for the single serotype (figure 4-14) and total seroprevalence. The dynamics do however change as the enhancement intensity increases for certain enhancement prevalences. In figure 4-14(a) we see that when $\chi = 2$ the system always has a stable endemic equilibrium in the $(\rho - \mu)$ parameter space, however this is not the case when the enhancement intensity is increased to $\chi = 3$ (figures 4-14(b)). The white area represents where there is oscillatory behaviour under one or both of the transmission rates. Therefore, the type I error cannot be calculated. Increasing the enhancement intensity further to $\chi = 5$ (figures 4-14 (c)) moves the point at which the oscillatory behaviour occurs to the right, meaning that the system is unstable for a greater region of the $(\rho - \mu)$ parameter space. This is also seen for total seroprevalence.

These graphs show that an endemic equilibrium is not always attained. Therefore we consider the bifurcation points as the enhancement prevalence is varied. Figure 4-15(a) shows the maximum and minimum number of individuals seroprevalent with serotype 1, either once the endemic equilibrium has been reached, or in the last 50 years if the endemic equilibrium has not been reached by $t = 2,500$ years, when the age–dependent contact rate is implemented. When $\chi = 2$ the system is stable for all ages, however as χ is increased we see that for larger enhancement prevalences

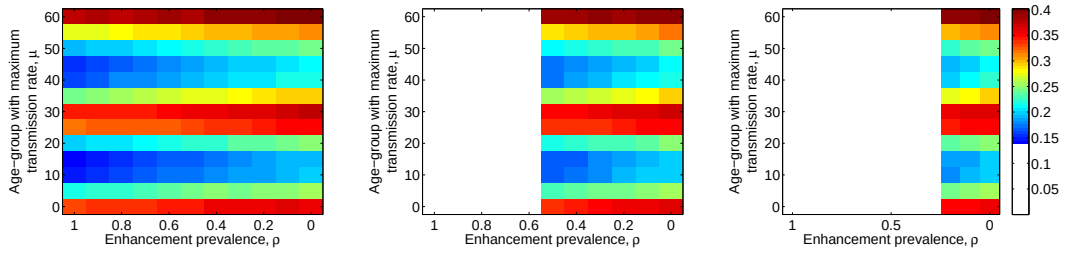

Figure 4-14: Probability of type I error at the endemic equilibrium as the enhancement prevalence and the age–group with the greatest transmission rate are varied for serotype 1. In (a) $\chi = 2$, in (b) $\chi = 3$ and in (c) $\chi = 5$. In all figures $\eta = 1$ and all other parameters are given in Table 4.1.

the system is no longer stable. Decreasing the enhancement prevalence changes the behaviour and allows for stability. Increasing χ again pushes the bifurcation point to the right, with oscillations occurring for smaller enhancement prevalences.

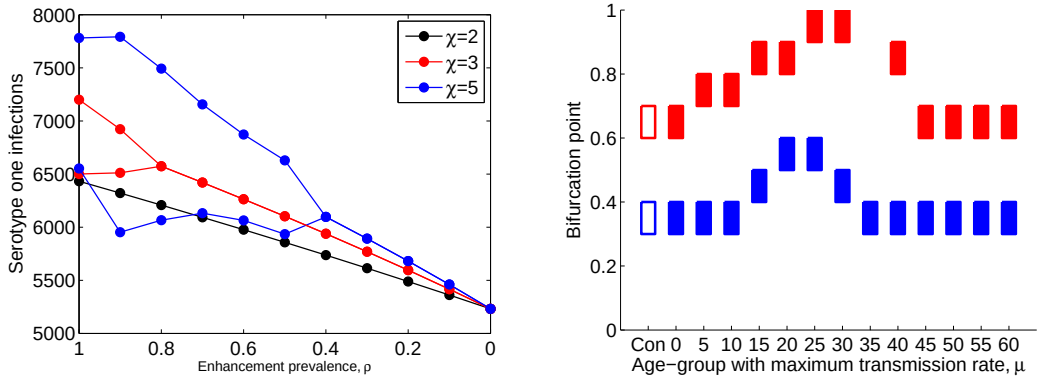

Figure 4-15: (a) Bifurcation diagram showing the total number of individuals who are infected with or have previously been infected with serotype 1 as the enhancement prevalence is varied for different enhancement intensities when the age–dependent transmission rate is implemented. (b) The area which the bifurcation point falls for the age–independent and age–dependent transmission rates. Red represents when $\chi = 3$ and blue represents when $\chi = 5$. In all graphs $\eta = 1$ and all other parameters are given in Table 4.1.

It is interesting to note that the bifurcation point does not occur for the same enhancement prevalence when different age–dependent transmission rates are implemented. This indicates that the transmission function has an impact on the point of

bifurcation. Figure 4-15(b) shows the region where the bifurcation point occurs for each of the different transmission rates; the empty blocks are the case for the age–independent transmission rate, whilst the age–dependent transmission rates are shown by the coloured blocks. As we only increase the enhancement prevalence by $\rho = 0.1$ in each case we are only able to estimate where the actual bifurcation occurs. As would be expected from the previous graphs, as the enhancement intensity increases, the point of bifurcation decreases - this is seen for all cases. For each enhancement intensity there is a similar shape; as the age–group which has the maximum transmission rate increases the enhancement prevalence at which the bifurcation occurs increases and then decreases. This does not happen in synchrony for all enhancement intensities. We see when $\chi = 3$ if the age–group with the maximum transmission rate is those aged 35 an endemic equilibrium can still be reached, whilst for the other age–groups it cannot. It is also worth noting that when the age–independent transmission rate is implemented the bifurcation points occur in similar places to those seen in Chapter 2, when the extended Ferguson et al. (1999a) model was implemented.

4.7.2 Varying the level of cross–protection, η

Figure 4-16(a) shows the seroprevalence profiles of serotype 1 at the endemic equilibrium under the age–independent and age–dependent transmission rates (equations (4.41) and (4.44) respectively) as the level of cross–protection is varied. Under both transmission rates as the level of cross–protection decreases the seroprevalence increases. This is to be expected; a decrease in cross–protection allows for greater infectivity in the population. As when varying the enhancement intensity, the seroprevalence profiles under the two transmission rates are qualitatively similar for each level of cross–protection. However, in contrast, varying the cross–protection has a greater impact on seroprevalence in the population (compare with figure 4-13(a)). The probability of type I error at the endemic equilibrium is qualitatively the same as when the enhancement intensity was varied. However, as the level of cross–protection decreases (η increases) the seroprevalence profiles are more different and therefore easier to differentiate between.

The generalities of theses findings are the same as the enhancement prevalence and age–group with the maximum transmission rate are varied. As the cross–protection decreases for individual serotypes it becomes easier to differentiate between seroprevalence profiles (see Appendix B.4). In contrast, for total seroprevalence there is no change as cross–protection decreases. The qualitative behaviour for each enhancement prevalence is similar to that found when varying the enhancement intensity.

As when varying the enhancement intensity, we find that for large enhancement prevalences there is not a stable endemic equilibrium and hence we cannot implement

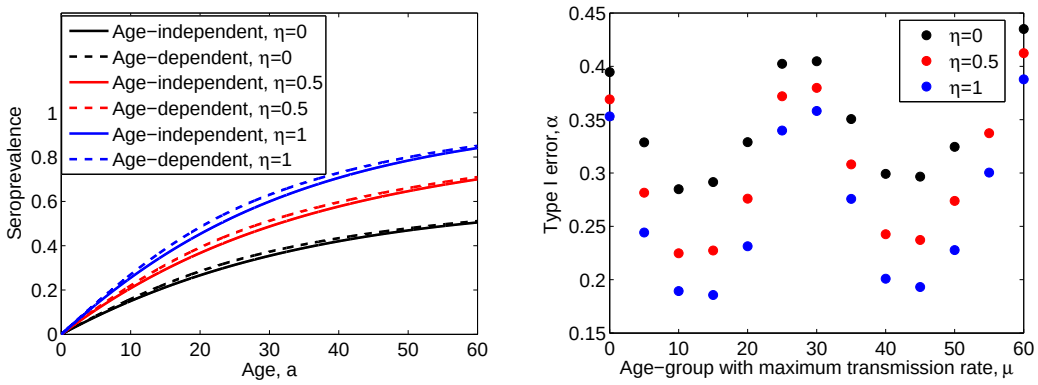

(a) (b)

Figure 4-16: (a) Seroprevalence profiles at the peak of the initial epidemic under the age–independent transmission rate (solid lines) and age–dependent transmission rate (dashed lines) when the level of cross–protection is $\eta = 0$ (black lines), $\eta = 0.5$ (red lines) and $\eta = 1$ (blue lines). (b) The probability of type I error at the peak of the initial epidemic as the age–group with the greatest transmission rate is increased for different levels of cross–protection. In (a) $\mu = 15$, $\rho = 0.2$ and $\chi = 3$ and in (b) $\rho = 0.2$ and $\chi = 3$. All other parameters are given in Table 4.1.

the likelihood analysis to find the type I error; this behaviour is expected. However, when $\eta = 0.25$ and $\eta = 0.5$ we also see oscillatory behaviour when $\rho = 0$ (see figure 4-17 for an example when $\mu = 15$). When $\rho = 0$ no infections are enhanced. If alongside this $\eta = 0$ then there are no secondary infections and an endemic equilibrium is quickly reached. If $\eta = 1$ there is no protection against infections which are not enhanced and the endemic equilibrium can be reached in a timely manner. However, for levels of cross–protection between, we see that if there is no enhancement of secondary infections ($\rho = 0$) and a high level of cross–protection (η small), this causes the system to be unable to reach a stable endemic equilibrium.

4.7.3 Oscillations when $\rho = 0$

We need to determine whether the oscillations seen when $\rho = 0$ are due to numerical error or because of the interaction of the parameters which is in some way causing the behaviour. In the simulations above we incremented time and age in steps sizes of $k, h = 0.01$. Therefore the first measure to test is if refining the step size has an effect at $\rho = 0$. Figure 4-18 shows examples where refining the step size means the system reaches the endemic equilibrium, for example under the age–independent transmission rate (figure 4-18(a)) and under the age–dependent transmission rate with

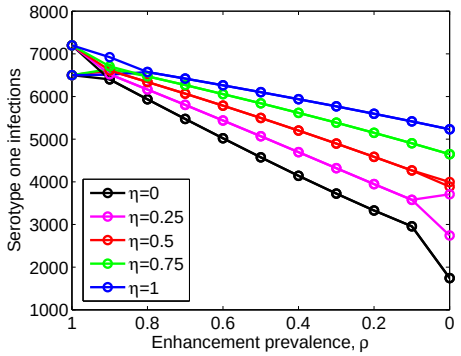

Figure 4-17: Bifurcation diagram showing the total number of individuals who are infected with or have previously been infected with serotype 1 as the enhancement prevalence is varied for different levels of cross protection when the age–dependent transmission rate is implemented. The enhancement intensity is $\chi = 3$, the age–group with maximum transmission rate is $\mu = 15$ and the intensity of contacts around μ is $\sigma = 10$. All other parameters are given in Table 4.1.

$\mu = 30$ (figure 4-18(b)). However, there are examples when under the age–dependent transmission rate oscillations still occur, for example when $\mu = 15$ (figures 4-18(c) and (d)). The regular oscillations that can be seen after a long transitional period would indicate that they may be a part of the system. If the oscillations were a numerical error we may expect them to propagate and worsen, however this does not happen.

We can use an alternative numerical scheme to see if this provides different results. Figure 4-19(a) shows the trajectory using both the forward–time backward–space (upwind) scheme and the splitting scheme. For details on the upwind scheme see Chapter 3. The figure shows that the oscillations are of a greater magnitude when the upwind scheme is implemented, however as with the splitting scheme there are still regular oscillations. The greater magnitude in oscillation is to be expected; the splitting scheme was shown to be more accurate than the upwind scheme (see Chapter 3). Figure 4-19(b) shows the oscillations over 100 years once transient behaviour has been removed. It appears that the period of the oscillations is different under the two schemes, and therefore we consider this in more detail.

Table 4.2 shows the dominant period for each of the immune status compartments using the two different schemes. The dominant periods in the oscillations are similar for the two schemes, and we see that in both cases the susceptible and recovered populations oscillate just over twice as quickly as the other compartments. We would also expect there to be a slight difference in the period as the magnitude of the oscillations is different. This is interesting to see, and again adds to the possibility that

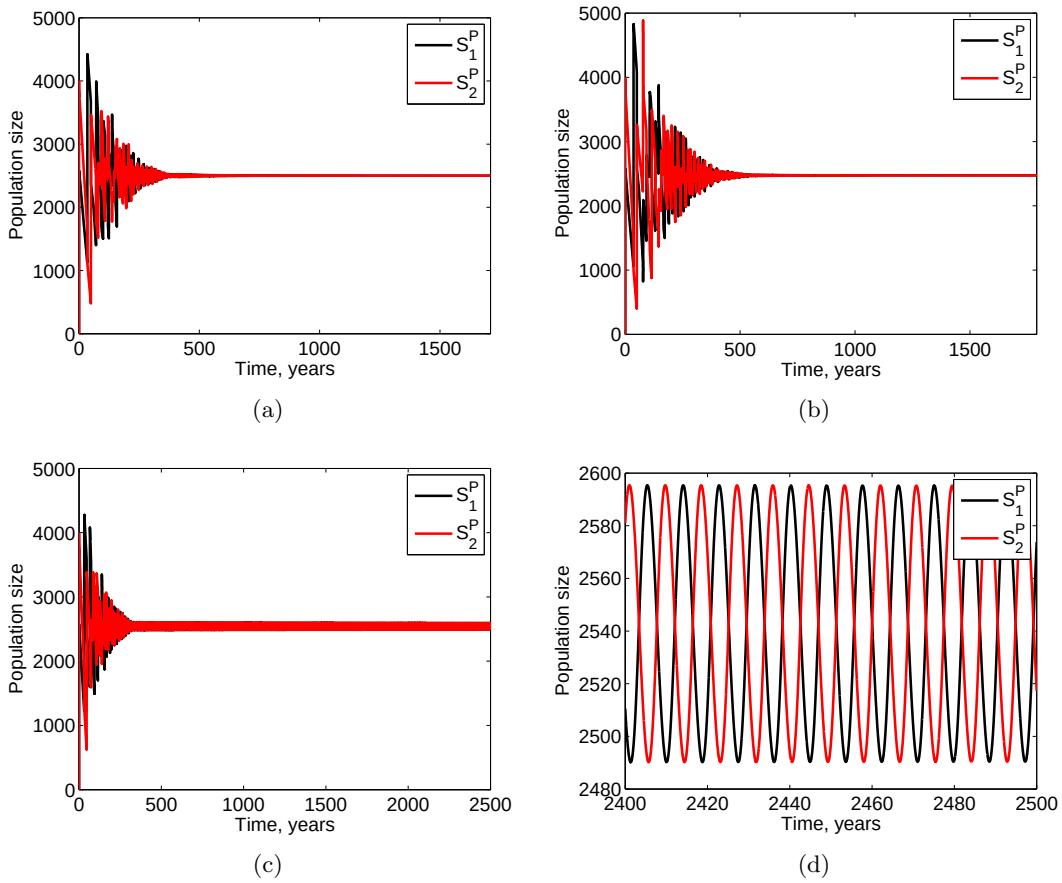

Figure 4-18: (a) Time series showing the number of individuals in the S_1^P (red line) and S_2^P (black line) compartments when the age–independent transmission rate is implemented. (b) Time series showing the number of individuals in the S_1^P (red line) and S_2^P (black line) compartments when the age–dependent transmission rate is implemented with $\mu = 30$. (c) Time series showing the number of individuals in the S_1^P (red line) and S_2^P (black line) compartments when the age–dependent transmission rate is implemented with $\mu = 15$ (d) 200 year time series showing the number of individuals in the S_1^P (black line) and S_2^P (red line) compartments when the age–dependent transmission rate is implemented with $\mu = 15$ once the transient behaviour has settled. The first 2,400 years have been discarded. In all figures $\rho = 0$, $\chi = 3$ and $\eta = 0.5$. All parameters are given in Table 4.1.

the oscillations being seen are not numerical error, but due to the interactions of the parameters.

Finally we consider the region the oscillations occur for when $\rho = 0$. If there is a continuous area in the $(\eta - \mu)$ parameter space that the oscillations occur for this would again indicate that the oscillations are not simply due to numerical error. We

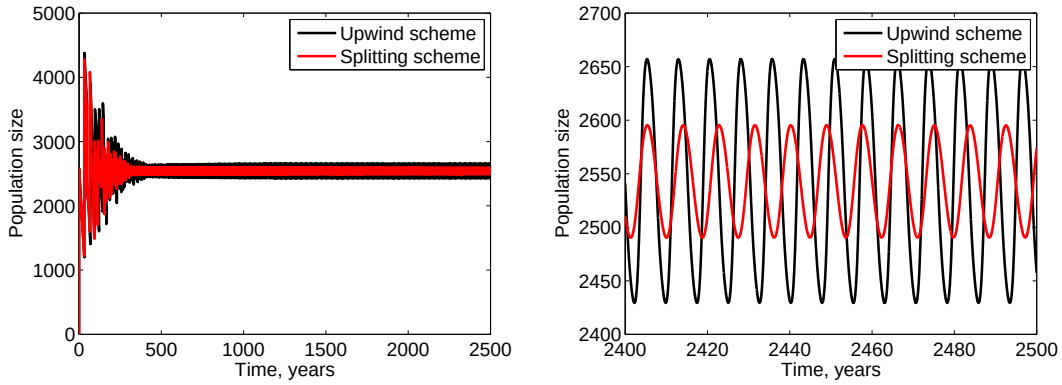

(a) (b)

Figure 4-19: (a) Time series showing the number of individuals in the S_1^P using the forward–time backward–space scheme (black line) and the splitting scheme (red line). (b) Time series for 200 years showing the number of individuals in the S_2^P compartments after the transient behaviour has been discarded when the forward–time back–ward space scheme (black line) and splitting scheme (red line) are implemented. In both graphs $k = h = 0.05$, $\rho = 0$, $\chi = 3$, $\eta = 0.5$ and the age–dependent transmission rate is implemented with $\mu = 15$. All other parameters are given in Table 4.1.

can see that for varying levels of cross–protection between $\eta = 0.1$ and $\eta = 0.5$ there is a continuous region where a stable endemic steady state is not reached (figure 4-20). This would indicate some interplay between the age–groups with the maximum transmission rate and the nature of the serotype cross–protection which is causing the oscillations.

4.7.4 Summary

When varying both the enhancement intensity and the cross–protection we see that this is little difference in the qualitative behaviour of the type I error at the endemic equilibrium. There can be some changes across enhancement prevalences (especially for high cross–protection), however there are not the scale of changes seen at the peak of the initial epidemic.

The main differences that can be seen when increasing the enhancement intensity and the cross–protection is that the solution is not always stable and oscillations can occur. Increasing the enhancement intensity causes the bifurcation point to exist for reducing enhancement prevalences. We have been able to give an estimate of where the bifurcation point may fall in the case of the age–independent and age–dependent transmission cases. This allows us to see that age–dependent transmission can greatly

Compartment	Forward-time backward-space	Splitting scheme
S_0	4	4.5
I_1	8.3	10
I_2	8.3	10
S_1^P	8.3	10
S_2^P	8.3	10
$I_{1,2}^P$	8.3	10
$I_{2,1}^P$	8.3	10
R	4	4.5

Table 4.2: The dominant period for each of the compartments when implementing the forward-time backward-space scheme with step size $k, h = 0.05$. The system is left to run for 2400 years and the dominant period found over the next 100 years.

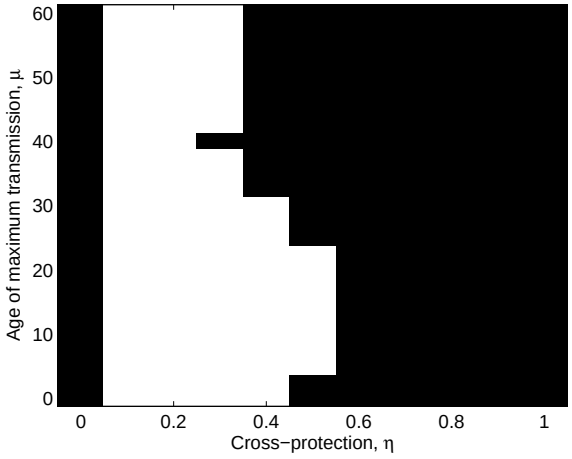

Figure 4-20: $(\eta - \mu)$ parameter space showing whether the endemic equilibrium is reached (black) or whether oscillations persist (white). The time series is incremented in steps of 0.005 to a time of 5,500 years.

affect the dynamics, stabilizing an unstable system in some cases. Finally, we have shown that if there is only cross–protection acting on the model then for high levels of cross–protection there can be oscillatory behaviour, i.e. age structure and immunity generate oscillations without any enhancement.

4.8 Discussion

In this chapter we have found the probability of type I error at the endemic equilibrium and at the peak of the initial epidemic under two sets of initial conditions. Considering

the size of the type I error has allowed us to examine how prominent age–dependence is in the two–serotype model for dengue by determining how similar seroprevalence profiles are under models which do and do not include age–dependent contact rates.

We found that if we introduce both serotypes into a naïve population the results differ from those obtained if one serotype is already endemic in the area. If infection is introduced into a naïve population at the peak of the initial epidemic the enhancement intensity does not affect the type I error. This implies that age–dependence in the transmission rate and the enhancement intensity do not interact that much. In contrast to this, varying the level of cross–protection has a greater effect; the lower the cross–protection the easier it is to differentiate seroprevalence profiles. It is also interesting to note that qualitatively the probability of type I error across age–groups with the greatest transmission rate does not change when both the enhancement intensity and cross–protection are varied.

When one serotype is endemic in the population the qualitative behaviour in the probability of type I error is affected, particularly in total seroprevalence. The behaviour then mimics what is seen at the endemic equilibrium rather than what has previously been seen at the peak of the initial epidemic.

A second difference that can be seen between the first set of initial conditions and the second set is in the values that the type I error takes. Under the first initial conditions it is harder to differentiate the seroprevalence profiles in the individual serotypes than total seroprevalence for (nearly all) parameter combinations. However, when one serotype is endemic in the population the opposite is true, meaning that it is harder to distinguish between the age-dependent and age-independent profiles when considering the total seroprevalence than that of serotype 2. This therefore has implications regarding population structure and whether one serotype is already endemic in the population or not. The results indicate that this could cause a difference in how readily age–dependence affects the ensuing dynamics.

For many of the results there is a similar probability of type I error across enhancement prevalences for a given age–group which have the maximum number of contacts. Studies showing the proportion of DHF in secondary infections (Guzmán et al., 2000, 2002; Sabchareon et al., 2012) indicate that not all secondary infections are enhanced. The result therefore suggests that as there is little change in how easy it is to differentiate seroprevalence profiles as the enhancement prevalence decreases, analysis for dengue may potentially be able to focus on the age–group which has the greatest number of infections, and hence finding an appropriate transmission rate to use in models. In contrast, when considering cross-protection it is important to know the enhancement prevalence in the population. If the enhancement prevalence is small this

makes it harder to differentiate seroprevalence profiles for children and young adults, particularly if there is cross-protection acting on secondary infections which are not enhanced.

The results indicate that, especially in a completely susceptible population, age-structure has an effect at the initial epidemic peak, as there is a difference in how easy it is to differentiate between seroprevalence profiles. The initial conditions also have an effect on the results. If a serotype is introduced into a naïve population, as it was in the 2002 epidemic in Chile (Chowell et al., 2013) and the 2012 epidemic in Madeira (Lourenço and Recker, 2014), the probability of type I error is different from that obtained if a serotype is introduced into a population where there has previously been an outbreak of a different serotype, such as the 1997 epidemic in Cuba (Guzmán et al., 2000). Therefore the make–up of the population when infection enters the population is also vital to know when studying age structure.

At the endemic equilibrium varying the enhancement level and the cross–protection did not have a great effect on the probability of type I error as the enhancement prevalence was varied. In contrast to this at the peak of the initial epidemic the probability of type I error changes with enhancement prevalence, particularly as the cross-protection is varied. However, what is seen when varying the enhancement intensity and cross–protection at the endemic equilibrium is a change in the dynamics of the system and a stable endemic steady state cannot always be achieved for different enhancement prevalences. Instead a bifurcation occurs, leading to oscillatory dynamics.

The probability of type I error at the endemic equilibrium follows similar qualitative behaviour for the individual serotypes and total seroprevalence as both the enhancement level and cross–protection are varied. This is similar to the behaviour for total seroprevalence at the initial epidemic peak when one serotype was endemic. It is not surprising that it is under these conditions that there are similarities; serotype 1 was already at an endemic equilibrium and therefore influencing the dynamics.

The results show that both at the peak of the initial epidemic and at the endemic equilibrium age-dependent transmission can have a large effect on the seroprevalence profiles, and therefore make it easier to differentiate between age-dependent and age-independent transmission. Research would indicate that it is the younger age groups who are most at risk of primary and secondary dengue infections (Kongsomboon et al., 2004; Balmaseda et al., 2006; Thai et al., 2011), and the type I error does vary in these categories. In most cases, particularly at the endemic equilibrium, increasing the age-group which has the maximum number of contacts initially decreases the type I error, meaning that it is easier to differentiate between the age-dependent and age-independent seroprevalence profiles. This in turn means that age-dependent transmis-

sion is having an effect on the seroprevalence profiles that are obtained. Therefore, if we are interested in how age structure affects seroprevalence, for example how it influences the epidemic trajectory and subsequent dynamics, then it is important to be included in a model for dengue.

CHAPTER 5

THE PROBABILITY OF AN EPIDEMIC FOR STOCHASTIC AGE STRUCTURED MODELS

Summary

In this chapter we introduce stochastic age structured models. We split the population into three age groups and assume that each can have a different exposure to mosquitoes. We initially consider a non–seasonal model and use offspring probability generating functions and stochastic simulations to determine the probability of an epidemic as the exposure weightings are varied. We then implement seasonality in the vector population and determine the probability of an epidemic. As the exposure of different age groups to the mosquito is varied we find that if infection starts in the host population the probability of an epidemic changes more dramatically than if infection starts in the vector population. This indicates that transmission from host to vector has a greater effect on the probability of an epidemic than transmission from vector to host. We also determine that as the mosquito population size increases the gradient of increase in the probability of an epidemic depends on which age group the outbreak starts in.

5.1 Introduction

Deterministic models such as those used in the previous chapters provide an excellent way of modelling epidemiological systems. However, due to their nature they do not allow for the variation that is often seen in the real world. In a deterministic model if the basic reproductive number (R_0) is large enough one person will always allow for an epidemic to occur, yet in reality this is not always the case (Diekmann and Heesterbeek, 2000). Therefore, we will now consider stochastic models, where variability within the model means that an epidemic may not always occur.

There are several different ways that stochastic models can be implemented, ranging from including noise in differential equations to event-driven approaches (Keeling and Rohani, 2008). Each of these has advantages and disadvantages, and can be used in different ways. For an event–driven epidemiological model, an event occurs when an individual moves in or out of a compartment in the model in each small time step. Gillespie's algorithm is often used in stochastic modelling when using an event-driven approach (Keeling and Rohani, 2008). In this case the probability that each event will happen is calculated, and in each time-step (which is not uniformly distributed) one of the events will occur. In this way the dynamics of the model vary with each simulation. Event–driven approaches differ from including noise in deterministic models as there has to be a whole number of individuals in a given state. This means we no longer have proportions of individuals in a compartment, which is also more realistic than the deterministic counterpart.

Epidemic stochastic models can be used for a number of different reasons. Due to their inclusion of probabilistic events and chance, they can be applied to model interventions and potentially how effective different controls will be (Gibson et al., 1999; Chowell et al., 2013). They can also be used to examine disease extinction (Keeling and Grenfell, 1997; Allen and van den Driessche, 2013), and hence the probability of whether an epidemic will in fact occur. There are several examples where dengue has been introduced into a naïve population. For example, there was a dengue epidemic in Madeira in 2012 (Lourenço and Recker, 2014), on Easter Island, Chile in 2002 (Chowell et al., 2013), and in 1997 a small outbreak in Cuba, where the previous epidemic (of a different serotype) had been between 1977–1979 (Guzmán et al., 2000). For a given population distribution knowing the probability of an epidemic in these circumstances is beneficial. Whilst the basic reproductive number is used for deterministic models and can give an indication of the severity of an epidemic, understanding the probability that an epidemic will occur if infection enters an entirely susceptible population is also important.

Stochastic models have previously been implemented for dengue. Aguiar et al. (2011b) use a stochastic model to show a realistic pattern for a two–serotype dengue model. Otero and Solari (2010) use an event–driven approach to show that in a seasonal dengue model the time at which an infected host enters the population affects the distribution of the final epidemic size. Christofferson et al. (2014) use a single serotype stochastic model which focuses on viraemia in the host. They find that understanding the contact relationship between hosts and vectors is vital to predict the likelihood and magnitude of an epidemic. We will use the stochastic model to focus on a different aspect relating to dengue; age structure.

In Chapters 3 and 4 we introduced age structure for single and two–serotype dengue models and explained the importance of age structure modelling for dengue. We now implement these ideas for a single–serotype stochastic model. Therefore, in this chapter we will use existing theory regarding the basic reproductive number and extinction thresholds for stochastic models to determine these for an age structured model. We will find the basic reproductive number for the deterministic ODE model, and then analyse the corresponding stochastic model. We follow existing theory to numerically find the probability of extinction by using offspring probability generating functions. We determine how varying the exposure weighting of different age groups and changing the initial conditions affects the probability of an epidemic. Finally, we examine the probability of an epidemic in a seasonal model, and also find how the time at which infection enters the population affects the probability of an epidemic. The first section of work uses theory on extinction thresholds given by Allen and Lahodny Jr (2012). When implementing the seasonal model we use the work of Bacaër and Ait Dads (2012) to determine the probability of an epidemic.

5.2 Methods of analysis

When studying the dynamics of infection there are different methods which can be used to analyse the system. These are dependent on the type of model which is implemented. For the deterministic ODE model we can use the basic reproductive number, R_0, which gives the expected number of secondary cases which are generated from one infected individual in a naïve population (Diekmann and Heesterbeek, 2000; Keeling and Rohani, 2008). If R_0 is less than 1 the disease will die out, whereas if R_0 is greater than 1 an epidemic will ensue. In contrast, when dealing with stochastic models we consider offspring probability generating functions and implement analysis using these to find the probability that extinction will occur (Allen and Lahodny Jr, 2012). Taking the complement of this we can find the probability of an epidemic.

We use these methods for a non-seasonal model, however seasonality adds to the complexity of the problem. It is necessary to consider the time infection enters the population, as the probability an epidemic will occur depends on both the periodicity in the population and when in the cycle infection starts. We therefore follow the work of Bacaër and Ait Dads (2012) to determine the probability of an epidemic in the seasonal model.

5.2.1 Non-seasonal deterministic model

For the non-seasonal deterministic ODE model we need to consider the next generation matrix to determine the basic reproductive number of the system. Further information can be found, for example, in van den Driessche and Watmough (2008). To find the basic reproductive number let $I = (I_1, I_2, ...I_n)'$ be the vector of infected individuals. We linearise the system of differential equations around the disease free equilibrium (DFE) to find

$$\frac{\mathrm{d}I}{\mathrm{d}t} = (F - V)I, \tag{5.1}$$

where $F - V$ is the Jacobian matrix at the DFE. F is termed the transmission matrix and V the transition matrix. There are five assumptions which matrices F and V have to satisfy to ensure the model is well posed (van den Driessche and Watmough, 2008). The basic reproductive number is the spectral radius of the next generation matrix, G, found by

$$G = FV^{-1}. \tag{5.2}$$

The basic reproductive number will give us information about the deterministic ODE model which corresponds to the stochastic model that we will study.

As well as examining the basic reproductive number for the whole population we can consider the reproductive number of different age groups. The type reproductive number is the number of secondary cases of a given type arising in a future generation from one infected individual of the same type (Diekmann et al., 2013). However, we are interested in the total number of infections generated by an individual of a given type, not just those infections of the same type. We will call this the "population–type" reproduction number. We can use the next–generation matrix to find this. Taking **I** as above we have

$$I^{t+1} = GI^t, \tag{5.3}$$

where G is the next generation matrix (equation (5.2)). The number of new infections

caused by an individual in I_i is given by

$$\begin{aligned} \bar{T}_i &= g_{1,i}I_i + g_{2,i}I_i + \ldots + g_{n,i}I_i \quad (5.4a) \\ &= \sum_j g_{j,i}I_i, \quad (5.4b) \end{aligned}$$

where $g_{i,j}$ is an element in G $(i, j = 1, \ldots, n)$. Therefore to find the population–type reproduction number for type i $(\bar{T}_i)$ we sum the elements in column i of the next–generation matrix.

5.2.2 Non-seasonal stochastic model

For the non-seasonal stochastic model we create a continuous-time Markov chain model which is analogous to the deterministic model. We need a quantity similar to the basic reproductive number which can be used to determine the probability of an epidemic in a stochastic model. Then we can use the model to derive thresholds for disease extinction (and consequently epidemic thresholds).

To derive the stochastic threshold for disease extinction using the Markov chain process we again approximate the system near the DFE. We then implement the following steps to determine the probability of an epidemic.

1. Find the transitions in the model and list the probability with which they occur.

2. Calculate the offspring probability generating function (PGF) for the different initial conditions that can arise from the model. The PGFs are given by $f_i(u_1, u_2, \ldots, u_n)$ where i is a given group of individuals and u_i is a number, $u_i \leq 1$ associated with infectious group I_i.

3. Calculate the expectation matrix, M. The elements m_{ji} correspond to the expected number of offspring of type j which an individual of type i produces. Note that the definition is similar to that of the next generation matrix, however, the next generation matrix looks at secondary infections which are new. In contrast the expectation matrix considers the number of offspring which could, for example, be a primary infection but an individual has aged and so moved into a different age group. The elements in the matrix M can be calculated using

$$m_{ji} = \left.\frac{\partial f_i}{\partial u_j}\right|_{\mathbf{u}=1} < \infty.$$

The spectral radius of the expectation matrix gives information regarding the probability of extinction (Athreya and Ney, 1972) when infection is first intro-

duced into the population:

(a) if $\rho(M) < 1$ the probability of extinction is 1.

(b) if $\rho(M) > 1$ the probability of extinction is less than 1.

As $t \to \infty$ the probability of an epidemic is 1, however we are interested in the probability of an epidemic when infection first enters a population.

4. If the probability of extinction is less than 1 there exists a unique fixed point of the PGF which is the probability of extinction given an initial condition. To find this let $0 < q_i < 1$ and for each i set $f_i(q_1, \ldots, q_n) = q_i$. If $I_j(0) = k_j$ the probability of extinction is given by

$$\lim_{t\to\infty} \text{Prob}\{\mathbf{I}(t) = \mathbf{0}\} = q_1^{k_1} \ldots q_n^{k_n} < 1. \tag{5.5}$$

5.2.3 Seasonal stochastic model

Seasonality can be included in a model in different ways, for example to represent changes in environmental factors such as the weather which may affect birth rates in mosquito driven diseases. For the seasonal stochastic model we have to implement a different methodology as the periodicity affects the underlying dynamics. If there is time dependence in the model the probability of an epidemic depends on at what point infection enters the population. We follow the work of Bacaër and Ait Dads (2012) to find the probability of an epidemic in our seasonal stochastic model.

We consider the analogous ODE model to the stochastic problem being solved. Let $\mathbf{I} = (I_1, I_2, ..., I_n)'$ denote the infected populations in the model linearised at the disease free state. Then we write the system as

$$\frac{\mathrm{d}\mathbf{I}}{\mathrm{d}t} = (A(t) - B(t))\mathbf{I}, \tag{5.6}$$

where $A(t)$ is a non-negative matrix, and $A\mathbf{I}$ represents the number of new infectious individuals created in a given time step t. The matrix $B(t)$ is formed using the other parameters and transition rates between the different compartments. Let $b_{ll}(t)$ be the exit rates of compartments and $b_{kl}(t)$, $k \neq l$ be the transfer rates from compartment l into compartment k. Then $B_{kl}(t) = -b_{kl}(t)$ $(k \neq l)$, and $B_{ll}(t) = b_{ll}(t) + \sum_{k\neq l} b_{kl}(t)$. Bacaër and Ait Dads (2012) gives the theoretical analysis (including the necessary assumptions to be made on matrices $A(t)$ and $B(t)$) of how to find the probability of extinction for a periodic system. Assuming that we wish to find the probability of extinction at time τ, given that at time t_0 there are $(I_1(t_0), I_2(t_0), ..., I_n(t_0)) \neq$

$(0, 0, ..., 0)$ individuals, this is found by

$$\omega(\tau) = \prod_i \left(1 - Y_i^{(\tau)}(\tau - t_0)\right)^{I_i(t_0)}, \tag{5.7}$$

where

$$\frac{\mathrm{d}Y_l^{(\tau)}}{\mathrm{d}s}(s) = \sum_k \left[A^*_{lk}(\tau - s)\left(1 - Y_l^{(\tau)(s)}\right) - B^*_{lk}(\tau - s)\right] Y_k^{(\tau)}(s). \tag{5.8}$$

In this equation A^* and B^* are the transposition matrices of A and B, and the initial conditions satisfy

$$Y_l^{(\tau)}(0) = 1. \tag{5.9}$$

This yields the probability of disease extinction. We therefore find the complement to calculate the probability that extinction does not occur (equally the probability of an epidemic).

5.2.4 General model information

We implement a single serotype age structured model for dengue. As we are considering the probability of an epidemic near the DFE (or the DF state in the seasonal model) we are only interested in the invasion of a single serotype. The hosts can be in one of three age-groups; children ($i = 1$), working age ($i = 2$) and retired ($i = 3$). We return to a model for dengue similar to Ferguson et al. (1999a), where individuals are susceptible, infected with or recovered. However, as we are considering the probability of an epidemic we are only interested in a single serotype. Therefore, in each of the age groups an individual can be susceptible (S_i), infected (I_i) or recovered (R_i) ($i = 1, 2, 3$). A vector can be susceptible (S_V) or infected (I_V) at any given time t. The dynamics are shown in figure 5-1. There is a constant host population, with birth and mortality rate μ. Individuals become infected through an infectious bite at rate λ_{Vi}, where i corresponds to the age-group ($i = 1, 2, 3$) and infectious hosts recover at a rate γ. We assume that the recovery rate is the same for all age groups. Progression from child to adult occurs at rate δ_1 and from adult to retired at rate δ_2. The vector population is also constant, with birth and mortality rate μ_V. Mosquitoes become infectious upon biting an infectious host at rate $\lambda_H(t)$, however due to their short lifespan there is no recovered compartment for the infected vector.

The model being implemented determines whether the different rates act concurrently or sequentially. This is explained further in Section 5.3. The parameters used in each of the models, where kept identical, are given in Table 5.1.

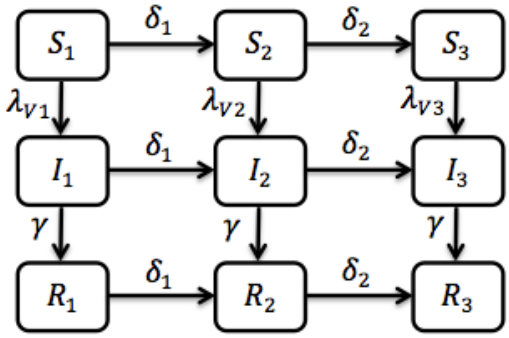

(a)

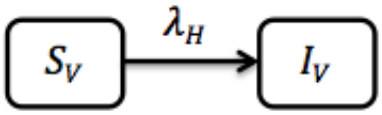

(b)

Figure 5-1: (a) Flow diagram showing the compartmentalized SIR model for three age groups (b) Flow diagram showing the vector dynamics. In both flow diagrams for clarity births and mortality have not been included.

Parameter	Definition	Value
μ	Host mortality rate	0.0167
N	Host population size	500
κ	Average number of vectors per host	5
δ_1	Rate of change child to working age	0.0667
δ_2	Rate of change working age to retired	0.0222
β	Transmission rate	70
γ	Host recovery rate	52
σ_i, $i = 1, 2, 3$	Exposure weighting of age-group i	
$N_V = \kappa N$	Vector population size	2500
μ_V	Vector mortality rate	26
a	Amplitude of oscillation in vector birth rate - seasonal model	0.25

Table 5.1: Parameter definitions and values where kept constant. All rates are given per year.

5.3 Model I: Non–seasonal model

5.3.1 Non–seasonal deterministic model

We initially implement a compartmentalized, deterministic ODE SIR type model, given by

$$\begin{aligned}
\frac{\mathrm{d}S_1}{\mathrm{d}t} &= \mu N - (\lambda_{V1} + \delta_1 + \mu)S_1, && (5.10a)\\
\frac{\mathrm{d}S_2}{\mathrm{d}t} &= \delta_1 S_1 - (\lambda_{V2} + \delta_2 + \mu)S_2, && (5.10b)\\
\frac{\mathrm{d}S_3}{\mathrm{d}t} &= \delta_2 S_2 - (\lambda_{V3} + \mu)S_3, && (5.10c)\\
\frac{\mathrm{d}I_1}{\mathrm{d}t} &= \lambda_{V1} S_1 - (\gamma + \delta_1 + \mu)I_1, && (5.10d)\\
\frac{\mathrm{d}I_2}{\mathrm{d}t} &= \lambda_{V2} S_2 + \delta_1 I_1 - (\gamma + \delta_2 + \mu)I_2, && (5.10e)\\
\frac{\mathrm{d}I_3}{\mathrm{d}t} &= \lambda_{V3} S_3 + \delta_2 I_2 - (\gamma + \mu)I_3, && (5.10f)\\
\frac{\mathrm{d}R_1}{\mathrm{d}t} &= \gamma I_1 - (\delta_1 + \mu)R_1, && (5.10g)\\
\frac{\mathrm{d}R_2}{\mathrm{d}t} &= \gamma I_2 + \delta_1 R_1 - (\delta_2 + \mu)R_2, && (5.10h)\\
\frac{\mathrm{d}R_3}{\mathrm{d}t} &= \gamma I_3 + \delta_2 R_2 - \mu R_3, && (5.10i)\\
\frac{\mathrm{d}S_V}{\mathrm{d}t} &= \mu_V N_V - (\lambda_H + \mu_V)S_V, && (5.10j)\\
\frac{\mathrm{d}I_V}{\mathrm{d}t} &= \lambda_H S_V - \mu_V I_V. && (5.10k)
\end{aligned}$$

The force of infection exerted by the vector on the host is given by

$$\lambda_{Vi} = \frac{\beta \sigma_i I_V}{\sum_j \sigma_j N_j}, \tag{5.11}$$

where β is the transmission rate. This is the number of bites per vector per unit time multiplied by the per bite vector to host transmission probability. σ_i is the exposure weighting of host age group i to the vectors. The force of infection exerted by the host on the vector is

$$\lambda_H = \frac{\beta(\sigma_1 I_1 + \sigma_2 I_2 + \sigma_3 I_3)}{\sum_i \sigma_i N_i}, \tag{5.12}$$

where σ_i is as in equation (5.11). We assume that the per bite host to vector transmission probability is equal to the per bite vector to host transmission probability, meaning that β is commutable between the two forces of infection.

To find the basic reproductive number we need to calculate the spectral radius of the next generation matrix at the DFE. At the DFE all infected and recovered compartments have no individuals in them. The stable population sizes in the susceptible host and vector compartments are given by

$$\bar{S}_1 = \frac{\mu N}{\delta_1 + \mu}, \qquad \bar{S}_2 = \frac{\delta_1 \mu N}{(\delta_1 + \mu)(\delta_2 + \mu)}, \tag{5.13a}$$

$$\bar{S}_3 = \frac{\delta_1 \delta_2 N}{(\delta_1 + \mu)(\delta_2 + \mu)}, \qquad \bar{S}_V = N_V. \tag{5.13b}$$

Note that at the DFE $\bar{N}_i = \bar{S}_i$ $(i = 1, 2, 3)$. Therefore we linearise the system at the DFE and, letting

$$\rho = \sum_i \sigma_i N_i, \tag{5.14}$$

write the transmission and transition matrices from equation (5.1) as

$$F = \begin{pmatrix} 0 & 0 & 0 & \frac{\beta\sigma_1\bar{S}_1}{\rho} \\ \delta_1 & 0 & 0 & \frac{\beta\sigma_2\bar{S}_2}{\rho} \\ 0 & \delta_2 & 0 & \frac{\beta\sigma_3\bar{S}_3}{\rho} \\ \frac{\beta\sigma_1\bar{S}_V}{\rho} & \frac{\beta\sigma_2\bar{S}_V}{\rho} & \frac{\beta\sigma_3\bar{S}_V}{\rho} & 0 \end{pmatrix} \tag{5.15}$$

and

$$V = \begin{pmatrix} \gamma + \delta_1 + \mu & 0 & 0 & 0 \\ 0 & \gamma + \delta_2 + \mu & 0 & 0 \\ 0 & 0 & \gamma + \mu & 0 \\ 0 & 0 & 0 & \mu_V \end{pmatrix} \tag{5.16}$$

respectively. Therefore, the next generation matrix is given by,

$$G = \begin{pmatrix} 0 & 0 & 0 & \frac{\beta\sigma_1\bar{S}_1}{\mu_V\rho} \\ \frac{\delta_1}{\gamma+\delta_1+\mu} & 0 & 0 & \frac{\beta\sigma_2\bar{S}_2}{\mu_V\rho} \\ 0 & \frac{\delta_2}{\gamma+\delta_2+\mu} & 0 & \frac{\beta\sigma_3\bar{S}_3}{\mu_V\rho} \\ \frac{\beta\sigma_1\bar{S}_V}{\rho(\gamma+\delta_1+\mu)} & \frac{\beta\sigma_2\bar{S}_V}{\rho(\gamma+\delta_2+\mu)} & \frac{\beta\sigma_3\bar{S}_V}{\rho(\gamma+\mu)} & 0 \end{pmatrix}, \tag{5.17}$$

and R_0 is the largest real eigenvalue of G.

The population–type reproduction numbers are therefore given by

$$\bar{T}_1 = \frac{\rho\delta_1 + \beta\sigma_1\bar{S}_V}{\rho(\gamma + \delta_1 + \mu)}, \qquad \bar{T}_2 = \frac{\rho\delta_2 + \beta\sigma_2\bar{S}_V}{\rho(\gamma + \delta_2 + \mu)}, \tag{5.18a}$$

$$\bar{T}_3 = \frac{\beta\sigma_3\bar{S}_V}{\rho(\gamma + \mu)}, \qquad \bar{T}_V = \frac{\beta\sum_i \sigma_i\bar{S}_i}{\mu_V\rho}, \tag{5.18b}$$

where ρ is as given in equation (5.14).

5.3.2 Non–seasonal stochastic model

We now create the continuous-time Markov chain model which is analogous to the deterministic model in Section 5.3.1. As stated previously, the methodology follows Allen and Lahodny Jr (2012).

Transitions in the model

We initially need to list the transitions that can occur in the model and the frequency with which they happen. This is shown in Table 5.2. Each event changes the population from one state to another in one of three ways; one compartment decreases in population size by one (for example an individual dies), one compartment increases in population size by one (for example a birth), or both of these things happen at the same time (for example if someone recovers from infection). Hosts and vectors move from initial state **a** given by

$$\mathbf{a} = (S_1, S_2, S_3, I_1, I_2, I_3, R_1, R_2, R_3, S_V, I_V) \tag{5.19}$$

to state **b** which is given in Table 5.2. State **a** is therefore the population state which changes due to individual transitions.

Offspring PGFs

Figure 5-1 and Table 5.2 show that there are 11 discrete random variables and 26 possible transitions that can occur. We assume the population is at the DFE and let the initial conditions for the susceptible and recovered compartments be given by

$$S_1(0) = \bar{S}_1, \qquad S_2(0) = \bar{S}_2, \qquad S_3(0) = \bar{S}_3, \qquad S_V(0) = \bar{S}_V$$
$$R_1(0) = 0, \qquad R_2(0) = 0, \qquad R_3(0) = 0,$$

where $\bar{S}_1$, $\bar{S}_2$, $\bar{S}_3$ and $\bar{S}_V$ are given in equation (5.13). We let the initial conditions for the infected compartments be

$$(I_1(0), I_2(0), I_3(0), I_V(0)) = (\delta_{i1}, \delta_{i2}, \delta_{i3}, \delta_{i4}), \tag{5.20}$$

where δ_{ij} is Kronecker delta ($\delta_{ij} = 0$ if $i \neq j$, $\delta_{ii} = 1$). We then generate the offspring probability generating functions (PGFs) for the system.

Let us initially make some new definitions for simplification purposes. As stated previously we are considering the system near the DFE. Therefore we let the infection

Description	State transition $\mathbf{b}$	Rate $P(\mathbf{a}, \mathbf{b})$
Host birth	$(S_1+1, S_2, S_3, I_1, I_2, I_3, R_1, R_2, R_3, S_V, I_V)$	μN
Ageing S_1	$(S_1-1, S_2+1, S_3, I_1, I_2, I_3, R_1, R_2, R_3, S_V, I_V)$	$\delta_1 S_1$
Infection S_1	$(S_1-1, S_2, S_3, I_1+1, I_2, I_3, R_1, R_2, R_3, S_V, I_V)$	$\lambda_{V1} S_1$
Mortality S_1	$(S_1-1, S_2, S_3, I_1, I_2, I_3, R_1, R_2, R_3, S_V, I_V)$	μS_1
Ageing S_2	$(S_1, S_2-1, S_3+1, I_1, I_2, I_3, R_1, R_2, R_3, S_V, I_V)$	$\delta_2 S_2$
Infection S_2	$(S_1, S_2-1, S_3, I_1, I_2+1, I_3, R_1, R_2, R_3, S_V, I_V)$	$\lambda_{V2} S_2$
Mortality S_2	$(S_1, S_2-1, S_3, I_1, I_2, I_3, R_1, R_2, R_3, S_V, I_V)$	μS_2
Infection S_3	$(S_1, S_2, S_3-1, I_1, I_2, I_3+1, R_1, R_2, R_3, S_V, I_V)$	$\lambda_{V3} S_3$
Mortality S_3	$(S_1, S_2, S_3-1, I_1, I_2, I_3, R_1, R_2, R_3, S_V, I_V)$	μS_3
Ageing I_1	$(S_1, S_2, S_3, I_1-1, I_2+1, I_3, R_1, R_2, R_3, S_V, I_V)$	$\delta_1 I_1$
Recovery I_1	$(S_1, S_2, S_3, I_1-1, I_2, I_3, R_1+1, R_2, R_3, S_V, I_V)$	γI_1
Mortality I_1	$(S_1, S_2, S_3, I_1-1, I_2, I_3, R_1, R_2, R_3, S_V, I_V)$	μI_1
Ageing I_2	$(S_1, S_2, S_3, I_1, I_2-1, I_3+1, R_1, R_2, R_3, S_V, I_V)$	$\delta_2 I_2$
Recovery I_2	$(S_1, S_2, S_3, I_1, I_2-1, I_3, R_1, R_2+1, R_3, S_V, I_V)$	γI_2
Mortality I_2	$(S_1, S_2, S_3, I_1, I_2-1, I_3, R_1, R_2, R_3, S_V, I_V)$	μI_2
Recovery I_3	$(S_1, S_2, S_3, I_1, I_2, I_3-1, R_1, R_2, R_3+1, S_V, I_V)$	γI_3
Mortality I_3	$(S_1, S_2, S_3, I_1, I_2, I_3-1, R_1, R_2, R_3, S_V, I_V)$	μI_3
Ageing R_1	$(S_1, S_2, S_3, I_1, I_2, I_3, R_1-1, R_2+1, R_3, S_V, I_V)$	$\delta_1 R_1$
Mortality R_1	$(S_1, S_2, S_3, I_1, I_2, I_3, R_1-1, R_2, R_3, S_V, I_V)$	μR_1
Ageing R_2	$(S_1, S_2, S_3, I_1, I_2, I_3, R_1, R_2-1, R_3+1, S_V, I_V)$	$\delta_2 R_2$
Mortality R_2	$(S_1, S_2, S_3, I_1, I_2, I_3, R_1, R_2-1, R_3, S_V, I_V)$	μR_2
Mortality R_3	$(S_1, S_2, S_3, I_1, I_2, I_3, R_1, R_2, R_3-1, S_V, I_V)$	μR_3
Vector birth	$(S_1, S_2, S_3, I_1, I_2, I_3, R_1, R_2, R_3, S_V+1, I_V)$	$\mu_V N_V$
Infection S_V	$(S_1, S_2, S_3, I_1, I_2, I_3, R_1, R_2, R_3, S_V-1, I_V+1)$	$\lambda_H S_V$
Mortality S_V	$(S_1, S_2, S_3, I_1, I_2, I_3, R_1, R_2, R_3, S_V-1, I_V)$	$\mu_V S_V$
Mortality I_V	$(S_1, S_2, S_3, I_1, I_2, I_3, R_1, R_2, R_3, S_V, I_V-1)$	$\mu_V I_V$

Table 5.2: Table showing transitions probabilities for the non-seasonal stochastic model when the initial state $\mathbf{a}$ is given by equation (5.19), where $\lambda_{Vi} S_i$ is given in equations (5.21)–(5.22) and $\lambda_H S_V$ is given in equations (5.23)–(5.24)

from vector to host transition be given by

$$\begin{aligned} \lambda_{Vi} S_i &= \lambda_{Vi} \bar{S}_i && \text{(5.21a)} \\ &= \frac{\beta \sigma_i I_V \bar{S}_i}{\rho} && \text{(5.21b)} \\ &= \beta_{Vi} I_V, && \text{(5.21c)} \end{aligned}$$

where

$$\beta_{Vi} := \frac{\beta \sigma_i \bar{S}_i}{\rho} \qquad (5.22)$$

and ρ is given in equation (5.14). Similarly, the infection from host to vector transition

can be given by

$$\begin{aligned} \lambda_H S_V &= \lambda_H \bar{S}_V && (5.23a) \\ &= \frac{\beta\sigma_1 I_1 + \beta\sigma_2 I_2 + \beta\sigma_3 I_3}{\rho} S_V && (5.23b) \\ &= \beta_{H1} I_1 + \beta_{H2} I_2 + \beta_{H3} I_3, && (5.23c) \end{aligned}$$

where

$$\beta_{Hi} := \frac{\beta\sigma_i S_V}{\rho}. \tag{5.24}$$

There are four offspring PGFs for the system as infection can start in any one of the host age groups or in the vector compartment. To demonstrate the offspring PGFs we will use the example where $i = 1$ in equation (5.20) so

$$(I_1(0), I_2(0), I_3(0), I_V(0)) = (1, 0, 0, 0). \tag{5.25}$$

The infected child can either infect a vector at rate β_{H1}, age at rate δ_1, recover at rate γ or die at rate μ. The probability of recovery or mortality is given by

$$p_0 = \frac{\gamma + \mu}{\beta_{H1} + \delta_1 + \gamma + \mu},$$

the probability of ageing is given by

$$p_1 = \frac{\delta_1}{\beta_{H1} + \delta_1 + \gamma + \mu},$$

and the probability of infecting a vector is given by

$$p_3 = \frac{\beta_{H1}}{\beta_{H1} + \delta_1 + \gamma + \mu}.$$

When the child ages there is no longer anyone in the I_1 compartment, as they have moved into the I_2 compartment. However, when infection of the vector occurs there is a birth, which is defined as a successful transmission of infection. When successful transmission occurs and the vector becomes infected there are two infectious agents; the child in the I_1 compartment and an infected vector in the I_V compartment. In the PGFs we use u_i to represent each of the different infected groups (with 4 representing the vectors). Therefore the offspring PGF when there is initially an infected child is

$f : [0,1] \to [0,1]$

$$f_1(u_1,u_2,u_3,u_4) = p_3u_1u_4 + p_1u_2 + p_0 \tag{5.26a}$$
$$= \frac{\beta_{H1}u_1u_4 + \delta_1u_2 + \gamma + \mu}{\beta_{H1} + \delta_1 + \gamma + \mu}. \tag{5.26b}$$

The first term in the numerator is the probability of infecting a vector, which leaves the initially infected child (u_1) and produces the infected vector (u_4). The second term is the probability of ageing which leaves us with the infected working–age person (u_2), and the third term is the probability of recovering or dying, neither of which leaves an infected individual in any compartment. The offspring PGFs can be generated for the second, third and fourth initial conditions. For $i = 2$ $((I_1(0), I_2(0), I_3(0), I_V(0)) = (0,1,0,0))$ we have

$$f_2(u_1,u_2,u_3,u_4) = \frac{\beta_{H2}u_2u_4 + \delta_2u_3 + \gamma + \mu}{\beta_{H2} + \delta_2 + \gamma + \mu}, \tag{5.27}$$

for $i = 3$ $((I_1(0), I_2(0), I_3(0), I_V(0)) = (0,0,1,0))$ we have

$$f_3(u_1,u_2,u_3,u_4) = \frac{\beta_{H3}u_3u_4 + \gamma + \mu}{\beta_{H3} + \gamma + \mu}, \tag{5.28}$$

and for $i = 4$ $((I_1(0), I_2(0), I_3(0), I_V(0)) = (0,0,0,1))$

$$f_4(u_1,u_2,u_3,u_4) = \frac{\beta_{V1}u_1u_4 + \beta_{V2}u_2u_4 + \beta_{V3}u_3u_4 + \mu_V}{\beta_{V1} + \beta_{V2} + \beta_{V3} + \mu_V}. \tag{5.29}$$

The offspring PGFs can now be used to find the expectation matrix and the fixed points associated with epidemic probability for the stochastic model.

Expectation matrix

As stated previously, the elements m_{ji} in the expectation matrix correspond to the expected number of offspring of type j which an individual of type i produces. Therefore, for example, m_{34} is the expected number of infectious retired hosts which an infected vector produces. For the three-age stochastic model being implemented the expectation matrix is given by

$$M = \begin{pmatrix} \frac{\beta_{H1}}{\beta_{H1}+\delta_1+\gamma+\mu} & 0 & 0 & \frac{\beta_{V1}}{\beta_{V1}+\beta_{V2}+\beta_{V3}+\mu_V} \\ \frac{\delta_1}{\beta_{H1}+\delta_1+\gamma+\mu} & \frac{\beta_{H2}}{\beta_{H2}+\delta_2+\gamma+\mu} & 0 & \frac{\beta_{V2}}{\beta_{V1}+\beta_{V2}+\beta_{V3}+\mu_V} \\ 0 & \frac{\delta_2}{\beta_{H2}+\delta_2+\gamma+\mu} & \frac{\beta_{H3}}{\beta_{H3}+\gamma+\mu} & \frac{\beta_{V3}}{\beta_{V1}+\beta_{V2}+\beta_{V3}+\mu_V} \\ \frac{\beta_{H1}}{\beta_{H1}+\delta_1+\gamma+\mu} & \frac{\beta_{H2}}{\beta_{H2}+\delta_2+\gamma+\mu} & \frac{\beta_{H3}}{\beta_{H3}+\gamma+\mu} & \frac{\beta_{V1}+\beta_{V2}+\beta_{V3}}{\beta_{V1}+\beta_{V2}+\beta_{V3}+\mu_V} \end{pmatrix}. \tag{5.30}$$

The largest real eigenvalue of M subsequently determines the extinction threshold of the non-seasonal stochastic model.

Fixed points

Due to the complexity of our system it is not possible to give analytical expressions for the fixed points. However they can be calculated numerically using MATLAB.

5.3.3 Results I: Varying the exposure weightings

It is important to note that the exposure weightings in the model are relative to each other. Therefore, the probability of an epidemic if $\sigma_1 = \sigma_2 = \sigma_3 = 0.1$ is the same as if $\sigma_1 = \sigma_2 = \sigma_3 = 1$. This is because the exposure weighting affects the whole age-group, not just infected individuals. The transmission term for each age-group does not change; it is the frequency that all hosts come into contact with vectors that is being varied. Therefore we consider how the exposure weightings of the age groups compare to each other. For example, if $\sigma_1 = \sigma_3 = 0.5$ and $\sigma_2 = 1$ the working age group are exposed to vectors twice as much as the other ages. Once exposed the probability of a transmission event is the same for all age-groups.

We initially consider the non–seasonal deterministic model. Figure 5-2(a) shows the population–type reproduction numbers ($\bar{T}_i$) for infected compartments I_i ($i = 1, 2, 3, V$) as the exposure weighting of the working age group is varied. As the exposure weighting of the working age group increases the population–type reproduction number decreases for the children's and retired age groups. This is because the exposure of the working age group is increasing, meaning that the distribution of bites changes across the population. As previously stated the exposure weightings are relative to each other. Therefore, as the exposure weighting of the working age group increases, the relative exposure that the children and the retired age groups have to vectors becomes less important. This means the population–type reproduction number decreases as more vectors are biting the working age group instead. In contrast, the population type reproduction number for the working age group increases. This is to be expected; the working age group are having a greater impact, thereby increasing the expected number of infections that they can make. Varying the exposure weighting has no effect on the population–type reproduction number of the vectors; the vectors bite at the same rate, it is just the composition of the population that they bite that changes. Therefore, the population–type reproduction number itself is identical as the exposure weighting is varied.

We then consider the corresponding non–seasonal stochastic model. Figure 5-2(b)

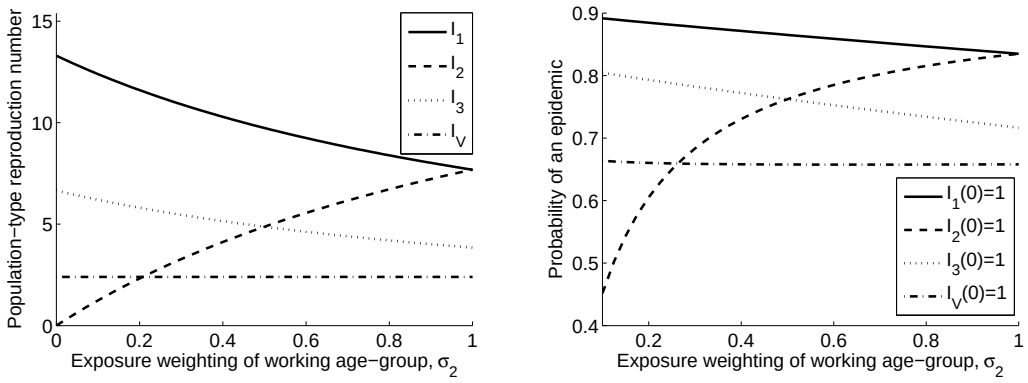

(a) (b)

Figure 5-2: (a) The population–type reproduction numbers for the children's age group (solid line), working age group (dashed line), retired age group (dotted line) and vectors (dot-dashed line) as the exposure weighting of the working age group is increased. (b) The probability of an epidemic using the PGFs (equations (5.26)–(5.29)) as the exposure weighting of the working age-group is varied. The initial conditions are $I_1(0) = 1$ (solid line), $I_2(0) = 1$ (dashed line), $I_3(0) = 1$ (dotted line) and $I_V(0) = 1$ (dot–dashed line). In both figures the exposure weighting of the children's and retired age-groups are $\sigma_1 = 1$ and $\sigma_3 = 0.5$ respectively. All other parameters are given in Table 5.1.

gives an example of how the probability of an epidemic changes when the exposure weighting of the working age group is varied and the exposure weightings of the other age groups are kept constant, calculated using the PGFs (equations (5.26) – (5.29)). The qualitative behaviour in the figure is similar to that of the population–type reproduction numbers (compare with figure 5-2(a)). If infection starts in the youngest or oldest age group then as the exposure weighting of the working age group increases the probability of an epidemic decreases. The reasoning for this is the same as in the deterministic case; the exposure of the population changes and therefore the vectors are distracted by the working–age group. If infection starts in the working age group there is initially a steep increase in the probability of an epidemic as the exposure weighting increases. This is unsurprising; the more exposure the group has to mosquitoes, the more likely the vector is to bite in that group (i.e. where the infected host is) rather than bite an individual in a different age group. The host exposure weighting is important to the overall probability of an epidemic. For example, the probability of an epidemic is smaller if infection starts in the oldest age-group rather than the youngest age group, as the exposure weighting for the older age-group is half that of children. Similarly, the probability of an epidemic if infection starts in the working age-group is always less than (or equal to in the case of $\sigma_2 = 1$) the probability of an epidemic if

infection starts in the children's age-group.

In contrast to when infection starts in the host population, the probability of an epidemic is relatively constant when infection starts in the vector population as the exposure of the working age group is increased. Once the exposure weighting of the working age group is greater than $\sigma_2 = 0.3$ the probability of an epidemic is always smaller if infection starts in the vector population than any host age group. This implies that it is only the first two generations of transmission (vector to host to vector) which are important in determining the probability of an epidemic if infection starts in the vector population. This is because one infected vector has to bite and pass on infection to hosts, whereas one infected host can be bitten by many susceptible mosquitoes. This is also an indication of where prevention strategies should be implemented. We now extend this to consider how the probability of an epidemic changes as the exposure weighting of another age-group varies as well.

Figure 5-3 shows the probability of an epidemic found using the PGFs (equations (5.26)–(5.29)) as the exposure weighting of the working and retired age groups are varied. The children's exposure weighting is fixed at $\sigma_1 = 1$ meaning that in these simulations the exposure weightings being varied are always less than or equal to that of the children. When infection initially starts in the children's age-group (figure 5-3 (a)) as the exposure weighting of the other age-groups increases the probability of an epidemic decreases. This is because the distribution of bites changes; the increase in exposure weighting decreases the importance of the exposure weighting of the children. Therefore the probability of a vector biting an infected child relative to the other age groups decreases. If infection starts in the working age-group the dynamics differ (figure 5-3(b)). For each exposure weighting for the working ages, as the exposure weighting for the retired age group increases the probability of an epidemic decreases. This is again due to the distribution of bites changing and the retired age group receiving a greater proportion of bites. Therefore the probability a vector bites an infected adult host before recovery or death decreases. As the exposure weighting for the working age group increases (the group initially infected), the probability of an epidemic increases as the age-group is more exposed to the vectors relative to other ages. This increase in the probability of an epidemic is faster than the decrease that occurs as the exposure weighting for the retired age-group increases. If infection starts in the retired age-group (figure 5-3 (c)) then we see similar results to when infection starts in the working age-group but reflected along the diagonal (compare with figure 5-3(b)). However, the graphs are not symmetric; this is because, on average, individuals remain in the working age-group for longer than the retired age-group. This affects the number of individuals infected and therefore the probability that an epidemic will occur.

Figure 5-3(d) shows that if infection starts in the vector population there are different dynamics to any previous case. As the exposure weightings increase the probability of an epidemic decreases by a very small amount (note the scale). The variation in the probability of an epidemic is very small in comparison to when infection starts in any of the host age-groups and the probability itself lies between the maximum and minimum if infection starts in any other compartment.

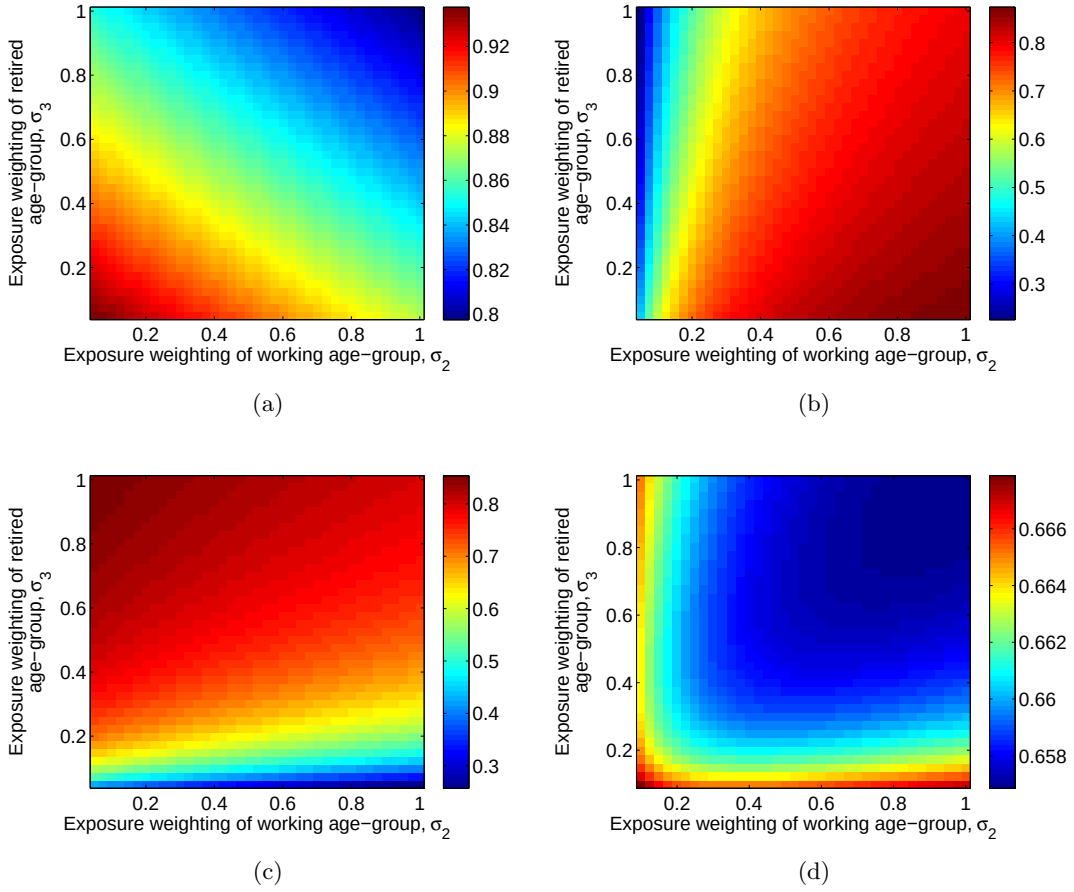

Figure 5-3: The probability of an epidemic found using the PGFs (equations (5.26)–(5.29)). In (a) the initial condition is $I_1(0) = 1$, in (b) is $I_2(0) = 1$, in (c) is $I_3(0) = 1$ and in (d) is $I_V(0) = 1$. The children's exposure weighting is $\sigma_1 = 1$. All other parameters are given in Table 5.1.

We can compare the results found using the PGFs (equations (5.26)–(5.29), figure 5-3) with the corresponding stochastic simulations (figure 5-4). When infection starts in the host population (figures 5-4(a)–(c)) using 1000 simulations of the stochastic model produces results which match well to those found using the PGFs. We see that as well

as matching qualitatively, quantitatively the ranges in the probability of an epidemic are similar (see Table 5.3). Figure 5-4 (d) shows the stochastic model when infection starts in the vector population. Although the probability of an epidemic has a greater range of values than when considering the result using the PGF, we can start to see the pattern of a lower probability of an epidemic for higher exposure weightings of the the working and retired age groups.

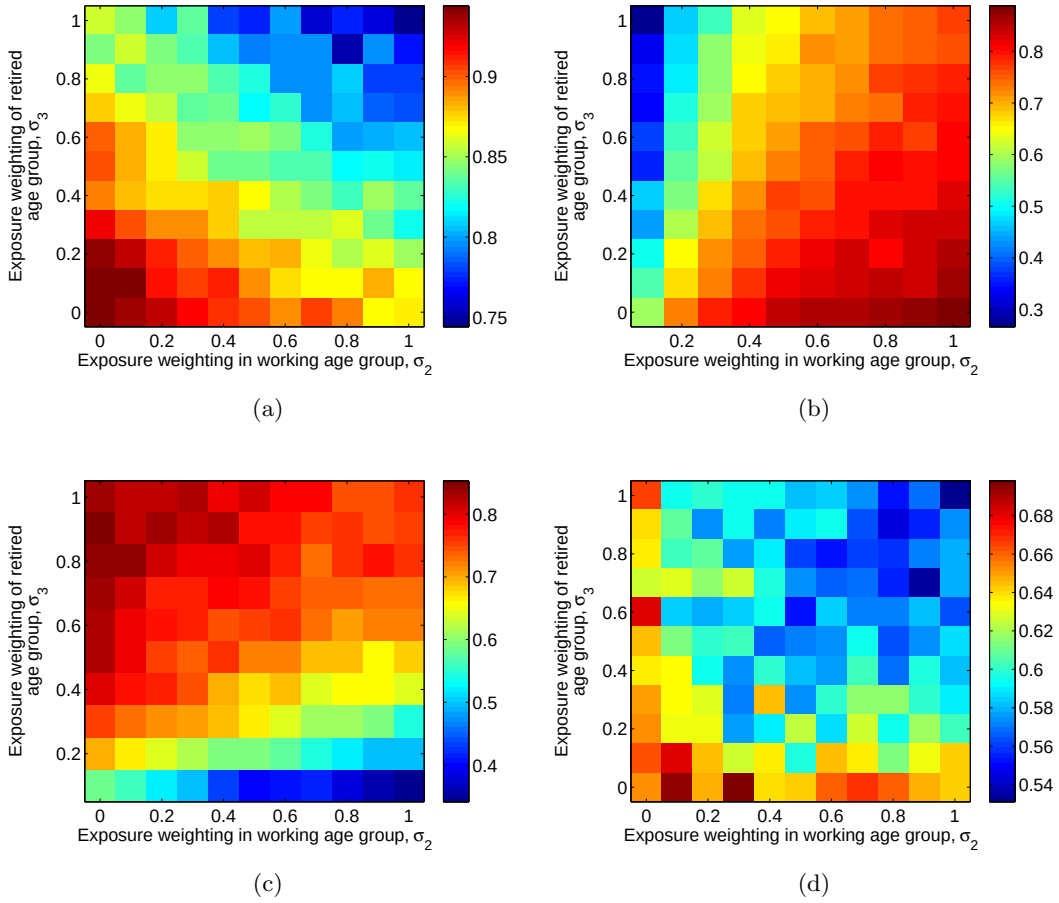

Figure 5-4: The probability of an epidemic found using stochastic simulations. In the stochastic model 1000 simulations have been run. An epidemic is said to have occurred if 5% of the total population (host and vector) are infected at any time. In (a) the initial condition is $I_1(0) = 1$, in (b) is $I_2(0) = 1$, in (c) is $I_3(0) = 1$ and in (d) is $I_V(0) = 1$. The children's exposure weighting is $\sigma_1 = 1$. All other parameters are given in Table 5.1.

As well as varying the exposure weightings of the working and retired age-groups, we can also see how changing the exposure weighting of the children's age-group affects the probability of an epidemic. We initially consider this for a single exposure weighting

Initial condition	**Range - PGFs (Figure 5-3)**	**Range - stochastic simulations (Figure 5-4)**
$I_1(0) = 1$	$0.7976 - 0.9286$	$0.744 - 0.944$
$I_2(0) = 1$	$0.3650 - 0.8900$	$0.266 - 0.888$
$I_3(0) = 1$	$0.3983 - 0.8501$	$0.341 - 0.853$
$I_V(0) = 1$	$0.6568 - 0.6679$	$0.531 - 0.698$

Table 5.3: The range that the probability of an epidemic takes using the PGFs and stochastic simulations under each of the different initial conditions.

for the retired age-groups, shown in figure 5-5. The underlying qualitative dynamics if infection starts in the host are the same as seen previously (compare with figure 5-2(b)). The results show that it makes a difference which population group should be targeted with prevention measures as decreasing the exposure weighting of one age group can increase the probability of an epidemic if infection starts in another. When infection starts in the vector compartment (figure 5-5 (d)) we find some interesting dynamics. Unlike when infection starts in any host age-group, the probability of an epidemic is qualitatively different as the child's exposure weighting is varied. The scale of the variation in epidemic probability is minimal when infection starts in the vector population and so we check this is not the results of numerical error (see Appendix C).

Figures 5-6 and 5-7 show the generalisation of this result. The exposure weightings of the working and retired age-groups are varied when the children's weightings are $\sigma_1 = 0.2$, $\sigma_1 = 0.5$ and $\sigma_1 = 1$ for comparison. If infection starts in the children's age-group (figures 5-6(a), (b) and (c)) then as the exposure weighting of the children's age-group increases so too does the epidemic probability. In contrast to this, if infection starts in the working age-group (figures 5-6(d), (e) and (f)) or the retired age-group (figures 5-6(g), (h) and (i)), then as the exposure weighting of the children increases the probability of an epidemic decreases. However, the change in the probability as the exposure weighting of the children is increased is far less than when infection starts in the children's age group. This exemplifies the importance of understanding how the exposure weightings, and where infection initially enters the population, are linked together. The overall qualitative behaviours of the graphs are to be expected from figures 5-3 and 5-5.

Figure 5-7 shows the probability of an epidemic when infection starts in the vector population as the exposure weightings are varied. The probability of an epidemic is fairly uniform across all exposure weightings. When infection starts in the host, as exposure weightings vary the qualitative behaviour of the graphs showing the probability of extinction is the same; it is the quantitative behaviour which is different. In con-

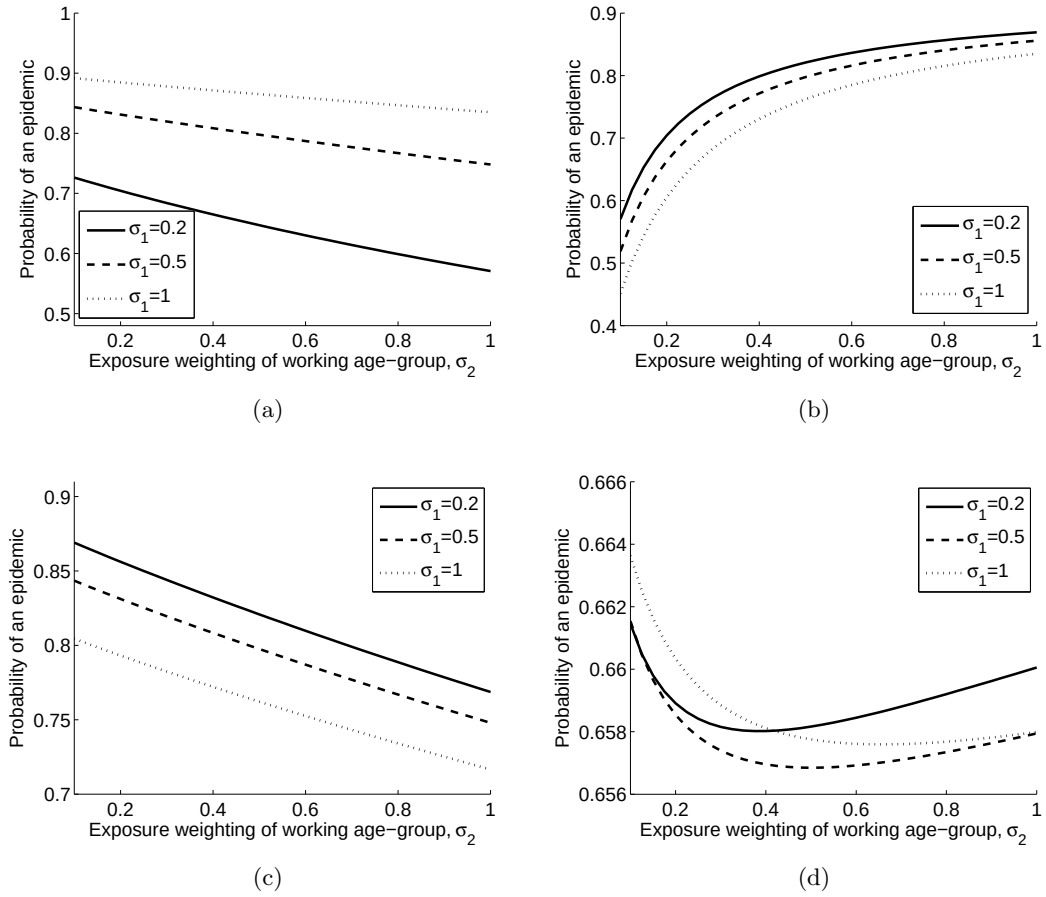

Figure 5-5: The probability of an epidemic under the PGFs (equations (5.26)–(5.29)). In (a) $I_1(0) = 1$, in (b) $I_2(0) = 1$, in (c) $I_3(0) = 1$ and in (d) $I_V(0) = 1$. In each graph solid, dashed and dotted lines are the children's exposure weighting $\sigma_1 = 0.2$, $\sigma_1 = 0.5$ $\sigma_1 = 1$ respectively. The retired age groups exposure weighting is $\sigma_3 = 0.5$. All other parameters are given in Table 5.1.

trast, when infection starts in the vector population the qualitative behaviour changes. When the exposure weighting of the children's age-group is $\sigma_1 = 0.2$ (figure 5-7(a)) the probability of an epidemic is least when all three exposure weightings are similar, and increases as the exposure weighting of the working and retired age-groups increase. When the exposure weighting of the children's age-group is $\sigma_1 = 0.5$ (figure 5-7(b)), the probability of an epidemic is again least when the other age-groups' exposure weightings are similar. However, as the exposure weightings of the working and retired age-groups decrease the probability of an epidemic increases. This is because any asymmetry in the weighting increases the epidemic probability as infection dynamics are more focussed on one age group, in this case the children's age group. Therefore if infection starts

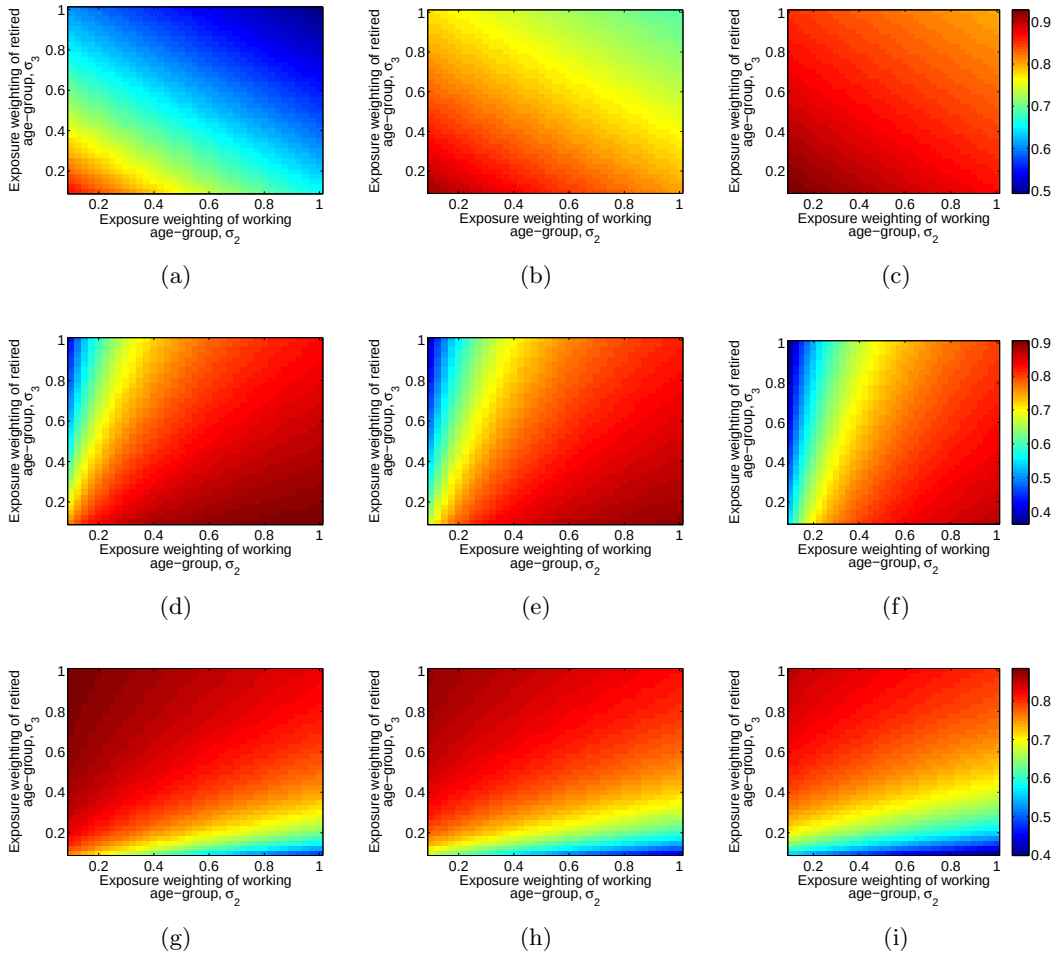

Figure 5-6: The probability of an epidemic under the PGFs (equations (5.26)–(5.29)). In (a), (b) and (c) the initial condition is $I_1(0) = 1$, with $\sigma_1 = 0.2$, 0.5, and 1 respectively. In (d), (e) and (f) the initial condition is $I_2(0) = 1$, with $\sigma_1 = 0.2$, 0.5, and 1 respectively. In (g), (h) and (i) the initial condition is $I_3(0) = 1$, with $\sigma_1 = 0.2$, 0.5, and 1 respectively. All other parameters are given in Table 5.1.

in the vector population to limit the probability of an epidemic we want the exposure weightings of all host age groups to be identical.

5.3.4 Results II: Varying the number of vectors to hosts

As well as varying the exposure weightings of the hosts, we can also vary the average number of vectors per host. This helps to determine thresholds that can be associated with epidemics if it is known the number of vectors to hosts that exist. We let the vector population size be $N_V = \kappa N$ and vary κ. We keep the exposure weighting of

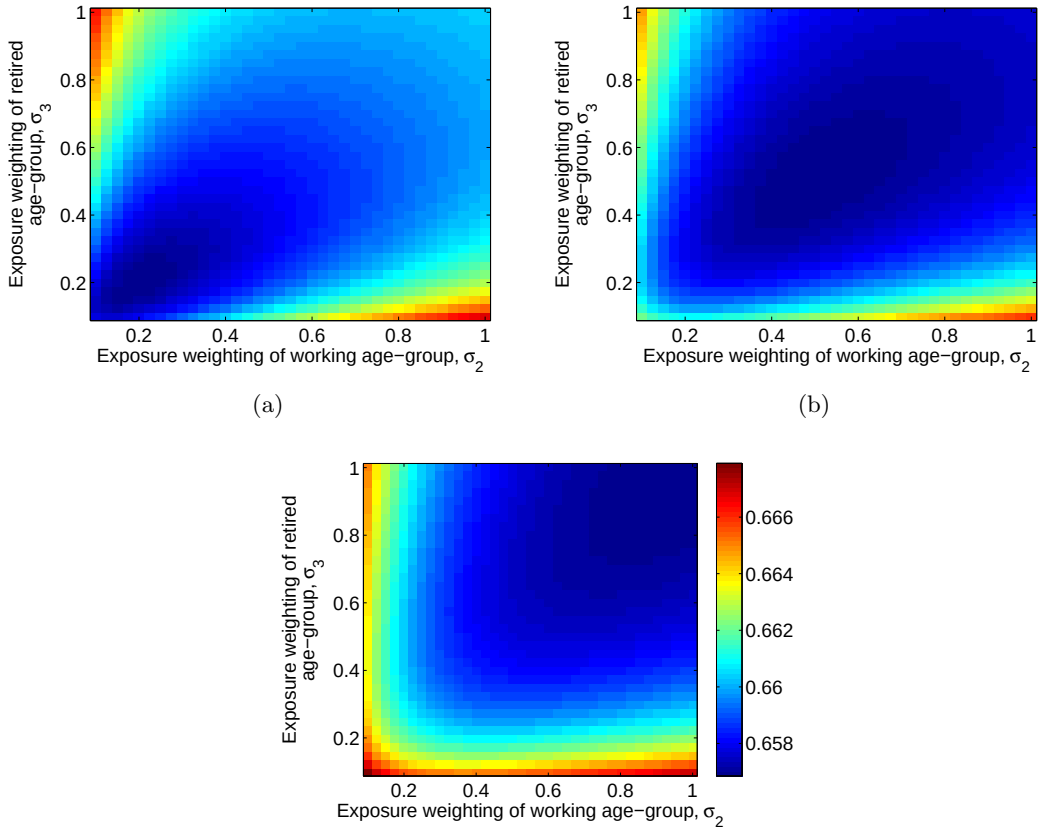

Figure 5-7: The probability of an epidemic under the PGFs (equations (5.26)–(5.29)). In (a), (b) and (c) the initial condition is $I_V(0) = 1$, with $\sigma_1 = 0.2$, 0.5, and 1 respectively. All other parameters are given in Table 5.1.

the retired age group constant and vary the exposure weightings of the children's and working age groups; we allow the children's and working age-groups to have exposure less than, equal to, and greater than that of the retired age-group.

When considering the probability of an epidemic as the average number of vectors per host increases there is the same qualitative behaviour whether infection starts in the host (figures 5-8(a), (b) and (c)) or in the vector (figure 5-8(d)); the probability of an epidemic increases. The probability tends towards an asymptote which is dependent on the exposure weightings of the different age-groups. If infection starts in the children's age-group (figure 5-8(a)) as the exposure weighting of the working age group increases the probability of an epidemic decreases (consider the solid lines), as the distribution of vector bites changes and hence the probability of an infected child being bitten

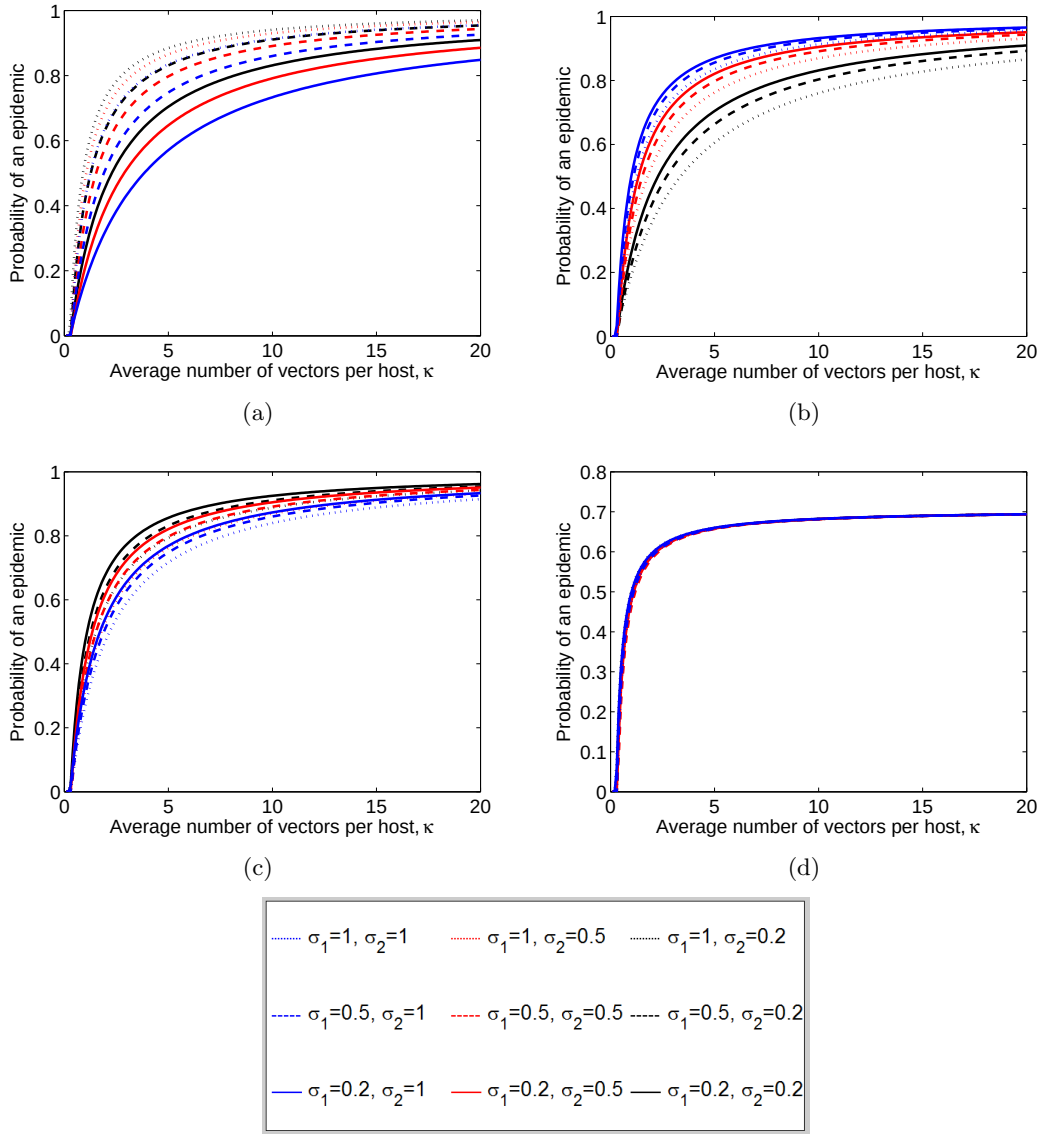

Figure 5-8: The probability of an epidemic using the PGFs (equations (5.26)–(5.29)) as the average number of vectors per host is varied. In (a) the initial condition is $I_1(0) = 1$, in (b) $I_2(0) = 1$, in (c) $I_3(0) = 1$ and in (d) $I_4(0) = 1$. (e) Shows the legend for each of the graphs. Solid, dashed and dotted lines represent $\sigma_1 = 0.2$, $\sigma_1 = 0.5$ and $\sigma_1 = 1$ respectively. Black, red and blue lines represent $\sigma_2 = 0.2$, $\sigma_2 = 0.5$ and $\sigma_2 = 1$ respectively. The retired age groups exposure weighting is $\sigma_3 = 0.5$. All other parameters are given in Table 5.1.

decreases. This is also true when infection starts in the retired age-group (figure 5-8(c)). In contrast, and as expected, when infection starts in the working age-group (figure 5-8(b)) when the exposure weighting of the working age-group increases the probability of an epidemic increases. These results mirror the qualitative behaviours which have already been established. The results as the exposure weighting of the children's age group is increased (consider the different coloured lines) are analogous to these results.

Figure 5-8(d) shows the probability of an epidemic when an infected vector is placed in a completely susceptible population. In contrast to when infection starts in the host, the probability of an epidemic as the number of vectors to hosts increases is nearly identical no matter the exposure weighting of the different age-groups. We also see that the probability of an epidemic if infection starts with a vector is less than when infection starts in the host population. When there are 20 times the number of vectors to hosts, the probability of an epidemic if infection starts in any host population is over 80%. However, if infection starts in the vector population it is just under 70%. This is a marked difference, and gives an indication of how the dynamics of infection may be different if initially started by a vector rather than a host. This is because one vector can make β bites per day, however one person may be bitten by many vectors in a day, and therefore infection is spread more easily.

Figure 5-9 shows the stochastic simulations and corresponding result using the PGFs under the different initial conditions. For this example we have chosen specific exposure weightings, however, as in this example, the stochastic model is a good approximation in all cases. We have also only run the stochastic model for 200 simulations, meaning that increasing this should increase the reliability of any results.

It is interesting to notice the different shapes of the curves depending on which age group infection originated. The initial gradient if infection starts in the host population is dependent on the exposure weighting of the age-group to vectors. The smaller the exposure weighting relative to other age-groups the shallower the gradient and hence the longer it takes to reach an asymptote for the maximum probability of an epidemic. When infection starts in the vector population we can see that the number of vectors to hosts is much smaller for the asymptote to be reached. This again indicates that the exposure weightings have a smaller impact on the probability of an epidemic if infection starts in the vector population rather than the host population.

5.3.5 Summary

We have shown that as the exposure weighting of different aged hosts to vectors are varied the probability of an epidemic is highly dependent on the initial conditions

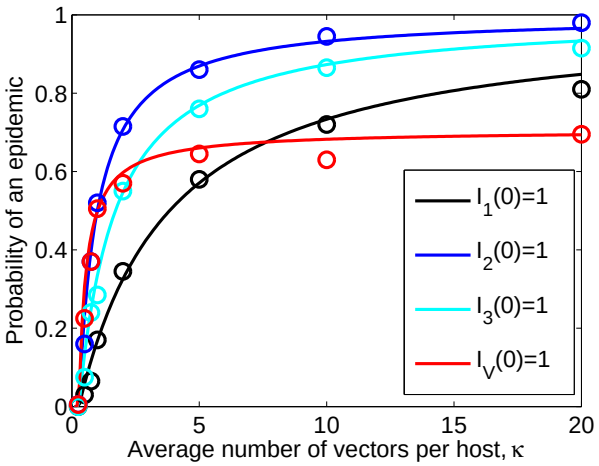

Figure 5-9: The probability of an epidemic as the number of vectors per host (κ) is varied. The solid line represents the result under the PGFs (equations (5.26)–(5.29)) and the circles are the stochastic approximation for the given κ value. In the stochastic model 200 simulations have been run. The black, blue, cyan and red colours correspond to the initial conditions $I_1(0) = 1$, $I_2(0) = 1$, $I_3(0) = 1$ and $I_V(0) = 1$ respectively. The exposure weightings for the children's, working age and retired age groups are $\sigma_1 = 0.2$, $\sigma_2 = 1$, $\sigma_3 = 0.5$ respectively. The vector population is $N_V = \kappa N$. All other parameters are given in Table 5.1.

of the system. If infection enters the population through an infected host there is much greater variability in the probability of an epidemic than if infection enters the population through a mosquito.

In the host population, if the exposure weighting being varied corresponds to the age-group where infection originates, an increase in exposure weighting causes a corresponding increase to the probability of an epidemic. Conversely, if infection starts in any of the other age-groups, the probability of an epidemic decreases. This is because the distribution of exposure has changed; hence the relative exposure to vectors that the initially infected age group has decreases.

The results show that there is greater variation in the probability of an epidemic if infection starts in the host population rather than the vector. The main loss of epidemic probability occurs when the vector infects a host. This is because a vector can only make β bites per day, however a host can be bitten multiple times by different mosquitoes. Therefore if infection starts in the vector population, when we have been through two generations of infection (vector to host to vector) the epidemic is either extinct or underway. In contrast, if infection starts in the host population we see that after two generations (host to vector to host) then there can be a greater possibility

that infection can still be passed on. Therefore imported human cases have a greater epidemic potential than imported vector cases. This is supported by the population–type reproduction numbers. These show that unless the exposure weightings are very small for an age group, the population–type reproduction number is smaller when infection starts in the vector population. We also see that the probability of an epidemic does not overly change if infection starts in the vector population. This implies that if infection does start with a mosquito, management strategies do not necessarily need to focus on the exposure of different aged individuals, but the host population as a whole.

Finally, we have shown that the probability of an epidemic increases as the average number of vectors to hosts increases. We have shown, for a given infection duration and set of exposure weightings, the probability of an epidemic quickly reaches 50% with less than five times the number of vectors to hosts. This is again important when considering prevention strategies. Unless the vector population can be significantly reduced with management strategies there may not be a marked impact on the reduction of the probability of an epidemic. Therefore an alternative strategy focusing on a different area may, in fact, be more appropriate.

5.4 Model II: Seasonal model

5.4.1 The model

We include seasonality in the model by introducing a time dependent birth rate for the vector population. Therefore, the host system is modelled by equations (5.10a)–(5.10i), with the vector population equations given by

$$\frac{\mathrm{d}S_V}{\mathrm{d}t} = N_V\left(1 - a\cos\left(\frac{2\pi t}{364}\right)\right)\mu_V - (\lambda_H + \mu_V)S_V \tag{5.31a}$$

$$\frac{\mathrm{d}I_V}{\mathrm{d}t} = \lambda_H S_V - \mu_V I_V, \tag{5.31b}$$

where λ_H, μ_V and N_V are as in the seasonal model (for parameter values see Table 5.1), and a describes the amplitude of the oscillation. If $a = 0$ there is no seasonality, and the non-seasonal model (equation (5.10)) is recovered.

Due to periodicity in the vector birth rate we no longer reach a DFE. However, we can find a disease free (DF) state where the vector population varies with time. Assuming that at $t_0 = 0$ $N_V = \kappa N$, the host and vector populations at the DF state

are given by

$$\bar{S}_1 = \frac{\mu N}{\delta_1 + \mu}, \qquad \bar{S}_2 = \frac{\delta_1 \mu N}{(\delta_1 + \mu)(\delta_2 + \mu)}, \qquad \bar{S}_3 = \frac{\delta_1 \delta_2 N}{(\delta_1 + \mu)(\delta_2 + \mu)}, \tag{5.32a}$$

$$\bar{S}_V(t) = \bar{N}_V(t) = \kappa N \exp\left(-a\mu_V \sin\left(\frac{2\pi t}{364}\right)\frac{364}{2\pi}\right). \tag{5.32b}$$

It is only the vector population which varies with time at the DF state; the host populations remain constant. These population sizes are used to find $A(t)$ and $B(t)$ in equation (5.6) and are used to compute the probability of an epidemic for a seasonal model. We therefore have

$$A(t) = \begin{pmatrix} 0 & 0 & 0 & \frac{\beta\sigma_1 S_1}{\rho} \\ \delta_1 & 0 & 0 & \frac{\beta\sigma_2 S_2}{\rho} \\ 0 & \delta_2 & 0 & \frac{\beta\sigma_3 S_3}{\rho} \\ \frac{\beta\sigma_1 S_V(t)}{\rho} & \frac{\beta\sigma_2 S_V(t)}{\rho} & \frac{\beta\sigma_3 S_V(t)}{\rho} & 0 \end{pmatrix} \tag{5.33a}$$

and

$$B(t) = \begin{pmatrix} \delta_1 + \gamma + \mu & 0 & 0 & 0 \\ 0 & \delta_2 + \gamma + \mu & 0 & 0 \\ 0 & 0 & \gamma + \mu & 0 \\ 0 & 0 & 0 & \mu_V \end{pmatrix}, \tag{5.33b}$$

where ρ is as in equation (5.14). Let $p(t, i_1, i_2, i_3, i_V)$ be the probability of having i_k individuals (hosts or vectors) in compartment I_k at time t, then assuming $i_V = i_4$

$$\begin{aligned} \frac{\mathrm{d}}{\mathrm{d}t}p(t, i_1, ..., i_V) \;=\; & \sum_{k=1}^{4}\left(A_{kk}(i_k - 1) + \sum_{l\neq k} A_{kl} i_l\right) p(t, i_1, ..., i_k - 1, ..., i_m) + \\ & + \sum_{k\neq l} b_{kk}(i_l + 1) p(t, i_1, ..., i_k - 1, ..., i_l + 1, ..., i_4) + \\ & + \sum_{k=1}^{4} b_{kk}(i_k + 1) p(t, i_1, ..., i_k + 1, ..., i_4) - \\ & + \sum_{k,l=1}^{4} (A_{kl} + b_{kl})\, i_l p(t, i_1, ..., i_4) \end{aligned} \tag{5.34}$$

We take an initial condition

$$p(t_0, i_1, i_2, i_3, i_4) = \begin{cases} 1 \text{ if } (i_1, i_2, i_3, i_4) = (I_1(t_0), I_2(t_0), I_3(t_0), I_V(t_0)), \\ 0 \text{ otherwise} \end{cases} \tag{5.35}$$

and find the extinction probability, ω, which is the limit of $p(t, 0, 0, 0, 0)$ as $t \to \infty$. Therefore we find the probability that the process is not extinct, or as we call it, the probability of an epidemic, $(1 - \omega)$. To do this we need to find $Y_l^{(\tau)}$ $(l = 1, \ldots, 4)$, which satisfy equation (5.8). For this we have to solve

$$\begin{aligned}
\frac{\mathrm{d}Y_1^{(\tau)}}{\mathrm{d}s}(s) &= -(\delta_1 + \gamma + \mu)Y_1^{(\tau)}(s) + \delta_1 \left(1 - Y_1^{(\tau)}(s)\right) Y_2^{(\tau)}(s) + \\
&\qquad \frac{\beta\sigma_1 S_V(\tau - s)}{\rho} \left(1 - Y_1^{(\tau)}(s)\right) Y_4^{(\tau)}(s), && \text{(5.36a)} \\
\frac{\mathrm{d}Y_2^{(\tau)}}{\mathrm{d}s}(s) &= -(\delta_2 + \gamma + \mu)Y_2^{(\tau)}(s) + \delta_2 \left(1 - Y_2^{(\tau)}(s)\right) Y_3^{(\tau)}(s) + \\
&\qquad \frac{\beta\sigma_2 S_V(\tau - s)}{\rho} \left(1 - Y_2^{(\tau)}(s)\right) Y_4^{(\tau)}(s), && \text{(5.36b)} \\
\frac{\mathrm{d}Y_3^{(\tau)}}{\mathrm{d}s}(s) &= -(\gamma + \mu)Y_3^{(\tau)}(s) + \frac{\beta\sigma_3 S_V(\tau - s)}{\rho} \left(1 - Y_3^{(\tau)}(s)\right) Y_4^{(\tau)}(s), && \text{(5.36c)} \\
\frac{\mathrm{d}Y_4^{(\tau)}}{\mathrm{d}s}(s) &= \frac{\beta\sigma_1 S_1}{\rho} \left(1 - Y_4^{(\tau)}(s)\right) Y_1^{(\tau)}(s) + \frac{\beta\sigma_2 S_2}{\rho} \left(1 - Y_4^{(\tau)}(s)\right) Y_2^{(\tau)}(s) \\
&\qquad \frac{\beta\sigma_3 S_3}{\rho} \left(1 - Y_4^{(\tau)}(s)\right) Y_3^{(\tau)}(s) - \mu_V Y_4^{(\tau)}(s), && \text{(5.36d)}
\end{aligned}$$

for $0 < s < \tau - t_0$ where t_0 is the initial time infection enters the population, and the initial conditions on the $Y^{(\tau)}$ variables are given by

$$Y_l^{(\tau)}(0) = 1, \qquad l = 1, 2, 3, 4. \tag{5.37}$$

Solving this system allows us to find the probability of an epidemic when infection enters the population at different times throughout the year.

5.4.2 Results

To study the seasonal model we need to understand the dynamics of the susceptible vector population at the DF state. The vector population size at the DF state (equation (5.32b)) over the course of one year can be seen in figure 5-10. The vector population size initially decreases before a minimum is reached. Then there is an increase in the population size. Once a maximum is reached between 8 and 9 months

into the year the population size of vectors again decreases. It is interesting to note that although we have sinusoidal forcing in the vector population, the population size itself is not sinusoidal.

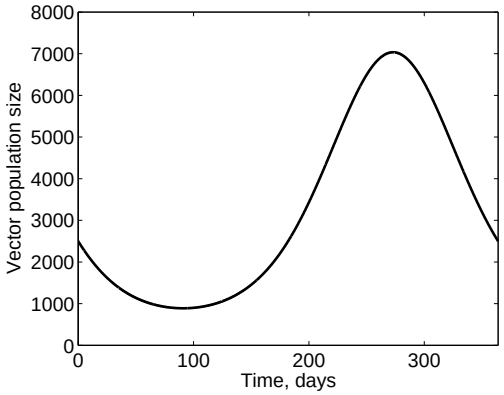

Figure 5-10: The vector population size over the course of one year at the DF state. The vector population is given by equation (5.32b). All other parameters given in Table 5.1.

We initially set the exposure weighting of each host age-group to be constant (greatest for the working age-group and least for the retired age-group) to determine how the probability of an epidemic is affected when infection is introduced at different times during the year (figure 5-11(a)). No matter which population infection starts in, there is initially a decrease in the probability of an epidemic; the vector population size has decreased and hence there is less chance that a transmission event will take place. As time goes on the probability of an epidemic then increases alongside the vector population size. As when studying the non-seasonal model we see that whilst there is large variation in the probability of an epidemic if infection starts in the host population, there is much smaller variation if infection starts in the vector population. Interestingly, when the vector population is at its largest, the probability of an epidemic is smallest if infection starts in the vector population. This indicates that infection starting in the host population poses a greater risk than infection starting in the vector population. This is exemplified by figures 5-11(b) and (c) which show the instantaneous population–type reproduction numbers (equation 5.4) throughout the year for the host and vector populations respectively. This is the population–type reproduction number if the vector population size at that time was to remain constant. The population–type reproduction number is always smaller for the vector population than for any host age group. It is also interesting to note that the gradient of the increase of the probability of an epidemic is not as steep as the increase in the vector population at the DF state

(compare figure 5-11(a) with figure 5-10). This means that although an increase in vectors causes an increase in the probability of an epidemic there may be a maximum population size, where anything above this does not dramatically change the probability of an epidemic. However, this could also be due to the probability of an epidemic being bound between 0 and 1 whereas the population size is not. Infact, when considering the estimate of transmission potential (the basic reproductive number at a given time if the vector population size was to remain constant for all time, figure 5-11(d)) we see that the sinusoidal function produced is more similar to the characteristics seen in the vector population at the DF state than in the probability of an epidemic.

Although we are mainly considering the method used in Bacaër and Ait Dads (2012), it is important to check that the stochastic simulation matches these results. We show this in figure 5-12, where the probability of an epidemic is shown using the method presented in Bacaër and Ait Dads (2012) and stochastic simulations as the vector population size changes throughout the year for each of the different initial conditions. No matter which group infection starts when running the stochastic model for 1000 simulations the results match well, with the sum of squared residuals ranging between 0.002 and 0.0061.

We have shown how the probability of an epidemic changes when infection is introduced at different times throughout the year as the vector population size at the DF state varies. So far, we have considered this for given exposure weightings. We now vary the exposure weighting of the working age group as well as the time infection is introduced into the population. No matter which group infection starts in, the qualitative behaviour is the same as in figure 5-11(a) for each exposure weighting; the probability of an epidemic decreases, increases and then decreases throughout the year. Figures 5-13 (a) and (c) show similar behaviour when infection starts in the children's or retired age groups. For each time when an infected individual enters the population, as the exposure weighting of the working age-group increases, the probability of an epidemic decreases. This is to be expected from the non-seasonal model. During the first half of the year, when the vector population is smaller, the difference in the probability of an epidemic is greater as the exposure weighting is varied than during the second half of the year when the vector population is larger. This implies that management strategies to control exposure to vectors may have greater implications when the vector population is smaller.

In contrast, if infection starts in the working age-group (figure 5-13 (b)), for each time as the exposure weighting increases the probability of an epidemic increases. This is again to be expected from the non-seasonal model results. When infection starts in the vector population (figure 5-13 (d)) we see uniformity of the probability of an

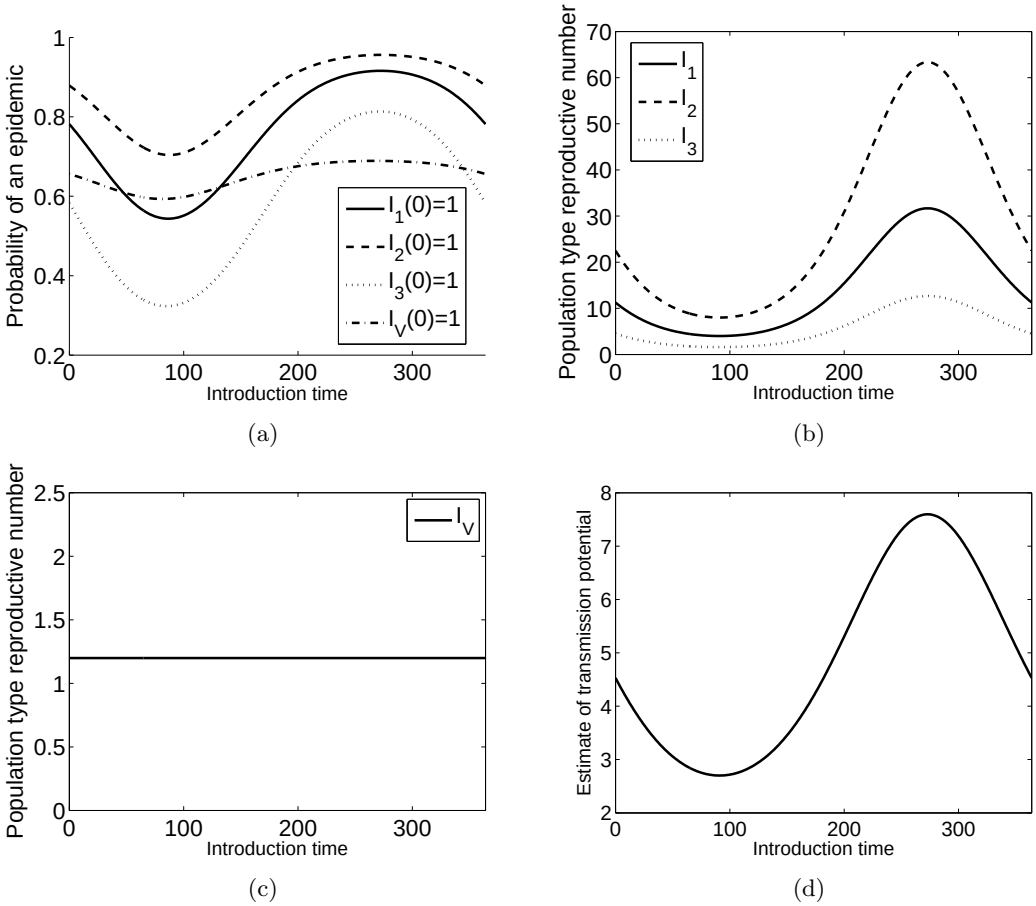

Figure 5-11: (a) The probability of an epidemic throughout one year as the vector population size at the DF state changes. (b) The instantaneous population–type reproduction numbers of the host population as the vector population size at the DF state changes. The solid, dashed and dotted lines represent the initial conditions $I_1(0) = 1$, $I_2(0) = 1$ and $I_3(0) = 1$ respectively. (c) The instantaneous population–type reproduction number of the vector population as the vector population size at the DF state changes. (d) The instantaneous estimate of transmission potential for the host–vector system as the vector population size at the DF state changes. In all graphs the exposure weightings for the children's, working–age and retired age groups are $\sigma_1 = 0.5$, $\sigma_2 = 1$ and $\sigma_3 = 0.2$ respectively. All other parameters are given in Table 5.1.

epidemic across the different exposure weightings. As we found in the non-seasonal model, the exposure weighting has a milder impact on the probability of an epidemic when infection starts in the vector population than in the host population. We also see that whilst for each exposure weighting there is oscillatory behaviour in the probability of an epidemic (as in the previous cases), the amplitude of oscillation is much smaller than when infection starts in any of the host age-groups.

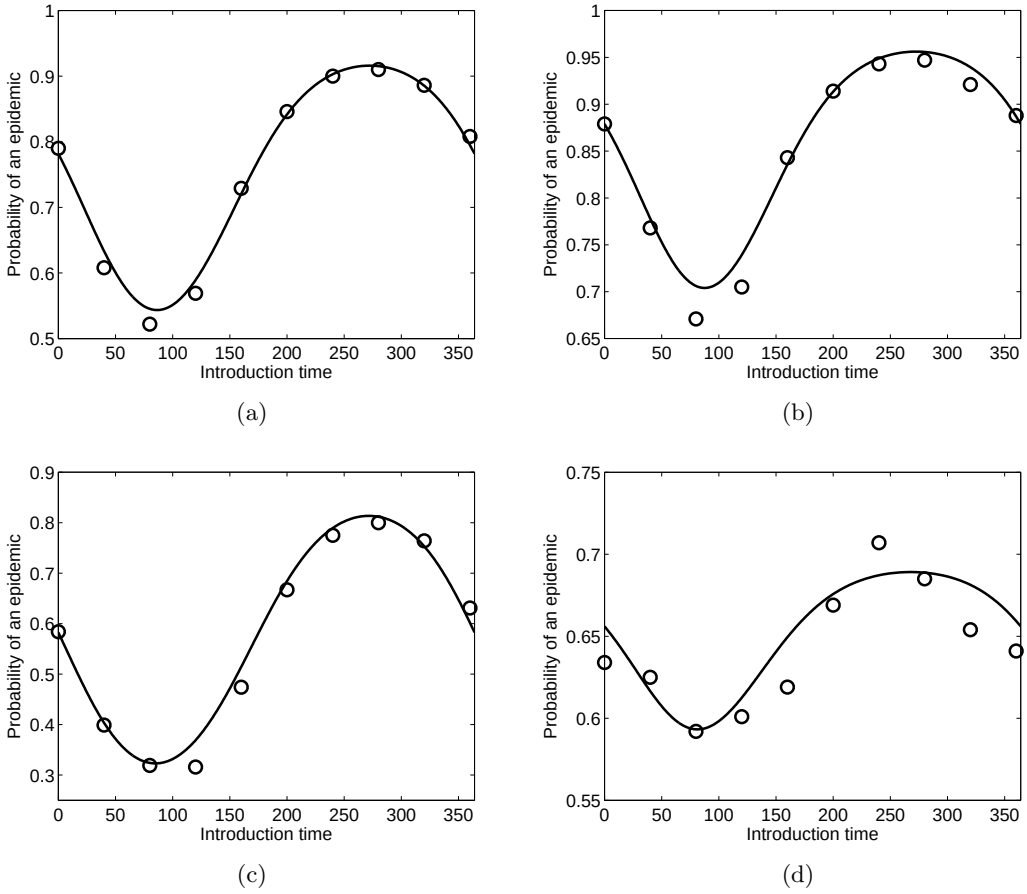

Figure 5-12: The probability of an epidemic as the vector population size at the DF state changes. The solid line represents the numerical model approach (equations 5.36) and the circles represent the stochastic approximation using 1000 simulations. In (a) the initial condition is $I_1(0) = 1$, in (b) $I_2(0) = 1$, in (c) $I_3(0) = 1$ and in (d) $I_V(0) = 1$. The children's, working ages and retired age groups are given by $\sigma_1 = 0.5$, $\sigma_2 = 1$ and $\sigma_3 = 0.2$ respectively. All other parameters are given in Table 5.1.

Figure 5-14 shows the probability that an epidemic will occur as two of the exposure weightings are varied, when infection is introduced at different points in time at the DF state. We are therefore studying the probability of an epidemic when infection is introduced for different sizes of vector populations at the start of the year, after four months and after eight months. This figure reiterates the fact that, no matter what the exposure weighting of the working and retired age-groups, when the vector population is smaller the probability of an epidemic is smaller than when the vector population is larger. For all sizes of vector population the qualitative behaviour is similar to when there is no seasonality in the model (compare with figures 5-5 and 5-6). Again we see

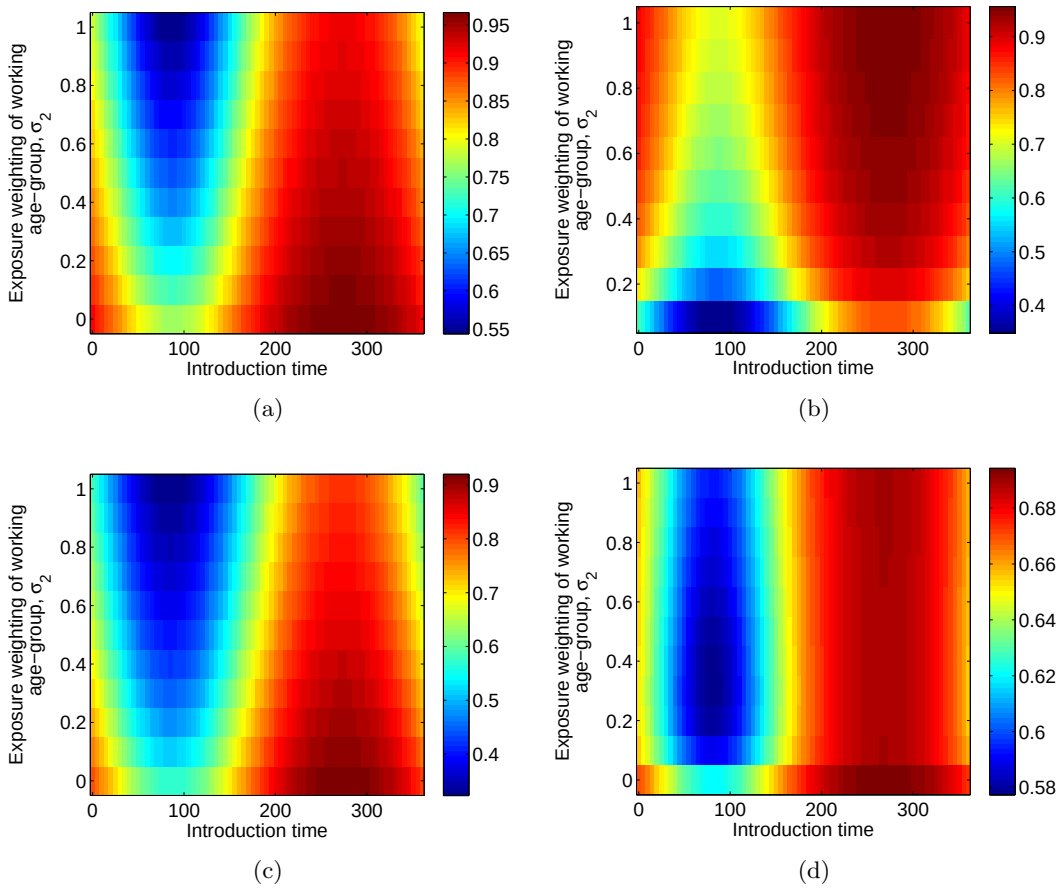

Figure 5-13: The probability of an epidemic as the vector population size at the DF state changes alongside the exposure weighting of the working age group to the vector. In (a) the initial condition is $I_1(0) = 1$, in (b) $I_2(0) = 1$, in (c) $I_3(0) = 1$ and in (d) $I_V(0) = 1$. The exposure weighting of the children's and retired age groups are $\sigma_1 = 0.5$ and $\sigma_3 = 0.2$ respectively. All other parameters are given in Table 5.1.

a difference if infection starts in the vector population; the probability of an epidemic has a smaller range of values across different exposure weightings. This again shows the transmission bottleneck occurs in vector to host transmission.

The previous graphs show the probability of an epidemic as $t \to \infty$. We can also look at the probability of an epidemic immediately after infection first enters the population (figure 5-15). In all cases as the time from when infection is introduced into the population increases the probability of an epidemic decreases. The figures show that it is during the first 5 days where the main changes in the probability occur, and it is in this time where there is variability in the probabilities between the different initial conditions. When infection starts in the host population (figures 5-15(a) – (c)) there are

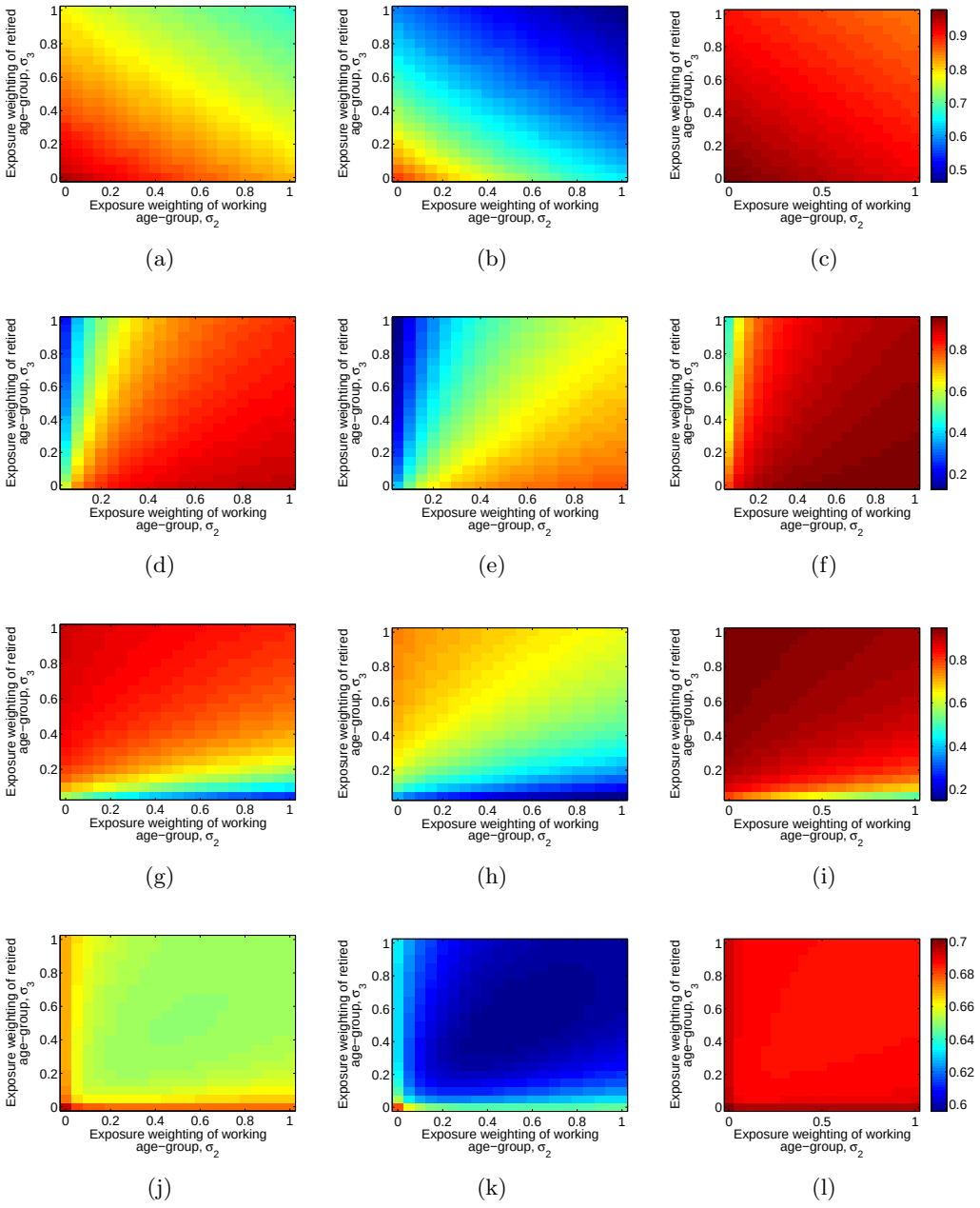

Figure 5-14: Probability of an epidemic as the exposure weightings of the working and retired age-groups are varied. (a), (d), (g) and (j) show the probability for $\bar{S}_V(0)$, (b), (e), (h) and (k) for $\bar{S}_V(120)$ and (c), (f), (i) and (l) for $\bar{S}_V(240)$. In (a), (b) and (c) the initial condition is given by $I_1(0) = 1$, in (d), (e) and (f) $I_2(0) = 1$, (g), (h) and (i) $I_3(0) = 1$ and (j), (k) and (l) $I_V(0) = 1$. The exposure weighting of the children's age group is $\sigma_1 = 1$. All other parameters are given in Table 5.1.

immediately different dynamics depending on the time infection is introduced. Hence the vector population size is affecting transmission probability. In contrast, if infection starts in the vector population (figure 5-15(d)) for the first five days the probability of an epidemic is very similar, and after this the vector population size dictates the probability of an epidemic. This again shows that the main transmission potential is lost in the vector to host transmission stage rather than host to vector transmission. This also shows that the time at which infection is introduced into the population affects which initial condition yields the greatest probability of an epidemic. This is in agreement to the results shown in figure 5-11(a).

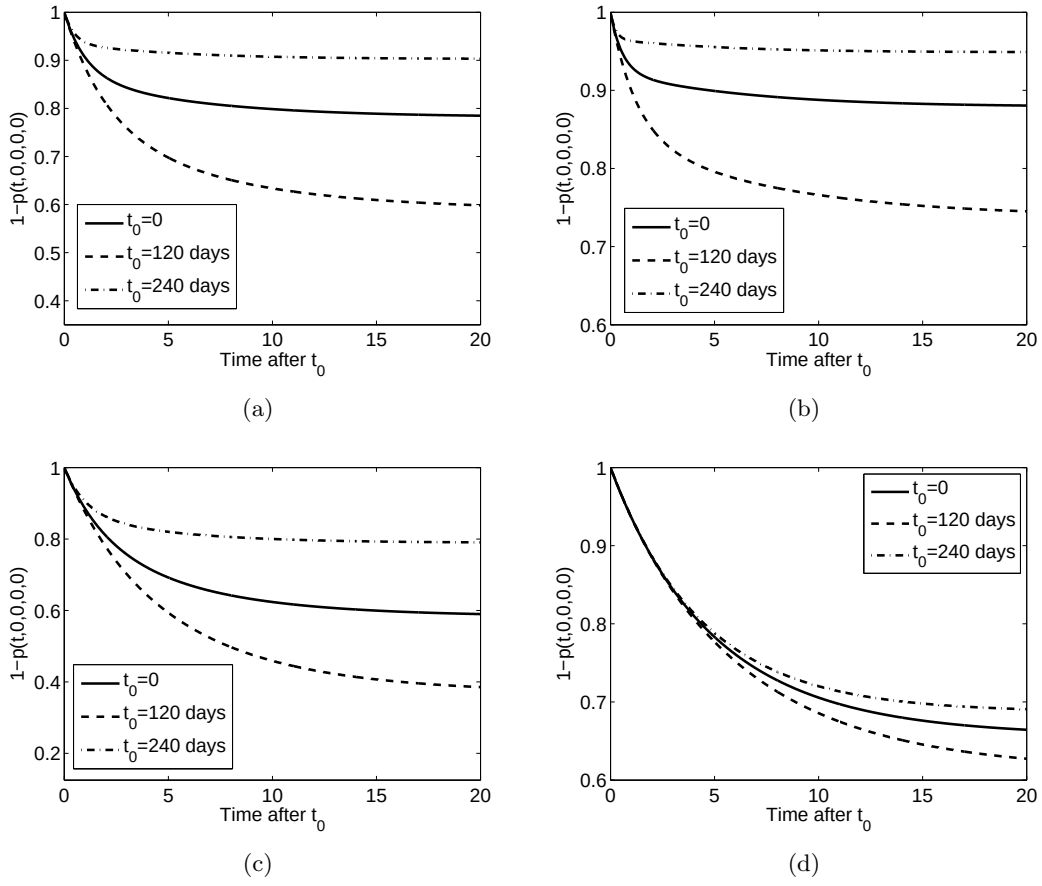

Figure 5-15: The probability of en epidemic at time τ as a function of τ (in days, $\tau \geq t_0$). In (a) the initial condition is $I_1(0) = 1$, in (b) $I_2(0) = 1$, in (c) $I_3(0) = 1$ and in (d) $I_V(0) = 1$. In each figure the solid, dashed and dot-dashed lines are for $t_0 = 0$, $t_0 = 120$ and $t_0 = 240$ respectively. The exposure weightings for the children's, working age and retired age groups are $\sigma_1 = 0.5$, $\sigma_2 = 1$ and $\sigma_3 = 0.2$ respectively. All other parameters are given in Table 5.1.

Figure 5-15 also complements the result shown in the non-seasonal model. Under each initial condition the probability of an epidemic is greatest when the vector population is greatest, decreasing accordingly. This is expected; a greater vector population size allows for greater transmission potential. Therefore the time an infected individual enters the population is important, as this determines the size of the vector population and therefore the probability of whether an epidemic will ensue.

5.4.3 Summary

In the seasonal model we have confirmed the results of the non-seasonal model; for each time point during the period we see similar results to the non-seasonal model as the exposure weightings are varied. This again highlights the insensitivity to exposure weightings that can be seen when infection starts in the vector population, and hence where the main transmission potential can be found. We have shown that the time infection enters the population is important if seasonality is included in the vector population. The smaller the vector population, the less the probability of an epidemic. As the vector population size increases the probability of an epidemic also increases.

The results from the seasonal model have additional implications to the non-seasonal model regarding whether hosts or vectors should be targeted in management strategies. When the vector population was at its largest and infection was introduced into the population, the probability of an epidemic was less when infection started in the vector population rather than the host population. This is true for a range of vector population sizes; therefore decreasing the vector population size may not be the most efficient management strategy. It is instead necessary to consider how infection is transmitted between the populations and control strategies related to this.

5.5 Discussion

We have shown that if infection starts in the host population the exposure weighting of the different age-groups to the vector can have a large impact on the probability of an epidemic. When infection starts in a given age-group, if the other age-groups' exposure weightings are fixed, the less exposure that age-group has the smaller the probability of an epidemic. This is because the exposure of the age-group relative to the others decreases, and hence there is less chance that a vector will bite the infected individual. In contrast, if infection starts in a different age-group, as the exposure weighting of the initial age group decreases the probability of an epidemic increases. This is because the distribution of bites changes and therefore there is a relative increase in the exposure of the individual initially infected. The results show that for each age-group the dominant

exposure weighting to focus on is their own; if infection starts in a given age-group then varying the exposure weighting of that age-group has a greater effect on the probability of an epidemic than varying the other age-groups exposure weightings.

Focusing on which age-groups have maximum exposure and trying to decrease this is therefore vital. Hence, management strategies which focus on this are important. The WHO states that transmission control should target the mosquito. However, they also state the importance of environmental management to decrease vector propagation and contact between hosts and vectors (World Health Organisation, 2014a). These environmental management strategies, including adapting human behaviours to reduce exposure, are vital; we have shown by decreasing the exposure of different age-groups the probability of an epidemic can be reduced by 30% when infection starts in the host population. However, the exposure weightings are relative to each other and where infection starts is important in determining the epidemic probability. An example of a possible strategy would be to implement a cost–benefit analysis to attempt to quantify the increase in epidemic risk associated to the other age groups if the exposure of one age group is reduced, for example by use of nets in houses or schools or some type of behavioural change.

In contrast, when infection starts in the vector population the exposure weightings have less impact on the probability of an epidemic than when infection starts in the host population. If infection starts in the vector population, the probability of an epidemic is least when the exposure weightings are identical for all age groups. Management strategies should therefore take this into account when being implemented, potentially prioritising strategies in areas where one age group is more exposed than others, for example if a school is close to a breeding ground for mosquitoes.

The average number of vectors per host is vitally important in predicting the probability of an epidemic; a greater number of vectors yields a larger probability of an epidemic. This is consistent with an increasing basic reproductive number as the number of mosquitoes increases (Anderson and May, 1991). However, a maximum probability of an epidemic will be reached as the mosquito population size increases, and further input of vectors will not cause a greater probability of an epidemic. This is because the maximum transmission potential of an area will be reached, and further increase in the number of vectors can not cause an increase in transmission. Many management strategies focus on reducing the number of vectors to try and decrease transmission between host and vector. These often include minimizing areas where free-standing water can form as these are a breeding ground for *Aedes aegypti* mosquitoes (World Health Organisation, 2014a). These strategies are important, however there needs to be a substantial decrease in vector population size to have a real impact on the prob-

ability of an epidemic. For given interventions at specific times after infection entered the population, Chowell et al. (2013) determined that with a high basic reproductive number decreasing the vector population by less than 30% was not always able to affect the final epidemic size of the dengue outbreak on Easter Island, where infection started in the host population. Their results showed that less effort was needed as the basic reproductive number decreased. Therefore intervention strategies, whatever form they take, need to be carefully analysed and adapted to the needs of a given situation.

Finally, we have shown that seasonality can play an additional role to the exposure weighting and number of vectors in whether an epidemic will occur. The results (combined with non-seasonal results) indicate that continued efforts to decrease the vector population size in the first half of the year when the vector population is smaller will continue to decrease the probability of an epidemic. However, in the second half of the year when the vector population is larger there is a relatively flat peak in the probability of an epidemic. Therefore, for many vector population sizes, particularly if infection starts in the vector compartment, a reduction in the number of mosquitoes may initially have little effect in decreasing the probability of an epidemic. Therefore, ensuring the host population is aware of, and understands, the importance of environmental strategies discussed above alongside individual and household protection, is vital to help reduce the probability of an epidemic. The results highlight that management strategies may need to change throughout the year to help ensure the probability of an epidemic is as low as possible when an infected individual (host or vector) enters the population. We consider this further in Chapter 6 where we implement epidemic prevention for a single serotype host–vector model.

CHAPTER 6

EPIDEMIC PREVENTION

Summary

In this chapter we implement epidemic prevention for a single serotype host–vector model, where the prevention strategy acts on both the host and vector populations. We use both control theory and Floquet theory to find the optimal prevention strategy in a seasonal model; that is, the optimal strategy such that the number of infected individuals at the start and end of a given time period are identical. We initially assume the exposure weightings of the hosts to vectors are fixed and find the optimal strategy. We find that for optimal prevention, whilst the strategies themselves for each age group differ, the intensity acting on the strategy is identical for each age group. We then determine how varying the exposure weighting of different aged hosts also affects the optimal prevention strategy. We find that varying the exposure weightings alters the total effort needed for optimal prevention.

6.1 Introduction

We have seen in Chapter 5 the importance of understanding epidemic thresholds. A single person or mosquito can cause an epidemic to occur, or the disease can die out depending on environmental factors or stochasticity. Seasonally forced variation can add to the complexity of the system and the ensuing dynamics. Therefore understanding how to minimise the effect of epidemics, or prevent them entirely, is vital.

We first need to understand how epidemic control and epidemic prevention differ.

In an epidemiological setting, control problems aim to limit the spread of a disease, for example by vaccination of a population. It is used, among other things, to make decisions about the best course of action for different epidemiological problems, such as the number of individuals to vaccinate to minimize both cost and the number of individuals infected (Lenhart and Workman, 2007). In contrast, epidemic prevention uses the same ideas as exclusion theory; attempting to exclude or maintain exclusion of a disease within a population (Greenman and Adams, 2015). We aim to examine epidemic prevention strategies for dengue in a seasonally forced model.

Epidemic prevention is highly related to the basic reproductive number (R_0). As stated in previous chapters, for a non–seasonal model R_0 is the average number of secondary infections from one infected individual in a naïve population (Diekmann and Heesterbeek, 2000). In a simple SIR model if a constant control u is implemented ($u < 1$ decreases the number of infected individuals) then the strategy needed for optimal prevention is $u = 1/R_0$. This is because if on average an infected individual generates R_0 new infections, of which a proportion $1/R_0$ survive the control, then there is approximately only one new infection per infected individual and hence zero growth in the population (Greenman and Adams, 2015). The definition of R_0 changes for a seasonal model, and Bacaër and Guernaoui (2006) determine a definition for the basic reproductive number in a periodic environment. This is then extended in Bacaër (2007) and an approximation of R_0 was found for models with periodicity in the vector population. Wang and Zhao (2008) determine threshold dynamics, giving examples where R_0 for the the time–averaged system is comparable with R_0 for the periodic epidemic model. It is worth noting that Wang and Zhao (2008) determine a simple model for dengue in which they implement their methodologies for finding R_0.

Controlling dengue is of vital importance, as over 40% of the world's population are at risk (World Health Organisation, 2014a). Most control efforts are aimed at reducing the number of vectors to decrease transmission probability, including using insecticides before and during epidemics, and ensuring that water supplies are clean and, where possible, covered to reduce breeding grounds for mosquitoes. Other controls involve individuals protecting themselves, for example by using screens or wearing long–sleeve clothing, to reduce the probability of a transmission event with a mosquito (World Health Organisation, 2014a). These methods can be modelled to help find when and how control measures should be applied. Oki et al. (2011) implement a model which finds the optimal time to use fogging of insecticide to target adult mosquitoes. They find that the optimal time for insecticide fogging is between when the wet season starts (and the vector density is greater than in the dry season) and when the prevalence is at its maximum. They also determine that seasonality and the transmission intensity

greatly influence the impact of the optimal control. Burattini et al. (2008) implement a model which simulates a variety of control measures. They find that as well as using insecticide fogging on adult mosquito populations, a mixed control measure which incorporates control strategies on larvae as well is, theoretically, effective. Rodrigues et al. (2013) study an optimal control problem where the cost of the disease, insecticide strategies on adults and larvae, and mechanical controls are considered. They find that if all controls are weighted identically the insecticide acting on adult mosquitoes is the best control method, as this is the greatest influence on the basic reproductive number.

These examples are where optimal control strategies have been implemented for dengue. However, to our knowledge, there are few examples where optimal prevention strategies have been modelled. This is especially true for host–vector models, including those which incorporate age structure. To this end, we find the optimal prevention strategy for an age structured host–vector model. We define a method implemented as a prevention strategy a control. We initially hold the controls on two age groups constant and find the optimal prevention strategy on the third. We gradually increase the complexity of the model until we find the optimal prevention strategy for all three age groups. Once this is found, we determine how the optimal strategy changes as the exposure weightings of the different age groups are varied, and in which age group the greatest effort needs to placed to ensure that introduction of isolated infections will not cause a large epidemic.

6.2 Model and methodologies

6.2.1 Terminology

As stated in Section 6.1 we are concerned with epidemic prevention for a three age group host–vector model. We briefly introduce some terminology we will use throughout the chapter for clarity.

- **Prevention strategies:** Methods implemented to ensure zero growth of individuals over a given time period.
- **(Optimal) control theory:** Theory used for 'standard' epidemiological optimal control problems to limit the spread of disease, which forms the start of the analysis for optimal prevention.
- **A control:** A method implemented on one (or more) age groups to find prevention strategies.

- **Optimal prevention strategies:** The best prevention strategy; the most desirable way to implement the controls on the different age groups which takes the least overall effort.

6.2.2 The model

We use a similar host–vector model to that given in Chapter 5. The host population is split into three age groups; children, working age and retired ($i = 1, 2, 3$ respectively). A host in any given age group can be susceptible (S_i), infected (I_i) or recovered (R_i). A vector can either be susceptible (S_V) or infected (I_V). Therefore the system is modelled by

$$\frac{\mathrm{d}S_1}{\mathrm{d}t} = \mu N - ((1-s_1)u_1\lambda_{V1} + \delta_1 + \mu)S_1, \tag{6.1a}$$
$$\frac{\mathrm{d}S_2}{\mathrm{d}t} = \delta_1 S_1 - ((1-s_2)u_2\lambda_{V2} + \delta_2 + \mu)S_2, \tag{6.1b}$$
$$\frac{\mathrm{d}S_3}{\mathrm{d}t} = \delta_2 S_2 - ((1-s_3)u_3\lambda_{V3} + \mu)S_3, \tag{6.1c}$$
$$\frac{\mathrm{d}I_1}{\mathrm{d}t} = s_1u_1\lambda_{V1}S_1 - (\gamma + \delta_1 + \mu)I_1, \tag{6.1d}$$
$$\frac{\mathrm{d}I_2}{\mathrm{d}t} = s_2u_2\lambda_{V2}S_2 + \delta_1 I_1 - (\gamma + \delta_2 + \mu)I_2, \tag{6.1e}$$
$$\frac{\mathrm{d}I_3}{\mathrm{d}t} = s_3u_3\lambda_{V3}S_3 + \delta_2 I_2 - (\gamma + \mu)I_3, \tag{6.1f}$$
$$\frac{\mathrm{d}R_1}{\mathrm{d}t} = \gamma I_1 - (\delta_1 + \mu)R_1, \tag{6.1g}$$
$$\frac{\mathrm{d}R_2}{\mathrm{d}t} = \gamma I_2 + \delta_1 R_1 - (\delta_2 + \mu)R_2, \tag{6.1h}$$
$$\frac{\mathrm{d}R_3}{\mathrm{d}t} = \gamma I_3 + \delta_2 R_2 - \mu R_3, \tag{6.1i}$$
$$\frac{\mathrm{d}S_V}{\mathrm{d}t} = \nu(t)N_V - (\lambda_H + \mu_V)S_V, \tag{6.1j}$$
$$\frac{\mathrm{d}I_V}{\mathrm{d}t} = \frac{\beta(s_1u_1\sigma_1I_1 + s_2u_2\sigma_2I_2 + s_3u_3\sigma_3I_3)}{\sum_i \sigma_i N_i}S_V - \mu_V I_V, \tag{6.1k}$$

where μ is the constant birth and mortality rate of the host, δ_i is the rate of ageing ($i = 1$ child to working age, $i = 2$ working age to retired), γ is the recovery rate of the hosts, $\lambda_{Vi}(t)$ is the force of infection acting on a host in age group i by the vector, σ_i is the exposure weighting of a host in age group i to the vector, $\nu(t)$ is the seasonal birth rate of the vectors, μ_V is the mortality rate of the vector and $\lambda_H(t)$ is the force of infection acting on the vector by the host. The control is formed of two terms; the control intensity acting on age group i ($s_i \in \mathbb{R}^+$) and the control function ($u_i(t)$ where $0 < u_i(t) \leq 1 \forall t$, $i = 1, 2, 3$). The control function determines the shape of the

control throughout the time period, while the control intensity adjusts the magnitude of the control function to ensure zero growth over a period, meaning the introduction of isolated infections does not lead to large epidemics. An example of the control would be using nets to avoid individuals being bitten, thus meaning that the individuals stay susceptible. The seasonal birth rate of the vector is given by

$$\nu(t) = \kappa N(1 + a\cos(\omega t))\mu_V, \tag{6.2}$$

where κ is the average number of vectors per host, N is the total host population size, a is the amplitude of the oscillations and ω is the phase of the oscillation. We note that this is different to the seasonality included in Chapter 5; the phase is adjusted by half a year. Therefore to compare with any results from the previous chapter we need to translate the results accordingly. The force of infection exerted by the vector on the host ($\lambda_{Vi}(t)$) is given by

$$\lambda_{Vi}(t) = \frac{\beta\sigma_i I_V}{\sum_i \sigma_i N_i} \tag{6.3}$$

and when the control is implemented by $\bar{\lambda}_{Vi}$ as

$$\bar{\lambda}_{Vi}(t) = s_i u_i(t)\lambda_{Vi}(t) = s_i u_i(t)\frac{\beta\sigma_i I_V}{\sum_i \sigma_i N_i}. \tag{6.4}$$

The force of infection exerted by the host on the vector ($\lambda_H(t)$) is given by

$$\lambda_H(t) = \frac{\beta(\sigma_1 I_1 + \sigma_2 I_2 + \sigma_3 I_3)}{\sum_i \sigma_i N_i} \tag{6.5}$$

and when the control is implemented by $\bar{\lambda}_H(t)$ as

$$\bar{\lambda}_H(t) = \frac{\beta(s_1 u_1(t)\sigma_1 I_1 + s_2 u_3(t)\sigma_2 I_2 + s_3 u_3(t)\sigma_3 I_3)}{\sum_i \sigma_i N_i}. \tag{6.6}$$

In all cases β is the transmission rate (the average number of bites of a vector on a host multiplied by the transmission probability of a bite involving an infectious host or vector). As in previous chapters we assume that the host to vector transmission potential is the same as the vector to host transmission potential. Note that if $s_i = 1$ $(i = 1, 2, 3)$ and $u_i(t) = 1 \ \forall \ t$ $(i = 1, 2, 3)$ there is no control acting on the system.

6.2.3 Control theory

As stated previously, the control being implemented for optimal prevention acts on both the host and vector populations. Therefore we assume that the control affects

the bite rate of the vector for a given age group, and that these bites are not shifted elsewhere. This is a reasonable assumption due to the short distance *Aedes aegypti* mosquitoes travel (a study showed this to be a maximum of 512m in Puerto Rico and Thailand (Harrington et al., 2005)). Although *Aedes aegypti* mosquitoes do not travel far, we also assume that the control is such that the bites are not moved elsewhere even in a location such as a house, for example by use of personal protection such as everyone in the location wearing long sleeves. An example of such a control would be putting up additional nets in schools or work places to decrease the biting rate of the vectors. For epidemic prevention we want to ensure that at the beginning and end of a given time period the number of infectious individuals are identical. To do this we initially find the rare invader approximation (RIA) (Greenman and Adams, 2015). At the RIA we assume that the number of infectious individuals entering an otherwise susceptible population is small (Greenman and Norman, 2007). Therefore we need to find the disease free (DF) state, given by

$$\bar{S}_1 = \frac{\mu N}{\delta_1 + \mu}, \qquad \bar{S}_2 = \frac{\delta_1 \mu N}{(\delta_1 + \mu)(\delta_2 + \mu)}, \qquad \bar{S}_3 = \frac{\delta_1 \delta_2 N}{(\delta_1 + \mu)(\delta_2 + \mu)}, \tag{6.7a}$$

$$\bar{S}_V = \kappa N \exp\left(\frac{\mu_V a \sin(\omega t)}{\omega}\right). \tag{6.7b}$$

For clarity we now drop the bar in the DF populations. At the RIA we can linearise the system and determine the optimal prevention problem (Greenman and Adams, 2015).

If the state variables satisfy the differential equation

$$\frac{\mathrm{d}\boldsymbol{x}}{\mathrm{d}t} = g(t, \boldsymbol{x}(t), \boldsymbol{u}(t)), \tag{6.8}$$

where $\boldsymbol{u}(t)$ is the control variable, the optimal control problem is to maximize (or minimize) the objective functional

$$\max_{\boldsymbol{u}} \int_{t_0}^{t_1} f(t, \boldsymbol{x}(t), \boldsymbol{u}(t))\mathrm{d}t, \tag{6.9}$$

subject to

$$\frac{\mathrm{d}\boldsymbol{x}}{\mathrm{d}t} = g(t, \boldsymbol{x}(t), \boldsymbol{u}(t)), \tag{6.10a}$$

$$\boldsymbol{x}(t_0) = \boldsymbol{x}_0 \text{ and } \boldsymbol{x}(t_1) = \boldsymbol{x}_1 \text{ free}, \tag{6.10b}$$

where $\boldsymbol{x}_1$ free means it can take any value (Lenhart and Workman, 2007). Following

this our optimal control problem is given by

$$\min_{\boldsymbol{su}} \int \frac{1}{3p}\left(\frac{1}{s_1u_1}+\frac{1}{s_2u_2}+\frac{1}{s_3u_3}\right)\mathrm{d}t, \tag{6.11}$$

subject to

$$\frac{\mathrm{d}I_1}{\mathrm{d}t} = g_1(\cdot) = s_1u_1\frac{\beta\sigma_1S_1}{\sum\sigma_jN_j}I_V-(\delta_1+\gamma+\mu)I_1, \tag{6.12a}$$

$$\frac{\mathrm{d}I_2}{\mathrm{d}t} = g_2(\cdot) = s_2u_2\frac{\beta\sigma_2S_2}{\sum\sigma_jN_j}I_V+\delta_1I_1-(\delta_2+\gamma+\mu), \tag{6.12b}$$

$$\frac{\mathrm{d}I_3}{\mathrm{d}t} = g_3(\cdot) = s_3u_3\frac{\beta\sigma_3S_3}{\sum\sigma_jN_j}I_V+\delta_2I_2-(\gamma+\mu), \tag{6.12c}$$

$$\frac{\mathrm{d}I_V}{\mathrm{d}t} = g_4(\cdot) = \frac{\beta(s_1u_1\sigma_1I_1S_V(t)+s_2u_2\sigma_2I_2+s_3u_3\sigma_3I_3)S_V(t)}{\sum\sigma_jN_j} -\mu_VI_V, \tag{6.12d}$$

with conditions

$$I_1(0)=I_1(p), \qquad I_2(0)=I_2(p), \qquad I_3(0)=I_3(p), \qquad I_V(0)=I_V(p). \tag{6.13}$$

The minimum period of the vector population at the DF state ($S_V(t)$) is p, and so equation (6.13) corresponds to zero growth over a single cycle for each of the sub–populations. We assume that the cost of the control is the same for each of the age groups, independent of its population size. Therefore in equation 6.11 the minimisation problem has been divided into three for consistency; if all the controls are equal ($s_1u_1 = s_2u_2 = s_3u_3 = su$) we have the usual optimal prevention problem.

The basic prevention problem looks to find a constant value u such that the DF state is stable. When this occurs $u = 1/R_0$, where R_0 is the basic reproductive number for seasonal systems (Bacaër and Guernaoui, 2006; Wang and Zhao, 2008). We wish to find an optimal prevention strategy which is variable in time for a multi–variable problem.

For a multi–variable problem, following Lenhart and Workman (2007), the Hamiltonian is given by

$$H(t,\boldsymbol{x},\boldsymbol{u},\boldsymbol{\lambda}) = f(t,\boldsymbol{x},\boldsymbol{u})+\sum_{i=1}^{n}\lambda_i(t)g_i(t,\boldsymbol{x},\boldsymbol{u}), \tag{6.14}$$

where $f(t,\boldsymbol{x},\boldsymbol{u})$ is the objective function, λ_i are the adjoint variables corresponding to I_i and the functions $g_i(\cdot)$ are given in equation (6.12). For the multi–variable problem

the system must satisfy

$$\frac{\mathrm{d}I_i}{\mathrm{d}t} = \frac{\partial H}{\partial \lambda_i} = g_i(\cdot), \;\; I_i(0) = I_i(p) \quad \text{for } i = 1,2,3,4 \tag{6.15}$$

$$\frac{\mathrm{d}\lambda_j}{\mathrm{d}t} = -\frac{\partial H}{\partial I_j} \quad \text{for } j = 1,2,3,4 \tag{6.16}$$

$$0 = \frac{\partial H}{\partial u_k} \text{ at } u_k^* \quad \text{for } k = 1,2,3,4. \tag{6.17}$$

For simplification purposes in our model let

$$x_i = \frac{\beta\sigma_i S_i}{\sum \sigma_j N_j}, \qquad y_i = \frac{\beta\sigma_i S_V(t)}{\sum \sigma_j N_j}. \tag{6.18}$$

The Hamilton for system (6.12) is then given by

$$H = f + \lambda_1 g_1 + \lambda_2 g_2 + \lambda_3 g_3 + \lambda_4 g_4 \tag{6.19}$$

$$\begin{aligned} = \frac{1}{3p}\left(\frac{1}{s_1u_1} + \frac{1}{s_2u_2} + \frac{1}{s_3u_3}\right) &+ \lambda_1\left(s_1u_1x_1I_V - (\delta_1+\gamma+\mu)I_1\right) + \\ &\lambda_2\left(s_2u_2x_2I_V + \delta_1I_1 - (\delta_2+\gamma+\mu)I_2\right) + \\ &\lambda_3\left(s_3u_3x_3I_V + \delta_2I_2 - (\gamma+\mu)I_3\right) + \\ &\lambda_4\left(s_1u_1y_1I_1 + s_2u_2y_2I_2 + s_3u_3y_3I_3 - \mu_V I_V\right). \end{aligned} \tag{6.20}$$

The adjoint equations are

$$\frac{\mathrm{d}\lambda_i}{\mathrm{d}t} = -\frac{\partial H}{\partial I_i}, \tag{6.21}$$

so

$$\frac{\mathrm{d}\lambda_1}{\mathrm{d}t} = \lambda_1(\delta_1+\gamma+\mu) - \lambda_2\delta_1 - \lambda_4 s_1u_1y_1, \tag{6.22a}$$

$$\frac{\mathrm{d}\lambda_2}{\mathrm{d}t} = \lambda_2(\delta_2+\gamma+\mu) - \lambda_3\delta_2 - \lambda_4 s_2u_2y_2, \tag{6.22b}$$

$$\frac{\mathrm{d}\lambda_3}{\mathrm{d}t} = \lambda_3(\gamma+\mu) - \lambda_4 s_3u_3y_3, \tag{6.22c}$$

$$\frac{\mathrm{d}\lambda_4}{\mathrm{d}t} = -\lambda_1 s_1u_1x_1 - \lambda_2 s_2u_2x_2 - \lambda_3 s_3x_3 + \lambda_4\mu_V. \tag{6.22d}$$

The optimality condition acts on each of the different control elements in the Hamil-

tonian. Therefore $\frac{\partial H}{\partial s_i u_i} = 0$. This yields

$$\frac{\partial H}{\partial s_1 u_1} = 0 = -\frac{1}{3p(s_1 u_1)^2} + \lambda_1 x_1 I_V + \lambda_4 y_1 I_1, \tag{6.23a}$$

$$\frac{\partial H}{\partial s_2 u_2} = 0 = -\frac{1}{3p(s_2 u_2)^2} + \lambda_2 x_2 I_V + \lambda_4 y_2 I_2, \tag{6.23b}$$

$$\frac{\partial H}{\partial s_3 u_3} = 0 = -\frac{1}{3p(s_3 u_3)^2} + \lambda_3 x_3 I_V + \lambda_4 y_3 I_3. \tag{6.23c}$$

Therefore

$$u_1^{-1}(t) = s_1\sqrt{3p(\lambda_1 x_1 I_V + \lambda_4 y_1 I_1)}, \tag{6.24a}$$

$$u_2^{-1}(t) = s_2\sqrt{3p(\lambda_2 x_2 I_V + \lambda_4 y_2 I_2)}, \tag{6.24b}$$

$$u_3^{-1}(t) = s_3\sqrt{3p(\lambda_3 x_3 I_V + \lambda_4 y_3 I_3)}. \tag{6.24c}$$

If the intensity parameters s_i are equal in the system then each s_i can be replaced by s in equation (6.24) for the control functions u_i. Therefore, if $s_i u_i$ is the control needed for prevention at time t, the effort needed for prevention is defined as $1/s_i u_i$ $(i = 1, 2, 3)$. The total effort needed for optimal prevention over one time period for age group i $(i = 1, 2, 3)$ is given by

$$E_i = \int_p \frac{1}{s_i u_i(\tau)} \mathrm{d}\tau. \tag{6.25}$$

The total effort over the whole population for one time period is then given by

$$E = \int_p \frac{1}{s_1 u_1(\tau)} + \frac{1}{s_2 u_2(\tau)} + \frac{1}{s_3 u_3(\tau)} \mathrm{d}\tau = E_1 + E_2 + E_3 \tag{6.26}$$

In order to scale the u_i functions appropriately we need to use Floquet theory to ensure that we have zero growth over one cycle. This is because whilst the control functions are found using the Hamiltonian process, there is no guarantee of zero growth over a period. This is why the control intensity then scales the control function.

6.2.4 Floquet theory

Floquet's theorem states that if $P(t)$ is an $n \times n$ matrix with minimal period p, then the system of n differential equations

$$\dot{\boldsymbol{x}} = P(t)\boldsymbol{x} \tag{6.27}$$

has at least one non–trivial solution $\boldsymbol{x} = \boldsymbol{\chi}(t)$ such that

$$\boldsymbol{\chi}(t+p) = \zeta\boldsymbol{\chi}(t) \tag{6.28}$$

where ζ is a constant (Jordan and Smith, 1999; Agarwal and O'Regan, 2008). The constant ζ is called the Floquet multiplier and is instrumental in determining the dynamics of the solution. If $\zeta > 1$ the solution shows growing oscillations, if $\zeta < 1$ the solution shows decaying oscillations and if $\zeta = 1$ the solution is periodic, with minimal period p (Jordan and Smith, 1999; Klausmeier, 2008). Therefore, for epidemic prevention we are interested in when the Floquet multiplier of a system equals 1, corresponding to zero growth over a period.

The proof of Floquet's theory requires the implementation of a fundamental matrix and the monodromy matrix. If $\boldsymbol{\phi}_1(t), \boldsymbol{\phi}_2(t), ..., \boldsymbol{\phi}_n(t)$ are n linearly independent solutions of equation (6.27), then the fundamental matrix $\Phi(t)$ is the $n \times n$ matrix

$$\Phi(t) = \begin{pmatrix} \boldsymbol{\phi}_1(t) & \boldsymbol{\phi}_2(t) & \dots & \boldsymbol{\phi}_n(t) \end{pmatrix} \tag{6.29}$$

(Jordan and Smith, 1999). The monodromy matrix (which is an example of a fundamental matrix) is then given by M where $\Phi(t+p) = \Phi(t)M \ \forall \ t$ and hence

$$M = \Phi^{-1}(t_0)\Phi(t_0+p) \tag{6.30}$$

(Agarwal and O'Regan, 2008). The proof of Floquet's theorem is found by exploiting the characteristics of these matrices (Jordan and Smith, 1999; Agarwal and O'Regan, 2008). Therefore, to solve the optimal prevention problem we also need to use these structures.

Floquet theory also tells us that if the monodromy matrix for system (6.27) has a dominant eigenvalue $\zeta = 1$ (and therefore Floquet multiplier of 1) then for t large enough the other solutions become negligible and the solution to the system is

$$\boldsymbol{\chi}(t) = \Phi(t)\boldsymbol{w} \tag{6.31}$$

where $\boldsymbol{w}$ is the eigenvector associated with $\zeta = 1$ (Jordan and Smith, 1999). This is an important result in finding the optimal prevention strategy and is explained further in Section 6.2.5. To find the controls for optimal prevention (equation 6.24) we also need to find the solution to the adjoint system. If the dominant eigenvalue of the monodromy matrix for the system is equal to one, then so too is the dominant eigenvalue of the monodromy matrix of the adjoint (Greenman and Adams, 2015) and we check this numerically. Solving for both the state variables and adjoint allows us to find the

control strategies that should be implemented for optimal prevention.

6.2.5 Application of Floquet theory and numerical method

We now show steps for how Floquet theory should be implemented for the optimal prevention problem, both theoretically (in italic) and the procedure numerically.

1. Choose a value for the control intensity s and a control function $\boldsymbol{u}(t)$.

2. *To satisfy the boundary conditions of state equations* (6.12) *we need to find a control which has a Floquet multiplier exactly equal to 1 i.e. the largest eigenvalue of the monodromy matrix is 1.*
   The only free parameter available is the control intensity s. We do not attempt to change the shape of the control function at this stage.

   (a) *Find the fundamental matrix. One way to construct this is to take linearly independent initial conditions. Let $\boldsymbol{\phi}_i$ be a column vector of length n with all elements 0 except the the ith element, which is 1. Solving the system with initial conditions $\boldsymbol{\phi}_i$ for $i = 1 \dots n$ we get n linearly independent solutions $\boldsymbol{\phi}_i(t)$. Putting these solutions together as in equation* (6.29) *creates an $n \times n$ fundamental matrix. These particular initial conditions mean that the monodromy matrix $M = \Phi^{-1}(t_0)\Phi(t_0 + p) = \Phi(p)$.*
   Find the monodromy matrix $\Phi(p) = \begin{pmatrix} \boldsymbol{\phi}_1(p) & \boldsymbol{\phi}_2(p) & \boldsymbol{\phi}_3(p) & \boldsymbol{\phi}_4(p) \end{pmatrix}$ where $\boldsymbol{\phi}_1(0) = \begin{pmatrix} 1 & 0 & 0 & 0 \end{pmatrix}^T$, $\boldsymbol{\phi}_2(0) = \begin{pmatrix} 0 & 1 & 0 & 0 \end{pmatrix}^T$, $\boldsymbol{\phi}_3(0) = \begin{pmatrix} 0 & 0 & 1 & 0 \end{pmatrix}^T$ and $\boldsymbol{\phi}_4(0) = \begin{pmatrix} 0 & 0 & 0 & 1 \end{pmatrix}^T$. Therefore, we solve the state equations from $t = 0$ to $t = p$ with initial conditions $\boldsymbol{\phi}_1(0)$, $\boldsymbol{\phi}_2(0)$, $\boldsymbol{\phi}_3(0)$ and $\boldsymbol{\phi}_4(0)$.

   (b) *Determine the dynamics of the solution.*
   Find the dominant eigenvalue ζ of the monodromy matrix M.

   (c) If $\zeta > 1$, increase the control intensity and repeat 2a,b. If $\zeta < 1$, decrease the control intensity and repeat 2a,b. If $\zeta = 1$, or is sufficiently close, stop.

3. *If the monodromy matrix is given by $M = \Phi(p)$, the asymptotic solution to the state equations is $\boldsymbol{\chi}(t) = \Phi(t)\boldsymbol{w}\ \forall\ t$. Therefore $\boldsymbol{\chi}(0) = \Phi(0)\boldsymbol{w} = \boldsymbol{w}$ where $\boldsymbol{w}$ is the eigenvector associated with $\zeta = 1$.*
   Find the asymptotic solution to the state equations by solving them for one cycle from $t = 0$ with an initial condition $\boldsymbol{w}$ where $\boldsymbol{w}$ is the eigenvector corresponding to the dominant eigenvalue found in 2.

4. *Find the fundamental matrix of the adjoint system in the same way as in 2. These particular initial conditions mean that the monodromy matrix of the adjoint system is* $\hat{M} = \Psi(p)$.
   Find the monodromy matrix $\Psi(p) = \begin{pmatrix} \boldsymbol{\psi}_1(p) & \boldsymbol{\psi}_2(p) & \boldsymbol{\psi}_3(p) & \boldsymbol{\psi}_4(p) \end{pmatrix}$ where $\boldsymbol{\psi}_1(0) = \begin{pmatrix} 1 & 0 & 0 & 0 \end{pmatrix}$, $\boldsymbol{\psi}_2(0) = \begin{pmatrix} 0 & 1 & 0 & 0 \end{pmatrix}$, $\boldsymbol{\psi}_3(0) = \begin{pmatrix} 0 & 0 & 1 & 0 \end{pmatrix}$ and $\boldsymbol{\psi}_4(0) = \begin{pmatrix} 0 & 0 & 0 & 1 \end{pmatrix}$. In other words, solve the adjoint equations from $t = 0$ to $t = p$ with initial conditions $\boldsymbol{\psi}_1(0)$, $\boldsymbol{\psi}_2(0)$, $\boldsymbol{\psi}_3(0)$ and $\boldsymbol{\psi}_4(0)$.

5. *The dominant eigenvalue of the adjoint monodromy matrix* $\hat{M}$ *will be 1, because the state equations already satisfy the zero growth conditions.*
   This is checked numerically. Find the corresponding eigenvector $\hat{\boldsymbol{w}}$ to the dominant eigenvalue of the adjoint system.

6. Find the asymptotic solution to the adjoint equations by solving backwards in time for one cycle from $t = p$ with an initial condition $\hat{\boldsymbol{w}}$. This is the same as solving forwards in time from $t = 0$ as since there is zero growth the solution trajectory should be the same.

7. *Using Floquet theory we now have all the components necessary to construct a new approximation for the control.*
   Construct a new approximation for the shape of the control function $\boldsymbol{u}(t)$ from the optimality equations (6.24).

8. Repeat 2 - 7 until $\boldsymbol{u}$ has converged sufficiently.

6.2.6 Pseudo-code

We will explain the methods used in the programming to obtain the results in Section 6.3. The code is given for the case where the control intensity on the retired age group (s_3) is held constant and the optimal prevention strategy over s_1u_1 and s_2u_2 is found where $s_1 = s_2 = s$. This can easily be simplified or extended for the other cases. At the end we will highlight the pieces of code which have to be amended for this.

1. Set all global variables (all parameters used in the model other than s_1, s_2, s_3, u_1, u_2, u_3).

2. Define global variables and set u_3.

3. Call programme which finds the initial guess at the control (which is constant over time) and returns the control functions u_1, u_2 and control intensity s which satisfies a Floquet multiplier of 1.

(a) Set u_1 and u_2 as initial guesses of constant control functions.

(b) Set initial values y_1 and y_2 as two guesses of control intensity.

(c) Set controls $z_1 = y_1 u_1$ and $z_2 = y_1 u_2$.

i. Solve the system under each of the four initial conditions to find the monodromy matrix.

ii. Find the Floquet multiplier of the monodromy matrix.

(d) Set controls $z_1 = y_2 u_1$ and $z_2 = y_2 u_2$.

i. Solve the system under each of the four initial conditions to find the monodromy matrix.

ii. Find the Floquet multiplier of the monodromy matrix.

Note: y_1 and y_2 should be such that the Floquet multiplier in one case is less than one and in the second case is greater than one.

(e) While the Floquet multiplier is more than 0.001 away from 1

i. Set $y_{\text{new}}=(y_1 + y_2)/2$

ii. Set controls $z_1 = y_{\text{new}} u_1$ and $z_2 = y_{\text{new}} u_2$

iii. Solve the system under each of the four initial conditions to find the monodromy matrix.

iv. Find the Floquet multiplier of the monodromy matrix.

v. If the Floquet multiplier is less than 1 set $y_1 = y_{\text{new}}$ or if the Floquet multiplier is greater than 1 set $y_2 = y_{\text{new}}$.

vi. Repeat steps 3(e)i–3(e)v until the condition on the while loops stops being true.

(f) Return control functions u_1 and u_2 to the main program and the control intensity $s = y_{new}$.

4. Set the four initial conditions for the forward and adjoint systems.

5. Define all time spaces, limits etc. needed. Set the initial tolerance as 1 to enter the while loop.

6. Set s_3 as the pre–determined constant value. Discretize su_1, su_2, $s_3 u_3$ over the time period to be used in the Runge–Kutta 4 (RK4) method.

7. While the tolerance between the old and new controls and old and new solutions has not been met

(a) Set $oldu1 = su_1$, $oldu2 = su_2$ etc. to be used to find the tolerance.

(b) Solve the system using the RK4 method under each of the four initial conditions to find the monodromy matrix.

(c) Find the Floquet multiplier of the monodromy matrix and the associated eigenvector.

Note: In the first case due to finding the initial guess the Floquet multiplier should be 1. In later cases the control intensity to ensure zero growth has been found so again the Floquet multiplier should be 1.

(d) If the eigenvector found in 7c is negative multiply by (-1) to make positive.

(e) Run the system forwards using the RK4 method using the eigenvector found in 7c as the initial condition.

Note: The solution found yields zero growth over the period.

(f) Solve the adjoint system backwards using the RK4 method under each of the four initial conditions to find the monodromy matrix.

(g) Find the Floquet multiplier of the monodromy matrix and the associated eigenvector.

Note: The monodromy matrix of the adjoint automatically has Floquet multiplier of 1 if the system does.

(h) If the eigenvector found in 7g is negative multiply by (-1) to make positive.

(i) Run the adjoint system backwards using the RK4 method using the eigenvector found in 7g as the initial condition.

(j) Use the solution to the system and adjoint (found in 7e and 7i respectively) to find u_1, u_2, u_3 (using equations (6.24a), (6.24b) and (6.24c) respectively).

(k) Set $u_1 = \min(1, u_1)$, $u_2 = \min(1, u_2)$, $s_3u_3 = \min(1, s_3u_3)$ to adhere to boundary conditions.

(l) Call programme which takes as input u_1, u_2, s_3u_3 and finds the control intensity s to act on control functions u_1, u_2 which yields a Floquet multiplier of 1.

Note: The value of the control functions which have been found give the correct shape for control but do not necessarily yield a dominant eigenvalue of one and hence zero growth. We therefore have to find the control intensity which the control function is multiplied by to ensure that we have zero growth.

Note u_1 and u_2 do not change in this programme; their shape is determined from the Hamiltonian. It is only the control intensity s which is being changed in this programme.

i. Set initial values y_1 and y_2 as initial guesses for the control intensity.

ii. Set controls $z_1 = y_1 u_1$ and $z_2 = y_1 u_2$.

A. Solve the system under each of the four initial conditions to find the monodromy matrix.

B. Find the Floquet multiplier of the monodromy matrix.

iii. Set $z_1 = y_2 u_1$ and $z_2 = y_2 u_2$.

A. Solve the system under each of the four initial conditions to find the monodromy matrix.

B. Find the Floquet multiplier of the monodromy matrix.

Note: y_1 and y_2 should be such that the Floquet multiplier in one case is less than one and in the second case is greater than one.

iv. While the Floquet multiplier is more than 0.001 away from 1

A. Set $y_{\text{new}}=(y_1 + y_2)/2$

B. Set controls $z_1 = y_{\text{new}} u_1$ and $z_2 = y_{\text{new}} u_2$

C. Solve the system under each of the four initial conditions to find the monodromy matrix.

D. Find the Floquet multiplier of the monodromy matrix.

E. If the Floquet multiplier is less than 1 set $y_1 = y_{\text{new}}$ or if the Floquet multiplier is greater than 1 set $y_2 = y_{\text{new}}$.

F. Repeat steps 7(l)ivA–7(l)ivE until the condition on the while loops stops being true.

v. Return the control intensity $s = y_{\text{new}}$ to the main program.

Note: the controls to be implemented in the next iteration are therefore su_1, su_2 and $s_3 u_3$.

(m) Set $u_1 = su_1$ and $u_2 = su_2$

(n) Find the norm of the new values for su_1, su_2, $s_3 u_3$ and the solutions to the system and adjoint. Find the maximum of all of these. Set as new tolerance.

(o) Repeat steps 7a to 7n until the condition on the while loop stops being true.

8. Plot the effort needed for prevention.

When amended for the simpler or more complex case the input arguments in point 3 change accordingly. Similarly either an extra control intensity is defined in point 6 or no control intensities are pre–defined for the optimal prevention strategy. Points 7k–7m change according to which controls are fixed or varied and how they subsequently need to be defined in the programme(s).

6.2.7 Implementation

In Section 6.3 our aim is to find the optimal prevention strategy over all three age groups. To this end we gradually build up to this, and therefore we work through several steps to calculate the optimal prevention strategy. Initially we optimise over one age group; we hold two of the control intensities equal and allow the third control intensity to be varied to find the solution which yields zero growth. To do this we find the control functions ($u_i(t)$, $i = 1, 2, 3$) for each age group by solving the Hamiltonian. This means that the shape of all control functions is influenced by the seasonality in the vector population. For the two age groups that the control intensity is fixed, we multiply the control function by the control intensity to find the overall control acting on that age group. We then use a bisection method to find the control intensity which is needed to act on the third age group so that epidemic prevention can occur (i.e. the Floquet multiplier is 1). We repeat this process until the optimal solution over one age group is found. We then extend this to optimisation over two age groups. After the control functions have been found, only one control intensity is held fixed. We assume that the control intensities acting on the age groups being optimised are identical and find the control intensity needed for zero growth. Repeating this process yields the optimal solution over two age groups. Finally, we optimise over all three age groups, thus finding the optimal prevention strategy. All parameters used in the model are given in Table 6.1.

Parameter	**Definition**	**Value**
μ	Host mortality rate	0.02
N	Host population size	1000
κ	Average number of vectors per host	5
δ_1	Rate of change child to working age	0.066
δ_2	Rate of change working age to retired	0.022
β	Transmission rate	70
γ	Host recovery rate	60.8
σ_i, $i = 1, 2, 3$	Exposure weighting of age-group i	
μ_V	Vector mortality rate	26.2
p	Period	1
a	Amplitude of oscillation in vector birth rate - seasonal model	0.2

Table 6.1: Parameter definitions and values where kept constant. All rates are given per year.

6.3 Results

6.3.1 Optimisation over one age group

We initially find the control needed on the working age group for epidemic prevention when the control intensities acting on the children's and retired are–groups are held constant. We set the control intensity acting on the children's and retired age groups to be identical ($s_1 = s_3 = 2$, figure 6-1 (a)), and find the optimal prevention strategy for the working age group to ensure zero growth. To do this we use a bisection method with given initial conditions to determine a constant control to be implemented over time which yields zero growth over the time period. This is done by fixing u_1, u_2, u_3, s_1 and s_3 and using the bisection method to find what value of control intensity s_2 is needed for the dominant eigenvalue of the monodromy matrix to be one. This constant rate is then implemented and the system and the adjoint solved using the Hamiltonian to find updated values for $u_1(t), u_2(t), u_3(t)$ by solving equations (6.24a), (6.24b) and (6.24c) respectively. u_1 and u_3 are then multiplied by their control intensities and the new control intensity for the working age group is found (again using a bisection method) so that the dominant eigenvalue of the updated monodromy matrix is one. This process is repeated until the time–dependent optimal prevention strategy is found.

It is important to note that changing the initial condition used for the control function u_2 and changing the initial control functions of u_1 and u_3 do not greatly affect the results attained (see Table 6.2). Although the control intensity acting on the children's and retired age groups is the same, figure 6-1(a) shows that a greater effort is needed for prevention in the children's age group. This implies that the control functions are different for the two age groups, with the control function acting on the children's age group being the more dominant of the two. This is likely to be because the exposure weighting for the children's age group is greater than the retired age group, hence a greater effort is needed. In this example for optimal epidemic prevention over one age group, the effort needed for prevention in the working age group needs to be much higher than the other two age groups.

It is interesting to note that the maximum effort required in each control is found at $t = 0.247$ and the minimum effort required is at $t = 0.745$. Therefore the controls are in phase with each other. However, this is slightly out of phase with the susceptible vector population at the DF state, whose maximum and minimum are found at $t = 0.25$ and $t = 0.75$ respectively. Therefore the maximum control needs to be applied approximately one day before the vector population is at its largest. The shape of the effort and the vector population size at the DF state are slightly different; as the year progresses the minimum effort for prevention needs to be applied approximately two

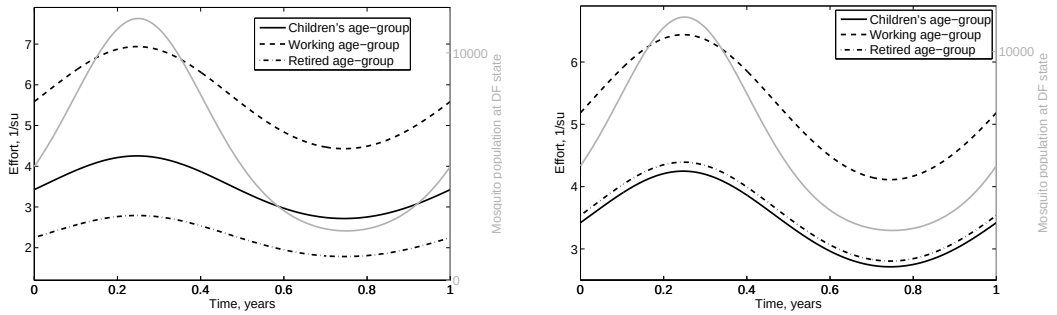

(a) (b)

Figure 6-1: The effort needed over one year for optimal prevention, where the control intensity on two of the controls is held constant. In (a) $s_1 = s_3 = 2$ with initial conditions $u_1(t) = 0.3$, $u_2(t) = 0.2$, $u_3(t) = 0.3 \ \forall \ t$ and in (b) $s_1 = 2 \neq s_3 = 1$ with initial conditions as $u_1(t) = 0.3$, $u_2(t) = 0.2$, $u_3(t) = 0.3 \ \forall \ t$. In both graphs the effort over time is shown for the control on the children's age group (solid line), the working age group (dashed line) and the retired age group (dot-dashed line). The vector population at the DF state is shown in grey. The exposure weightings of the children's, working and retired age groups are $\sigma_1 = 0.5$, $\sigma_2 = 1$ and $\sigma_3 = 0.2$ respectively. All other parameters are given in Table 6.1.

days before the minimum vector population size. Therefore the progression of the two does not occur at the same rate.

	$s_1 = s_3 = 2$ $u_1 = u_3 = 0.3$ $u_2 = 0.5$	$s_2 = s_3 = 2$ $u_1 = u_3 = 0.2$ $u_2 = 0.5$	$s_2 = s_3 = 2$ $u_1 = u_3 = 0.2$ $u_2 = 0.3$
Control 1	3.4481	3.4446	3.4449
Control 2	5.6494	5.6338	5.6336
Control 3	2.2173	2.2429	2.2431
Total effort	11.3148	11.3213	11.3216

Table 6.2: Table showing the total effort of each of the prevention strategies and their total effort over the course of one year.

We also consider the effort needed if the control intensities held constant are different ($s_1 = 2$, $s_3 = 1$, figure 6-1 (b)). The decrease in s_3 has caused the effort needed for epidemic prevention on the retired age group to increase. This has a subsequent effect on the optimal strategy for the working age group; reducing the effort needed throughout the year. As in the previous case the controls (and therefore effort needed) on each of the age groups are in phase, however they are out of phase by one or two

days with the susceptible vector population at the DF state.

We also consider the effort needed for the optimal prevention problem when s_1 and s_3 are fixed and then increased. We calculate the effort for each individual age group and the total effort (equations (6.25) and (6.26) respectively, figure 6-2). Figure 6-2(a) shows the total effort required for prevention in the children's age group decreases as the control intensity for children increases ($1/s_1$ decreases). This is because as s_1 increases the control intensity needed on the working age group decreases. These changes affect the controls that are implemented, causing the total effort which is needed on the children's age group to decrease. At the same time the effort required for prevention in the working age group (figure 6-2(b)) increases. As we are holding s_3 fixed the total effort required for the retired age-group stays fairly similar (see figure 6-2(c)). Therefore, the increase in effort so that optimal prevention can occur has to come from the working age group. An analogous argument can be made for the changes as s_3 is increased. Figure 6-2(d) shows the total effort required for prevention over the whole population. Interestingly, the graph appears symmetric just off the diagonal, with the minimum effort (therefore the true optimal solution) occurring when s_1 and s_3 take similar values. It is worth noting that the least effort required occurs when $s_1 = s_3 = 2.2$. Further, this leads to the control intensity on the working age group being optimised when $s = 2.2128$. Therefore, the prevention strategy appears to be optimised when the control intensities are similar. It is also interesting to note that for all of the parameter combinations used in figure 6-2 the maximum and minimum control needed is at the same time ($t = 0.247, t = 0.745$ respectively) indicating that, as in the previous case, the controls are in phase.

6.3.2 Optimisation over two age groups

The next step towards finding the optimal prevention strategy involves keeping only one control intensity constant, and allowing the other two control intensities to vary in the optimal prevention process. To do this we use a bisection method with given initial conditions to determine a constant control to be implemented over time which yields zero growth over the time period. This is done by fixing u_1, u_2, u_3 and s_3 and using the bisection method to find what value of control intensity s is needed for the dominant eigenvalue of the monodromy matrix to be one (assuming $s_1 = s_2 = s$). This constant rate is then implemented and the system and the adjoint solved using the Hamiltonian to find updated values for u_1, u_2, u_3 over time by solving equations (6.24a), (6.24b) and (6.24c) respectively. u_3 is then multiplied by its' control intensity and the new control intensity for the children's and working age group is found (again using a bisection method) so that the dominant eigenvalue of the updated monodromy matrix

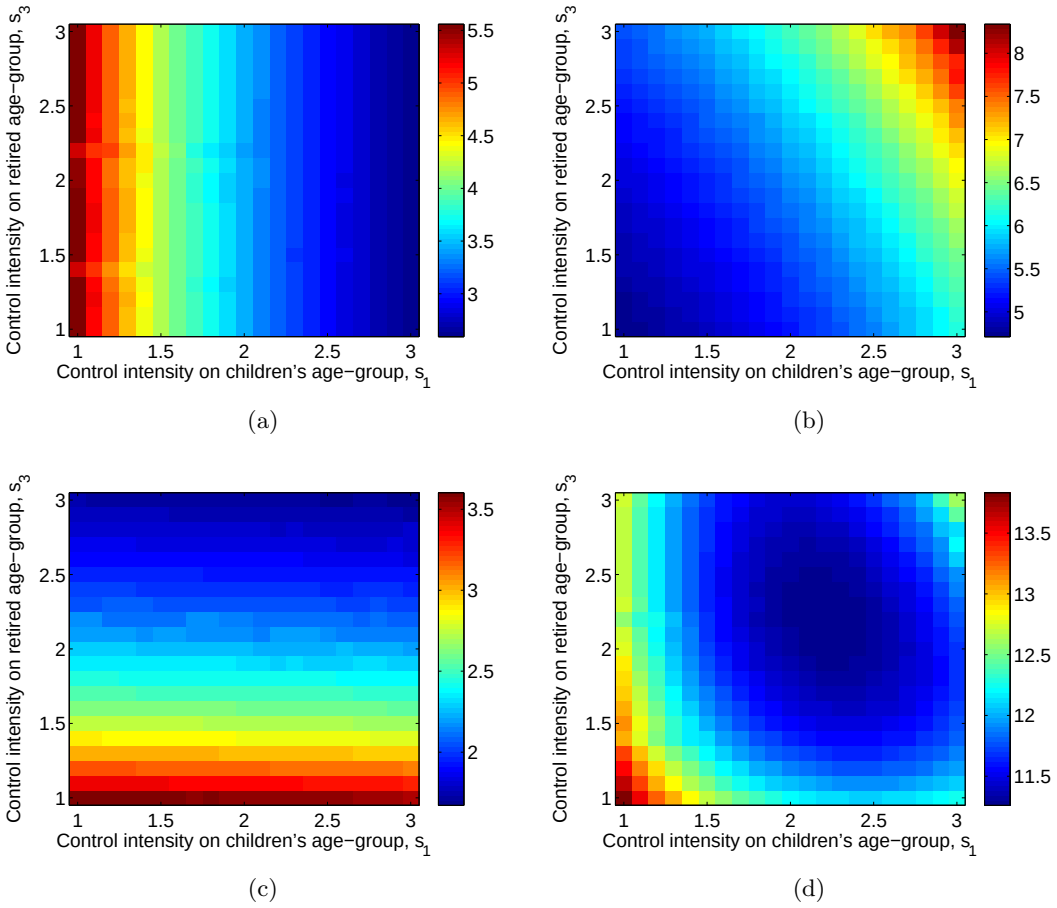

Figure 6-2: The total effort needed over one year for optimal prevention, where the control intensity on two of the controls are varied but fixed in each simulation. (a) The total effort required for prevention in the children's age group, (b) the total effort required for prevention in the working age group, (c) the total effort required for prevention in the retired age group and (d) the total effort required for prevention across the whole population. The exposure weightings of the children's, working and retired age groups are $\sigma_1 = 0.5$, $\sigma_2 = 1$ and $\sigma_3 = 0.2$ respectively. All parameters are given in Table 6.1.

is one. This process is repeated until the time–dependent optimal prevention strategy is found.

Figure 6-3 shows the effort needed over the course of a year for prevention when the control intensity acting on the retired population is held constant. In figure 6-3(a) the control intensity on the retired population is $s_3 = 1$. The effort needed for optimal prevention on each age group is in phase, with a greater effort focused on the working age group. However, by increasing s_3 to $s_3 = 2$ (decreasing $1/s_3$ and hence

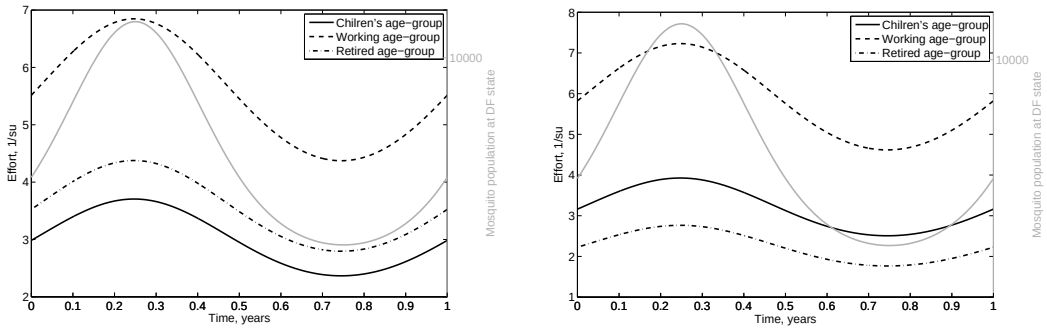

(a) (b)

Figure 6-3: The effort needed over one year for optimal prevention, where the control intensity on one of the controls is fixed. In (a) $s_3 = 1$ and in (b) $s_3 = 2$. In both graphs the effort over time is shown for the control on the children's age group (solid line), the working age group (dashed line) and the retired age group (dot–dashed line). The vector population at the DF state is shown in grey. The exposure weightings of the children's, working and retired age groups are $\sigma_1 = 0.2$, $\sigma_2 = 1$ and $\sigma_3 = 0.2$ respectively. All parameters are given in Table 6.1.

increasing the control intensity acting on the retired–age group), we see that there is a difference in the effort required (figure 6-3 (b)). The effort required on the retired age group for optimal prevention has decreased, whilst the effort required on the children's and working age groups for zero growth has increased slightly. The increase in control intensity has therefore affected the positioning of the control functions and hence the effort required for prevention across all ages. This can be seen further in Table 6.3; the total effort in the former case is higher than in the latter, meaning the latter choice of s_3 is better.

It is important to note that in each case the optimal solution has been found given s_3. For the different parameters used we get contrasting optimal controls to be implemented. Therefore, to find the true optimal solution we will have to optimise over all three controls which are used in the system. It is also noteworthy that, as in the previous case, the effort for the controls are in phase with each other; the maximum points are found at $t = 0.247$ and the minimum at $t = 0.745$. Therefore we again see that the time when effort is implemented is slightly out of phase with the susceptible vector population at the DF state by around 1-2 days.

	$s_3 = 1$ $u_3 = 0.3$ $u_1 = u_2 = 0.2$	$s_3 = 2$ $u_3 = 0.3$ $u_1 = u_2 = 0.2$
Control 1	3.0014	3.1803
Control 2	5.5466	5.8564
Control 3	3.5451	2.2389
Total effort	12.0931	11.2756

Table 6.3: Table showing the effort of each of the prevention strategies on the different age groups and the total effort over the course of one year. The exposure weightings of the children's, working and retired age groups are $\sigma_1 = 0.2$, $\sigma_2 = 1$ and $\sigma_3 = 0.2$ respectively.

6.3.3 Optimal prevention strategy

Finally, we use the processes implemented above to find the optimal prevention strategy over all the age groups if the control intensity is identical for each age group. To do this we initially find the optimised constant control, and then follow the same methodology previously implemented to find the control intensities over time to ensure zero growth over a period.

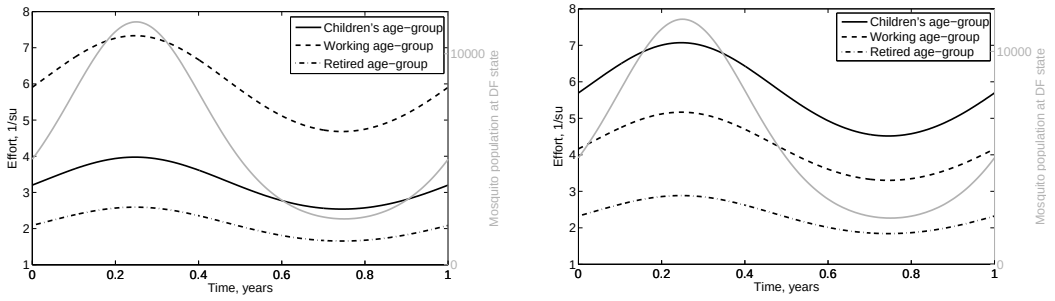

Figure 6-4: The effort needed over one year for optimal prevention. In (a) the exposure weightings are given by $\sigma_1 = 0.5, \sigma_2 = 1, \sigma_3 = 0.2$ and in (b) the exposure weightings are given by $\sigma_1 = 1, \sigma_2 = 0.5, \sigma_3 = 0.2$. The effort over time is shown for the control on the children's age group (solid line), the working age group (dashed line) and the retired age group (dot–dashed line). The vector population at the DF state is shown in grey. All parameters are given in Table 6.1.

Figure 6-4(a) shows the optimal prevention strategy for zero growth over a cycle when the exposure weightings for the children's, working and retired age groups are $\sigma_1 = 0.5, \sigma_2 = 1, \sigma_3 = 0.2$ respectively. We see that the efforts needed on each age group for optimal prevention are, as in previous cases, in phase with each other. This

means they are out of phase by one or two days with the susceptible vector population at the DF state. The age group which takes the most effort to control is the working age group. The effort is just under twice as much as the children's age group. Indeed, whilst the exposure weightings of the different age groups are relevant, it is important to note that the efforts needed for prevention on the different compartments are not in the same proportions as the exposure weightings. Therefore the optimal prevention strategy is not solely determined by the exposure weighting of the different age groups.

Figure 6-4(b) shows the optimal prevention strategy when the exposure weightings for the children's, working and retired age groups are $\sigma_1 = 0.5, \sigma_2 = 1, \sigma_3 = 0.2$ respectively. As before, the efforts needed for optimal prevention are in phase with each other. However, due to their increased exposure the maximum effort is now focussed on the children's age group for optimal prevention. It is interesting to note that this is not as high as the effort needed to control the working age group when they had the greatest exposure (compare with figure 6-4(a)). To compensate for this, we see a small increase in the effort focussed on the retired age group, and the effort focussed on the working age group for optimal prevention is greater than that of the children in the previous example.

It is interesting to consider the total effort needed for optimal prevention in each case. When children have the greatest exposure (figure 6-4(b)) the total effort for prevention is $E = 12.2513$. When the working age group have the greatest exposure (figure 6-4(a)) the total effort for prevention is $E = 11.2609$ (see Table 6.4). Therefore, simply switching which of the children and working age groups have the greatest exposure weighting not only affects where the effort for optimal prevention should lie throughout the year, but also the total effort required for epidemic prevention. Whilst for this combination of parameters the time averaged basic reproductive numbers (Wang and Zhao, 2008) are within 0.02 of each other, when the exposure weightings are switched between the two age groups this is not always the case. Therefore the time–averaged basic reproductive number helps to support the results found regarding the total effort required for epidemic prevention.

The examples shown have been plotted when the initial conditions for the control function used were $u_i(t) = 0.5 \; \forall \, t$, $(i = 1, 2, 3)$. Table 6.4 shows that under two different initial conditions the absolute difference between the results for total effort over the period is minimal, indicating that the initial conditions used do not matter in finding the optimal solution. This is because it is the Hamiltonian procedure which finds the optimal solution, which is not based on the initial conditions of the controls.

We check this further for a range of initial conditions. We randomly assigned u_1, u_2, u_3 as values between 0.1 and 0.9 for all time and subsequently followed the process

	$u_1 = 0.5$, $u_2 = 0.5$ $u_3 = 0.5$, $\sigma_1 = 0.5$ $\sigma_2 = 1$, $\sigma_3 = 0.2$	$u_1 = 0.2$, $u_2 = 0.3$ $u_3 = 0.5$, $\sigma_1 = 0.5$ $\sigma_2 = 1$, $\sigma_3 = 0.2$	**Norm**
Control 1	3.2204	3.2162	0.0042
Control 2	5.9409	5.9484	0.0075
Control 3	2.0996	2.0980	0.0016
Total effort	11.2609	11.2626	0.0017
	$u_1 = 0.5$, $u_2 = 0.5$ $u_3 = 0.5$, $\sigma_1 = 1$ $\sigma_2 = 0.5$, $\sigma_3 = 0.2$	$u_1 = 0.2$, $u_2 = 0.3$ $u_3 = 0.5$, $\sigma_1 = 1$ $\sigma_2 = 0.5$, $\sigma_3 = 0.2$	**Norm**
Control 1	5.7287	5.7186	0.0100
Control 2	4.1869	4.1835	0.0034
Control 3	2.3357	2.3469	0.0112
Total effort	12.2513	12.2491	0.0022

Table 6.4: Table showing the total effort of each of the prevention strategies and their total effort over the course of one year. The table also shows the norm (defined as $\sum |x^2|^{1/2}$) between the efforts calculated using two different sets of initial conditions, for two different exposure weightings.

to determine the effort for optimal prevention required by each of the age groups, the optimal effort on the total population and the control intensity that was found for 500 simulations. Figure 6-5(a)–(c) shows boxplots for the effort for each of the different age groups. We see that in each case the interquartile range is small, however there are outliers for each of the age groups. When considering the total effort over the whole population (figure 6-5(d)) there are only three outliers (less than 1% of the times run) and the difference between the maximum and minimum whiskers is 0.0235 (maximum at 11.2806, minimum at 11.2572). This shows that under different initial conditions the total effort is very similar and hence the optimal solution is found. We can also consider the control intensity (figure 6-5(e)). In this case there are no outliers from the 500 starting initial conditions. The difference between the whiskers is 0.0257 (maximum at 2.2217, minimum at 2.196), and between the interquartile range 0.0196 (25^{th} percentile at 2.2021, 75^{th} percentile at 2.2217). Again, this difference is minimal over the simulations. Furthermore, the value of control intensity s which is found corresponds to when the optimal problem was found in Section 6.3.1. When varying s_1 and s_3 and finding the optimal solution using only s_2 this was found at $s_1 = s_3 = 2.2$, $s_2 = 2.2128$ whilst finding the optimal solution over all age groups the median is 2.207. This further justifies the results when finding the optimal control strategy over all three populations.

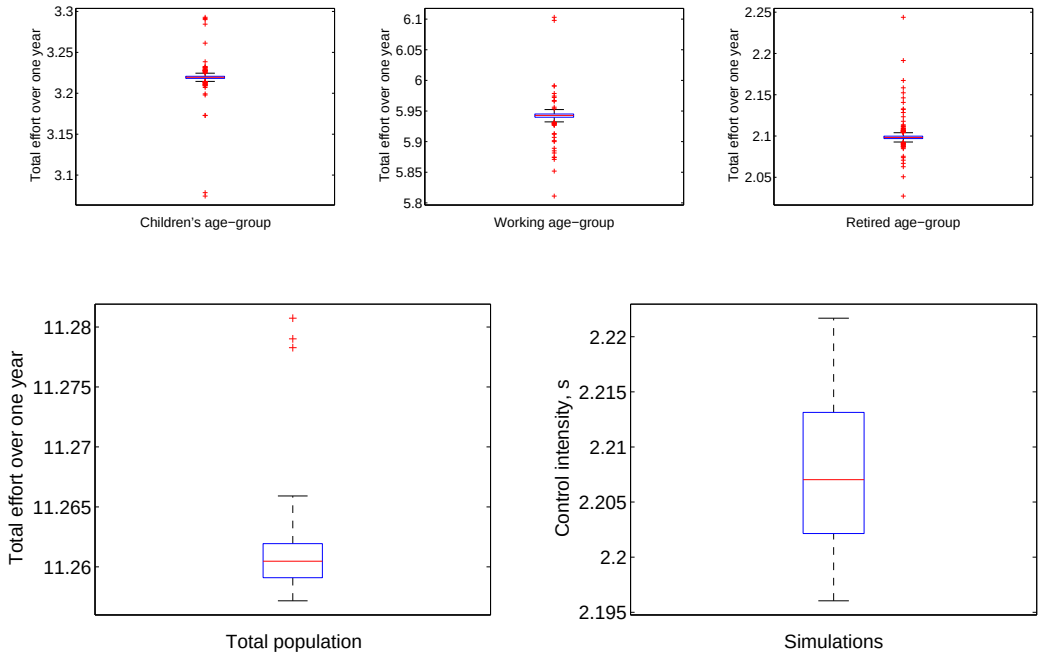

Figure 6-5: Boxplots showing the range of values for effort and the control intensity over 500 runs which start with random initial conditions on each of the different age groups. (a) is the effort for the children's age group, (b) is the effort for the working age group, (c) is the effort for the retired age group, (d) is the effort for the total population and (e) is the control intensity required for optimal control. The exposure weightings of the children's, working and retired age groups are $\sigma_1 = 0.5$, $\sigma_2 = 1$ and $\sigma_3 = 0.2$ respectively. All other parameters are given in Table 6.1.

6.3.4 Varying exposure weightings

We also see how varying the exposure weightings of the different age groups affects the effort required for epidemic prevention. Figure 6-6(a)–(c) shows the effort required on the different age groups throughout the year for optimal prevention as the exposure weighting of the working age group is varied. We see the same oscillatory dynamics for each of the different exposure weightings. However, the change in effort for the working age group is much greater as the exposure weighting is varied (compare figure 6-6(b) with figures 6-6(a) and (c)). We also see that as the exposure weighting of the working age group increases, the effort for optimal prevention decreases in the children's and retired age groups and increases in the working age group. This is because the distribution of vector bites is changing, and the vectors are biting more in the working age group. Therefore, the control (and hence the effort required for optimal prevention)

needs to be adapted accordingly.

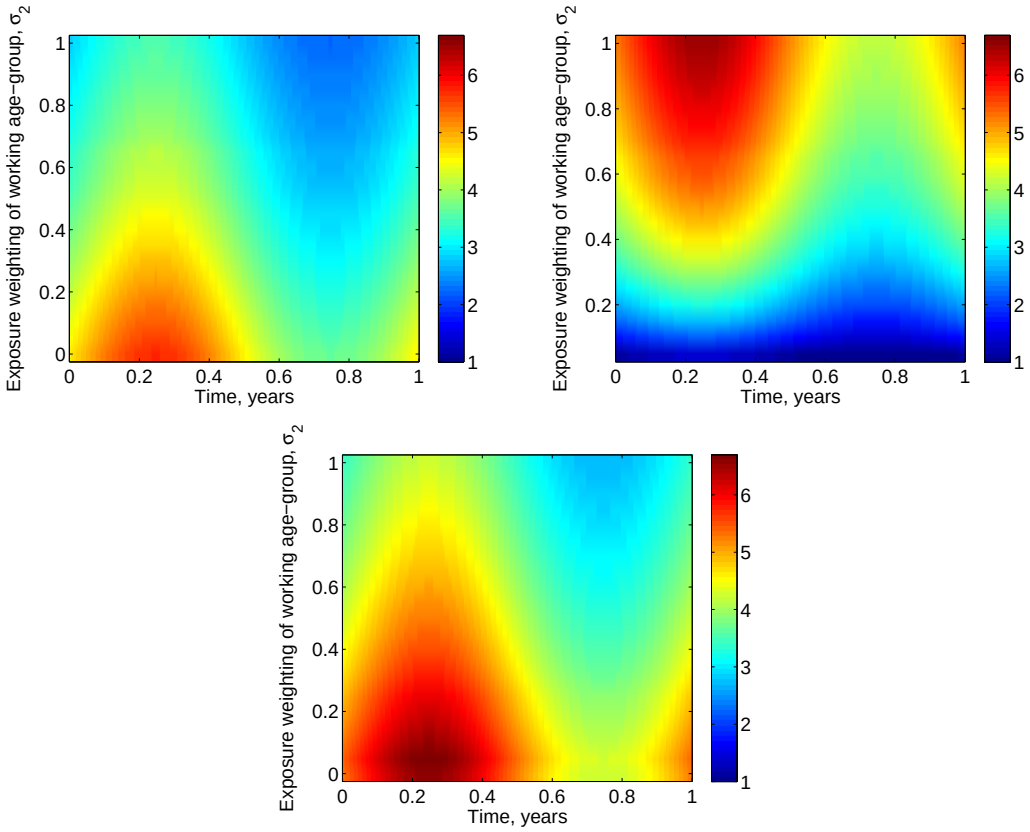

Figure 6-6: The effort needed for optimal prevention as the exposure weighting of the working age group is varied. (a) The effort needed for optimal prevention on the children's age groups over the course of the year (b) The effort needed for optimal prevention on the working age group over the course of the year (c) The effort needed for optimal prevention on the retired age group over the course of the year. In all graphs the exposure weightings of the children's and retired age groups are $\sigma_i = 0.5$, $(i = 1, 2, 3)$. All other parameters are given in Table 6.1.

Figure 6-7(a) shows the total effort (equations (6.25)) over the course of one period as the exposure weighting of the working age group is increased for each of the different age groups. There is a large increase in the effort needed for optimal prevention in the working age group as their exposure weighting increases. For the children's and retired age groups as the exposure weighting of the working age group increases the total effort required decreases. This is to be expected; more effort is being focussed on a different age group. It is interesting to note that the effort needed for optimal prevention is higher in the retired age group than in the children's age group, even though their exposure weighting is identical. One factor could be that individuals spend longer in

the children's age group than in the retired age group. Figure 6-7(b) shows the total effort over the whole population (equation (6.26)). As the exposure weighting of the working age group increases so too does the total effort required for optimal prevention. After a maximum is reached the total effort begins to reduce again. This shows the importance of understanding the exposure different age groups have to mosquitoes.

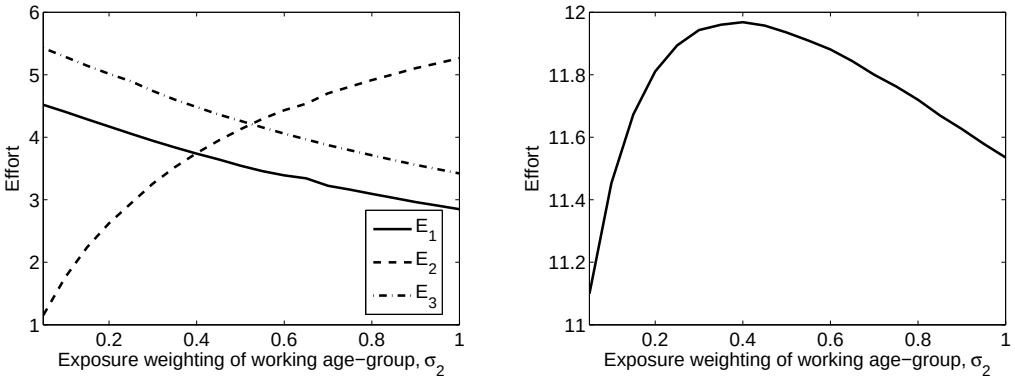

Figure 6-7: The effort needed for optimal prevention as the exposure weighting of the working age group is varied. (a) The total effort throughout the year as the exposure weighting is varied for the children's (solid line), working (dashed line) and retired (dot-dashed line) age groups (b) The total effort needed for optimal prevention over the whole population as the exposure weighting of the working age group is increased. In both graphs $\sigma_1 = 0.5$ and $\sigma_3 = 0.5$. All other parameters are given in Table 6.1.

This is further exemplified in figure 6-8. In this case the exposure weighting of the children's age group is $\sigma_1 = 0.5$ and the retired age group is $\sigma_3 = 0.2$. Whilst there are similar patterns in behaviour, the fact that children have a greater exposure than retired individuals means that a greater effort is needed on the children's age group for optimal prevention than on the retired age groups as the exposure weighting of the working age group is increased (figure 6-8 (a)). We again consider the total effort across the whole population (equations (6.26)) as we vary the exposure weighting of the working age group (figure 6-8 (b)). As the exposure weighting increases there is initially an increase in the effort needed for optimal prevention, followed by a decrease. The effort required decreases as the exposure weighting of the working age group gets comparatively bigger to the exposure weightings of the other age groups.

We have therefore shown that whilst we can find the optimal solution for epidemic prevention over the course of a year, the exposure weighting of different age groups is important. Whilst it may not always be possible to adapt the exposure that different age groups have to the vectors, knowing that different effort will have to be implemented

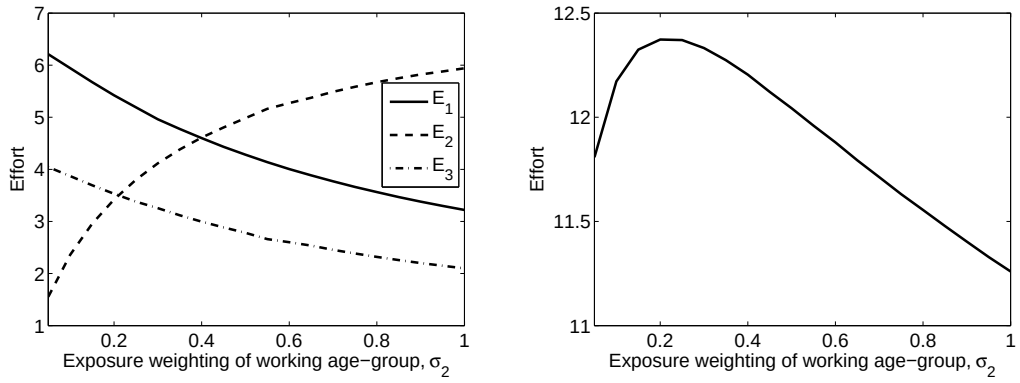

Figure 6-8: The effort needed for optimal prevention as the exposure weighting of the working age group is varied. (a) The total effort throughout the year as the exposure weighting is varied for the children's (solid line), working (dashed line) and retired (dot-dashed line) age groups (b) The total effort needed for optimal prevention over the whole population as the exposure weighting of the working age group is increased. In both graphs $\sigma_1 = 0.5$ and $\sigma_3 = 0.2$. All other parameters are given in Table 6.1.

in each case could help with epidemic prevention and to contain the spread of disease.

6.4 Discussion

In this chapter we have implemented a strategy for optimal prevention in a three age group host–vector SIR model for dengue. We have used a mixture of control theory and Floquet theory as seasonality is implemented in the vector population.

We find the optimal prevention strategy to ensure that the infected population size is the same at the start and end of a given time period. This is desired rather than a guaranteed decline, as by controlling throughout the year constantly it means that a potential epidemic is avoided. If infection is decreased so that control is no longer needed, then an infected individual introduced into the population could cause a rapid epidemic, as there is no controls in place. In contrast, by controlling throughout the year it means that the possibility of this is reduced.

We have found that the optimal prevention strategy to ensure that the infected population is the same size at the start and end of a given period follows a similar trajectory to the vector population size at the DF state. When the vector population size is larger a greater effort is needed for prevention than when the vector population size is smaller. The effort needed for optimal prevention and the susceptible mosquito population size are not exactly in phase; there is a difference of a day or two as to

when the most and least effort should be implemented and when the vector population size is at its maximum and minimum. Oki et al. (2011) determined that in an optimal control problem, the control should be implemented during the wet season, when the vector population size increases. For our optimal prevention model, we find that the maximum effort should be implemented just before the mosquito population reaches their peak size. Therefore, for optimal prevention and control strategies some results appear to coincide.

We find that the exposure weighting of the different age groups affects the amount of effort needed for optimal prevention. However, the exposure weighting interacts with the controls in different ways for the different age groups; simply switching the exposure weightings of two age groups does not mean the effort needed for optimal prevention switches. Therefore there is an interaction between the controls that the different groups need, perhaps influenced by the size of the age groups. We also found that varying the exposure weightings of the different age groups affected the total effort needed for prevention in the population. Therefore, if given age groups have a greater exposure this can ultimately mean that for prevention to occur a greater effort across the whole population is needed.

In our model we account for seasonality in the vector population. However we only split the host population according to age, not the mosquitoes. Therefore to implement prevention strategies to eradicate dengue which focus on larvae of the vector population (for control examples see Burattini et al. (2008); Rodrigues et al. (2013)), we would need to use more complex models.

We found that a high level of effort is needed across all age groups for epidemic prevention. This was exemplified by the results showing optimal control on all three age groups; the control was not identical across them, but the intensity on all age groups was found to be similar. A level of control acting on all groups was necessary, rather that simply trying to prevent the spread in one age group. Therefore, the results show that it is important to think, no matter what the exposure weightings of the different age groups, about the host population as a whole rather than simply each of the different age groups.

CHAPTER 7

CONCLUSIONS

We have used a combination of ordinary differential equations, partial differential equations and stochastic models to analyse the dynamics of dengue. We have implemented new frameworks, and determined methodologies to quantify differences in seroprevalence profiles which implement contrasting contact rates. We have examined the probability of an epidemic and optimal prevention strategies that should be implemented to ensure isolated infections do not lead to large epidemics. In doing so, we have presented new ideas and added to the growing research area surrounding infectious diseases, specifically dengue.

Transmission dynamics of dengue, particularly with reference to secondary infections, are not completely understood. After a primary infection a host has complete immunity to that serotype, but only partial and temporary immunity to heterologous serotypes (World Health Organisation, 2014a). However, it is not known for how long temporary immunity lasts, or exactly how subsequent infections are affected by antibody–dependent enhancement (ADE). Despite this uncertainty, we have implemented a new framework which can help us better understand the dynamics of dengue. We have used existing empirical data regarding secondary infections and reasoned that not all secondary infections are enhanced through ADE (Balmaseda et al., 2006; Sabchareon et al., 2012). Nevertheless, most existing models assume that all secondary infections are enhanced (Ferguson et al., 1999a; Wearing and Rohani, 2006; Recker et al., 2009). We implemented our new framework where only a proportion of the population suffer an enhanced secondary infection, and compared the results with well–known models in which all secondary infections are enhanced. In doing so

we have shown that the enhancement parameters associated with the new framework can interact to cause strikingly different dynamics to conventional models where all secondary infections are enhanced. A low enhancement prevalence and low levels of cross–protection can cause annual oscillations for longer durations of temporary cross–immunity than when enhancement acts on all secondary infections. This then has implications on the spread of infection and the frequency with which multi–annual oscillations occur as the duration of temporary cross–immunity increases. Our results, agreeing with Wearing and Rohani (2006), indicate that it is the duration of cross–protection after a primary infection which is the greatest determinant in achieving multi–annual oscillations that are in-line with the 8–10 years seen in empirical data (Nisalak et al., 2003; Recker et al., 2009). However we show that by separating the population into those who suffer an enhanced secondary infection and those that do not there are a greater range of dynamics seen as the enhancement and infection parameters interact.

Our initial results on age structure at the peak of the initial epidemic and endemic equilibrium show that it is possible to determine and quantify differences in seroprevalence profiles when age–independent and age–dependent contact rates are applied. Whilst there is much theory on age structure in PDE models (for example Schenzle (1984); Greenhalgh (1987); Iannelli et al. (1997)) we did not find literature which directly compared and looked for differences in models which implemented age structure in contact rates and those which did not. For a simple SIR model we found that the age group who have the greatest contact rate is influential in determining how easy it is to differentiate between seroprevalence profiles. We found that it is possible to determine distinct differences in the seroprevalence profiles at the peak of the initial epidemic and the endemic equilibrium if certain age groups have a higher contact rate. Therefore different contact patterns that age groups have (Edmunds et al., 1997; Mossong et al., 2008) are important to study and implement in models.

We extended the age structure model and considered a two–serotype model which is potentially more applicable to dengue in areas where more than one serotype are present, for example in Thailand (Nisalak et al., 2003; Adams et al., 2006; Bianco et al., 2009). We initially found that including the mosquito has a great impact on the results quantifying the difference between seroprevalence profiles which apply age–independent and age–dependent contact. This indicates that including the mosquito is important; this is reasonable as dengue is transmitted via a mosquito and so any changes in dynamics that occur because of this should be accounted for. We found that varying the proportion of the population with an enhanced secondary infection can affect how easy it is to quantify differences between age–independent and age–

dependent seroprevalence profiles. This is especially true when there is high cross protection in the population that do not suffer enhanced infections. Therefore this is important to consider further, as while sources such as Balmaseda et al. (2006) and Sabchareon et al. (2012) indicate that not everyone who has a secondary infection has an enhanced secondary infection, it is not known what proportion of the population have an enhanced secondary infection. Therefore this could potentially have large implications on how age–dependence should be included in models for dengue.

Our age structure results are important in a public health setting; if a school or workplace is near an area with a lot of standing water where mosquitoes flourish the people there have a greater exposure to mosquitoes than others. Understanding how this can be included in a model, and how this affects results from a model where all people have equal exposure is therefore important. Whilst the trajectory of an epidemic may be similar, the make–up of those infected differs. This could potentially affect how a new serotype may enter the population, particularly if, as in Cuba, it is entering a population where one serotype is already endemic (Guzmán et al., 2000). Therefore understanding these differences and quantifying them is important if we wish to determine if it significant for age structure to be included in transmission dynamics. If it is necessary, it is vital that the age structure of an area and the contact patterns between different age groups and the mosquitoes are known. Exposure to mosquitoes by different age groups can vary, for example through the behaviours that people exhibit such as using nets, or by location of work places or schools which may be closer to areas where mosquitoes are. If one age group has a lot more exposure than others to the mosquito this can greatly influence how easy it is to differentiate between seroprevalence profiles, particularly in the early stages of an epidemic.

Our methodology has the potential to be expanded to determine whether seroprevalence data from countries where dengue is endemic has been influenced by age–dependent contact. By using MCMC methods on data, parameter estimates could be generated. Likelihood methods could then be applied to determine whether there is any apparent age–dependence in the population. Data from different countries could then be analysed to see whether, for example, age–dependence varies by country. As well as examining seroprevalence data it could be possible to extend the model so that the age distribution of the population is different. Determining the effect, if any, that this has on the influence of age–dependence in the contact rate, and any interactions between the population distribution and age groups with the maximum contacts, may further help to determine how age structure should be included in models for dengue.

Age structure is further examined in a stochastic framework to determine the probability that an epidemic will occur. We considered a single serotype model; an infected

human or mosquito enters a population which is completely susceptible, such as the epidemic on Easter Island in Chile in 2002 (Chowell et al., 2013) or in Madeira in 2012 (Lourenço and Recker, 2014). If infection is brought into the population through an infected mosquito the probability of an epidemic is lowest when all age groups have equal exposure to the mosquito. However, the differences in the probability as the exposure weightings are varied are marginal. Therefore we found that vector to host transmission is less important in whether an epidemic may occur than if infection starts in the host population. From a public health perspective it is important to consider the exposure of all age groups. If one age group has more exposure to mosquitoes there is more chance of an epidemic if infection enters the population in that age group than any other. That is not to say that the probability of an epidemic is low if infection enters in a different age group, and therefore ensuring that all age groups are properly informed of how best to reduce transmission occurrences is important. Cost–benefit analysis may also be needed to ensure that decreasing the exposure of one age group is not detrimental to the population as a whole.

Control strategies are often aimed at the vector population, particularly for dengue where there are no vaccines available (World Health Organisation, 2014a). Optimal control has previously been implemented to determine the best time to use a method, such as insecticide fogging, to control the vector population size (Oki et al., 2011). Conversely, the method we have used considers the effort needed for prevention of disease. We want to retain the same number of infected hosts and vectors at the beginning and end of a given period if isolated infections enter a population. For this to occur, effort has to be implemented throughout the year, with a greater amount of effort when the susceptible vector population is at its largest.

Understanding both the probability of an epidemic and prevention strategies to stop large epidemics are therefore important. In this work we have considered a single serotype entering an entirely susceptible population, however there are many areas in the world where dengue is endemic such as in South America (World Health Organisation, 2014a). For public health strategies in these places it would be beneficial to know the probability of an epidemic, both of the endemic serotype and the invading serotype. With a two–serotype model we could also consider the interactions of the enhancement parameters which act on secondary infections, and use sensitivity analysis to determine if the epidemic probability is more affected by certain parameters. By understanding the probability of an epidemic in these cases, it will then be possible to consider the optimal prevention strategies if a different serotype were to enter a population already endemic. There may potentially be different effort needed throughout the year as there may be sequential infections of different serotypes.

The effective and accurate modelling of dengue is vital. The emerging infectious disease is a large threat in areas where it is endemic due to the lack of vaccinations. Therefore it is imperative that accurate and reliable modelling can be implemented to help understand the dynamics of the disease. This work shows the importance of this in many ways. Firstly, we have shown that it is necessary to understand the underlying dynamics of dengue and secondary infections, as this affects the subsequent dynamics. Secondly, we have shown that age structure in the transmission term can have a large impact on the seroprevalence profiles, which in turn can have epidemiological effects. Age structure, and the different exposure age groups have, can affect the probability of an epidemic and the effort needed for optimal prevention. We have explored these ideas and shown their significance and how, potentially, new methodologies can be used to help advance modelling, and therefore understanding, of the dynamics of dengue.

BIBLIOGRAPHY

Abia, L., Angulo, O., and López-Marcos, J. (2005). Age-structured population models and their numerical solution. *Ecological Modelling*, 188:112–136.

Adams, B. and Boots, M. (2006). Modelling the relationship between antibody–dependent enhancement and immunological distance with application to dengue. *Journal of Theoretical Biology*, 242(2):337–346.

Adams, B., Holmes, E., Zhang, C., Mammen, M., Nimmannitya, S., Kalayanarooj, S., and Boots, M. (2006). Cross–protective immunity can account for the alternating epidemic pattern of dengue virus serotypes circulating in Bangkok. *PNAS*, 103(38):14234–14239.

Agarwal, R. and O'Regan, D. (2008). *An Introduction to Ordinary Differential Equations*. Springer-Verlag New York, New York, NY.

Aguiar, M., Ballesteros, S., Kooi, B., and Stollenwerk, N. (2011a). The role of seasonality and import in a minimalistic multi-strain dengue model capturing differences between primary and secondary infections: Complex dynamics and its implications for data analysis. *Journal of Theoretical Biology*, 289:181–196.

Aguiar, M., Kooi, B., and Stollenwerk, N. (2008). Epidemiology of dengue fever: A model with temporary cross-immunity and possible secondary infection shows bifurcations and chaotic behaviour in wide parameter regions. *Mathematical Modelling of Natural Phenomena*, 3(4):48–70.

Aguiar, M., Stollenwek, N., and Kooi, B. (2011b). The stochastic multi–strain dengue

model: Analysis of the dynamics. *Numerical Analysis and Applied Mathematics ICNAAM*, 1389:1224–1227.

Alexanderian, A., Gobbert, M., Fister, K., Gaff, H., Lenhart, S., and Schaefer, E. (2011). An age-structured model for the spread of epidemic cholera: Analysis and simulation. *Nonlinear analysis: Real World Applications*, 12:3483–3498.

Allen, L. and Lahodny Jr, G. (2012). Extinction thresholds in deterministic and stochastic epidemic models. *Journal of Biological Dynamics*, 6(2):590–611.

Allen, L. and van den Driessche, P. (2013). Relations between deterministic and stochastic thresholds for disease extinction in continuous - and discrete-time infectious disease models. *Mathematical Biosciences*, 243:99–108.

Anders, K., Nguyet, N., Chau, N., Hung, N., Thuy, T., Lien, L., Farrar, J., Wills, B., Hien, T., and Simmons, C. (2011). Epidemiological Factors Associated with Dengue Shock Syndrome and Mortality in Hospitalized Dengue Patients in Ho Chi Minh City, Vietnam. *American Journal of Tropical Medicine and Hygiene*, 84(1):127–134.

Anderson, R. and May, R. (1991). *Infectious Diseases of Humans*. Oxford University Press.

Aparicio, J. and Castillo-Chavez, C. (2009). Mathematical modelling of tuberculosis epidemics. *Mathematical Bioscienes and Engineering*, 6:209–237.

Athreya, K. and Ney, P. (1972). *Branching Processes*. Springer-Verlag, New York.

Bacaër, N. (2007). Approximation of the basic reproduction number R_0 fr vector–borne diseases with a periodic vector population. *Bulletin of Mathematical Biology*, 69:1067–1091.

Bacaër, N. and Ait Dads, E. (2012). On the probability of extinction in a periodic environment. *Mathematical Biology*.

Bacaër, N. and Guernaoui, S. (2006). The epidemic threshold of vector–borne diseases with seasonality. the case of cutaneous leishmaniasis in Chichaoua, Morocco. *Mathematical Biology*, 53:421–436.

Balmaseda, A., Hammond, S., Tellez, Y., Imhoff, L., Rodriguez, Y., Saborío, S., Mercado, J., Perez, L., Videa, E., Almanza, E., Kuan, G., Reyes, M., Saenz, L., Amador, J., and Harris, E. (2006). High seroprevalence of antibodies against dengue virus in a prospective study of schoolchildren in Managua, Nicaragua. *Tropical Medicine and International Health*, 11(6):935–942.

Bhatt, S., Gething, P., Brady, O., Messina, J., Farlow, A., Moyes, C., Drake, J., Brownstein, J., Hoen, A., Sankoh, O., Myers, M., George, D., Jaenisch, T., Wint, G., Simmons, C., Scott, T., Farrar, J., and Hay, S. (2013). The global distribution and burden of dengue. *Nature*, 496(7446):504–507.

Bianco, S., Shaw, L., and Schwartz, I. (2009). Epidemics with multistrain interactions: The interplay between cross immunity and antibody-dependent enhancement. *CHAOS*, 19:043123–1–043123–9.

Braga, C., Luna, C., Martelli, C., de Souza, W., Cordeiro, M., Alexander, N., de Albuquerque, M., Silveira Júnior, J., and Marques, E. (2010). Seroprevalence and risk factors for dengue infection in socio–economically distinct areas of Recife, Brazil. *Acta Tropica*, 113:234–240.

Burattini, M., Chen, M., Chow, A., Couinho, F., Goh, K., Lopez, L., Ma, S., and Massad, E. (2008). Modelling the control strategies against dengue in Singapore. *Epidemiology and Infection*, 139:309–319.

Chikaki, E. and Ishikawa, H. (2009). A dengue transmission model in Thailand considering sequential infections with all four serotypes. *Journal of Infection in Developing Countries*, 3(9):711–722.

Chowell, G., Fuentes, R., Olea, A., Aguilera, X., Nesse, H., and Hyman, J. (2013). The basic reproductive number R_0 and effectiveness of reactive interventions during dengue epidemics: The 2002 dengue outbreak in Easter Island, Chile. *Mathematical Biosciences and Engineering*, 10(5–6):1455–1474.

Christofferson, R., Mores, C., and Wearing, H. (2014). Characterizing the likelihood of dengue emergence and detection in naïve populations. *Parasites & Vectors*, 7(282).

Cochran, J. and Xu, Y. (2014). Age–structured dengue epidemic model. *Applicable Analysis*.

Cummings, D., Iamsirithaworn, S., Lessler, J., McDermott, A., Prasanthong, R., Nisalak, A., Jarman, R., Burke, D., and Gibbons, R. (2009). The impact of the demographic transition on dengue in Thailand: insights from a statistical analysis and mathematical modelling. *PLoS Medicine*, 6(9):e1000139.

Del Valle, S., Hyman, J., Hethcote, H., and Eubank, S. (2007). Mixing patterns between age groups in social networks. *Social Networks*, 29:539–554.

Diekmann, O. and Heesterbeek, J. (2000). *Mathematical Epidemiology of Infectious Diseases: Model Building, Analysis and Interpretation*. John Wiley & Sons Ltd.

Diekmann, O., Heesterbeek, J., and Britton, T. (2013). *Mathematical Tools for Understanding Infectious Diseases Dynamics*. Princeton University Press.

Dietz, K. (1967). Epidemics and rumours: a survey. *Journal of the Royal Statistical Society. Series A*, 130(4):505–528.

Edmunds, W., O'Callaghan, C., and Notes, D. (1997). Who mixes with whom? A method to determine the contact patterns of adults that may lead to the spread of airborne infections. *Proceedings of the Royal Society B: Biological Sciences*, 264:949–957.

Ferguson, N., Anderson, R., and Gupta, S. (1999a). The effect of antibody-dependent enhancement on the transmission dynamics and persistence of multiple-strain pathogens. *Population Biology*, 96:790–794.

Ferguson, N. and Andreasen, V. (2002). The influence of different forms of cross–protective immunity on the population dynamics of antigenetically diverse populations. In Castillo-Chavez, C., Blower, S., Kirschner, D., van den Driessche, P., and Yakubu, A., editors, *Mathematical Approaches for Emerging and Reemerging Infectious Diseases: Models, Methods and Theory*, volume 126 of *IMA Volumes Mathematics and its Applications*, pages 157–169. Springer-Verlag, New York.

Ferguson, N., Donnelly, C., and Anderson, R. (1999b). Transmission dynamics and epidemiology of dengue: insights from age-stratified sero-prevalence surveys. *Phil. Trans. R. Soc. Lond. B*, 354:757–768.

Garciá, G., Sierra, B., Pérez, A., Aguirre, E., Rosado, I., Gonzalez, N., Izquierdo, A., Pupo, M., Díaz, D., Sánchez, L., Marcheco, B., Hirayama, K., and Guzmán, M. (2010). Asymptomatic dengue infection in a Cuban population confirms the protective role of the RR variant of the FcγRIIa polymorphism. *American Journal of Tropical Medicine and Hygiene*, 82(6):1153–1156.

Gibson, G., Gilligan, C., and Kleczowski, A. (1999). Predicting variability in biological control of a plant-pathogen system using stochastic models. *Proceedings of the Royal Society B: Biological Sciences*, 266:1743–1753.

Glass, K., Kelly, H., and Mercer, G. (2012). Pandemic influenza H1N1 reconciling serosurvey data with estimates of the reproduction number. *Epidemiology*, 23(1):86–94.

Greenhalgh, D. (1987). Analytical results on the stability of age–structured recurrent epidemic models. *IMA Journal of Mathematics Applied in Medicine and Biology*, 4:109–144.

Greenman, J. and Adams, B. (2015). The exclusion problem in seasonally forced epidemiological systems. *Journal of Theoretical Biology*, 367:49–60.

Greenman, J. and Norman, R. (2007). Environmental forcing, invasion and control of ecological and epidemiological systems. *Journal of Theoretical Biology*, 247:492–506.

Gubler, D. (2002). Epidemic dengue/denuge hemorrhagic fever as a public health, social and economic problem in the 21st century. *Trends in Microbiology*, 10(2):100–103.

Gubler, D. and Kuno, G. (2004). *Dengue and Dengue Hemorrhagic Fever*. CABI Publishing, Oxon, United Kingdom.

Guzman, M. and Kouri, G. (2002). Dengue: an update. *The Lancet*, 2:33–42.

Guzmán, M., Kouri, G., Braco, J., Valdes, L., Vazquez, S., and Halstead, S. (2002). Effect of age on outcome of secondary dengue 2 infections. *International Journal of Infectious Diseases*, 6:118–124.

Guzmán, M., Kouri, G., Valdes, L., bravo, J., Alvarez, M., Vazques, S., Delgado, I., and Halstead, S. (2000). Epidemiological studies on dengue in Santiago de Cuba. *American Journal of Epidemiology*, 152(9):793–799.

Guzman, M. and Vazquez, S. (2010). The complexity of antibody-dependent enhancement of dengue virus infection. *Viruses*, 2:2649–2662.

Halstead, S. (1976). Observations related to pathogenesis of dengue hemorrhagic fever. VI. Hypotheses and discussion. *Yale Journal of Biology and Medicine*, 42:350–362.

Halstead, S., Lan, N., Myint, T., Shwe, T., Nisalak, A., Kalyanarooj, S., Nimmannitya, S., Soegijanto, S., Vaughn, D., and Endy, T. (2002). Dengue hemorrhagic fever in infants: research opportunities ignored. *Emerging Infectious Diseases*, 8(12):1474–1479.

Halstead, S., Streit, T., Lafontant, J., Putvatana, R., Russell, K., Sun, W., Kanesa-Thasan, N., Hayes, C., and Watts, D. (2001). Haiti: Absence of dengue hemorrhagic fever despite hyperendemic dengue virus transmission. *American Journal of Tropical Medicine and Hygiene*, 65(3):180–183.

Harrington, L., Scott, T., Lerdthusnee, K., Coleman, R., Costero, A., Clark, G., Jones, J., Kitthawee, S., Kittayapong, P., Sithiprasasna, R., and Edman, J. (2005). Dispersal of the dengue vector *Aedes aegypti* within and between rural communities. *American Journal of Tropical Medicine and Hygiene*, 72(2):209–220.

Hens, N., Ayele, G., Goeyvaerts, N., Aerts, M., Mossong, J., Edmunds, J., and P, B. (2009). Estimating the impact of school closure on social mixing behaviour and the transmission of close contact infections in eight European countries. *BMC Infectiuos Diseases*, 9(187):doi:10.1186/1471–2334–9–187.

Hethcote, H. (1996). Modelling heterogeneous mixing in infectious disease dynamics. In Isham, V. and Medley, G., editors, *Models for Infectious Human Diseases: Their Structure and Relation to Data*, pages 215–238. Cambridge University Press.

Hethcote, H. (2000). The mathematics of infectious diseases. *SIAM Review*, 42(4):599–653.

Iannelli, M. (1995). *Mathematical Theory of Age-Structured Population Dynamics*. Giardini Editori e Stampatori.

Iannelli, M., Kim, M.-Y., and Park, E.-J. (1997). Splitting methods for the numerical approximation of some models of age–structured population dynamics and epidemiology. *Applied Mathematical and Computations*, 87:69–93.

Inaba, H. (1990). Threshold and stability results for an age-structured epidemic model. *Journal of Mathematical Biology*, 28:411–434.

Jordan, D. and Smith, P. (1999). *Nonlinear Ordinary Differential Equations*. Oxford University Press, New York, USA, third edition.

Kawaguchi, I., Sasaki, A., and Boots, M. (2003). Why are dengue virus serotypes so distantly related? Enhancement and limiting serotype similarity between dengue virus strains. *Proceedings of the Royal Society B: Biological Sciences*, 270:2241–2247.

Keeling, M. and Grenfell, B. (1997). Disease extinction and community size: Modeling the persistence of measles. *Science*, 275:65–68.

Keeling, M. and Rohani, P. (2008). *Modeling Infectious Diseases in Humans and Animals*. Princeton University Press.

Kermack, W. and McKendrick, A. (1927). A contribution to the mathematical theory of epidemics. *Proceedings of the Royal Society A*, 115:700–721.

Klausmeier, C. (2008). Floquet theory: a useful tool for understanding nonequilibrium dynamics. *Theoretical Ecology*, 1:153–161.

Kongsomboon, K., Singhasivanon, P., Kaewkungwal, J., Nimmannitya, S., Jr, M. M., Nisalak, A., and Sawanpanyalert, P. (2004). Temporal trends of dengue fever/dengue hemorrhagic fever in Bangkok, Thailand from 1981 to 2000: an age-period-cohort analysis. *Southeast Asian Journal of Tropical Medicine and Public Health*, 35(4):913–917.

la C. Sierra, B. D., Kourí, G., and Guzmán, M. (2007). Race: a risk factor for dengue hemorrhagic fever. *Archives of Virology*, 152:533–542.

Laverty, S. and Adler, F. (2010). The role of age structure in the persistence of a chronic pathogen in a fluctuating population. *Journal of Biological Dynamics*, 3(2-3):224–234.

Lenhart, S. and Workman, J. (2007). *Optimal Control Applied to Biological Models*. Chapman and Hall/CRC, Taylor and Francis Group.

Li, J. and Brauer, F. (2008). *Continuous-Time Age-Structured Models in Population Dynamics and Epidemiology*, volume 1945, pages 205–227. Springer eBooks.

Loke, H., Bethell, D., Phuong, C., Day, N., White, N., Farrar, J., and Hill, A. (2002). Susceptibility to dengue hemorrhagic fever in Vietnam: Evidence of an association with variation in vitamin D receptor and FCγ receptor IIA genes. *American Journal of Tropical Medicine and Hygiene*, 67(1):102–106.

Lourenço, J. and Recker, M. (2014). The 2012 Madeira dengue outbreak: Epidemiological determinants and future epidemic potential. *PLoS Neglected Tropical Diseases*, 8(8):e3083.

MacDonald, G. (1957). *The Epidemiology and Control of Malaria*. Oxford University Press, London.

Mathew, A. and Rothman, A. (2008). Understanding the contribution of cellular immunity to dengue disease pathogenesis. *Immunological Reviews*, 225:300–313.

Mello, R. and Castilho, C. (2014). A structured discrete model for dengue fever infections and the determination of R_0 from age–stratified serological data. *Bulletin of Mathematical Biology*, 76:1288–1305.

Mossong, J., Hans, N., Jit, M., Beutels, P., Auranen, K., Mikolajczyk, R., Massari, M., Salmaso, S., Tomba, G., Wallinga, J., Heijne, J., Sadkowska-Todya, M., Rosinska,

M., and Edmunds, W. (2008). Social contacts and mixing patterns relevant to the spread of infectious diseases. *PLOS Medicine*, 5(3):0381–0391.

Nagao, Y. and Koelle, K. (2008). Decreases in dengue transmission may act to increase the incidence of dengue hemorrhagic fever. *PNAS*, 105(6):2238–2243.

Newton, E. and Reiter, P. (1992). A model of the transmission of dengue fever with an evaluation of the impact of ultra–low volume (ULV) insecticide applicatinos on dengue epidemics. *American Journal of Tropical Medicine and Hygiene*, 47:709–720.

Nisalak, A., Endy, T., Nimmannitya, S., Kalayanarooj, S., Thisayakorn, U., Scott, R., Burke, D., Hoke, C., Innis, B., and Vaughn, D. (2003). Serotype–specific dengue virus circulation and dengue disease in Bangkok, Thailand from 1973 to 1999. *American Journal of Tropical Medicine and Hygiene*, 68(2):191–202.

Oki, M., Sunahara, T., Hashizume, M., and Yamamoto, T. (2011). Optimal timing of insecticide fogging to minimize dengue cases: modeling dengue transmission among various seasonalities and transmission intensities. *PLOS Neglected Tropical Diseases*, 5(10):e1367.

Otero, M. and Solari, H. (2010). Stochastic eco-epidemiological mode of dengue disease transmission by *Aedes aegypti* mosquito. *Mathematical Biosciences*, 223:32–46.

Pancharoen, C. and Thisyakorn, I. (2001). Dengue virus infection during infancy. *Transactions of the Royal Society of Tropical Medicine and Hygiene*, 95:307–308.

Pongsumpun, P. and Tang, I. (2001). A realistic age structures transmission model for dengue hemorrhagic fever in Thailand. *Southeast Asian Journal of Tropical Medicine and Public Health*, 32(2):336–340.

Pongsumpun, P. and Tang, I. (2003). Transmission of dengue hemorrhagic fever in an age structured population. *Mathematical and Computer Modelling*, 37:949–961.

Recker, M., Blyuss, K., Simmons, C., Hien, T., Wills, B., Farrar, J., and Gupta, S. (2009). Immunological serotype interactions and their effect on the epidemiological pattern of dengue. *Proceedings of the Royal Society B: Biological Sciences*, 276:2541–2548.

Reich, N., Shrestha, S., King, A., Rohani, P., Lessler, J., Kalayanarooj, S., Yoon, I.-K., Gibbons, R., Burke, D., and Cummings, D. (2013). Interactions between serotypes of dengue highlight epidemiological impact of cross–immunity. *Journal of the Royal Society Interface*, 10(86):20130414.

Reiner, Jr., R., Perkins, T., Barker, C., Niu, T., Fernando Chaves, L., Ellis, A., George, D., Le Menach, A., Pulliam, J., Bisanzio, D., Buckee, C., Chiyaka, C., Cummings, D., Garcia, A., Gatton, M., Gething, P., Hartley, D., Johnston, G., Klein, E., Michael, E., Lindsay, S., Lloyd, A., Pigott, D., Reisen, W., Ruktanonchai, N., Singh, B., Tatem, A., Kitron, U., Hay, S., Scott, T., and Smith, D. (2013). A systematic review of mathematical models of mosquito-borne pathogen transmission: 1970-2010. *Journal of the Royal Society Interface*, 10(81):20120921.

Rodrigues, H., Monteiro, M., and Torres, D. (2013). Bioeconomic perspectives to an optimal control dengue model. *International Journal of Computer Mathematics*, 90(10):2126–2136.

Rodriguez–Barraquer, I., Mier–y–Teran–Romero, L., Schwartz, I., Burke, D., and Cummings, D. (2014). Potential opportunities and perils of imperfect dengue vaccines. *Vaccine*, 32:514–520.

Ross, S. (1908). *Report on the prevention of malaria in Mauritius*. Waterlow & Sons Limited, London, UK.

Ross, S. (1911). *The prevention of malaria*. Dutton, New York, NY.

Sabchareon, A., Sirivichayakul, C., Limkittikul, K., Chanthavanich, P., Suvannadabba, S., Jiwariyavej, V., Dulyachai, W., Pengsaa, K., Margolis, H., and Letson, G. (2012). Dengue infection in children in Ratchaburi, Thailand: a cohort study. I. Epidemiology of symptomatic acute dengue infection in children, 2006–2009. *PLOS Neglected Tropical Diseases*, 6(7):e1732.

Sabin, A. (1952). Research on dengue during world war II. *American Journal of Tropical Medicine and Hygiene*, 1(1):30–50.

Schenzle, D. (1984). An age-structured model of pre- and post-vaccination measles transmission. *IMA Journal of MAthematics Applied in Medicine and Biology*, 1:169–191.

Schwartz, I., Shaw, L., Cummings, D., Billings, L., McCrary, M., and Burke, D. (2005). Chaotic desynchronization of multistrain diseases. *Physical Review E*, 72:066201.

Sierra, B., Alegre, R., Pérez, A., García, G., Sturn-Ramirez, K., Obasanjo, O., Aguirre, E., Alvarez, M., Rodriguez-Roche, R., Valdés, L., Kanki, P., and Guzmán, M. (2007). HLA–A, –B, –C, and –DRB1 allele frequencies in cuban individuals with antecedents of dengue 2 disease: Advantages of the Cuban population for HLA studies of dengue virus infection. *Human Immunology*, 68:531–540.

Strikwerda, J. C. (1989). *Finite Difference Schemes and Partial Differential Equations*. The Wadsworth & Brooks/Cole Mathematics Series.

Sulsky, D. (1993). Numerical solution of structured population models. I Age structure. *Journal of Mathematical Biology*, 31:817–839.

Supriatna, A., Soewono, E., and van Gils, S. (2008). A two-age-classes dengue transmission model. *Mathematical Biosciences*, 216:114–121.

Thai, K., Nishiura, H., Hoang, P., Tran, N., Phan, G., Le, H., Tran, B., Nguyen, N., and de Vries, P. (2011). Age-specificity of clinical dengue during primary and secondary infections. *PLOS Neglected Tropical Diseases*, 5(6):e1180.

Thavara, U., Siriyasatien, P., Tawatsin, A., Asavadachanukorn, P., Anantapreecha, A., Wongwanich, R., and Mulla, M. (2006). Double infection of heteroserotypes of dengue viruses in field populations of *Aedes aegypti* and *Aedes albopictus* (Diptera: Culicidae) and serological features of dengue viruses found in patients in Southern Thailand. *Southeast Asian Journal of Tropical Medicine and Public Health*, 37(3):468–476.

Thieme, H. (2001). Disease extinction and disease persistence in age structured epidemic models. *Nonlinear Analysis*, 47:6181–6194.

van den Driessche, P. and Watmough, J. (2008). Further notes on the basic reproduction number. In Brauer, F., van den Driessche, P., and Wu, J., editors, *Mathematical Epidemiology*, volume 1945 of *Lecture Notes in Mathematics*, pages 159–178. Springer, Berlin.

Wang, W. and Zhao, X.-Q. (2008). Threshold dynamics for compartmental epidemic models in periodic environments. *Journal of Dynamics and Differential Equations*, 20:699–717.

Wearing, H. and Rohani, P. (2006). Ecological and immunological determinants of dengue epidemics. *PNAS*, 103(31):11802–11807.

Whitehorn, J. and Simmons, C. (2011). The pathogenesis of dengue. *Vaccine*, 29:7221–7228.

WHO–VMI Dengue Vaccine Modelling Group (2012). Assessing the potential of a candidate dengue vaccine with mathematical modeling. *PLOS Neglected Tropical Diseases*, 6(3):e1450.

Woodall, H. and Adams, B. (2014). Partial cross–enhancement in models for dengue epidemiology. *Journal of Theoretical Biology*, 351:67–73.

World Health Organisation (2014a). Dengue. http://www.who.int/topics/dengue/en/.

World Health Organisation (2014b). Questions and answers on dengue vaccines: Phase III study of CYD–TDV. http://www.who.int/immunization/research/development/WH0_dengue_vaccine_QA_July2014.pdf?ua=1.

APPENDIX A

AGE-STRUCTURED EPIDEMIOLOGICAL MODELS

A.1 Numerical schemes: L_2 norm

Figure A-1 shows the error found by implementing the L_2 norm (equation (3.29)). For each compartment the total number of individuals is found and the error then calculated. Figures A-1(a) and (b) show very similar trends to the previous method of calculating the L_2 norm using each individual age–group for the susceptible and infected compartments (compare with figure 3-1). For larger step sizes the error is smaller when the splitting scheme is implemented. As the step size is reduced the error is very similar for both numerical schemes. The results are slightly more varied for the recovered compartment (figure A-1(c)). However, in general for larger step sizes the splitting scheme has a smaller error than the upwind scheme. As when using the method in Section 3.2.4 we find that the error is smaller for the susceptible and recovered compartments than it is for the infected compartment.

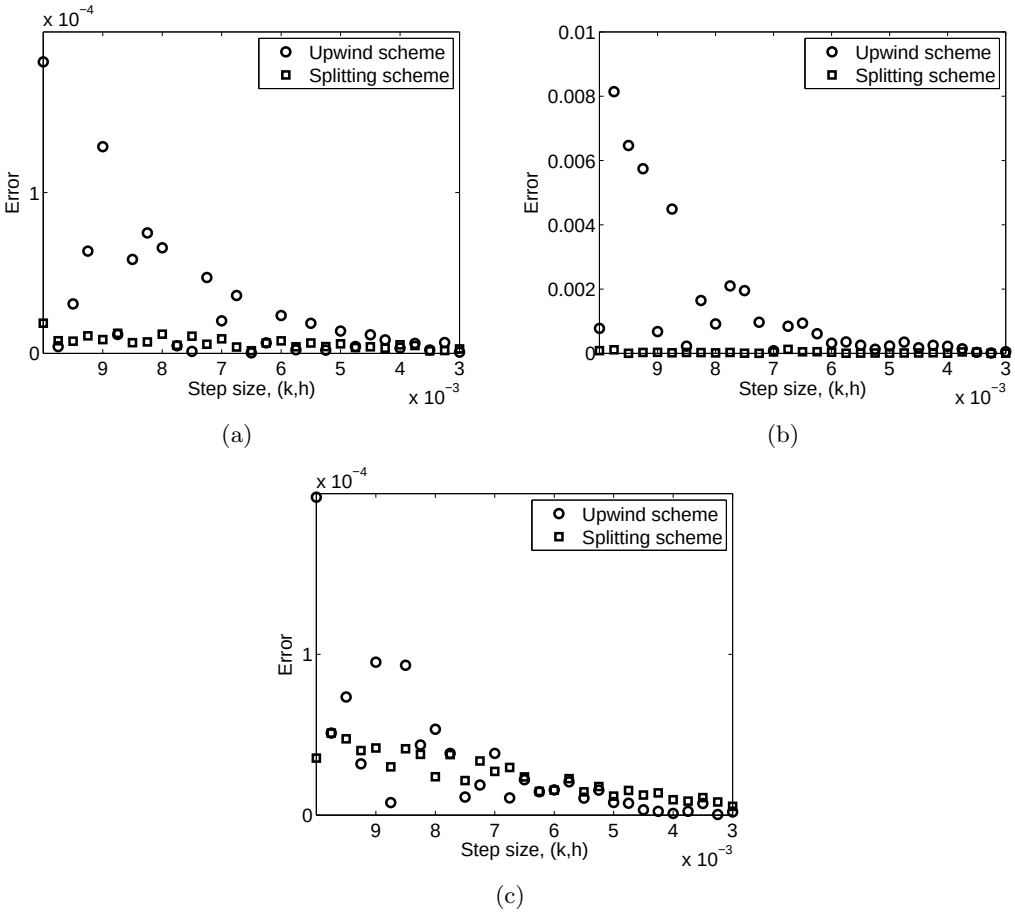

Figure A-1: The relative error (equation (3.29)) for the upwind scheme (circles) and the splitting scheme (squares) when $t = 1000$ years as the step size is reduced. The error is calculated by finding the total number of individuals in each compartment and then finding the error. (a) Shows the error in the schemes for the susceptible compartment, (b) shows the error in the schemes for the infected compartment and (c) shows the error in the schemes for the recovered compartment. The parameters are given by $N = 10000$, $\gamma = 60$, $\beta = 2\gamma$ and $b = 1/60$.

APPENDIX B

AGE–STRUCTURE IN THE TWO SEROTYPE DENGUE MODEL

B.1 Calculating the basic reproductive number for the single serotype host–vector model

To find the basic reproductive number (R_0) for the host–vector model we use the next generation matrix near the disease free equilibrium (DFE). We discretize the population into age groups i, $i = 1, 2, \ldots, n$. Therefore we can model the population by

$$\begin{aligned}
\frac{\mathrm{d}S_i}{\mathrm{d}t} &= N_i, && \text{(B.1a)}\\
\frac{\mathrm{d}I_i}{\mathrm{d}t} &= (\Lambda_V)_i N_H^i - \gamma I_H^i, && \text{(B.1b)}\\
\frac{\mathrm{d}S_V}{\mathrm{d}t} &= N_V, && \text{(B.1c)}\\
\frac{\mathrm{d}I_V}{\mathrm{d}t} &= \Lambda_H N_V - \delta_V I_V && \text{(B.1d)}
\end{aligned}$$

where

$$(\Lambda_V)_i(t) = qb\frac{\bar{p}_i I_V(t) S_i(t)}{\sum_k \bar{p}_k N_k(t)}, \qquad (\Lambda_H)(t) = b\frac{\sum_i \bar{p}_i I_i(t)}{\sum_k \bar{p}_k N_k}. \qquad \text{(B.2)}$$

There is no mortality rate included in the host equations as we are assuming type I mortality (equation (3.24)). After linearising about the DFE, focusing on the infected

compartments, we have

$$\begin{pmatrix} \dot{I}_1 \\ \dot{I}_2 \\ \vdots \\ \dot{I}_n \\ \dot{I}_V \end{pmatrix} = \begin{pmatrix} 0 & 0 & \cdots & 0 & \frac{qb\bar{p}_1(N_1)^2}{\sum_k \bar{p}_k N_k} \\ 0 & 0 & \cdots & 0 & \frac{qb\bar{p}_2(N_2)^2}{\sum_k \bar{p}_k N_k} \\ \vdots & \vdots & \ddots & \vdots & \vdots \\ 0 & 0 & \cdots & 0 & \frac{qb\bar{p}_n(N_n)^2}{\sum_k \bar{p}_k N_k} \\ \frac{qb\bar{p}_1 N_V}{\sum_k \bar{p}_k N_k} & \frac{qb\bar{p}_2 N_V}{\sum_k \bar{p}_k N_k} & \cdots & \frac{qb\bar{p}_n N_V}{\sum_k \bar{p}_k N_k} & 0 \end{pmatrix} \begin{pmatrix} I_1 \\ I_2 \\ \vdots \\ I_n \\ I_V \end{pmatrix} + \begin{pmatrix} -\gamma & 0 & \cdots & 0 & 0 \\ 0 & -\gamma & \cdots & 0 & 0 \\ \vdots & \vdots & \ddots & \vdots & \vdots \\ 0 & 0 & \cdots & -\gamma & 0 \\ 0 & 0 & \cdots & 0 & -\delta_V \end{pmatrix} \begin{pmatrix} I_1 \\ I_2 \\ \vdots \\ I_n \\ I_V \end{pmatrix} \tag{B.3a}$$

$$= (T + \Sigma)\mathbf{I}. \tag{B.3b}$$

The next generation matrix is then $G = -T\Sigma^{-1}$

$$G = \begin{pmatrix} 0 & 0 & \cdots & 0 & \frac{qb\bar{p}_1(N_1)^2}{\delta_V \sum_k \bar{p}_k N_k} \\ 0 & 0 & \cdots & 0 & \frac{qb\bar{p}_2(N_2)^2}{\delta_V \sum_k \bar{p}_k N_k} \\ \vdots & \vdots & \ddots & \vdots & \vdots \\ 0 & 0 & \cdots & 0 & \frac{qb\bar{p}_n(N_n)^2}{\delta_V \sum_k \bar{p}_k N_k} \\ \frac{qb\bar{p}_1 N_V}{\gamma \sum_k \bar{p}_k N_k} & \frac{qb\bar{p}_2 N_V}{\gamma \sum_k \bar{p}_k N_k} & \cdots & \frac{qb\bar{p}_n N_V}{\gamma \sum_k \bar{p}_k N_k} & 0 \end{pmatrix}. \tag{B.4}$$

Taking the spectral radius of this matrix then yields the square of the basic reproductive number for the host-vector model.

B.2 Probability of type I error

IC1: $S_0(0) = 9997$, $I_1(0) = 1$, $I_2(0) = 2$

B.2.1 Varying the enhancement intensity χ

Figures B-1(a), (b) and (c) show the probability of type I error for serotype one at the peak of the initial epidemic as the enhancement intensity is increased when the enhancement prevalence and age–group with maximum transmission rate are varied. Increasing the enhancement intensity does not overly influence the probability of type I error that is seen in the $(\rho - \mu)$ parameter space. This is also seen for serotype two (figures B-1(d), (e) and (f)) and the total seroprevalence (figures B-1(g), (h) and (i)).

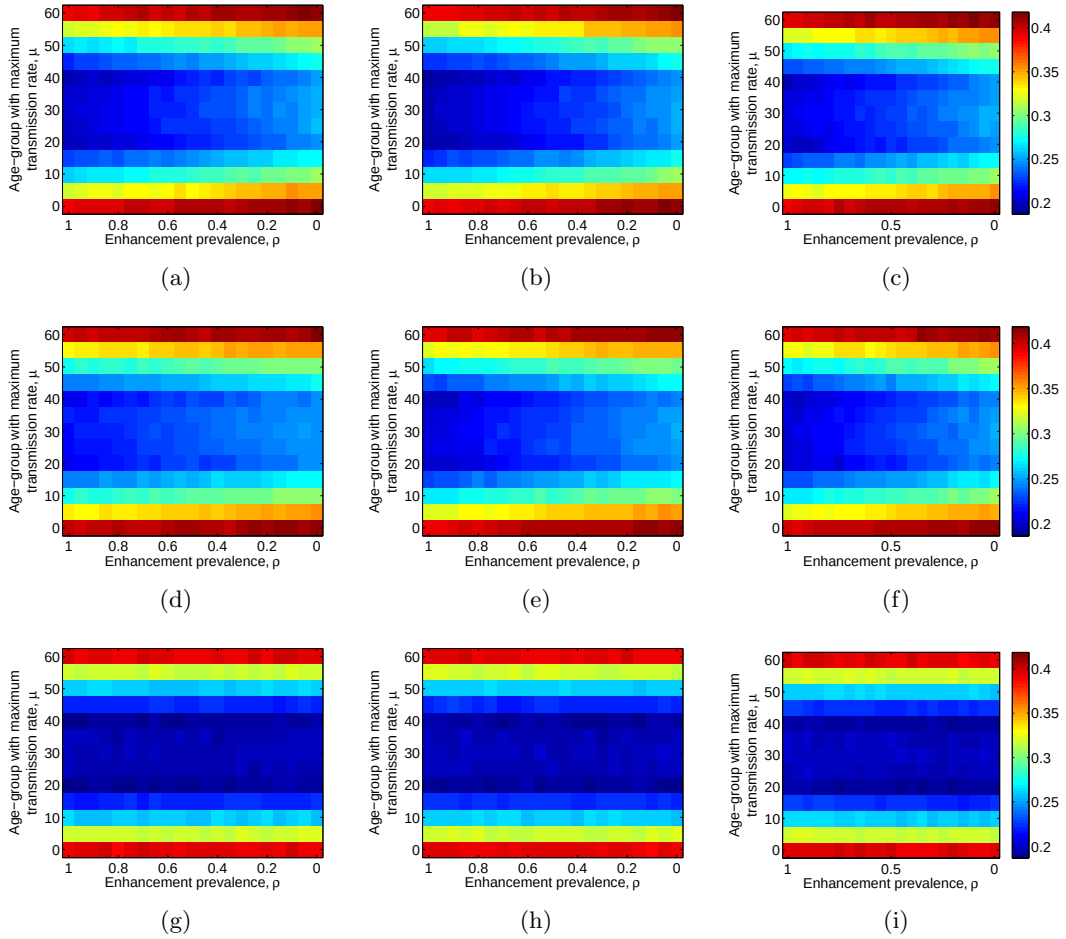

Figure B-1: Probability of type I error at the peak of the initial epidemic as the enhancement prevalence and the age–group with the greatest transmission rate are varied. (a) (b) and (c) show the probability of type I error for serotype one. In (a) $\chi = 2$, in (b) $\chi = 3$ and in (c) $\chi = 5$. (d) (e) and (f) show the probability of type I error for serotype two. In (d) $\chi = 2$, in (e) $\chi = 3$ and in (c) $\chi = 5$. (g) (h) and (i) show the probability of type I error for total seroprevalence. In (g) $\chi = 2$, in (h) $\chi = 3$ and in (i) $\chi = 5$. In all figures $\eta = 1$ and all other parameters are given in Table 4.1.

B.2.2 Varying the cross–protection η

Figure B-2 shows the probability of type I error for serotype two at the peak of the initial epidemic as the cross–protection is decreased when the enhancement prevalence and age–group with the maximum transmission rate are varied. We see similar characteristics as for serotype one (compare with figure 4-7(a), (b) and (c)), however the type I error is smaller across the parameter combinations. This means that it is harder to differentiate between the seroprevalence profiles for serotype one than serotype two.

As the level of cross–protection decreases (η increases) there is a greater uniformity across the different enhancement prevalences.

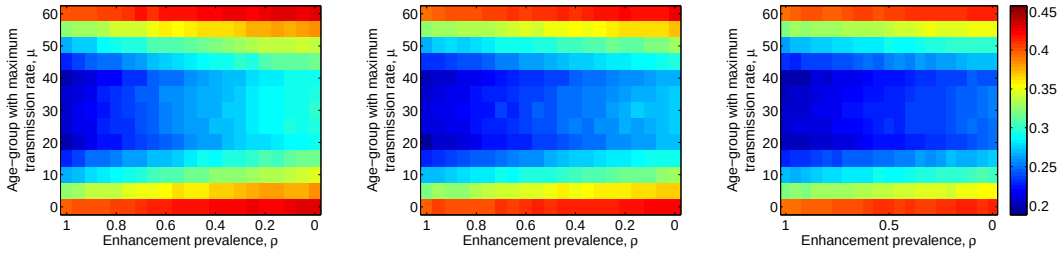

(a) (b) (c)

Figure B-2: Probability of type I error for serotype two at the peak of the initial epidemic as the enhancement prevalence and the age–group with the greatest transmission rate are varied. In (a) $\eta = 0$, in (b) $\eta = 0.5$ and in (c) $\eta = 1$. In all figures $\chi = 3$ and all other parameters are given in Table 4.1.

B.3 Probability of type I error IC2: Serotype one endemic

B.3.1 Varying the enhancement intensity χ

Figures B-3(a), (b) and (c) show the probability of type I error for serotype two for increasing enhancement intensity as the enhancement prevalence and age–group with the maximum transmission rate are varied. As the enhancement intensity increases it becomes more difficult to differentiate between the seroprevalence profiles and consequently age–dependence is having less of an effect in the model. It is easiest to differentiate between the seroprevalence profiles when the greatest transmission rate is in the middle ages.

Figures B-3(d), (e) and (f) show the probability of type I error for the total seroprevalence at the peak of the initial epidemic. For each enhancement intensity there is little change in how easy it is to differentiate seroprevalence profiles as the enhancement prevalence is varied. For each enhancement prevalence the qualitative behaviour is the same as seen in figure 4-10.

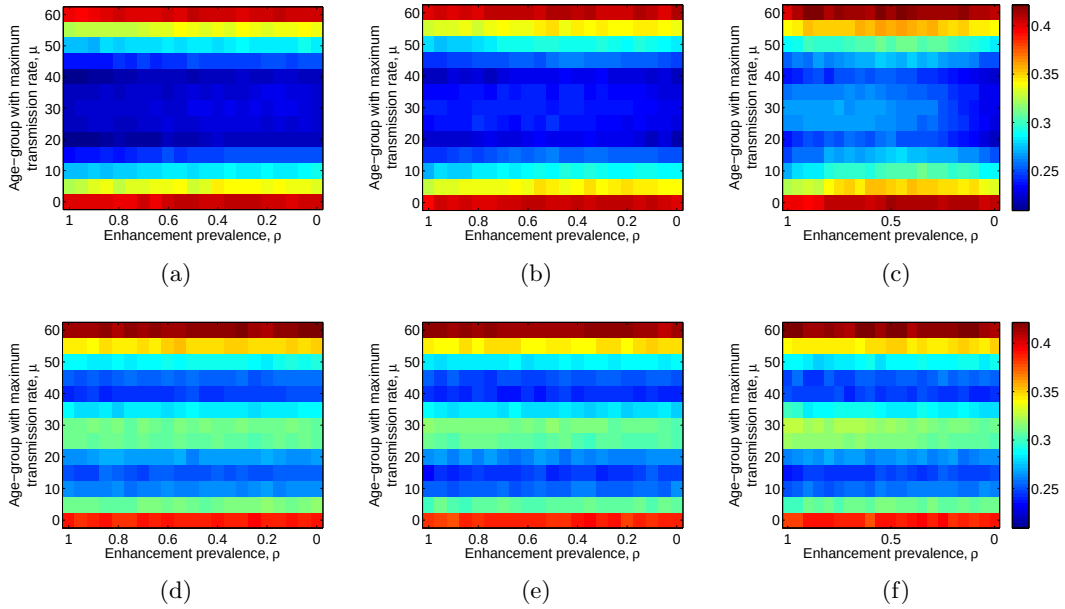

Figure B-3: Probability of type I error at the peak of the initial epidemic as the enhancement prevalence and the age–group with the greatest transmission rate are varied. (a) (b) and (c) show the probability of type I error for serotype one. In (a) $\chi = 2$, in (b) $\chi = 3$ and in (c) $\chi = 5$. (d) (e) and (f) shows the probability of type I error for total seroprevalence. In (d) $\chi = 2$, in (e) $\chi = 3$ and in (f) $\chi = 5$. In all figures $\eta = 1$ and all other parameters are given in Table 4.1.

B.4 Probability of type I error at the endemic equilibrium

Figure B-4 shows the probability of type I error at the endemic equilibrium for serotype one as the enhancement prevalence and age–group with the maximum transmission rate are varied. As cross protection decreases (η increases) the oscillatory behaviour occurs for lower enhancement prevalences. When the maximum transmission rate is between those aged 5 to 45 if the endemic equilibrium can be reached then decreasing the enhancement prevalence makes it harder to differentiate between the age–independent and age–dependent seroprevalence profiles.

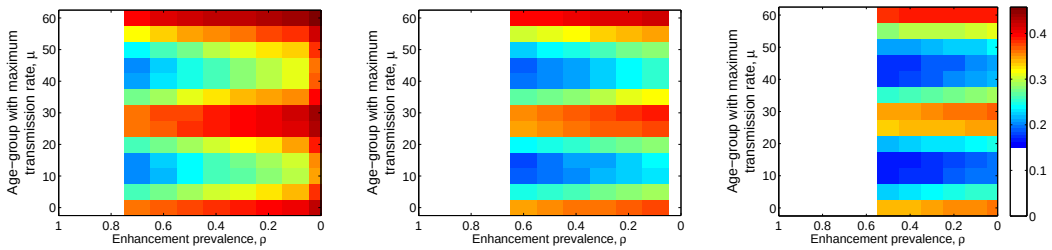

(a) (b) (c)

Figure B-4: Probability of type I error at the endemic equilibrium as the enhancement prevalence and the age–group with the greatest transmission rate are varied for serotype one. In (a) $\eta = 0$, in (b) $\eta = 0.5$ and in (c) $\eta = 1$. In all figures $\chi = 3$ and all other parameters are given in Table 4.1.

APPENDIX C

THE PROBABILITY OF AN EPIDEMIC FOR STOCHASTIC AGE-STRUCTURED MODELS

C.1 Probability of an epidemic when infection starts in the vector population

To confirm the qualitative variation when infection starts in the vector population is not the result of numerical error we look at the largest eigenvalues of the expectation matrix, stochastic simulations, and the expected number of infections after two generations given a particular initial condition. As previously stated, the largest real eigenvalue of the expectation matrix determines whether the system is subcritical (an epidemic will not occur), critical, or supercritical (an epidemic will occur with a probability determined by the fixed points) (Athreya and Ney, 1972; Allen and Lahodny Jr, 2012). Figure C-1(a) shows the largest real eigenvalue as the exposure weighting of the working age-group is varied. The qualitative behaviours seen in figure 5-5(d) can be seen, and hence this complements the result. The stochastic simulations (figure C-1(b)) do not give us much further insight, however the probability of an epidemic is similar as the exposure weighting increases. This is to be expected; such small differences will be almost impossible to detect by simulation.

Finally, we consider the expected number of infections after two generations if infection starts in each of the different age-groups. To do this we consider a generation

based approach. Let the initial conditions be given by $\mathbf{\Phi}_0$. The number of individuals in each population in the subsequent two generations are then given by

$$\begin{aligned}\mathbf{\Phi}_1 &= G\mathbf{\Phi}_0,\\ \mathbf{\Phi}_2 &= G\mathbf{\Phi}_1 \quad = G^2\mathbf{\Phi}_0.\end{aligned}$$

where G is the next generation matrix given by equation (5.17) (Diekmann and Heesterbeek, 2000). We consider the sum of the elements of Φ_2 under each of the different initial conditions, shown in figures C-1(c)–(f). When infection starts in each of the host populations the results coincide with the probability of an epidemic as the exposure weighting of the working and children's age-groups are varied. Similarly when infection starts in vector population (figure C-1(f)) the expected number of secondary infections after two generations initially decreases and then increases, showing qualitative changes for different exposure weightings. Although the dynamics are not exactly the same as for the probability of an epidemic, the two results are not showing the same thing. Rather, we are showing that there are similar behaviours in the graphs, indicating that if infection starts in the vector population there is some qualitative behaviour which is potentially harder to explain.

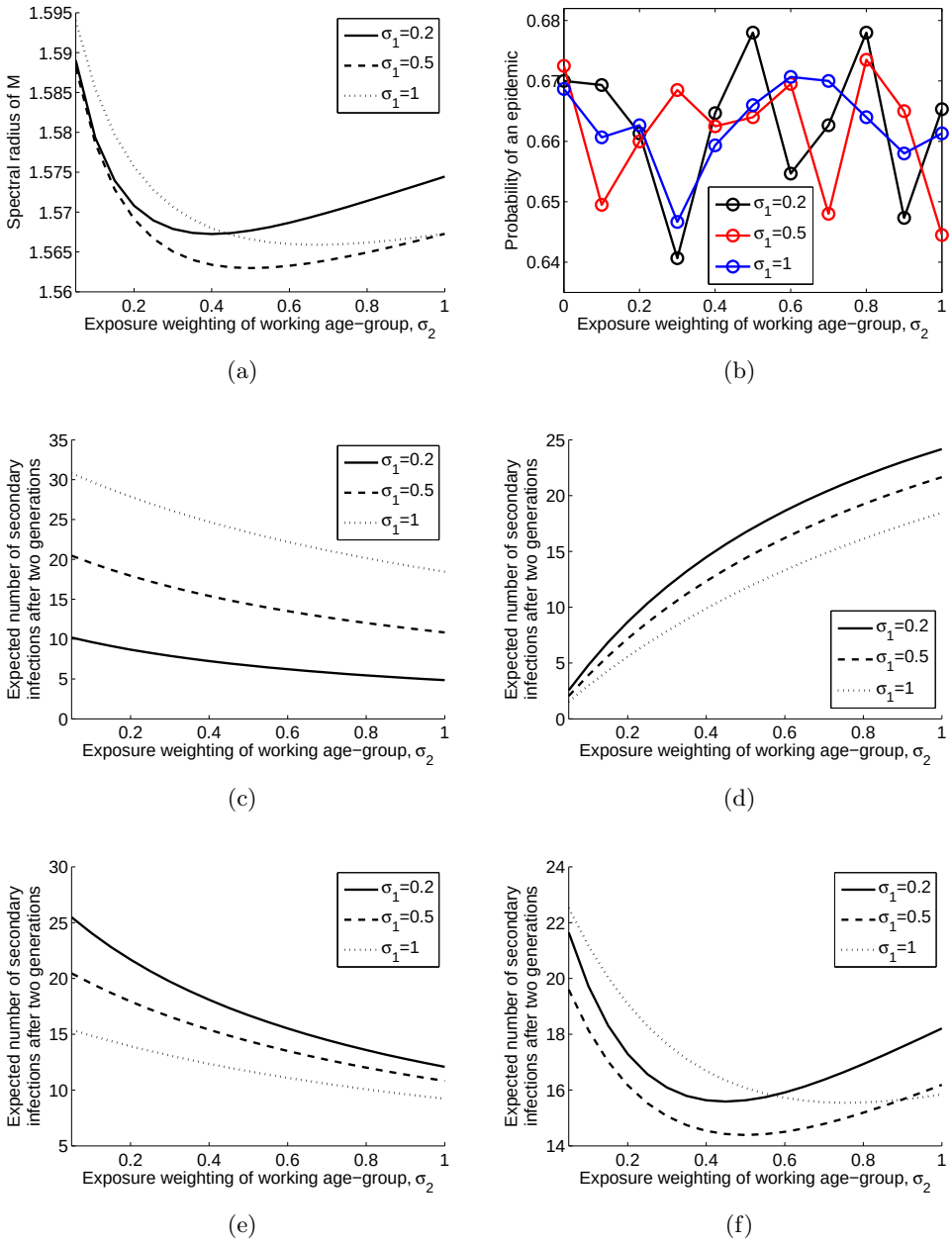

Figure C-1: (a) The spectral radius of the expectation matrix as the exposure weighting of the working age-group is increased. (b) The probability of an epidemic found using stochastic simulations as the exposure weighting of the working age-group is increased. (c)–(f) The expected number of secondary infections after two generations with initial conditions $I_1(0) = 1$, $I_2(0) = 1$, $I_3(0) = 1$ and $I_V(0) = 1$ respectively. In all graphs the solid, dashed and dotted lines represent $\sigma_1 = 0.2$, $\sigma_1 = 0.5$ and $\sigma_1 = 1$. The exposure weighting of the retired age–group is $\sigma_3 = 0.5$. All other parameters are given in Table 5.1.